MULTIFUNCTIONAL BIOCONJUGATES FOR DRUG CARRIERS AND

MOLECULAR PROBES

A Dissertation

Presented to the Faculty of the Graduate School

of Cornell University

In Partial Fulfillment of the Requirements for the Degree of

Doctor of Philosophy in Chemical and Biomolecular Engineering

by

Joshua Aaron Walker

August 2019

MULTIFUNCTIONAL CHEMICAL CROSS-LINKERS FOR DRUG CARRIERS AND MOLECULAR PROBES

Joshua Aaron Walker, Ph.D.

Cornell University 2019

Bioconjugates are an indispensable tool for molecular biology as well as an established modality for biomedical imaging and drug delivery. Broadly, bioconjugation is the use of a chemical cross-linker to covalently attach non-natural reporters, chemical handles, drug cargo, or targeting ligands to biologics to augment their innate properties and functions. Many bioconjugation strategies attach a single non-natural component to the biomolecule of interest. This limits the functional complexity of the resulting bioconjugate. Incorporating multiple functionalities and/or stimuli responsive units has the potential to enable new applications of bioconjugates as molecular probes and drug carriers. Herein, we present a survey of our work towards developing multifunctional bioconjugates. We develop a new strategy for the site-specific modification of native antibodies. This strategy enables dual "click" modification of native antibodies. We also develop new synthetic methods for the synthesis of oligothioetheramides. We apply this new synthesis to study the effect of cross-linker sequence on the biophysical properties of antibody-drug conjugates. Finally, we discuss our efforts to develop molecular probes to characterize the surface of extracellular vesicles and quantify endosomal escape for siRNA therapeutics. Taken together, these works highlight the importance of chemical cross-linkers in the design of multifunctional bioconjugates for a variety of applications.

Biographical Sketch

I was born on July 3rd, 1991 in Louisville, Kentucky. However, my parents, Vicky and David Walker, relocated the family shortly thereafter. I grew up in Lawrenceville, a small town in southern Illinois, with two brothers (Jeremy and James) and one sister (Jessica). I graduated from Lawrenceville High School in 2009.

In August 2009, I enrolled at the University of Illinois at Urbana-Champaign (UIUC) with a major in physics, but I quickly realized that physics was not the major for me. During my sophomore year, I settled on chemical and biomolecular engineering as my new major. At the start of my Junior year I joined the research group of Professor Charles Schroeder. In Professor Schroeder's group, I worked with Arnab Mukherjee to develop flavin-binding fluorescent proteins as a novel class of oxygen independent fluorescent probes.

In August 2013, I moved to Ithaca, New York, to pursue my Ph.D. in chemical and biomolecular engineering at Cornell University. In January 2014, I joined the lab of Professor Christopher Alabi as one of three students in his inaugural class. Shortly after joining the lab I was awarded the NSF graduate research fellowship. During my Ph.D. I have worked on a variety project of projects with varying levels of success. In 2019, I was a awarded a Provost Diversity Fellowship and best oral presentation at the graduate student symposium. Beyond any personal accomplishments, I have most enjoyed the opportunity to mentor undergraduate students.

In September 2019, I am beginning my postdoctoral research in the lab of Professor Alanna Schepartz at the University of California, Berkeley. I will be relocating to the San Francisco Bay Area with my partner, Michelle Sorkin, and our two dogs, Dumpling and Bowie.

To all the people that have supported me.

And to Jim Zlogar, a man with a strange name.

Acknowledgements

I would like to thank my advisor, Professor Christopher Alabi for allowing me to work on my projects with a high degree of freedom and for listening to all my half-baked ideas. I have always been too stubborn to listen to good advice. Working with such freedom has allowed me to discover my own failures and learn my own lessons – albeit more slowly than if I had just listened. Additionally, Chris was always willing to entertain my ideas and debate their merits. This has helped me understand both what makes for a good idea and how do you convince someone to believe in your idea. I believe these skills will help me greatly in my future career.

I would like to thank my committee members, Professor Barbara Baird and Professor Matthew DeLisa. I did not call on them for advice nearly as often as I should have. Nonetheless, they have always been accessible to me and willing to provide advice on my research and professional goals.

I would like to thank all the members of the Alabi Lab. Their collective knowledge has been an invaluable resource throughout my Ph.D. Michelle Sorkin and Dana Thornlow have provided me with a wealth of experience and advice regarding bioconjugation and assay development. I have also had the pleasure of working with several outstanding undergraduates: Xavier Mariano, Charles Jackan, Ameer Basrai, Akash Vaidya, Francis Ledesma, Sneha Kabaria, and John Bohn. Without them this work would not have been possible.

I would like to thank my high school chemistry teacher, Mr. David Atkins. Mr. A was my first academic role model. His passion for teaching is what inspired me to start applying myself during high school. Without his classes I would not be where I am at today. He made me believe that being interested in science can be fun and cool.

Table of Contents

List of Abbreviations

ADC	Antibody-drug Conjugate
ADCC	Antibody-dependent Cellular Cytotoxicity
AF488	Alexa Fluor 488
AF647	Alexa Fluor 647
ARC	Antibody-siRNA Conjugate
BBS	Borate Buffered Saline
βME	2-mercaptoethanol
CDC	Complement-dependent Cytotoxicity
CDCl$_3$	Deuterated Chloroform
CuAAC	Copper-catalyzed Azide-Alkyne Cycloaddition
DAR	Drug-to-Antibody Ratio
DBCO	Dibenzocyclooctyne
DCM	Dichloromethane
DIC	*N,N′*-Diisopropylcarbodiimide
DMA	Dimethylacetamide
DMEM	Dulbecco's Modified Eagle Media
DMF	Dimethylformamide
DMPA	2,2-Dimethoxy-2-phenylacetophenone
DMSO	Dimethyl Sulfoxide
DNA	Deoxyribonucleic Acid
DNP	2,4-dinitrophenol
ELISA	Enzyme-linked Immunosorbent Assay
EtOAc	Ethyl Acetate
Et$_3$N	Triethylamine
EVs	Extracellular Vesicles
FBS	Fetal Bovine Serum
FRET	Förster Resonance Energy Transfer
GalNAc	N-acetyl Galactosamine
GFP	Green Fluorescent Proteins
NHS	N-hydroxy Succinimide
HIC	Hydrophobic Interaction Chromatography
HIPS	Hydrazino-*iso*-Pictet-Spengler
IEDDA	Inverse Electron Demand Diels-Alder
K$_D$	Dissociation Constant
LC-MS	Liquid Chromatography-Mass Spectrometry
MALDI-MS	Matrix Assisted Laster Desorption Ionization-Mass Spectrometry
MeOH	Methanol
MMAE	Monomethyl Auristatin E
MTG	Microbial Transglutaminase
mTz	Methyltetrazine
NMR	Nuclear Magnetic Resonance
oligoTEA	Oligothioetheramide
OPSS	Ortho-pyridyl Disulfide
PBS	Phosphate Buffered Saline
PEG	Polyethylene Glycol
PNGase F	Peptide:N-glycosidase F
RNA	Ribonucleic Acid
RP-HPLC	Reverse Phase-High Performance Liquid Chromatography

SA	Streptavidin
SDS-PAGE	Sodium Dodecyl Sulfate-Polyacrylamide Gel Electrophoresis
SEC	Size Exclusion Chromatography
siRNA	Short Interfering RNA
SPAAC	Strain-Promoted Azide-Alkyne Cycloaddition
TCO	*Trans*-cyclooctene
TFA	Trifluoroacetic Acid
TGS	Target-guided Synthesis
THOP1	Thimet Oligopeptidase
THF	Tetrahydrofuran

List of Figures

List of Tables

Chapter 1 – The Functional Components of Bioconjugates

1.1 – Introduction

Broadly, bioconjugation seeks to chemically modify biologics such as lipids[1,2], carbohydrates[3,4], proteins[5,6], and nucleic acids[7,8] as a means augment their natural properties. These non-natural functions have made bioconjugates an indispensable tool for molecular biology[9,10], *in vivo* imaging[11,12], and medical diagnosis[13,14]. Further, therapeutic bioconjugates are an established modality for the delivery of small molecule chemotherapeutics[15], and are emerging as a platform for the delivery of small interfering RNA (siRNA)[16].
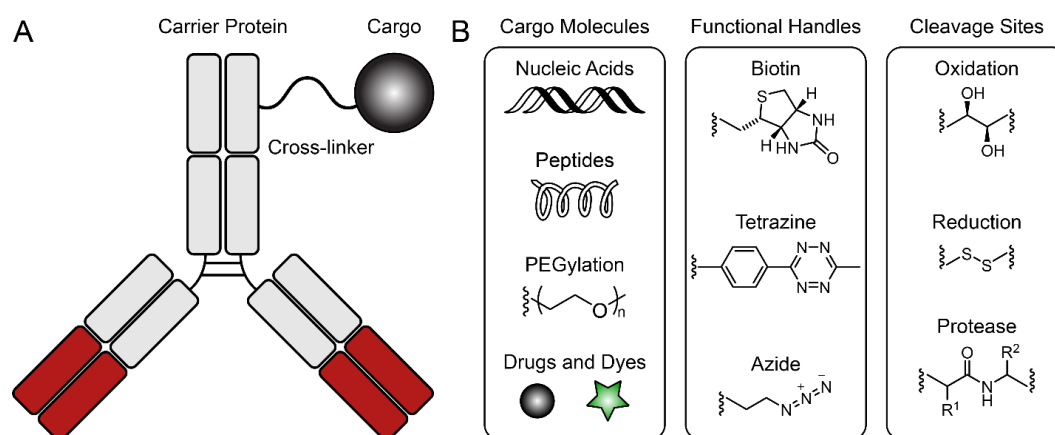
Figure 1.1. Structural and functional components of antibody-based bioconjugates. A) structural components of antibody bioconjugates and B) key functional features common to antibody bioconjugates.

Monoclonal antibodies, the prototypical affinity reagent, constitute a particularly powerful class of bioconjugates (**Figure 1.1**). Directed evolution techniques such as ribosome[17], phage[18], and yeast[19] display have enabled the rapid discovery of antibody fragments directed towards a variety of targets. In combination with antibody humanization[20], these techniques provide a powerful toolkit to develop novel, full-length therapeutic antibodies. In addition to the carrier protein, bioconjugates are comprised of two other structural features; a functional cargo and a chemical cross-linker. While

the antibody carrier directs a bioconjugate to its target, the non-natural cargo is what gives its specialized function. For example, modifying an antibody with a small molecule drug gives rise to an antibody-drug conjugate capable of inducing cell death[21,22]. Whereas, modifying the same antibody with a biotin functional handle yields a conjugate for immunofluorescence imaging applications[23]. The final structural component, the chemical cross-linker, is the central hub around which the rest of the bioconjugate is built. This covalent linkage is what allows the targeting ability of the antibody carrier to work in concert with the chosen non-natural cargo. Beyond serving as a passive physical attachment point, a cross-linker can also play an active role in the functional properties of a bioconjugate. Specifically, chemical cross-linkers can be designed to release therapeutic cargo at the appropriate time and location due to the presence of intracellular stimuli[24]. Ultimately, these three structural components are intimately linked and must be carefully considered when designing an antibody bioconjugate. Herein, we highlight the synthetic challenges, important biophysical properties, and functional limitations of antibody bioconjugates.

1.2 – Chemistry of Proteins and DNA

The Structural Features of DNA
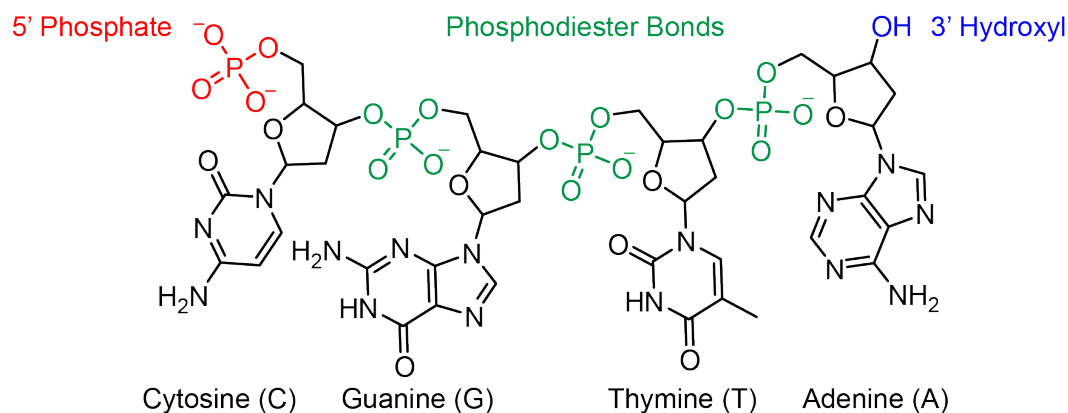
Figure 1.2. The structural features of nucleic acids. The 5' phosphate group is shown in red, phosphodiester backbone is highlighted in green, 3' hydroxyl group is shown in blue, and the structures of the four nucleotide bases are highlighted.

DNA, which is synthesized by DNA polymerases, is polymer comprised of deoxyribonucleotides (**Figure 1.2**). DNA synthesis proceeds in a 5' to 3' fashion through the sequential addition of nucleoside triphosphates to the 3' hydroxyl group of the growing nucleic acid chain. This synthesis yields a polymer backbone of deoxyribose sugars connected via negatively charged phosphodiester bonds[25]. These features result in a polymer backbone that is both highly rigid and negatively charged. The final nucleic acid chain is terminally modified with a 5' phosphate and a 3' hydroxyl. Finally, each nucleoside triphosphate building block is functionalized with a nucleobase. These nucleobases form pairs, guanine-cytosine and adenine-thymine, which participate in hydrogen bonding and π-stacking interactions. These interactions drive inter-strand self-assembly into the DNA double helix[26]. Further, the ability of nucleobases to recognize each other in a sequence-specific fashion is the basis for biological information storage and drives interest in adapting DNA for digital data storage[27].

The Structural Features of Polypeptide Chains
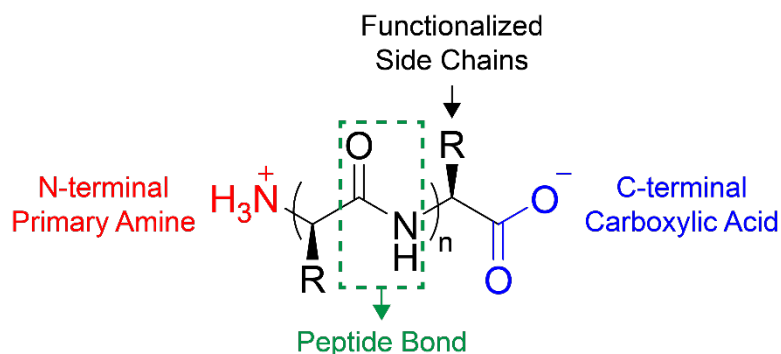
Figure 1.3. The structural features of polypeptide chains. The terminal primary amine is shown in red, peptide backbone is highlighted in green, the terminal carboxylic acid is shown in blue, and the functional side chain is indicated.

Proteins, which are synthesized by the ribosome, are polymers comprised of amino acids (**Figure 1.3**). Polymerization is achieved through the reaction of the amino group from one amino acid with the carboxyl group of another. This chemistry gives rise to the peptide bond that defines the polymer backbone. The partial double bond character of the peptide bond creates rigid linkages with restricted rotational freedom. This property along with the hydrogen bonding character of the peptide bond drives the formation of the secondary structural features such as the α-helix and β-sheet[28]. An additional structural relic of amino acid polymerization is the existence of a N-terminal primary amine and C-terminal carboxylic acid within each synthesized protein. Finally, functionalization of the polypeptide is achieved through the side chain of each amino acid monomer. These side chains participate in the formation of protein tertiary structure through intradomain hydrophobic and ionic interactions, the formation of disulfide bonds, and additional hydrogen bonding. Further, side chains define the numerous biological functions of proteins such as catalysis, molecular recognition, and self-assembly[29].

Reactivity of Amino Acid Side Chains
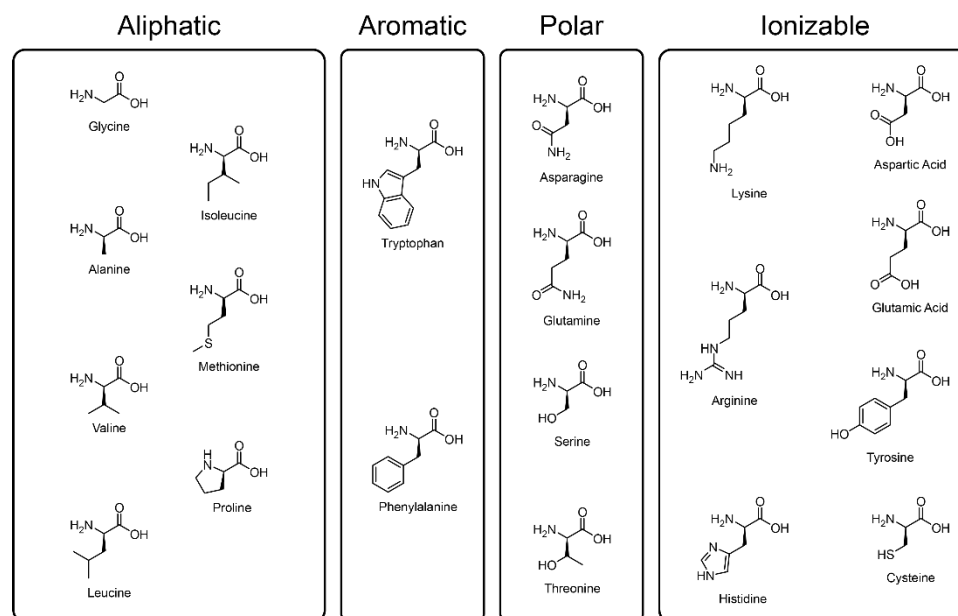
Figure 1.4. The chemistry of amino acid side chains. The twenty natural amino acids can be categorized as aliphatic, aromatic, polar, or ionizable. With respect to bioconjugation, ionizable side chains are generally considered to be reactive.

The twenty natural amino acids (**Figure 1.4**) provide a diverse palette from which to fine tune the structure and function of proteins. Broadly, these side chains can be subdivided into four categories that describe their chemical nature: aliphatic, aromatic, polar, and ionizable. These categories play varied roles in modulating the natural function of proteins. With respect to bioconjugation, the role of the amino acid side chains is to provide a point of covalent attachment for non-natural functional groups. Traditionally, the most common protein conjugation strategies have targeted the ionizable amino acids tyrosine, aspartic acid, glutamic acid, lysine, and cysteine as well as the N-terminal primary amine and the C-terminal carboxylic acid. Tyrosine can be modified alpha to the hydroxyl group using diazonium containing compounds[30] or primary amines via a Mannich condensation[31]. Carboxylic acid containing groups (aspartic acid, glutamic acid, and C-terminus) can be derivatized by conversion first to an activated ester intermediate. This is typically achieved by using a combination of 1-

Ethyl-3-[3-dimethylaminopropyl] carbodiimide (EDC) and *N*-hydroxy succinimide (NHS). Conjugation is completed by the addition of an amine-modified reagent which yields stable amide linkage[32]. Amine containing groups (lysine and N-terminus), can be acylated by reaction with a variety of activated carbonyl species[33]. The sulfhydryl group of cysteine provides the most versatile conjugation handle among the twenty natural amino acids. Cysteine can from an exchangeable thioester linkage upon reaction with an activated carbonyl. A stable thioether bond can be formed by reaction with an iodoacetyl group or via a thiol-Michael addition with maleimide-functionalized reagents. Finally, a reduction sensitive disulfide bond can be formed through thiol-disulfide exchange with labile pyridyl disulfide reagents[34]. Over the course of several decades the above chemistries have emerged as indispensable tools for bioconjugation. However, these methods are not without limitations. By their nature, these strategies target naturally occurring amino acids. For a given protein, there will invariable be numerous solvent accessible reactive amino acids. Therefore, a heterogeneous mixture of products containing multiple chemical modifications will be formed. Conjugation strategies which result in a heterogeneous mixture of products are called "non-specific". These strategies result in batch-to-batch variability wherein subtle differences in the reaction conditions yield a higher or lower degree of conjugation, which may affect conjugate performance. Non-specific conjugation can also inactivate the carrier protein by chance modification of amino acid residues that are important for binding or enzymatic activity. These limitations and others have inspired researchers to pursue methods to control the placement of chemical modifications within a protein carrier[35].

1.3 – Bioorthogonal Chemistry and Non-canonical Amino Acids
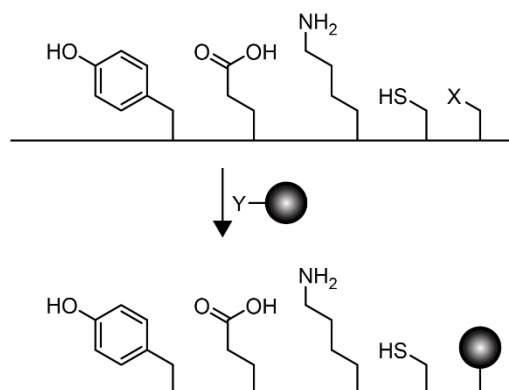
Figure 1.5. The principles of bioorthogonal chemistry. Bioorthogonal chemical handles (X and Y) react selectively in the presence of reactive amino acid side chains.

One approach to controlling the placement of chemical modifications within a protein is the use of bioorthogonal chemistry (**Figure 1.5**). Bioorthogonal reactions are reactions which occur selectively between two non-natural chemical handles within complex biological environments[36]. A variety of bioorthogonal chemistries have been developed[37] and employed to selectively label live cells[3], image living organisms[38], site-specifically modify proteins[39], discover novel small molecule inhibitors[40], and design peptide-based affinity reagents[41]. The preeminent bioorthogonal chemistries are the strain-promoted azide-alkyne cycloaddition (SPAAC) reaction[42] and the inverse electron demand Diels-alder (IEDDA) reaction[43].

Strain-Promoted Azide-Alkyne Cycloaddition (SPAAC) Reaction
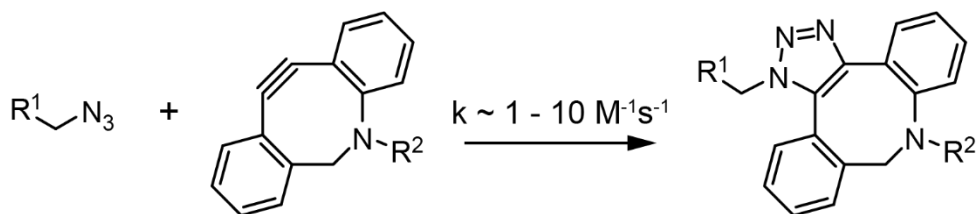
Figure 1.6. Strain-promoted azide-alkyne cycloaddition. Reaction shown between an azide and a dibenzocyclooctyne.

The SPAAC reaction, pioneered by the lab of Carolyn Bertozzi (**Figure 1.6**), was inspired by the 1,3-dipolar cycloaddition between an azide and a linear alkyne in the presence of a copper(I) catalyst and a stabilizing ligand This reaction, which generates a five-membered 1,2,3-triazole ring, is also known at the copper-catalyzed azide-alkyne cycloaddition (CuAAC)[44]. This reaction occurs rapidly and selectively in complex chemical environments with a second order rate constant of $10 - 200$ M^{-1} s^{-1}. However, the copper catalyst, which is toxic to live cells, limits its utility in biological applications[45]. The SPAAC reaction was developed to enable the same bioorthogonal reactivity without the need for a copper catalyst. This was achieved by placing the alkyne functional group within a cyclooctane ring to introduce ring strain. Using this methodology, a variety of cyclooctyne derivatives have been synthesized possessing a range of reactivities[46]. However, only derivatives with a second order rate constant of approximately 1 M^{-1} s^{-1} or greater can be practically useful for bioconjugation. The second order rate constant for the most widely commercially available cyclooctyne (dibenzocylcooctyne, DBCO) is reported to be $1 - 10$ M^{-1} s^{-1}. This rate constant is strongly dependent on both the composition of the reaction solvent and the nature of the azide reaction partner[47-50]. This rate is sufficient to allow for functionalization of biomolecules at a concentration of approximately $10 - 100$ µM. However, the cargo molecule to be attached must be provided in moderate molar equivalencies relative to

the carrier protein. For live cell imaging applications in which complete conversion is not necessary, it is possible that these conditions can be relaxed. One limitation of the SPAAC reaction is that all derivatives that display fast reaction kinetics contain bulky eight-membered rings and/or multi-ring structures[46]. These sterically bulky and hydrophobic features can have deleterious effects on stability and function of the conjugated biomolecule.

Inverse Electron Demand Diels-Alder (IEDDA) Reaction
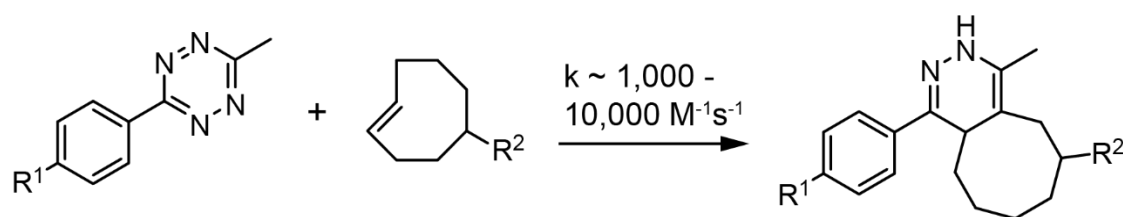
Figure 1.7. Inverse electron demand Diels-alder reaction. Reaction shown between a methyl tetrazine and a *trans*-cyclooctene.

The bioorthogonal IEDDA reaction between a tetrazine and a strained dienophile (**Figure 1.7**) was first reported by the labs of Scott Hilderbrand[51] and Joseph Fox[52]. This reaction proceeds through a Diels-Alder [4+2] cycloaddition yielding a strained bicyclic intermediate. Strain is relieved by a subsequent retro-Diels-Alder reaction, which releases nitrogen as the only byproduct of the reaction. Interestingly, the kinetics of this reaction can be tuned across several orders of magnitude by modifying the chemical nature of both reaction partners[43]. For example, the use of dienophiles such as norbornene[53], a methyl-substituted cyclopropene[51], *trans*-cyclooctene (TCO)[52], and trans-bicyclo[6.1.0]nonene[54] tunes the rate constant from 1 – 400,000 M^{-1} s^{-1}. Modulating the structure of the tetrazine has been shown to tune the reaction with TCO from 0.1 M^{-1} s^{-1} to greater than 100 M^{-1} s^{-1},[55]. The most common tetrazine-dienophile pair is the reaction between a methyl-substituted tetrazine and a *trans*-cyclooctene. This pair represents a balance between reactivity and solution-

phase stability with a second order rate constant of 2,000 M^{-1} s^{-1},[52]. The kinetics of this reaction are compatible with the functionalization of biomolecules at equimolar conditions and concentrations as low as approximately 1 µM. However, like the DBCO-azide SPAAC reaction, these reactive partners form a bulky and hydrophobic product, which may negatively impact the properties of the resulting bioconjugate. Further, recently, TCO has been shown to rapidly isomerize to the *cis* conformation when stored in solution[56]. The *cis* conformation does not participate in the IEDDA reaction. This adds an additional complexity to employing the TCO-tetrazine ligation and motivates the investigation of stable alternatives with fast reaction kinetics.

1.4 – Strategies for Site-specific Antibody Modification
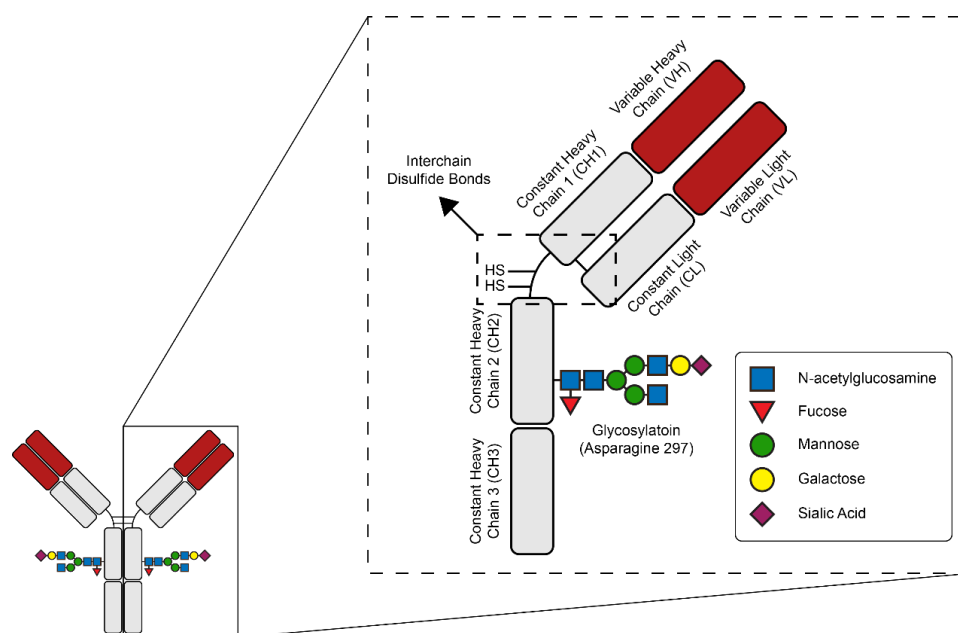
Figure 1.8. Structure and nomenclature of full length IgG1. The full length IgG1 is a symmetric, multidomain protein with a molecular weight of approximately 150 kDa. The structure consisting of four polypeptide chains connected via four interchain disulfide bonds. The light chain (approximately 25 kDa molecular weight) is comprised of two domains; constant and variable light chains. The heavy chain (approximately 50 kDa molecular weight) is comprised of four domains; variable heavy chain domain and three constant heavy chain domains. A single glycosylation site is located at asparagine 297 within the heavy chain.

The human IgG is a complex multidomain glycoprotein (**Figure 1.8**) that is a central component of the human immune response responsible for binding to exogenous species such as viruses and bacteria[57]. Like other protein-based carriers, antibodies are compatible with a variety of non-specific conjugation strategies targeted towards tyrosine, aspartic acid, glutamic acid, and lysine residues. However, antibodies are also compatible with site-directed conjugation strategies that yield a heterogeneous product but enable control over the localization of chemical modification. Antibodies contain no unpaired cysteine residues in their folded form. Therefore, the interchain disulfide bonds can be selectively reduced using reagents such as TCEP to liberate up to eight sulfhydryl groups for bioconjugation[58]. This directs conjugation to the hinge region between the binding domain and the Fc region. The human IgG1 also contains a single glycosylation site at asparagine 297 within the heavy chain[59], which can be used to control placement of cargo away from the binding domain. Oxidizing agents such as sodium periodate can be used to convert 1,2-diols within the glycan to reactive aldehyde functional groups. These aldehydes can be reacted with nucleophiles such as primary amines, hydrazides, or hydroxylamines to form reversible imine bonds. Reductive amination with reagents such as sodium cyanoborohydride can be used to generate stable secondary amine linkages[60]. These methods offer certain improvements over non-specific strategies, but still yield heterogeneous products that suffer from batch-to-batch variability.

In recent years, site-specific modification has been identified as a powerful handle to enhance the properties of antibody-based bioconjugates for applications in both immunodetection[9,61] and drug delivery[62-65]. These methods seek to precisely control both the localization and number of chemical modifications with the goal of achieving a homogeneous product. Broadly, site-specific antibody modification can be

categorized as utilizing either engineered antibodies (e.g. engineered cysteines[66,67], non-canonical amino acids[68,69], and chemoenzymatically-recognized peptide tags[70,71]) or native antibodies (interchain disulfide conjugation[58,72], disulfide re-bridging[73,74], glycan remodeling[4,75], and microbial transglutaminase[76-78]). Here we focus on the leading platforms for controlling the placement of cargo molecules at any site within an antibody of interest.

THIOMAB Platform
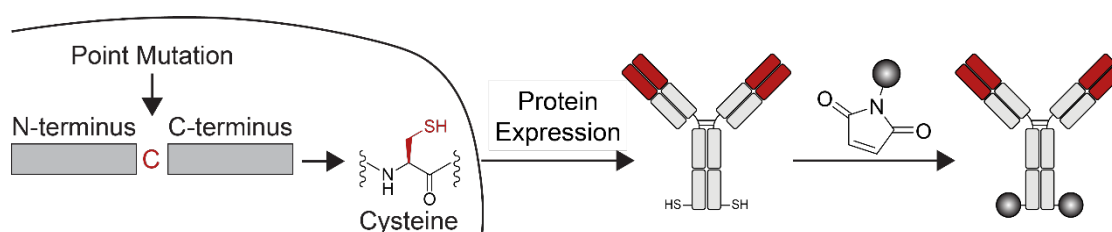
Figure 1.9. Overview of site-specific protein antibody modification via THIOMAB. A cysteine point mutation along the amino acid sequence of the protein, introducing a unique thiol chemical handle. Maleimide-thiol chemistry is used to covalently attach the cargo of interest.

Researchers at Genentech developed THIOMABs (**Figure 1.9**), which leverage the fact that antibodies contain no unpaired cysteine residues, to site-specifically modify antibodies[66]. THIOMABs are conceptually simple. A non-natural cysteine residue is engineered into the antibody at any site of interest. The antibody is then produced bearing a non-natural, unpaired cysteine residue. These residues can be derivatized through simple, commercially available maleimide linkers to covalently attach cargo. Despite the elegance of this approach, it is not without its drawbacks. Specifically, traditional maleimide linkers are prone to deconjugation in circulation[79]. This may necessitate the use of more advanced chemistries such as the self-hydrolyzing maleimide[58], which negates some potential benefits. Further, incorporation of non-natural cysteine residues can lead to scrambling of disulfide bonds within the

antibody[80,81]. Nevertheless, researchers at Genentech have applied this technology to screen the entire human IgG for stable conjugation sties[65].

Microbial Transglutaminase
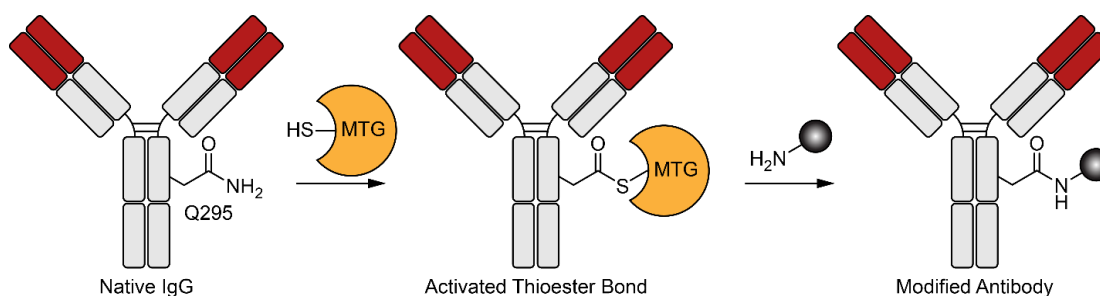
Figure 1.10. Mechanism of action for microbial transglutaminase (MTG)-based modification of the native human IgG. Glutamine 295 within the heavy chain of the antibody is recognized by MTG and converted into an activated thioester bond. An amine bearing cargo displaces the activated MTG and forms a stable isopeptide bond.

In addition to THIOMABs, chemoenzymatic approaches have been developed in which the catalytic activity and site specificity of an enzyme is coopted for bioconjugation. One such approach is microbial transglutaminase (MTG, **Figure 1.10**), which belongs to a family of enzymes that catalyze the formation of interprotein isopeptide bonds between glutamine and lysine residues[82,83]. Serendipitously, MTG recognizes glutamine 295 (Q295) within the heavy chain of aglycosylated, human IgGs[84]. Co-treatment with Peptide:N-glycosidase F (PNGase F) removes the N-linked glycan at asparagine 297 (N297) and facilitates efficient bioconjugation[78]. By supplying non-natural acyl acceptor substrates, this natural function has been co-opted for site-specific, homofunctional antibody modification[85,86]. Researchers have expanded beyond the natural Q295 site by introducing a N297Q point mutation that provides an additional conjugation site within the IgG heavy chain[78]. Moreover, recognition sequences have been designed that enable the incorporation of MTG conjugation sites at any point along the antibody backbone[62,87]. In addition to site-specific native antibody modification, a key advantage of MTG-based bioconjugation is compatibility with many

commercially available amine-bearing chemical cross-linkers. A key drawback of MTG-based conjugation is competition with native lysine residues. After MTG recognizes Q295, an activated thioester is formed between Q295 and MTG. Native lysine residues on the antibody or other antibodies in solution can displace this thioester bond forming intra- or intermolecular isopeptide bonds respectively. These unwanted side reactions must be suppressed by the addition of large equivalencies of acyl acceptor substrate. Otherwise, the antibody of interest will form a cross-linked network of proteins.

Formylglycine-generating Enzyme/HIPS Ligation
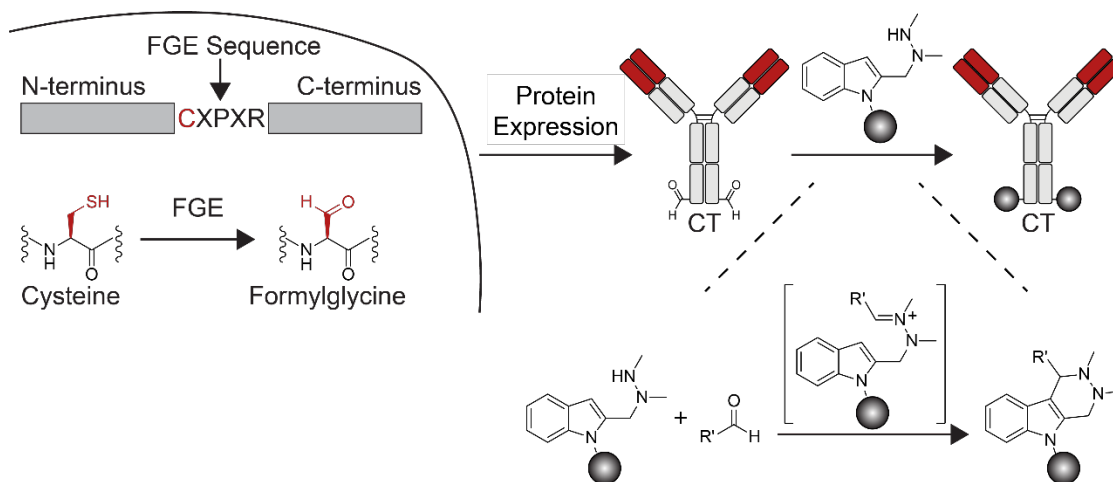
Figure 1.11. Overview of site-specific protein modification via formylglycine-generating enzyme. Bioorthogonal aldehyde tags are site specifically incorporated along the amino acid sequence of the protein. The Hydrazino-iso-Pictet-Spengler ligation is used to stably attach the cargo of interest.

Finally, a hybrid approach pioneered by the Bertozzi lab utilizes formylglycine-generating enzyme to site-specifically incorporate a bioorthogonal chemical handle (**Figure 1.11**). To install this chemistry, the protein of interest is engineered to contain a pentapeptide recognition sequence (CXPXR). The protein of interest is then co-expressed with formylglycine-generating enzyme which co-translationally converts the cysteine residue into an aldehyde-bearing fromylglycine residue[88]. This residue is compatible with hydrazide and hydroxylamine conjugation chemistries and undergoes

reversible cross-linking through imine formation with naturally occurring lysine residues. This technology was the basis of Redwood Bioscience, a start-up company founded by Bertozzi lab alumni. To suppress cross-linking and generate stable bioconjugates, Redwood Bioscience developed the Hydrazino-*iso*-Pictet-Spengler (HIPS) ligation[89]. This ligation proceeds initially through a traditional hydrazide-aldehyde imine reaction to form an intermediate hydrazonium ion. The proximity of this hydrazonium ion to a nucleophilic indole leads to intramolecular alkylation and the formation of a stable carbon-carbon bond. Redwood Bioscience has since been acquired by Catalent Biologics where they have refined this conjugation strategy[63]. Recently, Catalent Biologics has used the HIPS ligation to perform unbiased screening of conjugations sites throughout the human IgG[64].

1.5 – Synthesis of Multifunctional Chemical Cross-linkers

The chemical cross-linker is the component of a bioconjugate that provides a covalent linkage between the biologic and its reporter, cargo, chemical handle, or ligand. As such, the chemical cross-linker is the central hub that controls many of the properties of a bioconjugate. Traditional synthesis of chemical cross-linkers has utilized substituted aromatic derivatives[90,91], amino acid core structures[92,93], or bifunctionalized polyethylene glycol[94,95]. These approaches yield cross-linkers with no more than three attachment sites, which limits the functionality and valency of the resulting bioconjugate. Iterative synthesis methodologies have the potential to overcome this limitation.

DNA-based Cross-linkers
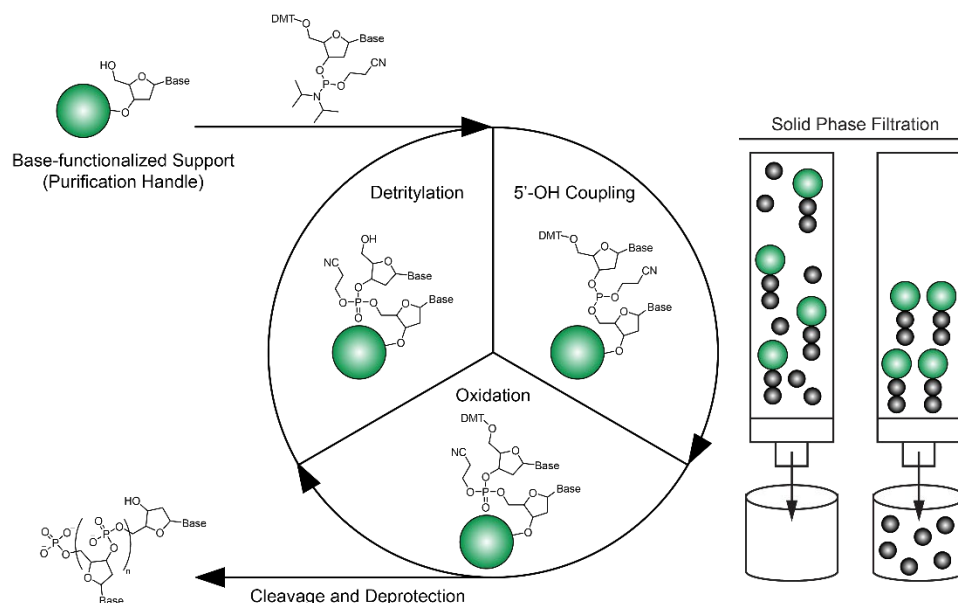
Figure 1.12. Overview of solid-phase DNA synthesis. Coupling of the free 5'-hydroxyl displaces the diisopropylamino group of the phosphoramidite monomer. Then the unstable phosphite triester is oxidized to a stable phosphate triester. Finally, the dimethoxytrityl protecting group is removed from the 5'-hydroxyl and the next protected nucleotide is added to the growing nucleic acid chain. Cleavage from the resin along deprotection of the phosphodiester backbone and nucleotide bases yields the final nucleic acid product. Stepwise filtration is used to remove excess reagents.

DNA can be chemically synthesized via a solid phase method using phosphoramidite chemistry (**Figure 1.12**)[96]. The synthetic accessibility of DNA makes it possible to consider DNA as a material for chemical cross-linker design. With respect to bioconjugation, DNA possesses several intriguing properties. The rigid nature of DNA, particularly in its double-stranded form[97], enables the assembly of structured bioconjugates with precisely defined geometries[98,99]. Further, DNA hybridization can be used to immobilize conjugated cargo on DNA-functionalized surfaces[100] as well as the program the assembly of multiprotein complexes[101]. Finally, DNA-based conjugates can be used in combination with polymerase chain reaction (PCR) to achieve sensitive detection of conjugated materials[9]. A variety of reagents have been developed for the solid-phase synthesis of DNA with non-natural chemical handles. Amino and sulfhydryl

groups can be placed on the 3' and 5' ends of DNA to allow for further user-defined modification via traditional amine- and thiol-compatible chemistries. Chemical spacers can be incorporated between nucleobases to modulate the structural properties of the cross-linker or introduce photocleavable chemistry. Non-natural nucleobases can be inserted that improve the melting temperature of the double stranded cross-linker or enable photo-initiated cross-linking[96]. Taken together, these features present DNA as a uniquely versatile material for cross-linker design. However, comparatively higher cost and nuclease sensitivity dictate that DNA-based chemical cross-linkers be used only when structural rigidity, self-assembly, or PCR-based amplification is needed.

Peptide-based Cross-linkers
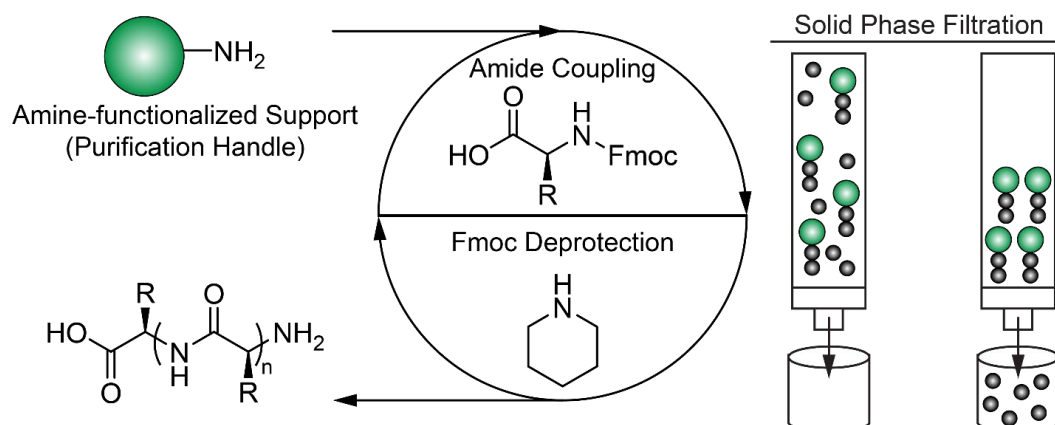
Figure 1.13. Overview of solid-phase peptide synthesis. Iterative amide coupling and deprotection reactions are used to extend the peptide chain. Stepwise filtration is used to remove excess reagents.

Peptide-based cross-linkers are built linearly using traditional solid-phase synthesis techniques (**Figure 1.13**)[102]. This yields heteromultifunctional chemical cross-linkers with the pendant group chemistry of both natural and non-natural amino acids[103]. These chemical handles can be further derivatized using traditional conjugation chemistries as well as bioorthogonal techniques to attach a variety of cargoes of interest. Traditionally, this has positioned peptides as the standard platform

17

for heteromultifunctional cross-linkers. However, the peptide backbone is a potential

biological liability and imposes chemical limitations. Being of biological origin, the

peptide backbone is sensitive to proteolysis. In therapeutic applications, it is critical to

maintain covalent attachment of the drug cargo during circulation to avoid systemic

toxicity or decreased potency. The biological origin of peptides also restricts their

functional diversity. For example, the peptide backbone is not capable of responding

to external queues such as oxidative reagents or photochemical cleavage. Such

diversity would enable bioorthogonal release mechanisms that complement biological

stimuli. Synthetic systems have the potential to overcome this shortcoming.

OligoTEA-based Cross-linkers
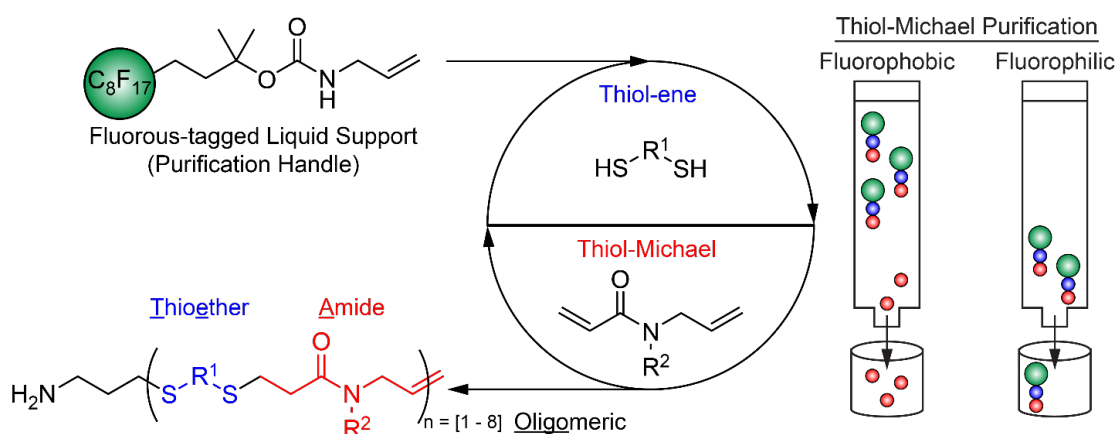
Figure 1.14. Overview of oligothioetheramide (oligoTEA) synthesis. Iterative thiol-ene
and thiol-Michael additions are used to extend the oligomer chain. Stepwise fluorous
purification is used to remove excess reagents.

Oligothioetheramides (oligoTEAs), a sequence-defined synthesis methodology

developed by our lab[104] holds the potential to circumvent many of the limitations of

peptide-based cross-linkers (**Figure 1.14**). OligoTEA synthesis utilizes an orthogonally

reactive *N*-allylacrylamide monomer, which can undergo alternating photoinitiated

thiol−ene "click" reactions and phosphine catalyzed thiol-Michael additions[104].

OligoTEAs are built off a fluorous tag liquid support, which enables stepwise fluorous

purification throughout synthesis. The fluorous purification handle is removed post synthesis by acid-catalyzed Boc deprotection. OligoTEA synthesis has been used as a platform to discover synthetic antibacterial agents[105] and cell penetrating oligomers[106] as well as to synthesize model systems to study the solution phase structure of polymers[107]. Previously, we have demonstrated that oligoTEAs can be used to synthesize cleavable, multifunctional chemical cross-linkers for bioconjugation[108]. The oligoTEA backbone is abiotic and is therefore stable in the biological milieu. Further, oligoTEA synthesis decouples the selection of backbone and pendant group chemistry. This enables the incorporation of a diverse selection of dithiol monomers. These monomers can be used to mimic the flexibility and hydrophilicity of polyethylene glycol-based cross-linkers or to incorporate biologically inert, chemically triggered cleavage sites.

1.6 – Design of Antibody-drug Conjugates
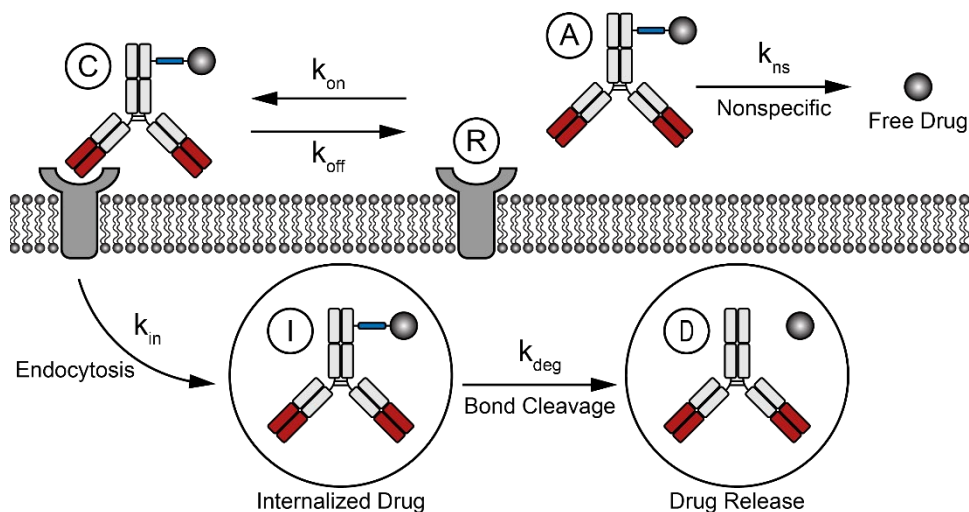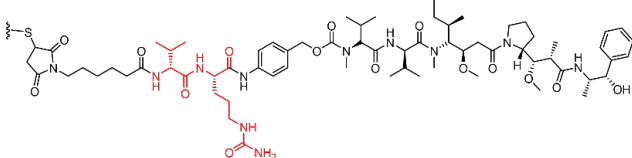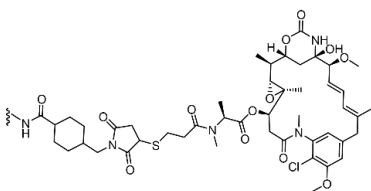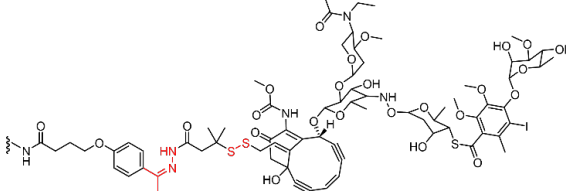
Figure 1.15. Mechanism of intracellular antibody-drug conjugate (ADC) processing. Circulating ADC (A) can be acted upon by extracellular factors to nonspecifically release the active payload. Once bound to the target receptor (R), the ADC-receptor complex (C) is taken up by the target cell via endocytosis. The internalized ADC (I) is acted upon by intracellular factors that degrade the ADC (D), releasing the active payload within the target cell.

Cancer is a disease in which genetic mutations cause normal tissue to develop a phenotype characterized in part by uncontrolled proliferation. In traditional chemotherapy, cancer is treated by the administration of a cytotoxic small molecule drug with the goal of killing the hyperproliferative cells[109]. However, these drugs passively diffuse into both healthy and diseased tissue which causes the serve side effects often associated with chemotherapy. Antibodies have also been used to treat cancer. First an antibody is discovered which selectively binds to a receptor protein over expressed on cancerous cells. Once bound to its target receptor, the antibody can interfere with cell signaling pathways to inhibit cell growth. The antibody can also stimulate an immune response leading to antibody-dependent cellular cytotoxicity (ADCC) or complement-dependent cytotoxicity (CDC)[110]. A third approach to the treatment of cancer, antibody-drug conjugates (ADCs), seek to combine the targeting capability of antibodies with the chemotherapeutic potential of small molecule drugs (**Figure 1.15**). In an ADC, a cytotoxic drug is inactivated by covalent attachment to an antibody-based carrier protein. Once bound to its target receptor, the ADC-receptor complex is internalized via endocytosis. Inside the target cell, intracellular stimuli release the cytotoxic drug in an active form. This conceptual framework has led to the FDA approval of five ADCs with dozens of compounds in clinical trials[15]. Here we highlight a few of the key functional components and outstanding challenges in the development of ADCs.

The Structure of FDA Approved ADCs

Table 1.1. Payload structures for FDA approved antibody-drug conjugates (ADCs). Stimuli-responsive chemistry is highlighted in red. Details regarding the construction of each ADC are provided on the right.

Payload Structure	FDA Approved Antbody-drug Conjugates	
	Brentuximab vedotin Target Antigen: CD30 D.A.R.: ~3 - 5 Approval Year: 2011	Polatuzumab vedotin Target Antigen: CD79b D.A.R.: ~ 3.5 Approval Year: 2019
	Trastuzumab emtansine Target Antigen: CD340 (HER2) D.A.R.: ~ 3.5 Approval Year: 2013	
	Inotuzumab ozogamicin Target Antigen: CD22 D.A.R.: ~ 2 - 3 Approval Year: 2017	Gemtuzumab ozogamicin Target Antigen: CD33 D.A.R.: ~ 2 - 3 Approval Year: 2017

The structures of the five FDA approved ADCs (**Table 1.1**) provide insights into the characteristics of successful ADCs. The first FDA approved ADC, Brentuximab vedotin (Adcetris), a product of Seattle Genetics, is targeted against the CD30 receptor. This receptor is overexpressed on tumor cells in Hodgkin's lymphoma and anaplastic large cell lymphoma (ALCL). The cytotoxic payload, tubulin binding monomethyl auristatin E (MMAE), is conjugated to the antibody via maleimide-thiol chemistry in a site-directed fashion using the interchain disulfide bonds. The payload is released intracellularly via lysosomal cleavage of a dipeptide linker[111]. The same payload-cross-linker combination was used in a collaborative effort between Seattle Genetics and Genentech. This work yielded Polatuzumab vedotin (Polivy), an ADC targeted against the CD79b receptor for the treatment of refractory diffuse large B-cell lymphoma. Conjugation was again achieved via maleimide-thiol chemistry. However, site-specific

conjugation via Genentech's THIOMAB technology was used[112]. Trastuzumab emtansine (Kadcyla), another product of Genentech, is targeted against the HER2 receptor, which is overexpressed in breast cancer. The payload, a tubulin binding maytansine derivative known as DM1, is conjugated non-specifically to lysine residues via a non-cleavable SMCC cross-linker. Therefore, lysosomal degradation must digest the entire antibody carrier to release the active, lysine conjugated DM1[113]. Finally, Inotuzumab ozogamicin (Bespona) and Gemtuzumab ozogamicin (Mylotarg), products of Pfizer, are targeted against the CD22 and CD33 receptors respectively. Their payload, a derivative of calicheamicin, binds and cuts double stranded DNA. Attachment is achieved through non-specific conjugation to lysine residues via a 4-(4'-acetylphenoxy) butanoic acid linker. The payload is linked to the antibody via two stimuli responsive chemistries, a reduction-sensitive disulfide bond and a hydrolysis-sensitive hydrazone bond[114,115].

The success of these five ADCs targeted against five different receptor proteins illustrates the broad utility of this concept. A variety of receptor pathways possess the correct balance of high receptor expression, fast internalization rate, and efficient intracellular release to support viable ADCs. Of these ADCs only one, Polivy, utilizes a site-specific conjugation chemistry. This indicates that precise control over the site of conjugation is not required for a successful ADC. However, site-specific conjugation, which has been shown to improve the properties of pre-clinical ADCs[62-65], is a relatively new technique. Therefore, it may take some time to determine the full scope of its application to ADC design. The only ADC that does not contain a stimuli responsive chemistry is Kadcyla. This highlights the importance of such groups in ADC design. A payload such as MMAE is known to require release in a free form to bind its target[116]. Interestingly, the calicheamicin payload of Bespona and Mylotarg contains two stimuli

responsive chemistries. Originally, these ADCs were designed such that intracellular reducing agents such as glutathione would release the active cargo. However, it was found that a hydrazone linkage in place of a stable amide bond increased potency[117]. This not only highlights the importance of cleavable chemistry in ADC design, but also underscores the importance of studying the intracellular trafficking and processing of ADC payloads. Some recent work has sought to address this deficiency in the literature[118]. Finally, none of the FDA approved ADCs contains more than approximately four drug molecules per antibody. This limit is a result of biophysical properties of ADCs and their cargo as discussed below.

Cargo Hydrophobicity

Direction of Flux — Surface Area (A) — Concentration Gradient (ΔC)

X

Partition Coefficient (K) — Diffusion Coefficient (D)

$$\text{Diffusion Rate} \longrightarrow \frac{dn}{dt} = A \frac{KD}{X} \Delta C$$
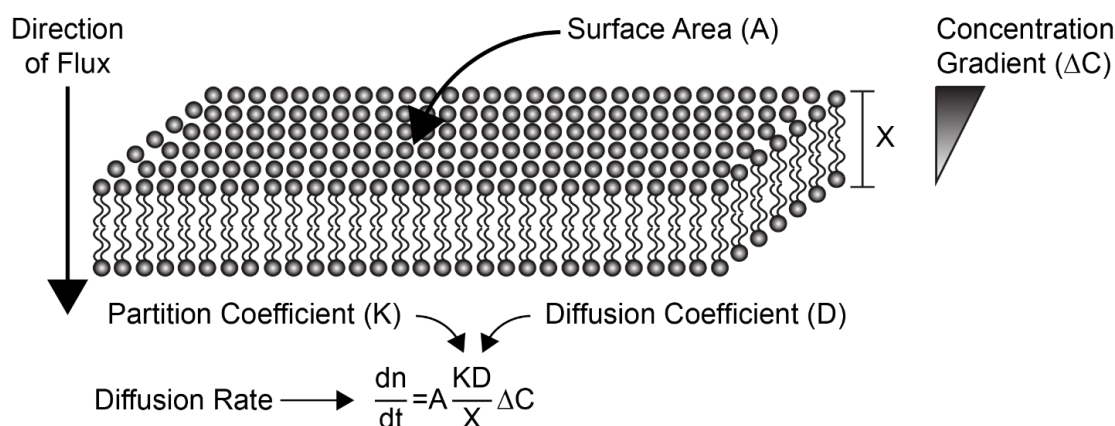
Figure 1.16. Physical description of lipid bilayer permeability of hydrophobic cargo molecules. The diffusion rate is directly proportional to the surface area of the membrane as well as the concentration gradient, partition coefficient, and diffusion coefficient of the cargo molecule. The diffusion rate is inversely proportional to the thickness of the lipid bilayer.

Upon release from the carrier protein inside the endocytic vesicle, the cytotoxic payload must cross the endosomal membrane to reach its intended target. This process can be described by Fick's first law of diffusion (**Figure 1.16**). In sort, payload is driven across the endosomal membrane by two key parameters, the concentration gradient between the endosomal and cytosolic compartments and the partition

coefficient of the payload. The endosomal concentration of drug is determined by the rate of drug release by either lysosomal antibody degradation or cleavage due to specific endosomal stimuli. Meanwhile, the partition coefficient is an intrinsic property of the drug payload. To efficiently cross the endosomal membrane, an ADC payload much have a degree of lipophilic character[119,120]. However, in ADC design, lipophilicity is also a liability. Upon chemical conjugation to the antibody, hydrophobic drugs change the biophysical properties of the carrier protein. These changes can destabilize the tertiary structure of ADCs, leading aggregation[121,122]. Further, studies have shown that ADC hydrophobicity decreases circulation half-life by increasing liver accumulation and subsequent premature clearance[123,124]. Therefore, drug hydrophobicity and degree of drug loading must be balanced to optimize the performance of ADCs. It has been shown that there is an inverse relationship between drug loading and efficacy when the drug to antibody ratio (DAR) is greater than approximately four[125]. This limits the number of drugs that can be conjugated per antibody and ultimately limits the potency of ADCs.

To address this problem, researchers at both Catalent Biologics[64] and Genentech[65] have adapted their respective site-specific conjugation strategies for unbiased screening and identification of stable conjugation sites. These techniques enable the identification of non-intuitive conjugation sites and may help identify the structural features of antibodies that mitigate aggregation. Additionally, researcher at Seattle Genetics have pioneered an approach in which the hydrophobicity of the conjugated payload is masked by modifying the chemical cross-linker with polyethylene glycol (PEG) chains[72,126]. This work has identified both the placement and length of PEG chains as tunable features to increase the circulation half-life and efficacy of ADCs.

1.7 – Antibody-RNA Conjugates for the Delivery of siRNA
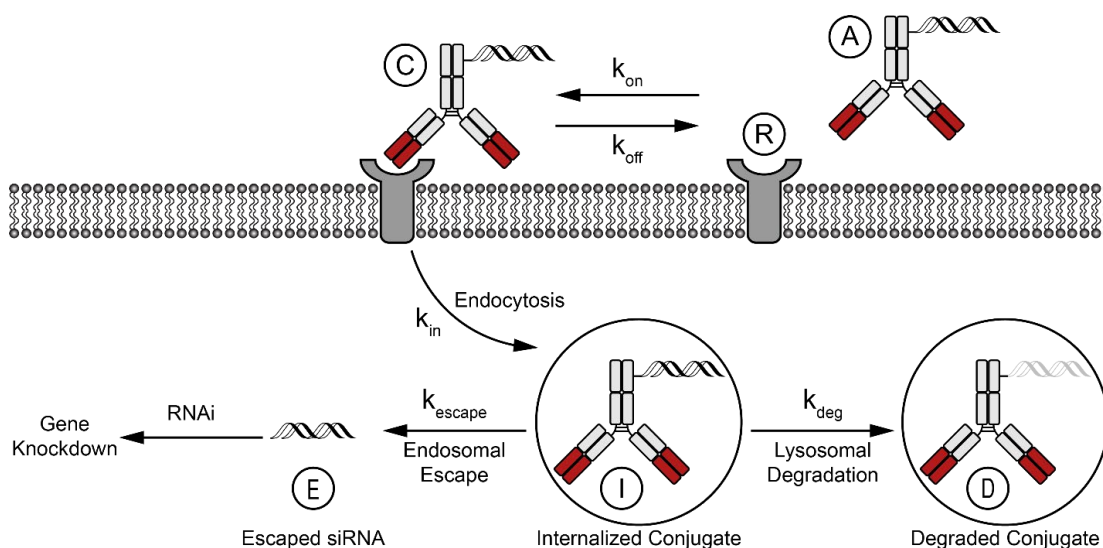
Figure 1.17. Mechanism of intracellular antibody-siRNA conjugate (ARC) processing. Circulating ARC (A) binds to the target receptor (R). The ARC-receptor complex (C) is taken up by the target cell via endocytosis. The internalized ARC (I) is trapped within the endocytic vesicle. The trapped ARC must undergo endosomal escape to facilitate delivery of functional siRNA (E) into the cytosol where it can initiate RNA interference (RNAi). ARC that does not escape the endosome is degraded in the lysosome yielding a nonfunctional conjugate (D).

Nucleic acid-based therapeutics such as short interfering RNA (siRNA) have the potential to fundamentally alter disease treatment by selectively[127] and reversibly[128] degrading otherwise undruggable protein targets[129]. However, due to their large size and highly negative charge, siRNAs cannot passively diffuse across the mammalian cell membrane. To deliver siRNA, researchers have relied primarily on nanoparticle encapsulation[130-135]. A limitation of these approaches is the propensity of nanoparticles to accumulate in the liver[136]. This necessitates the development of siRNA carriers capable of targeting organs other than the liver. Due to their ability to target specific tissues, antibody-based carriers have the potential to achieve extra-hepatic delivery[22,137,138].

Upon binding to its target receptor (**Figure 1.17**), an antibody-siRNA conjugate (ARC) is internalized via endocytosis. Upon endocytosis, the ARC is sequestered

inside of an endosome, a lipid bilayer-bound vesicle. During lysosomal maturation, nucleases are shuttled into the endosome to degrade exogenous nucleic acids. An effective ARC must facilitate escape from the endosome before lysosomal degradation. However, antibodies do not possess a natural mechanism to initiate endosomal escape[139]. Efforts have been made to incorporate active release mechanisms into ARCs[140-142]. Meanwhile, other reports indicate that an ARC can function without an active release mechanism[67,143]. These conflicting reports highlight a fundament deficit in the understanding of intracellular ARC processing. To date, there exists no technique capable of visualizing and quantifying ARC processing in a modular and high-throughput fashion[33,144-146]. Developing such a system would deepen our knowledge of intracellular ARC processing and accelerate the development of bioconjugate-based delivery of siRNA.

1.8 – Conclusion

Bioconjugates are a staple of molecular biology and pharmaceuticals. However, many bioconjugates are still made using heterogeneous conjugation strategies and monofunctional designs. That is, they function by attaching a single reporter molecule, chemical handle, cargo, or ligand to a biomolecule of interest. Comparatively few studies have sought to combine multiple functionalities into a single bioconjugate. Integrating multiple functionalities and/or stimuli-responsive units holds the potential to enhance the function of existing bioconjugates, enable new tools for molecular biology, and open the door to new therapeutic platforms. Herein, we present a survey of our work towards designing multifunctional bioconjugates to expand the toolbox for site-specific antibody modification, improve the stability of antibody-drug conjugates, characterize the surface of extracellular vesicles, and quantify the cytosolic delivery of nucleic acid therapeutics.

Chapter 1 References

1.Höglinger, D. *et al.* Trifunctional lipid probes for comprehensive studies of single lipid species in living cells. *Proc Natl Acad Sci USA* **114,** 1566–1571 (2017).

2.Hendrickson, H. S., Hendrickson, E. K., Johnson, I. D. & Farber, S. A. Intramolecularly quenched BODIPY-labeled phospholipid analogs in phospholipase A(2) and platelet-activating factor acetylhydrolase assays and in vivo fluorescence imaging. *Anal Biochem* **276,** 27–35 (1999).

3.Robinson, P. V., de Almeida-Escobedo, G., de Groot, A. E., McKechnie, J. L. & Bertozzi, C. R. Live-Cell Labeling of Specific Protein Glycoforms by Proximity-Enhanced Bioorthogonal Ligation. *J Am Chem Soc* **137,** 10452–10455 (2015).

4.Tang, F., Wang, L.-X. & Huang, W. Chemoenzymatic synthesis of glycoengineered IgG antibodies and glycosite-specific antibody-drug conjugates. *Nature protocols* **12,** 1702–1721 (2017).

5.Maruani, A. *et al.* A plug-and-play approach to antibody-based therapeutics via a chemoselective dual click strategy. *Nat Commun* **6,** 6645 (2015).

6.Gokarn, Y. R., McLean, M. & Laue, T. M. Effect of PEGylation on protein hydrodynamics. *Molecular pharmaceutics* **9,** 762 (2012).

7.Matsuda, S. *et al.* siRNA conjugates carrying sequentially assembled trivalent N-acetylgalactosamine linked through nucleosides elicit robust gene silencing in vivo in hepatocytes. *ACS Chemical Biology* **10,** 1181–1187 (2015).

8.Meade, B. R. *et al.* Efficient delivery of RNAi prodrugs containing reversible charge-neutralizing phosphotriester backbone modifications. *Nat Biotechnol* **32,** 1256–1261 (2014).

9.Kazane, S. A. *et al.* Site-specific DNA-antibody conjugates for specific and sensitive immuno-PCR. *Proc Natl Acad Sci USA* **109,** 3731–3736 (2012).

10. Tillberg, P. W. *et al.* Protein-retention expansion microscopy of cells and tissues labeled using standard fluorescent proteins and antibodies. *Nat Biotechnol* **34,** 987–992 (2016).

11. Han, H.-S. *et al.* Quantum dot/antibody conjugates for in vivo cytometric imaging in mice. *Proc Natl Acad Sci USA* **112,** 1350–1355 (2015).

12. Vandesquille, M. *et al.* Chemically-defined camelid antibody bioconjugate for the magnetic resonance imaging of Alzheimer's disease. *MAbs* **9,** 1016–1027 (2017).

13. Badu-Tawiah, A. K. *et al.* Polymerization-based signal amplification for paper-based immunoassays. *Lab Chip* **15,** 655–659 (2014).

14. Lee, K. H. & Zeng, H. Aptamer-Based ELISA Assay for Highly Specific and Sensitive Detection of Zika NS1 Protein. *Anal Chem* **89,** 12743–12748 (2017).

15. Beck, A., Goetsch, L., Dumontet, C. & Corvaïa, N. Strategies and challenges for the next generation of antibody-drug conjugates. *Nat Rev Drug Discov* **16,** 315–337 (2017).

16. Springer, A. D. & Dowdy, S. F. GalNAc-siRNA Conjugates: Leading the Way for Delivery of RNAi Therapeutics. *Nucleic Acid Ther* **28,** 109–118 (2018).

17. Groves, M. A. T. & Osbourn, J. K. Applications of ribosome display to antibody drug discovery. *Expert Opin Biol Ther* **5,** 125–135 (2005).

18. Kretzschmar, T. & Rüden, von, T. Antibody discovery: phage display. *Curr Opin Biotechnol* **13,** 598–602 (2002).

19. Feldhaus, M. J. & Siegel, R. W. Yeast display of antibody fragments: a discovery and characterization platform. *J Immunol Methods* **290,** 69–80 (2004).

20. Safdari, Y., Farajnia, S., Asgharzadeh, M. & Khalili, M. Antibody humanization methods - a review and update. *Biotechnol Genet Eng Rev* **29,** 175–186 (2013).

21.Casi, G. & Neri, D. Antibody-drug conjugates: basic concepts, examples and future perspectives. *Journal of controlled release : official journal of the Controlled Release Society* **161,** 422–428 (2012).

22.Hughes, B. Antibody-drug conjugates for cancer: poised to deliver? *Nat Rev Drug Discov* **9,** 665–667 (2010).

23.Berman, J. W. & Basch, R. S. Amplification of the biotin-avidin immunofluorescence technique. *J Immunol Methods* **36,** 335 (1980).

24.Bargh, J. D., Isidro-Llobet, A., Parker, J. S. & Spring, D. R. Cleavable linkers in antibody-drug conjugates. *Chemical Society Reviews* (2019). doi:10.1039/c8cs00676h

25.Bebenek, K. & Kunkel, T. A. Functions of DNA polymerases. *Adv Protein Chem* **69,** 137–165 (2004).

26.Sivakova, S. & Rowan, S. J. Nucleobases as supramolecular motifs. *Org Biomol Chem* **34,** 9–21 (2004).

27.Ceze, L., Nivala, J. & Strauss, K. Molecular digital data storage using DNA. *Nat Rev Genet* (2019). doi:10.1038/s41576-019-0125-3

28.Hubbard, R. E. Hydrogen Bonds in Proteins: Role and Strength. *Encyclopedia of Life Sciences* **10,** 58 (2001).

29.Lodish, H., Darnell, J. E., Berk, A., Kaiser, C. A. & Krieger, M. *Molecular cell biology.* (2008).

30.Jones, M. W. *et al.* Direct peptide bioconjugation/PEGylation at tyrosine with linear and branched polymeric diazonium salts. *J Am Chem Soc* **134,** 7406–7413 (2012).

31.Joshi, N. S., Whitaker, L. R. & Francis, M. B. A three-component Mannich-type reaction for selective tyrosine bioconjugation. *J Am Chem Soc* **126,** 15942–15943 (2004).

32. Hornick, N. I. *et al.* AML suppresses hematopoiesis by releasing exosomes that contain microRNAs targeting c-MYB. *Science …* **9,** ra88 (2016).

33. Gilleron, J. *et al.* Image-based analysis of lipid nanoparticle-mediated siRNA delivery, intracellular trafficking and endosomal escape. *Nat Biotechnol* **31,** 638–646 (2013).

34. Gunnoo, S. B. & Madder, A. Chemical Protein Modification through Cysteine. *Chembiochem* **17,** 529–553 (2016).

35. Agarwal, P. & Bertozzi, C. R. Site-specific antibody-drug conjugates: the nexus of bioorthogonal chemistry, protein engineering, and drug development. *Bioconjugate Chemistry* **26,** 176–192 (2015).

36. Sletten, E. M. & Bertozzi, C. R. From mechanism to mouse: a tale of two bioorthogonal reactions. *Acc Chem Res* **44,** 666–676 (2011).

37. Sletten, E. M. & Bertozzi, C. R. Bioorthogonal chemistry: fishing for selectivity in a sea of functionality. *Angew Chem Int Ed Engl* **48,** 6974–6998 (2009).

38. Baskin, J. M. *et al.* Copper-free click chemistry for dynamic in vivo imaging. *Proc Natl Acad Sci USA* **104,** 16793–16797 (2007).

39. Agarwal, P., van der Weijden, J., Sletten, E. M., Rabuka, D. & Bertozzi, C. R. A Pictet-Spengler ligation for protein chemical modification. *Proc Natl Acad Sci USA* **110,** 46–51 (2012).

40. Lewis, W. G. *et al.* Click chemistry in situ: acetylcholinesterase as a reaction vessel for the selective assembly of a femtomolar inhibitor from an array of building blocks. *Angew Chem Int Ed Engl* **41,** 1053–1057 (2002).

41. Nag, A. *et al.* A chemical epitope-targeting strategy for protein capture agents: the serine 474 epitope of the kinase Akt2. *Angew Chem Int Ed Engl* **52,** 13975–13979 (2013).

42. Pickens, C. J., Johnson, S. N., Pressnall, M. M., Leon, M. A. & Berkland, C. J. Practical Considerations, Challenges, and Limitations of Bioconjugation via Azide-Alkyne Cycloaddition. *Bioconjugate Chemistry* **29,** 686–701 (2018).

43. Knall, A.-C. & Slugovc, C. Inverse electron demand Diels-Alder (iEDDA)-initiated conjugation: a (high) potential click chemistry scheme. *Chemical Society Reviews* **42,** 5131–5142 (2013).

44. Hein, J. E. & Fokin, V. V. Copper-catalyzed azide-alkyne cycloaddition (CuAAC) and beyond: new reactivity of copper(I) acetylides. *Chemical Society Reviews* **39,** 1302–1315 (2010).

45. Das, S. *et al.* A General Synthetic Approach for Designing Epitope Targeted Macrocyclic Peptide Ligands. *Angew Chem Int Ed Engl* **54,** 13219–13224 (2015).

46. Dommerholt, J., Rutjes, F. P. J. T. & van Delft, F. L. Strain-Promoted 1,3-Dipolar Cycloaddition of Cycloalkynes and Organic Azides. *Top Curr Chem (Cham)* **374,** 16 (2016).

47. Steflova, J. *et al.* Investigation of Strain-Promoted Azide-Alkyne Cycloadditions in Aqueous Solutions by Capillary Electrophoresis. *J Org Chem* **83,** 604–613 (2018).

48. Davis, D. L. *et al.* Effect of Buffer Conditions and Organic Cosolvents on the Rate of Strain-Promoted Azide-Alkyne Cycloaddition. *J Org Chem* **81,** 6816–6819 (2016).

49. Mohan, S., Kerry, P. S., Bance, N., Niikura, M. & Pinto, B. M. Serendipitous discovery of a potent influenza virus a neuraminidase inhibitor. *Angew Chem Int Ed Engl* **53,** 1076–1080 (2013).

50. Karver, M. R., Weissleder, R. & Hilderbrand, S. A. Bioorthogonal reaction pairs enable simultaneous, selective, multi-target imaging. *Angew Chem Int Ed Engl* **51,** 920–922 (2011).

51. Yang, J., Šečkutė, J., Cole, C. M. & Devaraj, N. K. Live-cell imaging of cyclopropene tags with fluorogenic tetrazine cycloadditions. *Angew Chem Int Ed Engl* **51,** 7476–7479 (2012).

52. Blackman, M. L., Royzen, M. & Fox, J. M. Tetrazine ligation: fast bioconjugation based on inverse-electron-demand Diels-Alder reactivity. *J Am Chem Soc* **130,** 13518–13519 (2008).

53. Devaraj, N. K., Weissleder, R. & Hilderbrand, S. A. Tetrazine-based cycloadditions: application to pretargeted live cell imaging. *Bioconjugate Chemistry* **19,** 2297–2299 (2008).

54. Schoch, J., Staudt, M., Samanta, A., Wiessler, M. & Jäschke, A. Site-specific one-pot dual labeling of DNA by orthogonal cycloaddition chemistry. *Bioconjugate Chemistry* **23,** 1382–1386 (2012).

55. Wu, H. & Devaraj, N. K. Advances in Tetrazine Bioorthogonal Chemistry Driven by the Synthesis of Novel Tetrazines and Dienophiles. *Acc Chem Res* **51,** 1249–1259 (2018).

56. Umlauf, B. J., Mix, K. A., Grosskopf, V. A., Raines, R. T. & Shusta, E. V. Site-Specific Antibody Functionalization Using Tetrazine-Styrene Cycloaddition. *Bioconjugate Chemistry* **29,** 1605–1613 (2018).

57. Pancer, Z. & Cooper, M. D. The evolution of adaptive immunity. *annualreviewsorg* (2006).

58. Lyon, R. P. *et al.* Self-hydrolyzing maleimides improve the stability and pharmacological properties of antibody-drug conjugates. *Nat Biotechnol* **32,** 1059–1062 (2014).

59. Carter, P. J. Potent antibody therapeutics by design. *Nature Reviews Immunology* **6,** 343–357 (2006).

60. Abdel-Magid, A. F., Carson, K. G., Harris, B. D., Maryanoff, C. A. & Shah, R. D. Reductive Amination of Aldehydes and Ketones with Sodium Triacetoxyborohydride. Studies on Direct and Indirect Reductive Amination Procedures(1). *J Org Chem* **61,** 3849–3862 (1996).

61. Adumeau, P. *et al.* Site-Specifically Labeled Antibody-Drug Conjugate for Simultaneous Therapy and ImmunoPET. *Molecular pharmaceutics* **15,** 892–898 (2018).

62. Strop, P. *et al.* Location matters: site of conjugation modulates stability and pharmacokinetics of antibody drug conjugates. *Chem Biol* **20,** 161–167 (2013).

63. Drake, P. M. *et al.* Aldehyde tag coupled with HIPS chemistry enables the production of ADCs conjugated site-specifically to different antibody regions with distinct in vivo efficacy and PK outcomes. *Bioconjugate Chemistry* **25,** 1331–1341 (2014).

64. Huang, B. C. B. *et al.* Antibody-drug conjugate library prepared by scanning insertion of the aldehyde tag into IgG1 constant regions. *MAbs* **10,** 1182–1189 (2018).

65. Ohri, R. *et al.* High-Throughput Cysteine Scanning To Identify Stable Antibody Conjugation Sites for Maleimide- and Disulfide-Based Linkers. *Bioconjugate Chemistry* **29,** 473–485 (2018).

66. Bhakta, S., Raab, H. & Junutula, J. R. Engineering THIOMABs for site-specific conjugation of thiol-reactive linkers. *Methods Mol Biol* **1045,** 189–203 (2013).

67. Cuellar, T. L. *et al.* Systematic evaluation of antibody-mediated siRNA delivery using an industrial platform of THIOMAB-siRNA conjugates. *Nucleic Acids Res* **43,** 1189–1203 (2014).

68. Tian, F. *et al.* A general approach to site-specific antibody drug conjugates. *Proc Natl Acad Sci USA* **111,** 1766–1771 (2014).

69.Axup, J. Y. *et al.* Synthesis of site-specific antibody-drug conjugates using unnatural amino acids. *Proc Natl Acad Sci USA* **109,** 16101–16106 (2012).

70.Harmand, T. J. *et al.* One-Pot Dual Labeling of IgG 1 and Preparation of C-to-C Fusion Proteins Through a Combination of Sortase A and Butelase 1. *Bioconjugate Chemistry* **29,** 3245–3249 (2018).

71.Rabuka, D. Chemoenzymatic methods for site-specific protein modification. *Curr Opin Chem Biol* **14,** 790–796 (2010).

72.Lyon, R. P. *et al.* Reducing hydrophobicity of homogeneous antibody-drug conjugates improves pharmacokinetics and therapeutic index. *Nat Biotechnol* **33,** 733–735 (2015).

73.Nunes, J. P. M. *et al.* Functional native disulfide bridging enables delivery of a potent, stable and targeted antibody-drug conjugate (ADC). *Chem Commun (Camb)* **51,** 10624–10627 (2015).

74.Badescu, G. *et al.* Bridging disulfides for stable and defined antibody drug conjugates. *Bioconjugate Chemistry* **25,** 1124–1136 (2014).

75.Zhou, Q. *et al.* Site-specific antibody-drug conjugation through glycoengineering. *Bioconjugate Chemistry* **25,** 510–520 (2014).

76.Anami, Y. *et al.* Enzymatic conjugation using branched linkers for constructing homogeneous antibody-drug conjugates with high potency. *Org Biomol Chem* **15,** 5635–5642 (2017).

77.Dennler, P. *et al.* Transglutaminase-based chemo-enzymatic conjugation approach yields homogeneous antibody-drug conjugates. *Bioconjugate Chemistry* **25,** 569–578 (2014).

78.Jeger, S. *et al.* Site-specific and stoichiometric modification of antibodies by bacterial transglutaminase. *Angew Chem Int Ed Engl* **49,** 9995–9997 (2010).

79. Ponte, J. F. *et al.* Understanding How the Stability of the Thiol-Maleimide Linkage Impacts the Pharmacokinetics of Lysine-Linked Antibody-Maytansinoid Conjugates. *Bioconjugate Chemistry* **27,** 1588–1598 (2016).

80. Junutula, J. R. *et al.* Rapid identification of reactive cysteine residues for site-specific labeling of antibody-Fabs. *J Immunol Methods* **332,** 41–52 (2008).

81. Junutula, J. R. *et al.* Site-specific conjugation of a cytotoxic drug to an antibody improves the therapeutic index. *Nat Biotechnol* **26,** 925–932 (2008).

82. Strop, P. Versatility of microbial transglutaminase. *Bioconjugate Chemistry* **25,** 855–862 (2014).

83. Rachel, N. M. & Pelletier, J. N. Biotechnological applications of transglutaminases. *Biomolecules* **3,** 870–888 (2013).

84. Farias, S. E. *et al.* Mass spectrometric characterization of transglutaminase based site-specific antibody-drug conjugates. *Bioconjugate Chemistry* **25,** 240–250 (2014).

85. Anami, Y. *et al.* Glutamic acid-valine-citrulline linkers ensure stability and efficacy of antibody-drug conjugates in mice. *Nat Commun* **9,** 2512 (2018).

86. Gundersen, M. T., Keillor, J. W. & Pelletier, J. N. Microbial transglutaminase displays broad acyl-acceptor substrate specificity. *Appl Microbiol Biotechnol* **98,** 219–230 (2013).

87. Ebenig, A. *et al.* Efficient Site-Specific Antibody-Drug Conjugation by Engineering of a Nature-Derived Recognition Tag for Microbial Transglutaminase. *Chembiochem* (2019). doi:10.1002/cbic.201900101

88. Rush, J. S. & Bertozzi, C. R. New aldehyde tag sequences identified by screening formylglycine generating enzymes in vitro and in vivo. *J Am Chem Soc* **130,** 12240–12241 (2008).

89. Agarwal, P. *et al.* Hydrazino-Pictet-Spengler ligation as a biocompatible method for the generation of stable protein conjugates. *Bioconjugate Chemistry* **24,** 846–851 (2013).

90. Viault, G. *et al.* The first 'ready-to-use' benzene-based heterotrifunctional cross-linker for multiple bioconjugation. *Org Biomol Chem* **11,** 2693–2705 (2013).

91. Chevalier, A., Hardouin, J., Renard, P.-Y. & Romieu, A. Universal dark quencher based on 'clicked' spectrally distinct azo dyes. *Org Lett* **15,** 6082–6085 (2013).

92. Frei, A. P. *et al.* Direct identification of ligand-receptor interactions on living cells and tissues. *Nat Biotechnol* **30,** 997–1001 (2012).

93. Beal, D. M. *et al.* Click-enabled heterotrifunctional template for sequential bioconjugations. *Org Biomol Chem* **10,** 548–554 (2011).

94. Loiseau, F. A., Hii, K. K. & Hill, A. M. Multigram synthesis of well-defined extended bifunctional polyethylene glycol (PEG) chains. *J Org Chem* **69,** 639–647 (2004).

95. Goswami, L. N., Houston, Z. H., Sarma, S. J., Jalisatgi, S. S. & Hawthorne, M. F. Efficient synthesis of diverse heterobifunctionalized clickable oligo(ethylene glycol) linkers: potential applications in bioconjugation and targeted drug delivery. *Org Biomol Chem* **11,** 1116–1126 (2013).

96. Goodchild, J. Conjugates of oligonucleotides and modified oligonucleotides: a review of their synthesis and properties. *Bioconjugate Chemistry* **1,** 165–187 (1990).

97. Peters, J. P. & Maher, L. J. DNA curvature and flexibility in vitro and in vivo. *Sci Transl Med* **43,** 23–63 (2010).

98. Sil, D., Lee, J. B., Luo, D., Holowka, D. & Baird, B. Trivalent ligands with rigid DNA spacers reveal structural requirements for IgE receptor signaling in RBL mast cells. *ACS Chemical Biology* **2,** 674–684 (2007).

99.Englund, E. A. *et al.* Programmable multivalent display of receptor ligands using peptide nucleic acid nanoscaffolds. *Nat Commun* **3,** 614 (2012).

100.Boozer, C., Ladd, J., Chen, S. & Jiang, S. DNA-directed protein immobilization for simultaneous detection of multiple analytes by surface plasmon resonance biosensor. *Anal Chem* **78,** 1515–1519 (2006).

101.Liang, S. I., McFarland, J. M., Rabuka, D. & Gartner, Z. J. A modular approach for assembling aldehyde-tagged proteins on DNA scaffolds. *J Am Chem Soc* **136,** 10850–10853 (2014).

102.Merrifield, R. B. *Solid phase peptide synthesis. I. The synthesis of a tetrapeptide*. *Journal of the American Chemical Society* (1963). doi:10.1016/b978-1-4832-2819-8.50015-5

103.McCarver, S. J. *et al.* Decarboxylative Peptide Macrocyclization through Photoredox Catalysis. *Angew Chem Int Ed Engl* **56,** 728–732 (2016).

104.Porel, M. & Alabi, C. A. Sequence-defined polymers via orthogonal allylacrylamide building blocks. *J Am Chem Soc* **136,** 13162–13165 (2014).

105.Porel, M., Thornlow, D. N., Phan, N. N. & Alabi, C. A. Sequence-defined bioactive macrocycles via an acid-catalysed cascade reaction. *Nat Chem* **8,** 590–596 (2016).

106.Phan, N. N., Li, C. & Alabi, C. A. Intracellular Delivery via Noncharged Sequence-Defined Cell-Penetrating Oligomers. *Bioconjugate Chemistry* **29,** 2628–2635 (2018).

107.Brown, J. S. *et al.* Synthesis and Solution-Phase Characterization of Sulfonated Oligothioetheramides. *Macromolecules* **50,** 8731–8738 (2017).

108.Sorkin, M. R., Walker, J. A., Brown, J. S. & Alabi, C. A. Versatile Platform for the Synthesis of Orthogonally Cleavable Heteromultifunctional Cross-Linkers. *Bioconjugate Chemistry* **28,** 907–912 (2017).

109. Chabner, B. A. & Roberts, T. G. Chemotherapy and the war on cancer. *Nat Rev Cancer* **5,** 65 (2005).

110. Scott, A. M., Wolchok, J. D. & Old, L. J. Antibody therapy of cancer. *Nat Rev Cancer* **12,** 278–287 (2012).

111. Doronina, S. O. *et al.* Development of potent monoclonal antibody auristatin conjugates for cancer therapy. *Nat Biotechnol* **21,** 778–784 (2003).

112. Dornan, D. *et al.* Therapeutic potential of an anti-CD79b antibody-drug conjugate, anti-CD79b-vc-MMAE, for the treatment of non-Hodgkin lymphoma. *Blood* **114,** 2721–2729 (2009).

113. Peddi, P. F. & Hurvitz, S. A. Trastuzumab emtansine: the first targeted chemotherapy for treatment of breast cancer. *Future Oncol* **9,** 319–326 (2013).

114. Shor, B., Gerber, H.-P. & Sapra, P. Preclinical and clinical development of inotuzumab-ozogamicin in hematological malignancies. *J Control Release* **67,** 107–116 (2014).

115. Baron, J. & Wang, E. S. Gemtuzumab ozogamicin for the treatment of acute myeloid leukemia. *Expert Rev Clin Pharmacol* **11,** 549–559 (2018).

116. McCombs, J. R. & Owen, S. C. Antibody drug conjugates: design and selection of linker, payload and conjugation chemistry. *AAPS J* **17,** 339–351 (2015).

117. Hamann, P. R. *et al.* Gemtuzumab ozogamicin, a potent and selective anti-CD33 antibody-calicheamicin conjugate for treatment of acute myeloid leukemia. *Bioconjugate Chemistry* **13,** 47–58 (2002).

118. Lee, B.-C. *et al.* FRET Reagent Reveals the Intracellular Processing of Peptide-Linked Antibody-Drug Conjugates. *Bioconjugate Chemistry* **29,** 2468–2477 (2018).

119. Menichetti, R., Kanekal, K. H. & Bereau, T. Drug-Membrane Permeability across Chemical Space. *ACS Cent Sci* **5,** 290–298 (2019).

120. Hansch, C., Steward, A. R., Anderson, S. M. & Bentley, D. L. Parabolic dependence of drug action upon lipophilic character as revealed by a study of hypnotics. *J Med Chem* **11,** 1 (1968).

121. Beckley, N. S., Lazzareschi, K. P., Chih, H.-W., Sharma, V. K. & Flores, H. L. Investigation into temperature-induced aggregation of an antibody drug conjugate. *Bioconjugate Chemistry* **24,** 1674–1683 (2013).

122. Buecheler, J. W., Winzer, M., Tonillo, J., Weber, C. & Gieseler, H. Impact of Payload Hydrophobicity on the Stability of Antibody-Drug Conjugates. *Molecular pharmaceutics* **15,** 2656–2664 (2018).

123. Strop, P. *et al.* Site-specific conjugation improves therapeutic index of antibody drug conjugates with high drug loading. *Nat Biotechnol* **33,** 694–696 (2015).

124. Sun, X. *et al.* Effects of Drug-Antibody Ratio on Pharmacokinetics, Biodistribution, Efficacy, and Tolerability of Antibody-Maytansinoid Conjugates. *Bioconjugate Chemistry* **28,** 1371–1381 (2017).

125. Hamblett, K. J. *et al.* Effects of drug loading on the antitumor activity of a monoclonal antibody drug conjugate. *Clin Cancer Res* **10,** 7063–7070 (2004).

126. Burke, P. J. *et al.* Optimization of a PEGylated Glucuronide-Monomethylauristatin E Linker for Antibody-Drug Conjugates. *Mol Cancer Ther* **16,** 116–123 (2016).

127. Janas, M. M. *et al.* Selection of GalNAc-conjugated siRNAs with limited off-target-driven rat hepatotoxicity. *Nat Commun* **9,** 723 (2018).

128. Zlatev, I. *et al.* Reversal of siRNA-mediated gene silencing in vivo. *Nat Biotechnol* **36,** 509–511 (2018).

129. Scherman, D., Rousseau, A., Bigey, P. & Escriou, V. Genetic pharmacology: progresses in siRNA delivery and therapeutic applications. *Gene Ther* **24,** 151–156 (2017).

130.Jayaraman, M. *et al.* Maximizing the potency of siRNA lipid nanoparticles for hepatic gene silencing in vivo. *Angew Chem Int Ed Engl* **51,** 8529–8533 (2012).

131.Semple, S. C. *et al.* Rational design of cationic lipids for siRNA delivery. *Nat Biotechnol* **28,** 172–176 (2010).

132.Whitehead, K. A., Langer, R. & Anderson, D. G. Knocking down barriers: advances in siRNA delivery. *Nat Rev Drug Discov* **8,** 129–138 (2009).

133.Alabi, C. A. *et al.* Multiparametric approach for the evaluation of lipid nanoparticles for siRNA delivery. *Proc Natl Acad Sci USA* **110,** 12881–12886 (2013).

134.Kumar, V. *et al.* Shielding of Lipid Nanoparticles for siRNA Delivery: Impact on Physicochemical Properties, Cytokine Induction, and Efficacy. *Molecular Therapy— …* **3,** e210 (2014).

135.Ball, R. L., Hajj, K. A., Vizelman, J., Bajaj, P. & Whitehead, K. A. Lipid Nanoparticle Formulations for Enhanced Co-delivery of siRNA and mRNA. *Nano Lett* **18,** 3814–3822 (2018).

136.Zhang, Y.-N., Poon, W., Tavares, A. J., McGilvray, I. D. & Chan, W. C. W. Nanoparticle-liver interactions: Cellular uptake and hepatobiliary elimination. *Journal of controlled release : official journal of the Controlled Release Society* **240,** 332–348 (2016).

137.Sievers, E. L. & Senter, P. D. Antibody-drug conjugates in cancer therapy. *Annu Rev Med* **64,** 15–29 (2012).

138.van Buggenum, J. A. G. L. *et al.* A covalent and cleavable antibody-DNA conjugation strategy for sensitive protein detection via immuno-PCR. *Scientific reports* **6,** 22675 (2016).

139.Varkouhi, A. K., Scholte, M., Storm, G. & Haisma, H. J. Endosomal escape pathways for delivery of biologicals. *Journal of controlled release : official journal of the Controlled Release Society* **151,** 220–228 (2010).

140.Ma, Y. *et al.* Humanized Lewis-Y specific antibody based delivery of STAT3 siRNA. *ACS Chemical Biology* **6,** 962–970 (2011).

141.Bäumer, N. *et al.* Antibody-coupled siRNA as an efficient method for in vivo mRNA knockdown. *Nature protocols* **11,** 22–36 (2015).

142.Song, E. *et al.* Antibody mediated in vivo delivery of small interfering RNAs via cell-surface receptors. *Nat Biotechnol* **23,** 709–717 (2005).

143.Sugo, T. *et al.* Development of antibody-siRNA conjugate targeted to cardiac and skeletal muscles. *Journal of controlled release : official journal of the Controlled Release Society* **237,** 1–13 (2016).

144.Verdurmen, W. P. R., Mazlami, M. & Plückthun, A. A Biotin Ligase-Based Assay for the Quantification of the Cytosolic Delivery of Therapeutic Proteins. *Methods Mol Biol* **1575,** 223–236 (2017).

145.Wittrup, A. *et al.* Visualizing lipid-formulated siRNA release from endosomes and target gene knockdown. *Nat Biotechnol* **33,** 870 (2015).

146.Deyle, K. M. *et al.* A protein-targeting strategy used to develop a selective inhibitor of the E17K point mutation in the PH domain of Akt1. *Nat Chem* **7,** 455–462 (2015).

Chapter 2 – Site-specific Dual "Click" Modification of Native Antibodies via Microbial Transglutaminase

2.1 – Background

Antibodies, the prototypical affinity reagent, are the foundational building block of numerous bioconjugate-based molecular probes[1-3] and *in vivo* imaging agents[4,5] as well as carriers for both small molecule[6-8] and macromolecular therapeutics.[9,10] In recent years, site-specific modification has been identified as a powerful handle to enhance the properties of antibody-based bioconjugates for applications in both immunodetection[11,12] and drug delivery[13-16]. Broadly, site-specific antibody modification can be categorized as utilizing either engineered antibodies (e.g. engineered cysteines[17,18], non-canonical amino acids[19,20], and chemoenzymatically-recognized peptide tags[21,22]) or native antibodies (interchain disulfide conjugation[7,23], disulfide re-bridging[24,25], glycan remodeling[26,27], and microbial transglutaminase[28-30]).

Modification of native antibodies is advantageous as it circumvents the need to manipulate the genetic code. This mitigates the risk of both negative effects on protein folding and function[31,32] and low titers due to the inefficient read-through of non-canonical amino acids[33]. Despite these advantages, native antibody modifications have traditionally been limited to conjugates modified at a single site with a single functional handle.

Recent work has sought to expand the scope of native antibody modifications. Seattle Genetics devised an approach based on interchain disulfide modification that enables the incorporation of two orthogonally protected cysteine residues[34]. With the use of stepwise purification, these cysteine residues can be deprotected and modified via maleimide conjugation chemistry. In another approach, the groups of Chudasama and Caddick employed disulfide re-bridging to install linear alkyne and cyclooctyne

functional handles within a full-length monoclonal antibody[35]. These handles react with an azide functional group under orthogonal reaction conditions. However, stepwise purification is needed to remove excess reagents.

An ideal approach to synthesizing heterobifunctional antibody conjugates would avoid stepwise purification by employing functional handles that are chemically orthogonal. To address this shortcoming, we were inspired by two bioorthogonal "click" chemistries, the strain-promoted azide-alkyne cycloaddition (SPAAC) reaction and the inverse electron demand diels-alder (IEDDA) reaction. With judicious selection of strained alkyne and dienophile, these chemistries are mutually orthogonal[36]. This property has been demonstrated via multicolor labeling of a co-culture of live cells[37].

We reasoned that these complimentary chemistries would enable simultaneous, one-pot synthesis of multifunctional antibody conjugates. To site-specifically incorporate these chemistries, we turned to the bioconjugation enzyme microbial transglutaminase (MTG). MTG belongs to a family of enzymes that catalyze the formation of interprotein isopeptide bonds between glutamine and lysine residues[38,39]. Serendipitously, MTG recognizes glutamine 295 (Q295) within the heavy chain of aglycosylated, human IgGs[40]. Co-treatment with Peptide:N-glycosidase F (PNGase F) removes the N-linked glycan at asparagine 297 (N297) and facilitates efficient bioconjugation[30]. By supplying non-natural acyl acceptor substrates, this natural function has been co-opted for site-specific, homofunctional antibody modification[41,42]. To realize our vision, we sought to design a heterobifunctional, dual "click" substrate for MTG.

2.2 – Results and Discussion
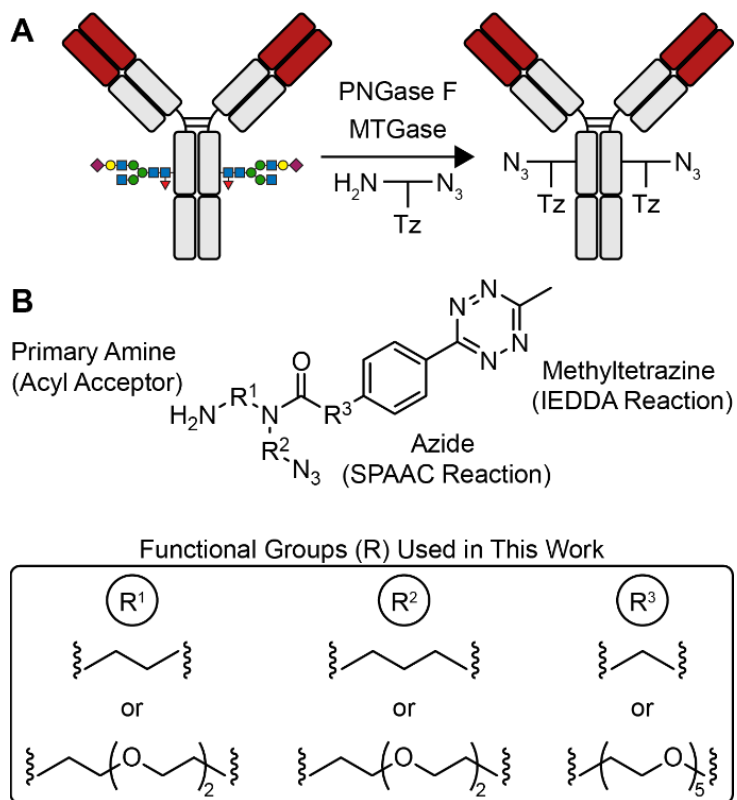
Figure 2.1. Dual "click" modification of native antibodies. A) Overview of site-specific conjugation scheme B) Design of heterobifunctional substrates containing either short, alkyl spacers or long, ethylene oxide-based spacers.

Herein, we report the design, synthesis, and characterization of five heterobifunctional substrates for MTG. These substrates contain two bioorthogonal chemical handles, azide and methyltetrazine (**Figure 2.1**). To the best of our knowledge, this represents the first report of heterobifunctional substrates for MTG.¶To demonstrate the potential for this methodology to yield therapeutically relevant bioconjugates, trastuzumab was selected as a model protein. Trastuzumab, a humanized monoclonal antibody against the Her2 receptor, is employed as the targeting component in a variety of bioconjugates including the FDA approved antibody-drug conjugate Kadcyla[43]. Trastuzumab was purified from the conditioned

media of a stably expressing HEK293F suspension cell line using established protocols[44].
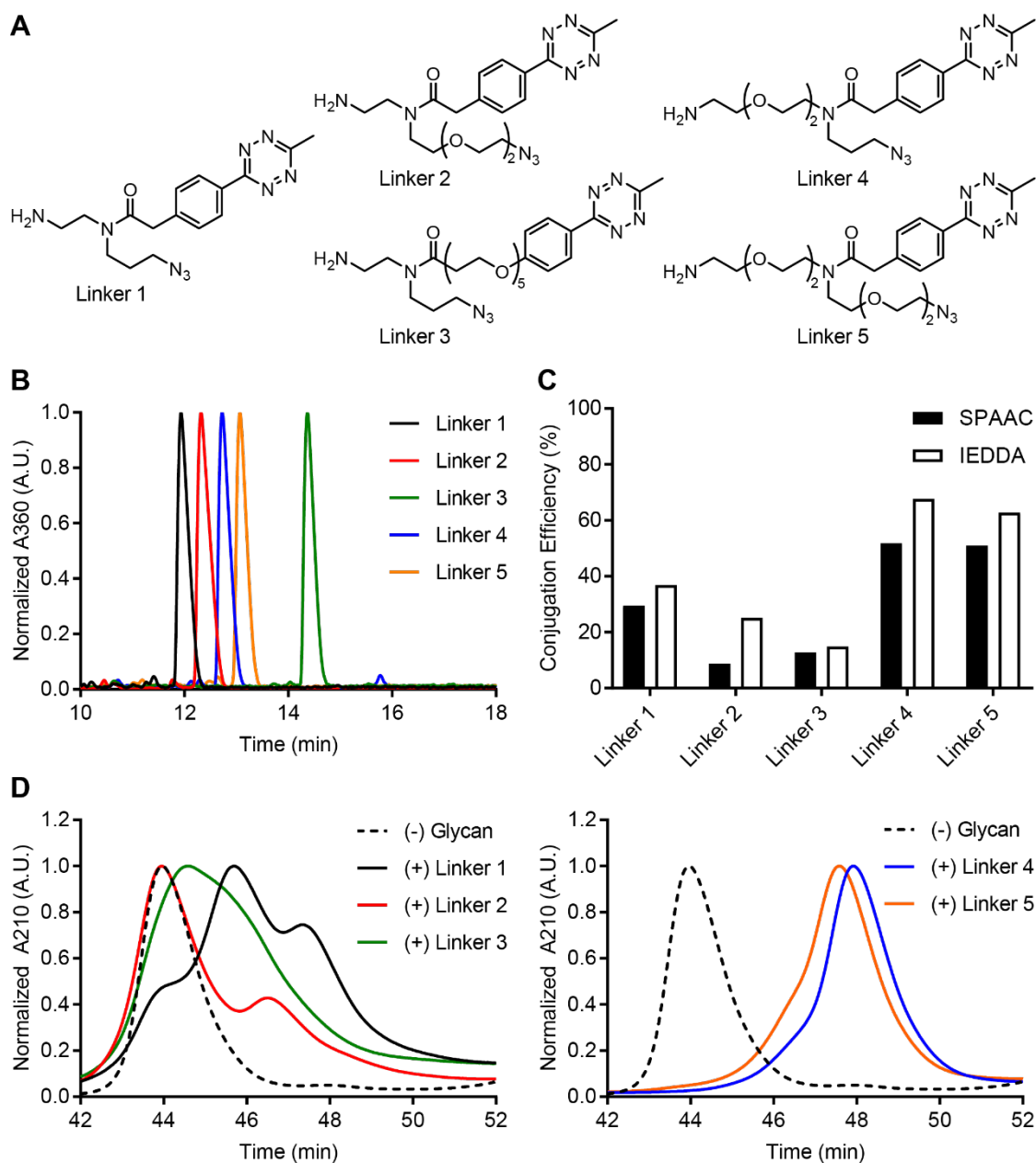
Figure 2.2. Characterization of MTG substrate library. A) Structures of linker 1 – 5. B) Analytical RP-HPLC of purified linkers. C) Quantification of linker conjugation efficiency via molecular weight shift SDS-PAGE assay. D) Analysis of linker conjugation efficiency via hydrophobic shift analyzed via HIC.

To synthesize the heterobifunctional substrates, first, either mono-Boc-protected bisamine or azide-functionalized, amine-bearing starting material was alkylated with

the corresponding alkyl halide. The resulting secondary amine intermediate was reacted with an NHS ester-activated methyltetrazine (mTz) to yield the acylated, tertiary amide product. Liberation of the terminal primary amine conjugation site was achieved by removal of the Boc protecting group via acid treatment. The final substrates (**Figure 2.2A**), henceforth referred to as linkers 1 – 5, were purified via reverse-phase high-performance liquid chromatography (RP-HPLC). All linkers were isolated in high purity and displayed a range of hydrophobicity as measured by analytical RP-HPLC (**Figure 2.2B**).

To elucidate structure-activity relationships for heterobifunctional MTG substrates, linker conjugation efficiency was evaluated in two ways. First, conjugation efficiency was quantified via an indirect SDS-PAGE assay (**Figure 2.2C**). In short, linker-modified trastuzumab, henceforth referred to as conjugates 1 – 5, were analyzed via SDS-PAGE for a molecular weight shift following incubation with a dibenzocyclooctyne (DBCO)- or transcyclooctene (TCO)-functionalized 5,000 g/mol polyethylene glycol (PEG5K) chain. DBCO and TCO functional handles are mutually orthogonal and compatible with the SPAAC and IEDDA "click" reactions, respectively[37]. In agreement with heavy chain-directed modification, each conjugate displayed a molecular weight increase in the 50 kDa band upon addition of DBCO- and TCO-PEG5K. However, the conjugates displayed clear differences in conjugation efficiency. The efficiency of conjugate 1 was quantified to be 29% and 37% for SPAAC and IEDDA reactions, respectively. When the short, two carbon spacer alpha to the primary amine is held constant, increasing the spacer length proximal to the azide and mTz handles decreases the conjugation efficiency. Specifically, the efficiency of conjugate 2 was determined to be 9% (SPAAC) and 25% (IEDDA) while conjugate 3 was found to be 13% (SPAAC) and 15% (IEDDA), respectively. Incorporation of a flexible ethylene oxide spacer alpha to the primary

amine increased the conjugation efficiency for both conjugate 4 (52% and 68%) and conjugate 5 (51% and 63%). Interestingly, with the exception of conjugate 3, there was a consistent difference between the conjugation efficiency as measured by the SPAAC and IEDDA reactions. This may speak to differences in the solvent accessibility of the chemical handles when conjugated to Q295 or the solvent accessibility of the DBCO and TCO functional groups when attached to a 5 kDa PEG chain.

By SDS-PAGE analysis, conjugation with all linkers yielded a heterogeneous antibody conjugate. Given the indirect nature of the SDS-PAGE assay, we sought to complement these results by directly evaluating the conjugation efficiency to linkers 1 – 5 via hydrophobic interaction chromatography (HIC) to remove confounding variables such as SPAAC and IEDDA reaction efficiency (**Figure 2.2D**). While trends remained the same, the HIC results suggest that SDS-PAGE underestimated MTG conjugation efficiency. Specifically, in agreement with SDS-PAGE, conjugates 1 – 3 showed a heterogeneous mixture of products. Each linker 1 – 3 showed a peak which eluted at the same retention time as the control antibody as well as two other peaks. We interpreted peaks eluted at approximately 46 and 48 minutes to corresponds to singly and double conjugated antibodies, respectively. However, conjugates 4 and 5 showed conversion to a single, homogeneous product. This result indicates that a large component of the incomplete conjugation in Figure 2.2C, especially with linker 4 and 5, is due to the SPAAC and IEDDA reactions, and not the MTG conjugation. Furthermore, this result emphasizes the importance of spacer flexibility alpha to the primary amine as both linker 4 and linker 5 served as efficient substrates for MTG.

A multi-miligram scale synthesis of conjugate 5 was performed for futher characterization and functional testing. Conjugate 5 was isolated via HIC and recovered in high purity at an overall yield of 1.1 mg (48%). Successful conjugation

was confirmed via matrix-assisted laser desorption/ioniztion mass spectrometry (MALDI-MS). Treatment of trastutuzmab with PNGase F to remove the N-linked glycan at N297 produced a decrease of approximately 2000 Da in the molecular weight of the heavy chain fragment. Simultaneous treatment with PNGase F, MTG, and linker 5 resulted in a 500 Da increase in the molecular weight of the aglycosylated control, consistent with incorporation of one linker per heavy chain.
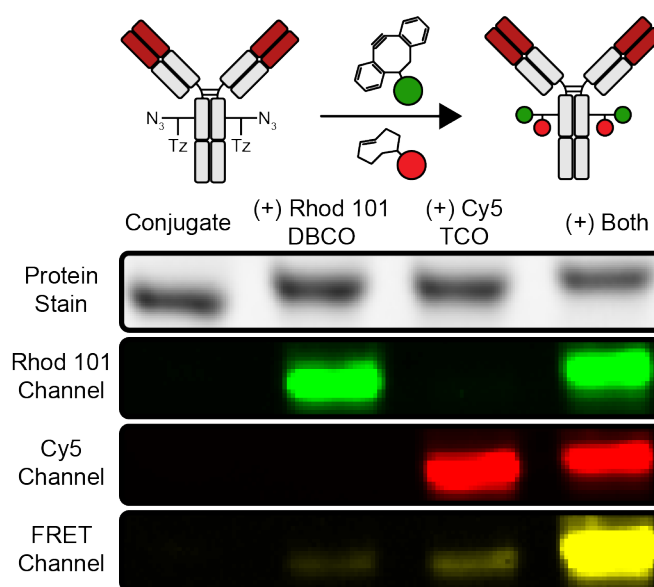

Figure 2.3. Validation of one-pot synthesis of multifunctional antibody conjugates. Fluorescence SDS-PAGE images of conjugate 5 upon treatment with DBCO-modified carboxyrhodamine 101 and/or TCO-modified sulfo-Cy5. Denatured and reduced 4 – 20% SDS-PAGE gel. Coomassie blue protein stain. Carboxyrhodamine 101 excitation: 488 nm, emission: 500 – 540 nm. Sulfo-Cy5 excitation: 633 nm, emission 655 – 685 nm. FRET excitation: 488 nm, emission: 655 – 685 nm.

Dual "click" modification of conjugate 5 was demonstrated via fluorescent SDS-PAGE analysis (**Figure 2.3**). Briefly, conjugate 5 was reacted with a Förster resonance energy transfer (FRET) pair of fluorophores, DBCO-modified carboxyrhodamine 101 and TCO-modified sulfo-Cy5. Upon excitation with 488 nm light, carboxyrhodamine 101 displays a characteristic fluorescence emission at 523 nm. Upon excitation with 633 nm light, sulfo-Cy5 displays a characteristic fluorescence emission at 655 nm. Dual

modification leads to intramolecular energy transfer and subsequent emission at 655 nm (sulfo-Cy5) upon excitation at 488 nm (carboxyrhodamine 101). This data validates that these chemistries (SPAAC and IEDDA) are mutually orthogonal, and therefore enable the one-pot synthesis of multifunctional antibody conjugates.

To further demonstrate the utility of our dual "click" approach, we sought to carry out a one-pot synthesis of a multifunctional antibody-drug conjugate (ADC). ADCs seek to combine the antigen specificity of antibodies with the non-targeted, chemotherapeutic potential of small molecule drugs. This conceptual framework has led to the development of ADCs targeted against a variety of cancer-specific antigens and carrying a wide range of therapeutic payloads. These efforts have led to the FDA approval of four ADCs with many more in the clinical pipeline[43].

Despite their clinical success, ADCs are not without their limitations. As with traditional chemotherapy, ADCs are susceptible to resistance due to tumor heterogeneity and acquired resistance[3,45-49]. Additionally, the inherent hydrophobicity of many chemotherapeutic drugs limits the therapeutic window of ADCs[7,50]. Conjugation of hydrophobic drugs to the solvent-exposed surface of an antibody can cause hydrophobicity-induced aggregation ultimately leading to premature clearance and reduced circulation time. Researchers have leveraged multifunctional antibody conjugates to ameliorate these shortcomings. With an eye towards drug resistance, synergistic ADCs containing two complimentary payloads have been shown to improve efficacy in a drug resistant mouse xenograft model[34]. Further, bifunctional ADCs containing branched, hydrophilic PEG-based side chains have been shown to mitigate the aggregation-inducing effects of high degrees of drug loading[7,50].
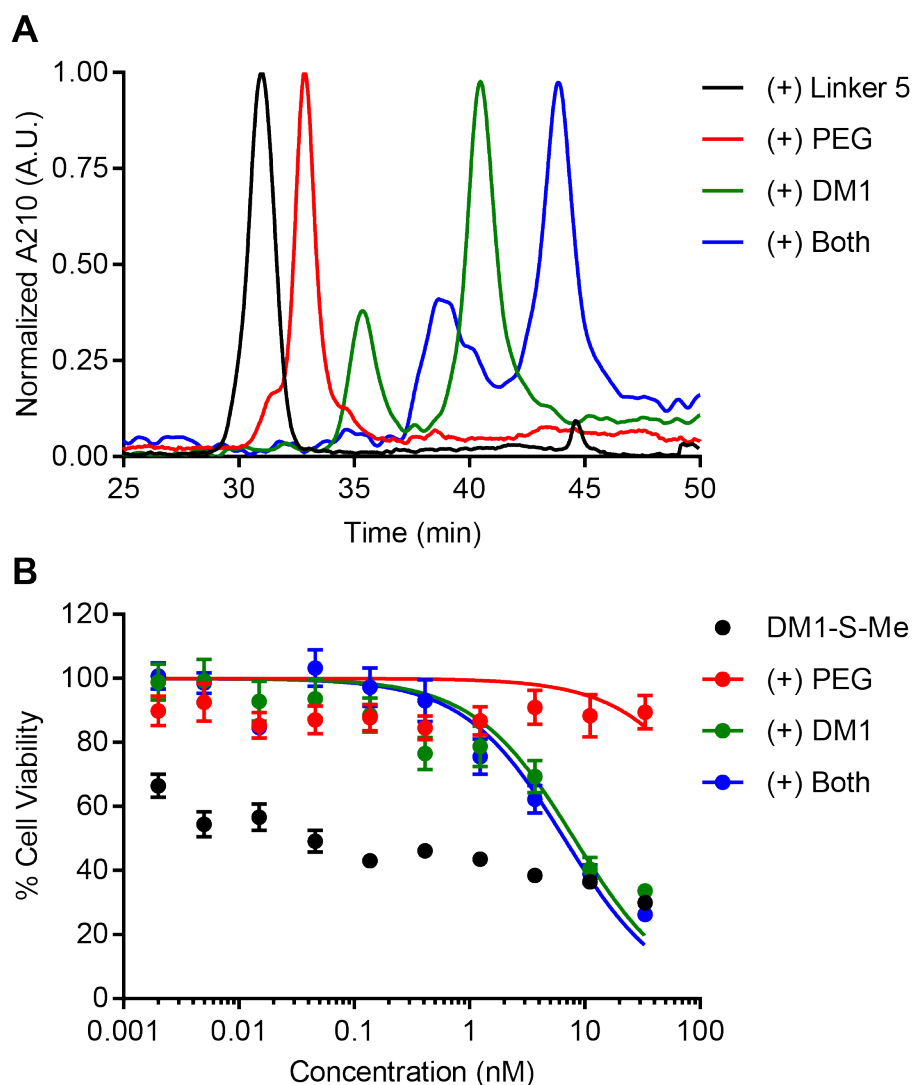
Figure 2.4. Synthesis of multifunctional antibody-drug conjugates. A) HIC analysis of both single and dual "click" modification efficiency. B) Evaluation of in vitro potency of DM1-loaded antibody-drug conjugates using SKOV3 cells, a model Her2 positive cell line (three biological replicates measured in triplicate).

We utilized our dual "click" approach to synthesize a multifunctional ADC containing DM1, a maytansine-derived cytotoxic payload, which inhibits microtubule assembly[51], and a hydrophobicity-masking PEG side chain. A DBCO-modified discrete PEG was synthesized via NHS ester chemistry. A TCO-modified, disulfide-linked version of DM1 was synthesized via the one-pot reaction of a discrete,

heterobifunctional PEG. Conjugate 5 was reacted with DBCO-PEG, TCO-DM1, or both and analyzed via HIC to assess conjugation efficiency (**Figure 2.4A**). Addition of DBCO-PEG fully consumed the parent conjugate to yield a homogeneous antibody conjugate with a degree of labelling (DOL) of 2. The molecular weight of this conjugate was confirmed via MALDI-MS. Addition of TCO-DM1 completely consumed the parent conjugate and yielded a mixed population of products. The peaks eluting at approximately 36 and 41 minutes were interpreted to correspond to a DOL of 1 and 2 respectively. Area under the curve (AUC) analysis estimated the DOL to be approximately 1.8. In agreement with this interpretation, MALDI-MS showed a mixture of conjugates corresponding to a DOL of 1 and 2. Reaction with both cargoes also yielded a mixture of conjugates. Given the complete conversion observed after the addition of DBCO-PEG, incomplete labelling was attributed to the reaction with TCO-DM1. Under this assumption, AUC analysis indicated the PEG and DM1 DOL to be approximately 2 and 1.7 respectively. MALDI-MS analysis was consistent with this interpretation. However, the similar molecular weight of the DBCO-PEG and TCO-DM1 modifications makes it difficult to definitively identify the source of incomplete labelling by MALDI-MS.

The potency of these ADCs was demonstrated using an *in vitro* cell viability assay of a model, Her2 positive cell line, SKOV3 cells (**Figure 2.4B**)[52]. Treatment of SKOV3 cells with the PEG-modified conjugate did not show appreciable toxicity at any of the test conditions. This is to be expected as PEG is inert and biocompatible, and thus should not be toxic. A positive control, DM1-S-Me, showed toxicity at all tested conditions. Analysis of the DM1-loaded conjugate demonstrated an approximate IC50 value of 8.1 nM, in line with previously reported values for DM1[53]. Dual modification of trastuzumab with DM1 and PEG did not negatively impact potency as the dual labeled

conjugate yielded an approximate IC50 value of 6.6 nM. MCF7 cells, a Her2 negative cell line were used to confirm the Her2-specific nature of conjugate-induced toxicity. These data demonstrate the potential for dual "click" conjugation to produce complex, bioactive antibody conjugates using native antibodies.

2.3 – Conclusions

In conclusion, we have synthesized, characterized, and tested the bioconjugation efficiency of five heterobifunctional substrates for MTG. Through this systematic approach, we identified spacer flexibility alpha to the primary amine as the critical structural component for efficient conjugation. A heterobifunctional, dual "click" conjugate was synthesized and characterized at multi-milligram scale. This conjugate was used to demonstrate the mutually orthogonal nature of the SPAAC and IEDDA reactions. This powerful feature was leveraged for the one-pot synthesis of a multifunctional ADC containing a maytansine-derived cytotoxic payload and hydrophobicity-masking PEG side chain. This bifunctional antibody conjugate was shown to induce Her2-specific toxicity in an *in vitro* cell viability assay. Taken together, these data demonstrate the power of substrate design in developing new approaches to site-specific antibody modification. An iterative methodology for linker synthesis, could be used to further elaborate on the principles outlined in this work. This could enable the design of complex, heteromultifunctional antibody conjugates containing a host of functional handles, reporter molecules, and stimuli-responsive moieties that would find use in a wide range of biological applications.

2.4 – Materials and Methods

Reagents for Chemical Synthesis

All chemicals were purchased from MilliporeSigma unless stated otherwise. N-(14-Amino-3,6,9,12-tetraoxatetradec-1-yl)-11,12-didehydro-γ-oxodibenz[b,f]azocine-5(6H)-butanamide (DBCO-PEG4-Amine), (E)-cyclooct-4-en-1-yl (3-aminopropyl)carbamate (TCO-Amine), DM1, mTz-NHS ester, mTz-PEG5-NHS ester, and tert-butyl (2-(2-(2-bromoethoxy)ethoxy)ethyl) carbamate were purchased from BroadPharm. Azidopropan-1-amine was purchased from Click Chemistry Tools. OPSS-PEG24-NHS ester and mPEG24-NHS ester were purchased from Quanta Biodesign. PEG5K-SVA was purchased from Laysan Bio. DM1-S-Me was purchased from Toronto Research Chemicals.

Reagents for Protein Expression and Purification

The plasmid pDJ1-3 was kindly provided by Professor Joelle Pelletier (Université de Montréal, Montreal, Canada). pDJ1-3 encodes the proenzyme of microbial transglutaminase from *S. mobaraensis* with its N-terminal pro-sequence and a C-terminal hexa-histidine tag inserted between the *Nde*I and *Xho*I restriction sites of the vector pET20b. The plasmid pVITRO-Trastuzumab-IgG1/k for expressing trastuzumab was purchased from Addgene (Plasmid# 61883). Ni-NTA agarose resin was purchased from Qiagen. NAb protein A/G resin was purchased from ThermoFisher Scientific. Sequencing primers (T7 forward and reverse) were purchased from Integrated DNA Technologies (IDT). Sequencing was performed at the Cornell University Genomics Facility using the Applied Biosystems Automated 370xl DNA Analyzer using Big Dye Terminator chemistry and ApliTag-FS DNA Polymerase.

Reagents for Gel Electrophoresis, Molecular Biology, and Cell Culture

Sulfo-Cy5 TCO was purchased from BroadPharm. DBCO-PEG4-Carboxyrhodamine 101 was purchased from Click Chemistry Tools. Precast protein gels (4 – 20% mini-PROTEAN® TGX™) and Bio-safe Coomassie Stain were purchased from Bio-Rad Laboratories. Peptide:N-glycosidase F (PNGase F) was purchased from New England Biolabs. All cell culture reagents were purchased from ThermoFisher Scientific unless stated otherwise. HEK293F cells were cultured in FreeStyle™ 293 Expression Medium. SKOV3 and MCF7 cells were cultured in Dulbecco's Modified Eagle Medium (DMEM) and DMEM supplemented with insulin (0.01 mg/mL), respectively. CellTiter 96® AQ$_{ueous}$ One Solution Cell Proliferation Assay (MTS) was purchased from Promega.

Nuclear Magnetic Resonance (NMR) Spectroscopy

^{1}H and ^{13}C NMR spectra were recorded on either an INOVA 400 MHz or 500 MHz spectrometer as specified. NMR data was analyzed by MestReNova software. ^{1}H and ^{13}C NMR chemical shifts are reported in units of ppm relative to chloroform.

Liquid Chromatography Mass Spectrometry (LC-MS)

LC-MS analysis was carried out on an Agilent 1100 Series LC with a Poroshell 120 EC-C18 column (100 × 3 mm, 2.7 μm, Agilent Technologies) and an Agilent G1956B Series Single Quadripole MS in positive ion mode for mass detection. The mobile phase for LC-MS (solvent A) was water with 0.1% (v/v) acetic acid, and the stationary phase (solvent B) was acetonitrile with 0.1% (v/v) acetic acid. Compounds were eluted at a flow rate of 0.6 mL/min using a gradient of 5-100% solvent B (0-10 minutes) followed by 100% solvent B (10-12 minutes) and equilibrated back to 5% solvent B (12-15 minutes).

Reverse Phase High Performance Liquid Chromatography (RP-HPLC)

HPLC purification was performed on an Agilent 1100 Series HPLC system equipped with a UV diode array detector and an 1100 Infinity fraction collector using a semi-preparative reversed-phase C18 column (Agilent Eclipse XDB-C18, 9.4 x 250 mm, 5 µm). The mobile phase for HPLC was water with 0.1% (v/v) trifluoroacetic acid (solvent A) and acetonitrile with 0.1% (v/v) trifluoroacetic acid (solvent B) unless specified otherwise. Compounds were eluted at a flow rate of 4 mL/min using a linear solvent gradient as specified below.

Hydrophobic Interaction Chromatography (HIC)

HIC was performed on an Agilent 1100 Series HPLC system equipped with a UV diode array detector and an 1100 Infinity fraction collector using a reversed-phase phenyl column (Tosoh Biosciences LLC, TSKgel Phenyl-5PW, 7.5 x 75 mm, 10 µm). The mobile phase for HIC was 25 mM phosphate, 1.5 M ammonium sulfate, pH 7.0 (solvent A) and 18.75 mM phosphate, 25% (v/v) isopropyl alcohol, pH 7.0 (solvent B). Compounds were eluted at a flow rate of 1 mL/min using a linear solvent gradient as specified below.

Gel Electrophoresis of Conjugates

All samples were denatured and reduced with 2-mercaptoethanol by boiling at 100 °C for 5 minutes. A precast 4-20% mini-PROTEAN® TGX™ gel was run for 60 minutes at 120V to separate the protein samples. Protein content was visualized using Bio-Safe Coomassie Stain according to the manufacturer's instructions and imaged using a Bio-Rad ChemiDoc™ MP Imaging System.

Synthesis of Linker 1 (Compound 3, Figure A2. 1 – Figure A2. 3)

Synthesis of (1): 1 equivalency (20 mg, 92 µmol) of tert-butyl (2-bromoethyl)carbamate was dissolved at 400 mM in dimethyl sulfoxide (solution 1). 2 equivalencies of

azidopropan-1-amine and 2 equivalencies of triethylamine were dissolved at 400 mM in dimethyl sulfoxide (solution 2). Solution 1 was added dropwise to solution 2 at room temperature over 2 hours. The resulting mixture was reacted at room temperature overnight and then purified via semi-preparative RP-HPLC. The reaction mixture was separated using a linear solvent gradient of 5 – 45% solvent B over 20 minutes. The product **(1)** eluted at 11.5 minutes and was recovered in 94% yield (21 mg, 87 µmol). The product was characterized by LC-MS (**(1)** calculated: 244.17, observed: 244.20 [M+H]$^+$).

Synthesis of (2): 1 equivalency (10.5 mg, 43 µmol) of **(1)** was dissolved at 300 mM in dimethyl sulfoxide in the presence of 5 equivalencies of triethylamine. To this solution, 1 equivalency of mTz-NHS ester dissolved at 300 mM in dimethylsulfoxide was added. The resulting mixture was reacted at room temperature overnight and then purified via semi-preparative RP-HPLC. The reaction mixture was separated using a linear solvent gradient of 5 – 95% solvent B over 30 minutes. The product **(2)** eluted at 22 minutes and was recovered in 60% yield (11.7 mg, 26 µmol). The product was characterized by ^{1}H NMR and LC-MS (**(2)** calculated: 478.24, observed: 478.00 [M+Na]$^+$).

Synthesis of (3): Removal of the Boc protecting group was achieved by dissolving **(2)** at 5 mM in 50% (v/v) trifluoroacetic acid in dichloromethane at room temperature for 1 hour. The solvent was then removed under vacuum, and the product was purified via semi-preparative RP-HPLC. The dried product was separated using a linear solvent gradient of 5 – 50% solvent B over 22.5 minutes. The product **(3)** eluted at 14.5 minutes and was recovered in 94% yield (8.6 mg, 24 µmol). The product was characterized by ^{1}H NMR and LC-MS (**(3)** calculated: 356.19, observed: 356.10 [M+H]$^+$).

Synthesis of 1-azido-2-(2-(2-bromoethoxy)ethoxy)ethane (Compound 6, Figure A2. 4 – Figure A2. 9)

Synthesis of (4): 1 equivalency of 4-methylbenzenesulfonyl chloride (3.5 g, 18.4 mmol) was dissolved at 175 mM in dichloromethane. Separately, 4 equivalencies of 2,2'-(ethane-1,2-diylbis(oxy))bis(ethan-1-ol) (11 g, 73 mmol) was dissolved at 110 mM in dichloromethane. To this solution was added 1.05 equivalencies of triethylamine (1.95 g, 19 mmol) and 0.02 equivalencies of 4-dimethylaminopyridine (46 mg, 0.3 mmol), and the mixture was allowed to equilibrate for 10 minutes on ice. The solution of 4-methylbenzenesulfonyl chloride in DCM was then added dropwise to the mixture over 2 hours. The mixture was subsequently removed from the ice and reacted at room temperature overnight. The reaction was quenched with 100 mL of water and extracted with dichloromethane (100 mL, 3x). The organic layer was collected, dried with sodium sulfate, and concentrated under vacuum. The crude product **(4)**, recovered in 98% yield (5.5 g, 18 mmol), was used without further purification. The product was characterized by ^{1}H and ^{13}C NMR.

Synthesis of (5): 1 equivalency (4.8 g, 16 mmol) of **(4)** was dissolved at 739 mM in dry dimethylformamide (DMF). To this solution was added 2 equivalencies of sodium azide (2 g, 32 mmol) and the mixture was reacted overnight at 80°C. The mixture was then concentrated under vacuum. The residue was suspended in diethyl ether and filtered through celite. The filtered product was collected and concentrated under vacuum. The crude product **(5)**, recovered in 96% yield (2.7 g, 15.4 mmol), was used without further purification. The product was characterized by ^{1}H NMR.

Synthesis of (6): 1 equivalency (1 g, 5.8 mmol) of **(5)** was dissolved at 342 mM in dry chloroform. To this solution was added 2 equivalencies of phosphorus tribromide (3.1 g, 12 mmol) over 5 minutes. The mixture was refluxed overnight at 50°C. The reaction

was quenched on ice over 30 minutes with 75 mL of saturated sodium bicarbonate solution and extracted with chloroform (100 mL, 3x). The organic layer was collected, dried with sodium sulfate, and concentrated under vacuum. The crude product **(6)**, recovered in 30% yield (0.4 g, 1.7 mmol), was used without further purification. The product was characterized by ^{1}H and ^{13}C NMR.

Synthesis of Linker 2 (Compound 9, Figure A2. 10 – Figure A2. 12)

Synthesis of (7): 1 equivalency (38 mg, 159 µmol) of **(6)** was dissolved at 400 mM in dimethyl sulfoxide (solution 1). 2 equivalencies of tert-butyl (2-aminoethyl)carbamate and 2 equivalencies of triethylamine were dissolved at 400 mM in dimethyl sulfoxide (solution 2). Solution 1 was added dropwise to solution 2 at room temperature over 2 hours. The resulting mixture was reacted at room temperature overnight and then purified via semi-preparative RP-HPLC. The reaction mixture was separated using a linear solvent gradient of 5 – 45% solvent B over 20 minutes. The product **(7)** eluted at 13.5 minutes and was recovered in 52% yield (26 mg, 83 µmol). The product was characterized by LC-MS (**(7)** calculated: 318.21, observed: 318.20 [M+H]$^+$).

Synthesis of (8): 1 equivalency (6.6 mg, 21 µmol) of **(7)** was dissolved at 300 mM in dimethyl sulfoxide in the presence of 5 equivalencies of triethylamine. To this solution, 1 equivalency of mTz-NHS ester dissolved at 300 mM in dimethylsulfoxide was added. The resulting mixture was reacted at room temperature overnight and then purified via semi-preparative RP-HPLC. The reaction mixture was separated using a linear solvent gradient of 5 – 95% solvent B over 30 minutes. The product **(8)** eluted at 21 minutes and was recovered in 28% yield (3.1 mg, 6 µmol). The product was characterized by ^{1}H NMR and LC-MS (**(8)** calculated: 552.28, observed: 552.10 [M+Na]$^+$).

Synthesis of (9): Removal of the Boc protecting group was achieved by dissolving **(8)** at 5 mM in 50% (v/v) trifluoroacetic acid in dichloromethane at room temperature for 1

hour. The solvent was then removed under vacuum, and the product was purified via semi-preparative RP-HPLC. The dried product was separated using a linear solvent gradient of 5 – 50% solvent B over 22.5 minutes. The product **(8)** eluted at 16 minutes and was recovered in 85% yield (2.6 mg, 6 µmol). The product was characterized by ^{1}H NMR and LC-MS (**(9)** calculated: 430.22, observed: 430.10 [M+H]+).

Synthesis of Linker 3 (Compound 11, Figure A2. 13 – Figure A2. 15)

Synthesis of (10): 1 equivalency (10.5 mg, 43 µmol) of **(1)** was dissolved at 300 mM in dimethyl sulfoxide in the presence of 5 equivalencies of triethylamine. To this solution, 0.36 equivalencies of mTz-PEG5-NHS ester dissolved at 300 mM in dimethylsulfoxide was added. The resulting mixture was reacted at room temperature overnight and then purified via semi-preparative RP-HPLC. The reaction mixture was separated using a linear solvent gradient of 5 – 95% solvent B over 30 minutes. The product **(10)** eluted at 22.5 minutes and was recovered in 74% yield (7.6 mg, 11.5 µmol). The product was characterized by ^{1}H NMR and LC-MS (**(10)** calculated: 684.35, observed: 684.10 [M+Na]+).

Synthesis of (11): Removal of the Boc protecting group was achieved by dissolving **(10)** at 5 mM in 50% (v/v) trifluoroacetic acid in dichloromethane at room temperature for 1 hour. The solvent was then removed under vacuum, and the product was purified via semi-preparative RP-HPLC. The dried product was separated using a linear solvent gradient of 5 – 50% solvent B over 22.5 minutes. The product **(3)** eluted at 18.5 minutes and was recovered in 79% yield (5.1 mg, 9 µmol). The product was characterized by ^{1}H NMR and LC-MS (**(11)** calculated: 562.30, observed: 562.20 [M+H]+).

Synthesis of Linker 4 (Compound 14, Figure A2. 16 – Figure A2. 18)

Synthesis of (12): 1 equivalency (24.6 mg, 79 µmol) of tert-butyl (2-(2-(2-bromoethoxy)ethoxy)ethyl) carbamate was dissolved at 400 mM in dimethyl sulfoxide

(solution 1). 2 equivalencies of azidopropan-1-amine and 2 equivalencies of triethylamine were dissolved at 400 mM in dimethyl sulfoxide (solution 2). Solution 1 was added dropwise to solution 2 at room temperature over 2 hours. The resulting mixture was reacted at room temperature overnight and then purified via semi-preparative RP-HPLC. The reaction mixture was separated using a linear solvent gradient of 5 – 45% solvent B over 20 minutes. The product **(12)** eluted at 13.5 minutes and was recovered in 75% yield (19.6 mg, 59 µmol). The product was characterized by LC-MS (**(12)** calculated: 332.22, observed: 332.20 $[M+H]^+$).

Synthesis of (13): 1 equivalency (7.4 mg, 22 µmol) of **(12)** was dissolved at 300 mM in dimethyl sulfoxide in the presence of 5 equivalencies of triethylamine. To this solution, 1 equivalency of mTz-NHS ester dissolved at 300 mM in dimethylsulfoxide was added. The resulting mixture was reacted at room temperature overnight and then purified via semi-preparative RP-HPLC. The reaction mixture was separated using a linear solvent gradient of 5 – 95% solvent B over 30 minutes. The product **(13)** eluted at 21 minutes and was recovered in 27% yield (3.3 mg, 6.1 µmol). The product was characterized by ^{1}H NMR and LC-MS (**(13)** calculated: 566.29, observed: 566.10 $[M+Na]^+$).

Synthesis of (14): Removal of the Boc protecting group was achieved by dissolving **(13)** at 5 mM in 50% (v/v) trifluoroacetic acid in dichloromethane at room temperature for 1 hour. The solvent was then removed under vacuum, and the product was purified via semi-preparative RP-HPLC. The dried product was separated using a linear solvent gradient of 5 – 50% solvent B over 22.5 minutes. The product **(14)** eluted at 16.5 minutes and was recovered in 92% yield (2.5 mg, 5.6 µmol). The product was characterized by ^{1}H NMR and LC-MS (**(3)** calculated: 444.24, observed: 444.10 $[M+H]^+$).

Synthesis of Linker 5 (Compound 17, Figures Figure A2. 19 – Figure A2. 21)

Synthesis of (15): 1 equivalency (38 mg, 159 µmol) of **(6)** was dissolved at 400 mM in dimethyl sulfoxide (solution 1). 2 equivalencies of tert-butyl (2-(2-(2-aminoethoxy)ethoxy)ethyl)carbamate and 2 equivalencies of triethylamine were dissolved at 400 mM in dimethyl sulfoxide (solution 2). Solution 1 was added dropwise to solution 2 at room temperature over 2 hours. The resulting mixture was reacted at room temperature overnight and then purified via semi-preparative RP-HPLC. The reaction mixture was separated using a linear solvent gradient of 5 – 45% solvent B over 20 minutes. The product **(15)** eluted at 15.5 minutes and was recovered in 26% yield (17 mg, 42 µmol). The product was characterized by LC-MS (**(15)** calculated: 406.25, observed: 406.10 [M+H]$^+$).

Synthesis of (16): 1 equivalency (8.6 mg, 21 µmol) of **(15)** was dissolved at 300 mM in dimethyl sulfoxide in the presence of 5 equivalencies of triethylamine. To this solution, 1 equivalency of mTz-NHS ester dissolved at 300 mM in dimethylsulfoxide was added. The resulting mixture was reacted at room temperature overnight and then purified via semi-preparative RP-HPLC. The reaction mixture was separated using a linear solvent gradient of 5 – 95% solvent B over 30 minutes. The product **(16)** eluted at 20.5 minutes and was recovered in 51% yield (6.7 mg, 11 µmol). The product was characterized by ^{1}H NMR and LC-MS (**(8)** calculated: 640.33, observed: 640.10 [M+Na]$^+$).

Synthesis of (17): Removal of the Boc protecting group was achieved by dissolving **(16)** at 5 mM in 50% (v/v) trifluoroacetic acid in dichloromethane at room temperature for 1 hour. The solvent was then removed under vacuum, and the product was purified via semi-preparative RP-HPLC. The dried product was separated using a linear solvent gradient of 5 – 50% solvent B over 22.5 minutes. The product **(17)** eluted at 17.5 minutes and was recovered in 91% yield (5.1 mg, 10 µmol). The product was

characterized by ^{1}H NMR and LC-MS (**(9)** calculated: 518.28, observed: 518.20 [M+H]$^+$).

Synthesis of DBCO-PEG5K (Compound 18, **Figure A2. 22** and **Figure A2. 23**)

1 equivalency (1.7 mg, 3.2 µmol) of DBCO-PEG4-Amine was dissolved at 100 mM in dimethyl sulfoxide in the presence of 5 equivalencies of triethylamine. To this solution, 1.25 equivalencies of PEG5K-SVA dissolved at 50 mM in dimethylsulfoxide was added. The resulting mixture was reacted at room temperature overnight and then purified via semi-preparative RP-HPLC. The reaction mixture was separated using a mobile phase of water (solvent A) and acetonitrile (solvent B) and a linear solvent gradient of 5 – 65% solvent B over 30 minutes. The product **(18)** eluted at 25 minutes and was recovered in 62% yield (10 mg, 1.8 µmol). The product was characterized by MALDI-MS.

Synthesis of TCO-PEG5K (Compound 19, Figure A2. 24 and Figure A2. 25)

1 equivalency (0.7 mg, 3.2 µmol) of TCO-Amine was dissolved at 100 mM in dimethyl sulfoxide in the presence of 5 equivalencies of triethylamine. To this solution, 1.25 equivalencies of PEG5K-SVA dissolved at 50 mM in dimethylsulfoxide was added. The resulting mixture was reacted at room temperature overnight and then purified via semi-preparative RP-HPLC. The reaction mixture was separated using a mobile phase of water (solvent A) and acetonitrile (solvent B) and a linear solvent gradient of 5 – 65% solvent B over 30 minutes. The product **(19)** eluted at 24.5 minutes and was recovered in 80% yield (12.8 mg, 2.5 µmol). The product was characterized by MALDI-MS.

Synthesis of DBCO-PEG28 (Compound 20, Figure A2. 26 and Figure A2. 27)

1 equivalency (2 mg, 3.8 µmol) of DBCO-PEG4-Amine was dissolved at 190 mM in dimethyl sulfoxide in the presence of 5 equivalencies of triethylamine. To this solution, 1 equivalency of mPEG24-NHS ester dissolved at 100 mM in dimethylsulfoxide was added. The resulting mixture was reacted at room temperature overnight and then

purified via semi-preparative RP-HPLC. The reaction mixture was separated using a linear solvent gradient of 5 – 95% solvent B over 45 minutes. The product **(20)** eluted at 24.5 minutes and was recovered in 47% yield (2.9 mg, 1.8 µmol). The product was characterized by LC-MS (**(20)** calculated: 1622.91, observed: 1622.60 [M+H]$^+$).

Synthesis of TCO-PEG24-DM1 (Compound 21, Figure A2. 28 and Figure A2. 29)

1 equivalency (2.6 mg, 9.9 µmol) of TCO-Amine was dissolved at 100 mM in dimethyl sulfoxide in the presence of 5 equivalencies of triethylamine. To this solution, 0.67 equivalencies of OPSS-PEG24-NHS ester dissolved at 100 mM in dimethyl sulfoxide was added. The resulting mixture was reacted at room temperature for 1 hour. To this solution, 0.67 equivalencies of DM1 dissolved at 100 mM in dimethyl sulfoxide was added. The resulting mixture was reacted at room temperature for 4 hours and then purified via semi-preparative RP-HPLC. The reaction mixture was separated using a linear solvent gradient of 5 – 75% solvent B over 35 minutes. The product **(21)** eluted at 27 minutes and was recovered in 76% yield (10.9 mg, 5 µmol). The product was characterized by LC-MS.

Analysis of Linker Purity and Hydrophobicity via HPLC

Linker purity and relative hydrophobicity were analyzed on an Agilent 1100 Series HPLC system equipped with a UV diode array detector and an 1100 Infinity fraction collector using a reversed-phase C18 column (Agilent Eclipse Plus C18, 4.6 x 150 mm, 5 µm). The mobile phase for HPLC was water with 0.1% (v/v) trifluoroacetic acid (solvent A) and acetonitrile with 0.1% (v/v) trifluoroacetic acid (solvent B). Compounds were eluted at a flow rate of 1 mL/min with a linear gradient of 5% to 95% solvent B over 30 minutes. Linkers were analyzed at a scale of 50 µg and monitored based on their methyltetrazine-specific absorption at 360 nm.

Expression and Purification of Microbial Transglutaminase

Microbial transglutaminase (MTG) was expressed and purified as previously described with minor modifications[42]. Briefly, plasmid pDJ1-3 was transformed into *E. coli* BL21 (DE3), using standard procedures, and maintained with 100 µg/mL ampicillin. Before protein expression, correct plasmid sequence was confirmed (**Table A2. 1**). A 5 mL starter culture was propagated overnight at 37°C with shaking at 240 rpm in ZYP-0.8G media. The starter culture (2.5 mL) was used to inoculate 250 mL of auto-inducing ZYP-5052 medium. The expression culture was grown for 2 hours at 37°C with shaking at 240 rpm. After 2 hours, the temperature was reduced to 22°C for 20 hours. Cells were collected by centrifugation at 3,000xg at 4°C for 30 minutes. The cell pellet was suspended in 8 mL of 0.2 M Tris-HCl, pH 6.0. The cells were disrupted by sonication at 4°C (Qsonica Model CL-18, 3 cycles of 30 second pulse at 20% intensity with 60 second pause). The N-terminal MTG pro-sequence was removed by treatment for 45 minutes at 30°C with 800 µL of trypsin at a concentration of 1 mg/mL in 0.2 M Tris-HCl, pH 6.0. Activated MTG was purified using a gravity flow column charged with 0.5 mL of Ni-NTA resin. The column was equilibrated in a buffer of 50 mM phosphate, 300 mM NaCl, and 2 mM reduced glutathione, pH 7.5. His-tagged enzyme was eluted using equilibration buffer containing increasing amounts of imidazole (0 – 200 mM). Purified enzyme was concentrated and exchanged into equilibration buffer using Amicon Ultra-0.5 mL centrifugal filters with a 10 kDa molecular weight cut off according to the manufacturer's instructions. MTG yield was quantified using absorbance at 280 nm (molar extinction coefficient of 55,408 M^{-1} cm^{-1}). The average MTG yield was 10 mg/L of *E. coli* culture. Purified MTG was snap frozen as single use aliquots containing 15% (v/v) glycerol.

Expression and Purification of Trastuzumab

HEK293F suspension cells were transfected with the plasmid pVITRO-Trastuzumab-IgG1/k using FreeStyle™ MAX transfection reagent. Transfected cells were selected with 50 µg/mL hygromycin B for two weeks to establish a stably expressing cell line. Stably expressing HERK293F cells were maintained at density of approximately 1 x 10^6 cells/mL for protein production. Trastuzumab was purified from sterile-filtered, conditioned media using a gravity flow column charged with 1 mL of protein A/G resin according to the manufacturer's instructions. Purified antibody was concentrated and exchanged into PBS buffer (100 mM phosphate, 150 mM NaCl, pH 7.4) using Amicon Ultra-0.5 mL centrifugal filters with a 30 kDa molecular weight cut off according to the manufacturer's instructions. Antibody yield was quantified using absorbance at 280 nm (molar extinction coefficient of 210,000 M^{-1} cm^{-1}). The average antibody yield was 1 – 2 mg per/L of conditioned media.

HIC Analysis of Linker Conjugation Efficiency

1 equivalency of trastuzumab (250 µg, 1.7 nmol) at a concentration of 5 mg/mL in PBS buffer was treated with PNGase F (600 U/mg of antibody), MTG (0.75 equivalencies), and amine-bearing substrate (160 equivalencies). Conjugation reactions were carried out at 37°C for 24 hours. Excess enzyme and substrate were removed using NAb Protein A/G 0.2 mL spin columns according to the manufacturer's instructions. Conjugation efficiency was analyzed via analytical HIC using a linear solvent gradient of 0 – 60% solvent B over 60 minutes.

Gel Electrophoresis Analysis of Linker Conjugation Efficiency

1 equivalency of trastuzumab (100 µg, 0.7 nmol) at a concentration of 5 mg/mL in PBS buffer was treated with PNGase F (600 U/mg of antibody), MTG (0.75 equivalencies), and amine-bearing substrate (160 equivalencies). Conjugation reactions were carried

out at 37°C for 24 hours. Excess enzyme and substrate were removed using NAb Protein A/G 0.2 mL spin columns according to the manufacturer's instructions. Purified conjugates were lyophilized and suspended at a concentration of 5 mg/mL. Conjugates were diluted to a concentration of 1 mg/mL in PBS buffer, pH 7.4 and reacted with 20 equivalencies of either DBCO-PEG5K (compound 18) or TCO-PEG5K (compound 19). Reactions were carried out at 37°C for 20 hours and analyzed by reduced and denatured SDS-PAGE. Conjugation efficiency was quantified by analyzing the relative band intensities for the IgG heavy chain and the PEG5K-modified heavy chain. Each band was quantified relative to the IgG light chain band as an internal control. Band intensities were quantified using the gel analysis tool of FIJI[54]. Raw images are provided (**Figure A2. 30**).

Large Scale Purification of Conjugate 5

1 equivalency of trastuzumab (2.3 mg, 15.3 nmol) at a concentration of 5 mg/mL in PBS buffer was treated with PNGase F (600 U/mg of antibody), MTG (0.75 equivalencies), and Linker 5 (160 equivalencies). The reaction was carried out at 37°C for 24 hours and then purified via analytical HIC using a linear solvent gradient of 0 – 60% solvent B over 60 minutes. The product (conjugate 5) eluted at 47 minutes. The product was concentrated and exchanged into PBS buffer, pH 7.4 using Amicon Ultra-0.5 mL centrifugal filters with a 30 kDa molecular weight cut off according to the manufacturer's instructions. Conjugate was recovered in 48% yield (1.1 mg, 7.3 nmol). Conjugate purity was assessed via analytical HIC using a linear solvent gradient from 0 – 100% solvent B over 60 minutes (**Figure A2. 31**). Conjugate molecular weight was characterized via MALDI-MS (**Figure A2. 32**).

Gel Electrophoresis Analysis of Dual "Click" Modification

1 equivalency of conjugate 5 (50 ug, 0.33 nmol) at a concentration of 6 mg/mL in PBS buffer was reacted with 2 equivalencies of DBCO-PEG4-Carboxyrhodamine101, sulfo-Cy5-TCO, or both. Reactions were carried out protected from light at room temperature for 20 hours and analyzed by reduced and denatured SDS-PAGE. Fluorescence imaging was performed using a GE Healthcare Typhoon 9400 image system set to a photomultiplier tube voltage of 400 with the following fluorescence settings: Carboxyrhodamine101 excitation 488 nm, emission 500 – 540 nm; sulfo-Cy5 excitation 633 nm, emission 655 – 685 nm; FRET excitation 488 nm, emission 655 – 685 nm. A reaction scheme is provided (**Figure A2. 33**).

One-pot Synthesis of Antibody-drug Conjugates

1 equivalency of conjugate 5 (80 ug, 0.53 nmol) at a concentration of 6 mg/mL in PBS buffer was reacted with 2 equivalencies of DBCO-PEG28 (compound 20), TCO-PEG24-DM1 (compound 21), or both. Reactions were carried out at room temperature for 20 hours. Excess reagents were removed using Amicon Ultra-0.5 mL centrifugal filters with a 30 kDa molecular weight cut off according to the manufacturer's instructions. Conjugation efficiency was assessed via analytical HIC using a linear solvent gradient from 0 – 100% solvent B over 60 minutes. A reaction scheme is provided (**Figure A2. 34**). Conjugate molecular weight was characterized via MALDI-MS (**Figure A2. 35**).

In Vitro Potency of Antibody-drug Conjugates

SKOV3 and MCF7 cells were plated at 6,000 and 1,500 cells/well, respectively, and allowed to adhere overnight. After overnight incubation, three-fold serial dilutions of the conjugates or DM1-S-Me control starting at 33 nM were added. Treated cells were then incubated for 4 days. Cell viability was measured using MTS according to the

manufacturer's instructions using a Tecan Infinite M1000 Pro microplate reader. Percent viability was calculated by comparison to untreated cells and media alone. Potency data for MCF7, a Her2 negative cell line, is provided (**Figure A2. 36**).

Chapter 2 Appendix

Site-specific Dual "Click" Modification of Native Antibodies

via Microbial Transglutaminase

Synthesis of Linker 1 (Compound 3)
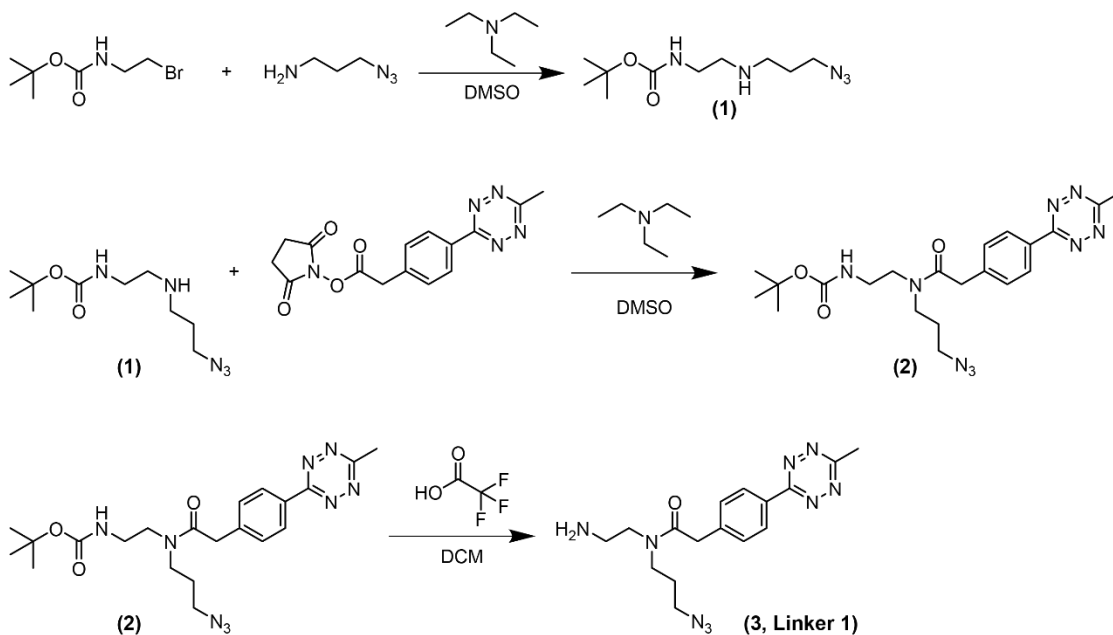
Figure A2. 1. Synthesis scheme for Linker 1.
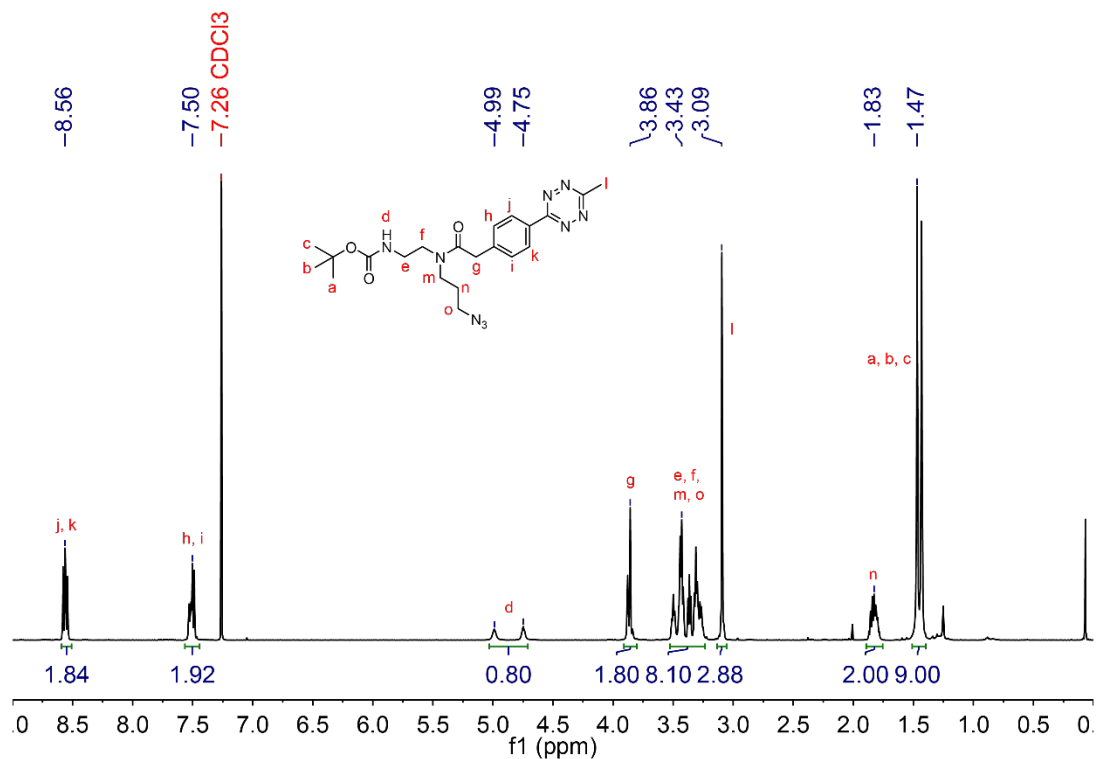
Figure A2. 2. ^{1}H NMR (500 MHz, CDCl$_3$) of compound **(2)**.
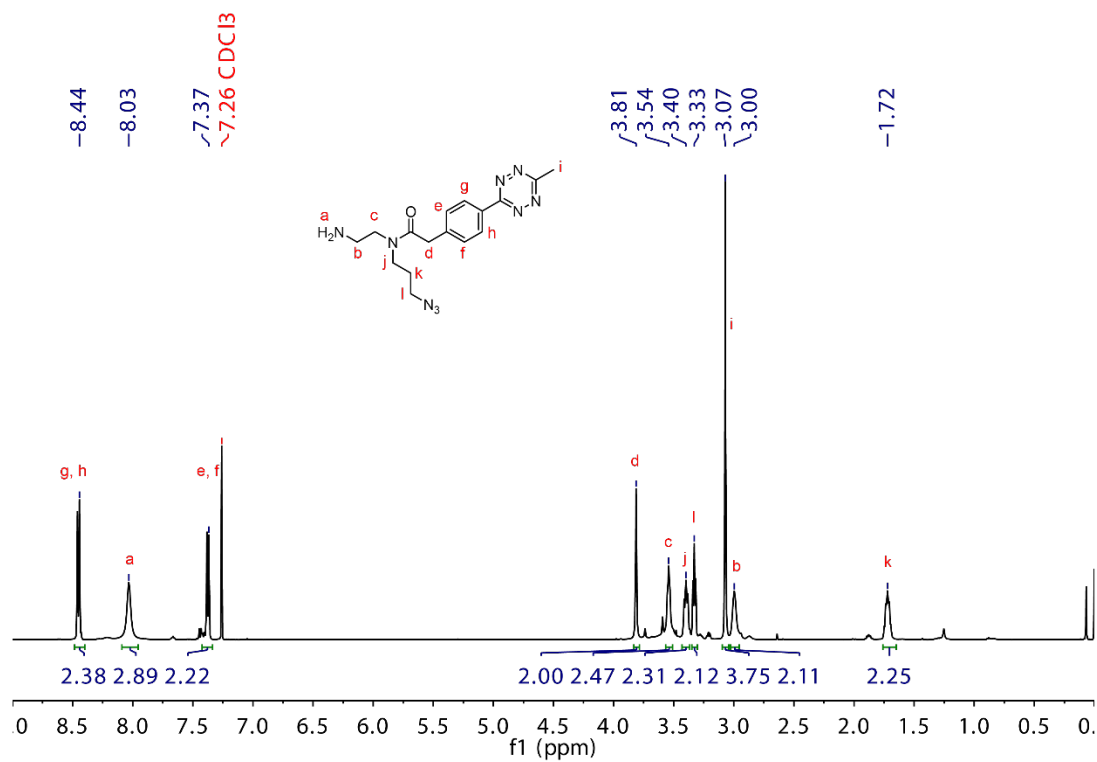
Figure A2. 3. ^{1}H NMR (500 MHz, CDCl$_3$) of compound **(3)**.

Synthesis of 1-azido-2-(2-(2-bromoethoxy)ethoxy)ethane (Compound 6)
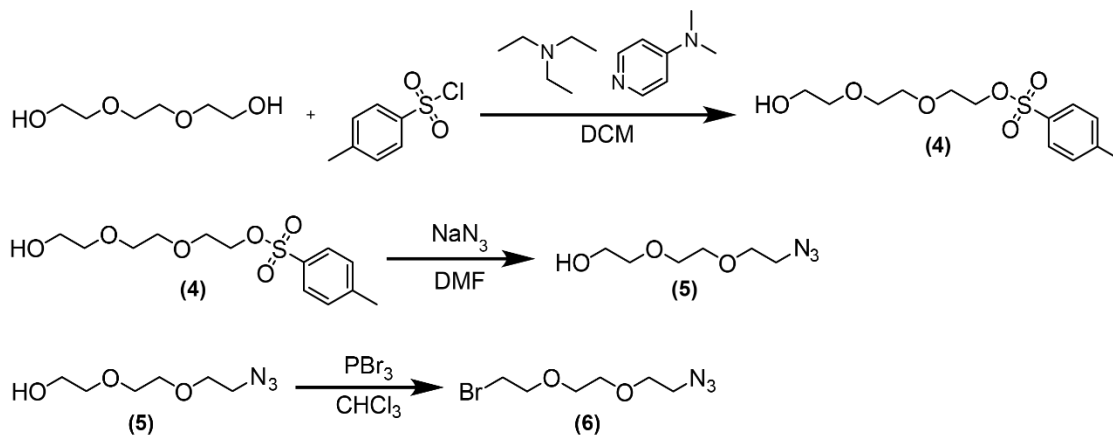
Figure A2. 4. Synthesis scheme for 1-azido-2-(2-(2-bromoethoxy)ethoxy)ethane.
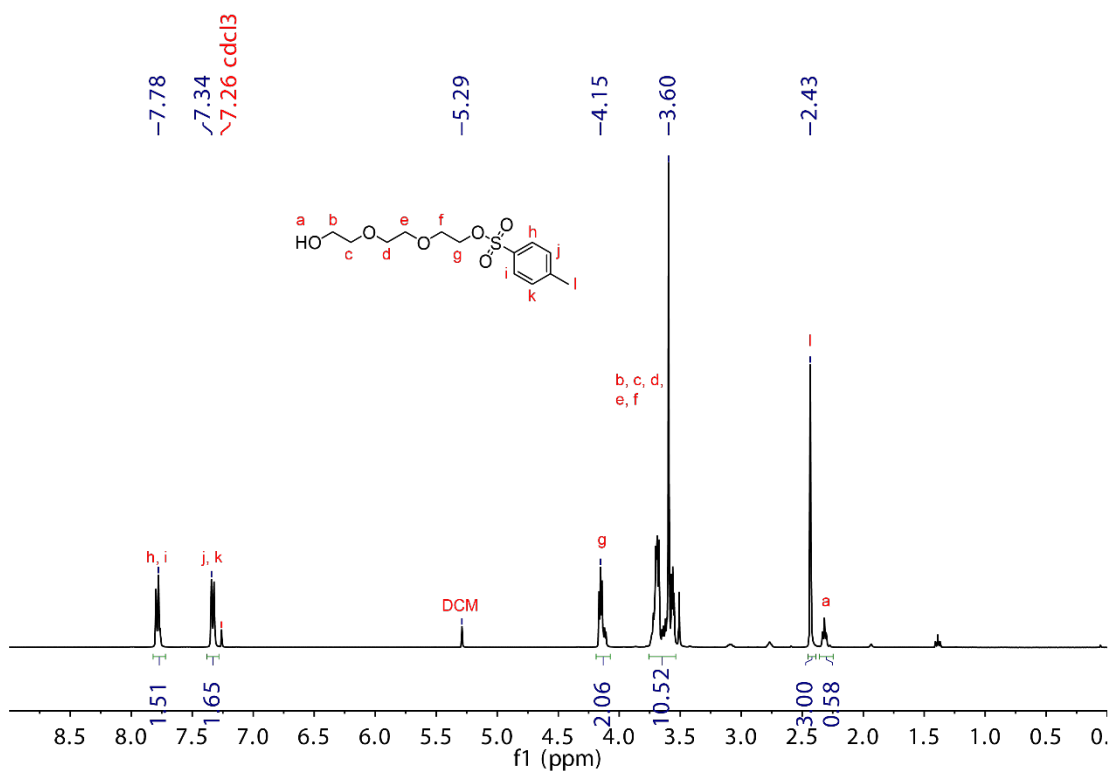
Figure A2. 5. ^{1}H NMR (400 MHz, CDCl$_3$) of compound **(4)**.
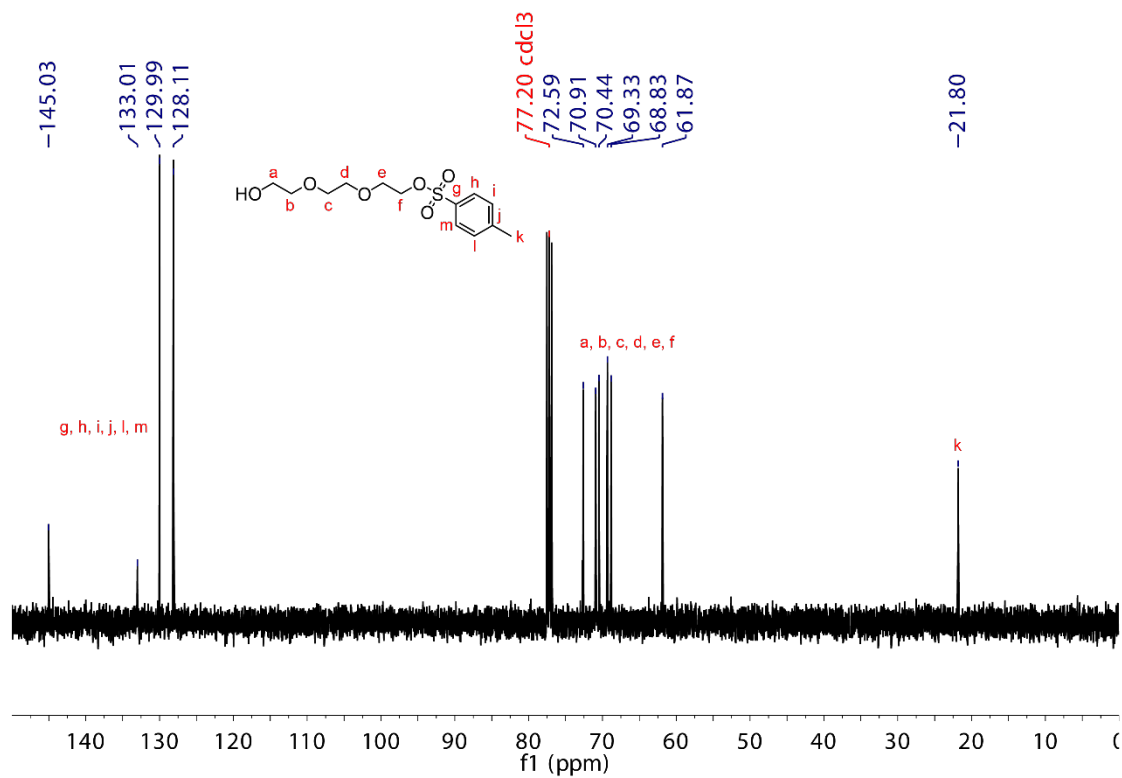
Figure A2. 6. ^{13}C NMR (400 MHz, CDCl$_3$) of compound **(4)**.
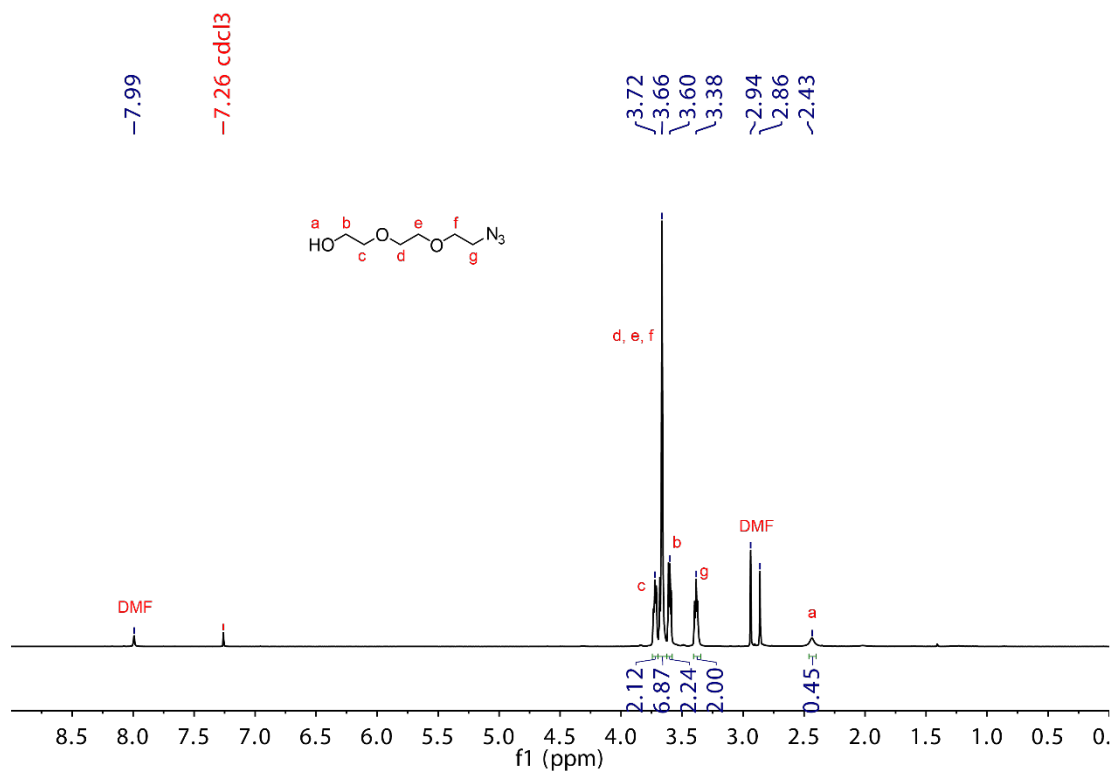
Figure A2. 7. ^{1}H NMR (400 MHz, CDCl$_3$) of compound **(5)**.
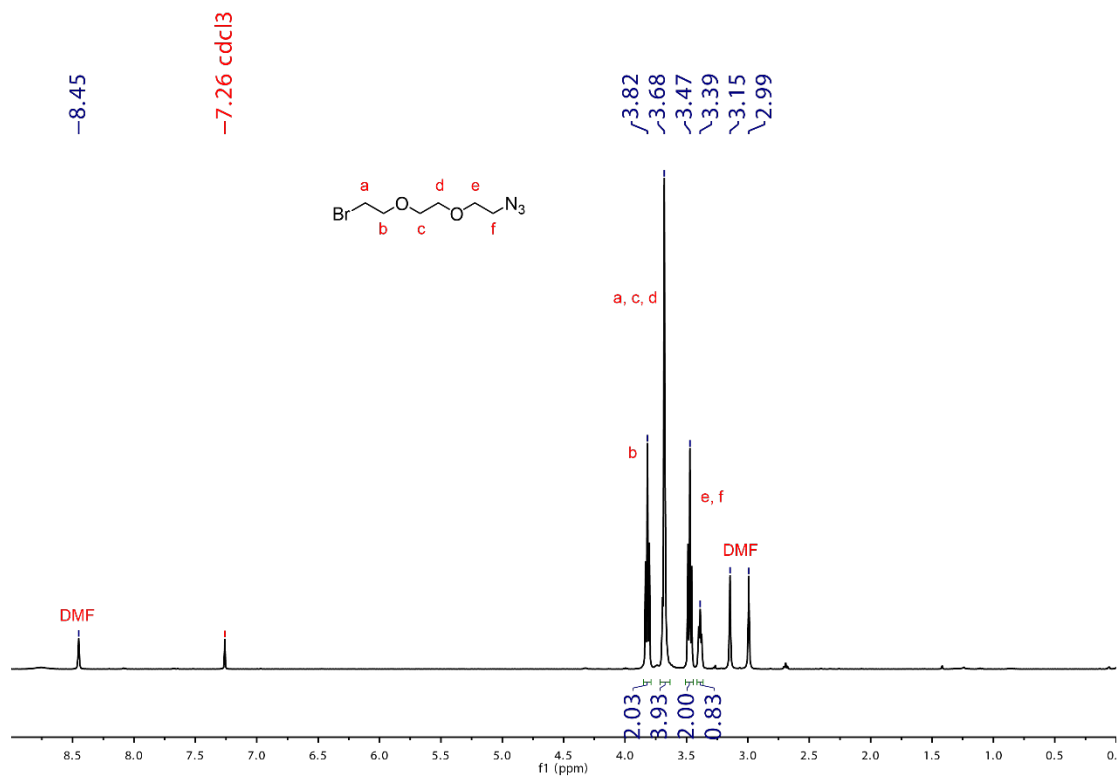
Figure A2. 8. ^{1}H NMR (400 MHz, CDCl$_3$) of compound **(6)**.
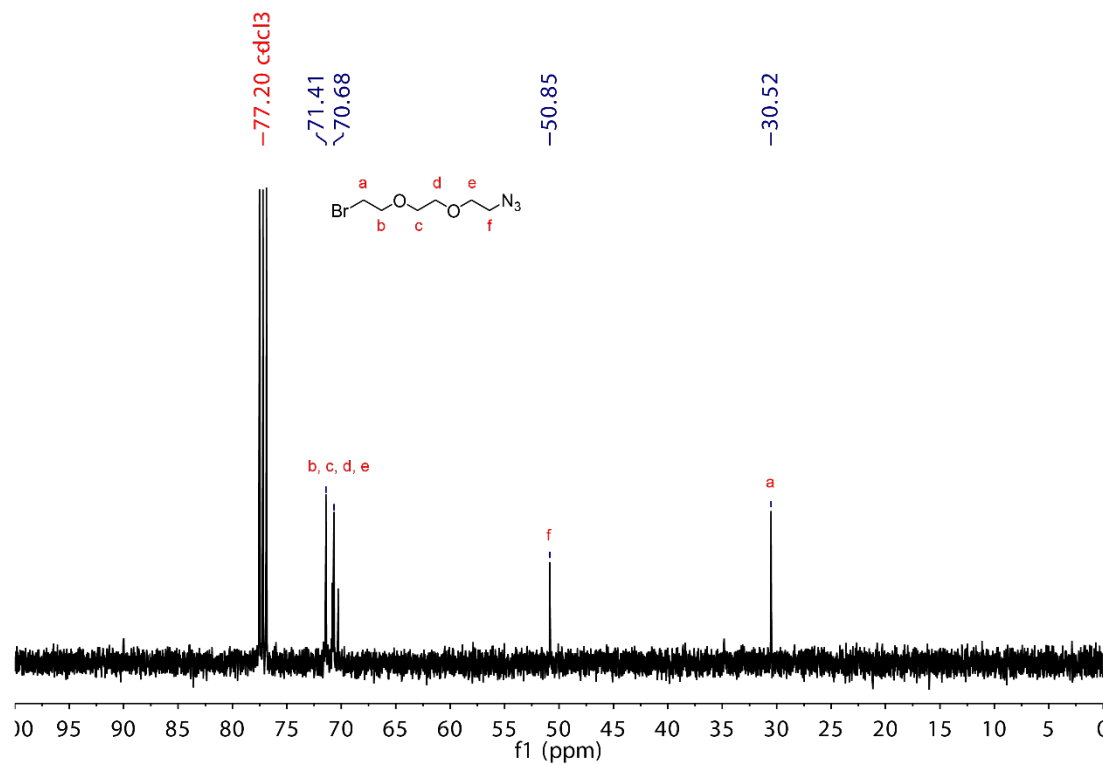
Figure A2. 9. ^{13}C NMR (400 MHz, CDCl$_3$) of compound **(6)**.

Synthesis of Linker 2 (Compound 9)
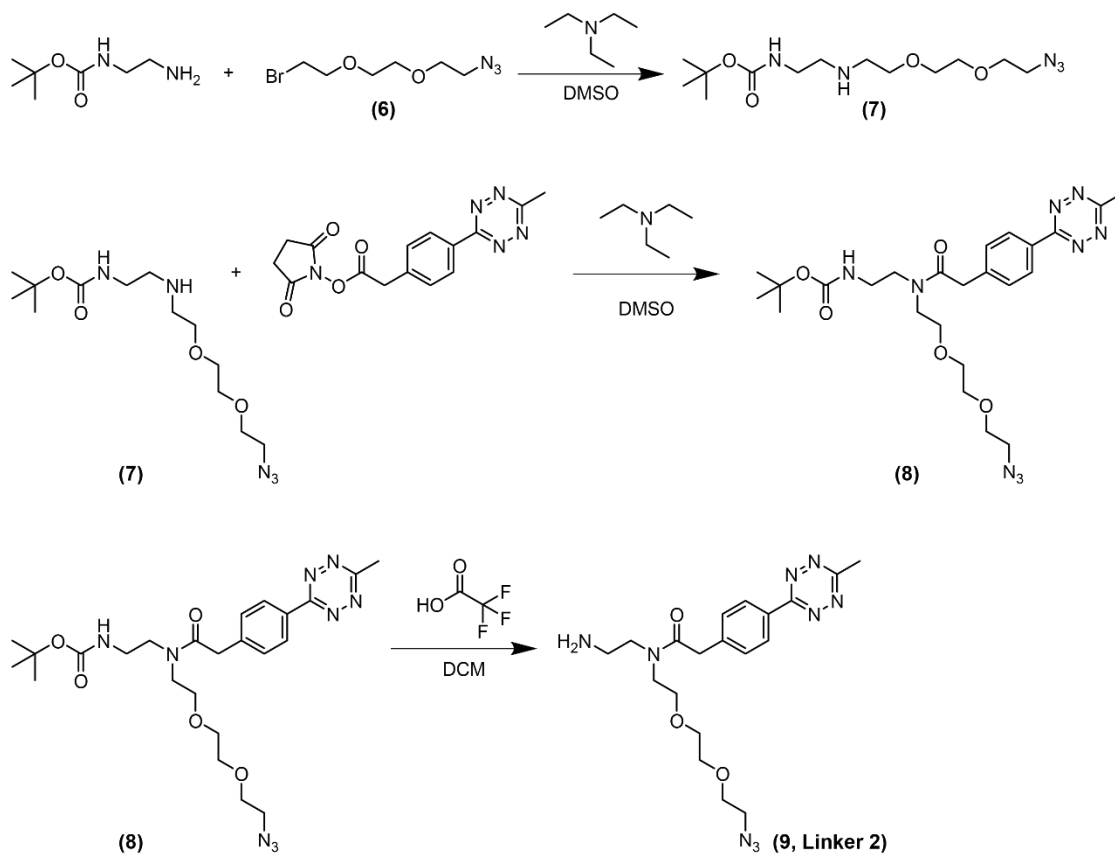
Figure A2. 10. Synthesis scheme for Linker 2.
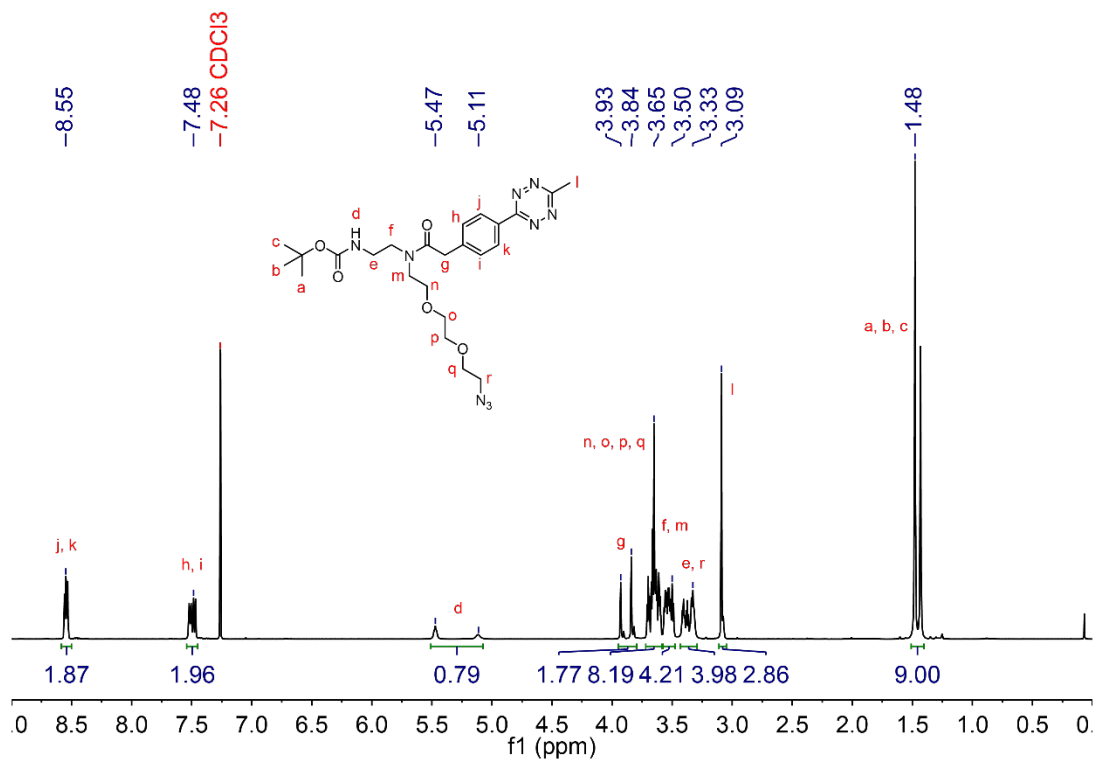
Figure A2. 11. ^{1}H NMR (500 MHz, CDCl$_3$) of compound **(8)**.
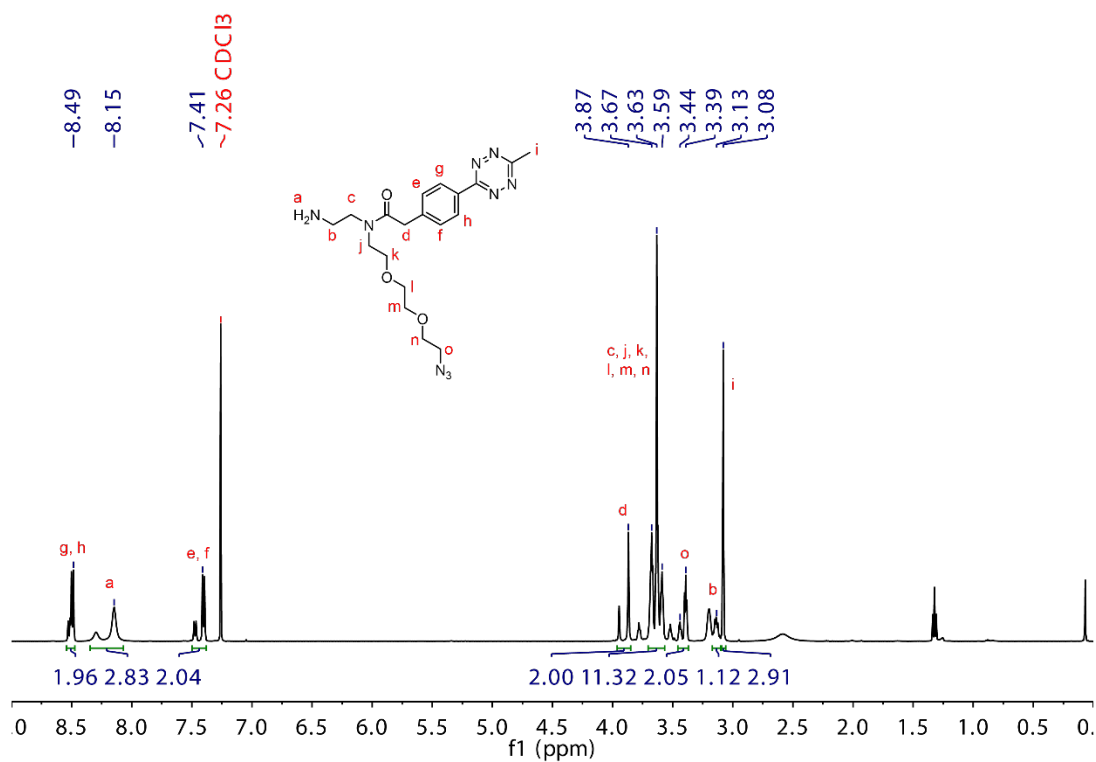
Figure A2. 12. ^{1}H NMR (500 MHz, CDCl$_3$) of compound **(9)**.
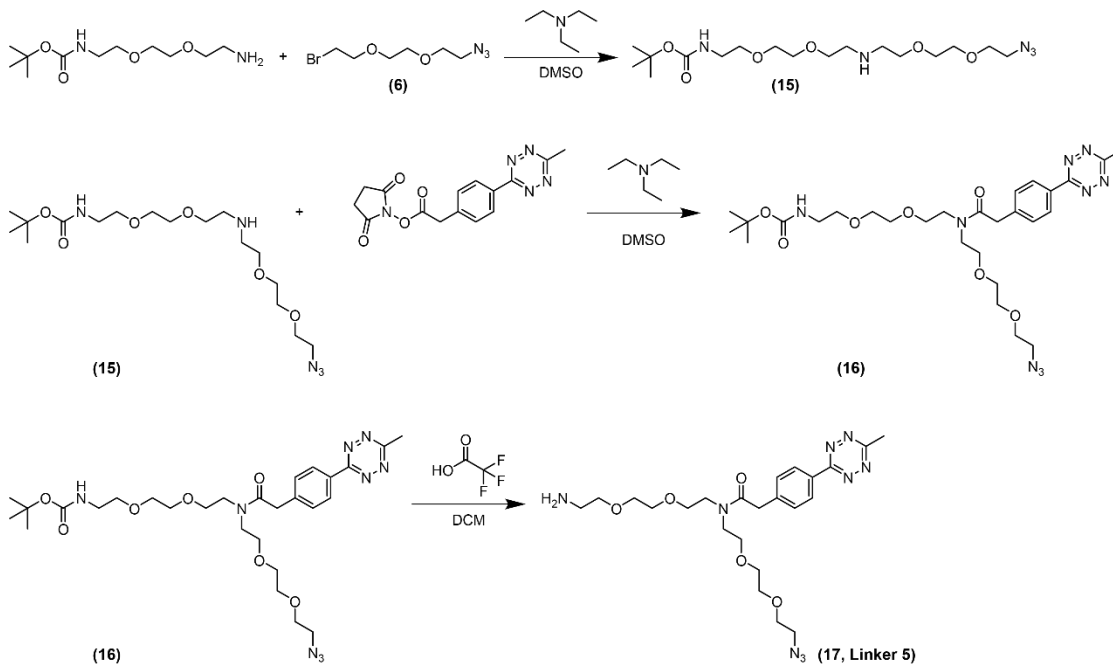
Synthesis of Linker 3 (Compound 11)

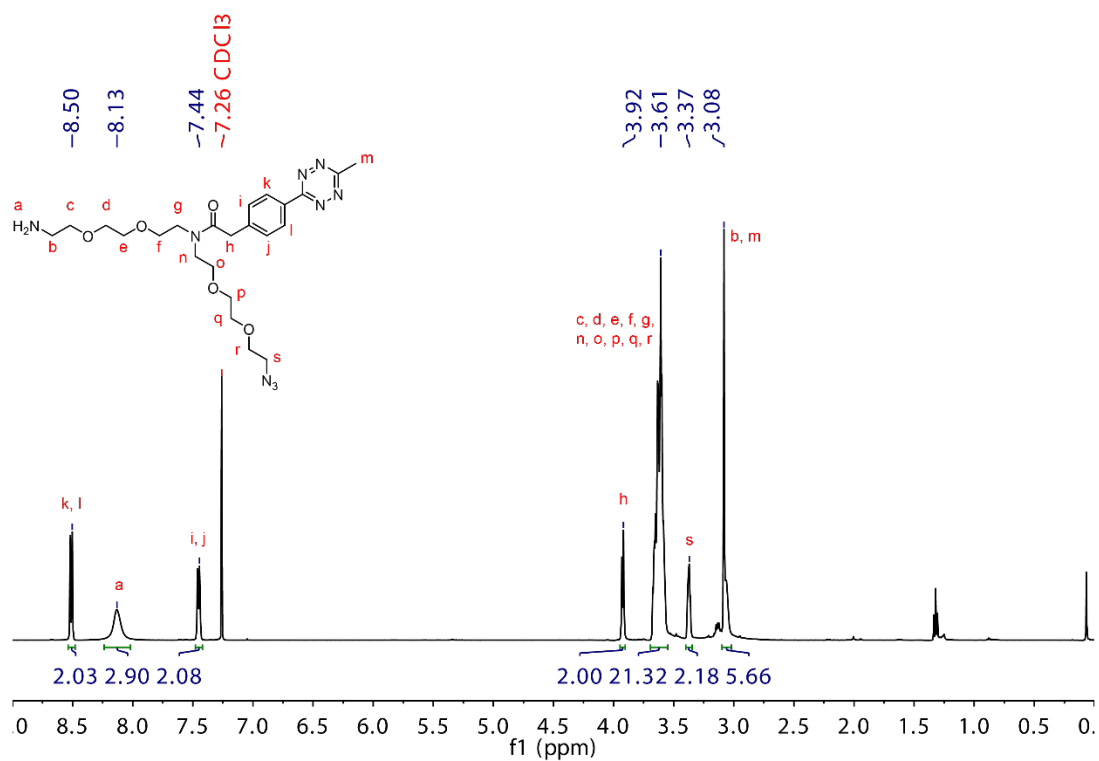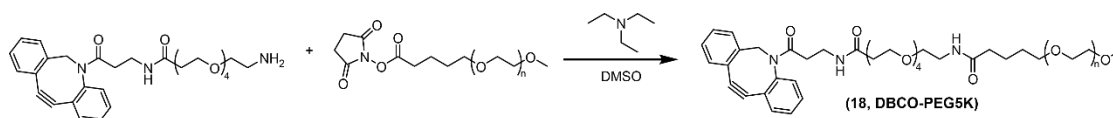**Figure A2. 13.** Synthesis scheme for Linker 3.

Figure A2. 14. ¹H NMR (500 MHz, CDCl₃) of compound **(10)**.

Figure A2. 15. ^{1}H NMR (500 MHz, CDCl$_3$) of compound **(11)**.

Synthesis of Linker 4 (Compound 14)
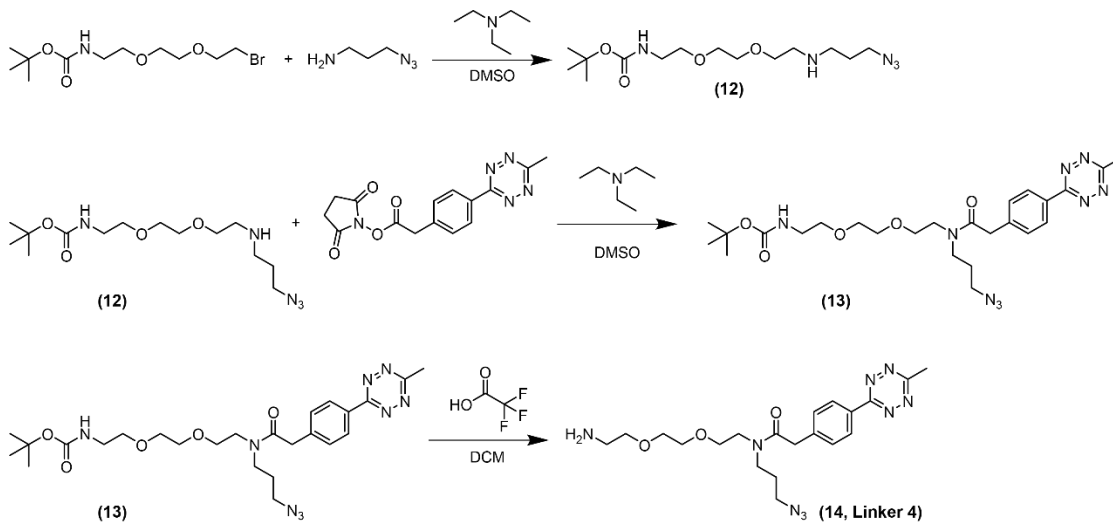
Figure A2. 16. Synthesis scheme for Linker 4.
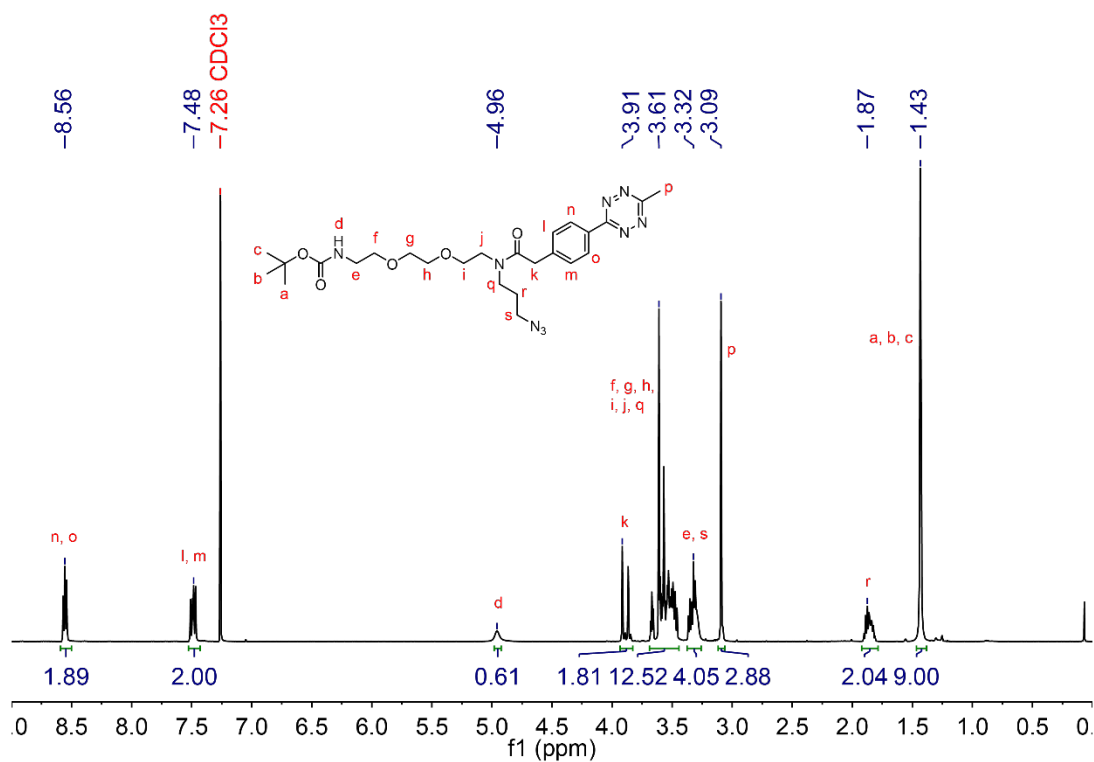
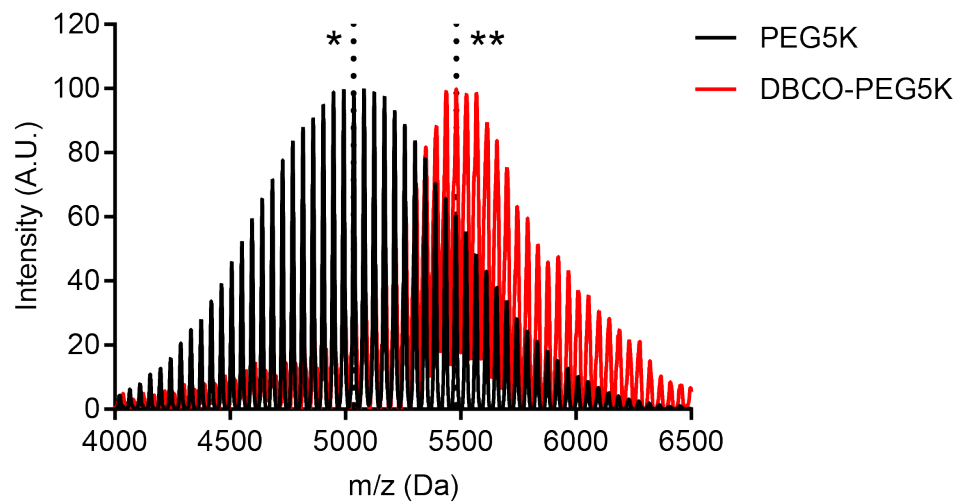**Figure A2. 17.** ¹H NMR (500 MHz, CDCl₃) of compound **(13)**.
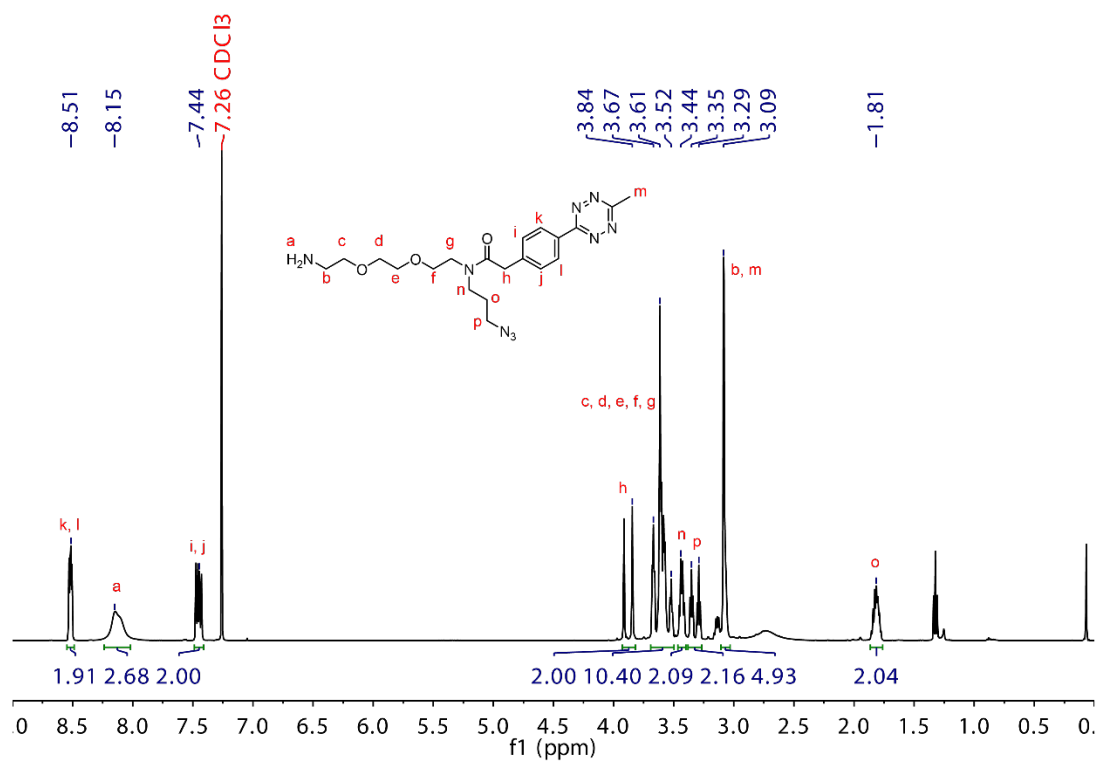
Figure A2. 18. ^{1}H NMR (500 MHz, CDCl$_3$) of compound **(14)**.

Synthesis of Linker 5 (Compound 17)

Figure A2. 19. Synthesis scheme for Linker 5.
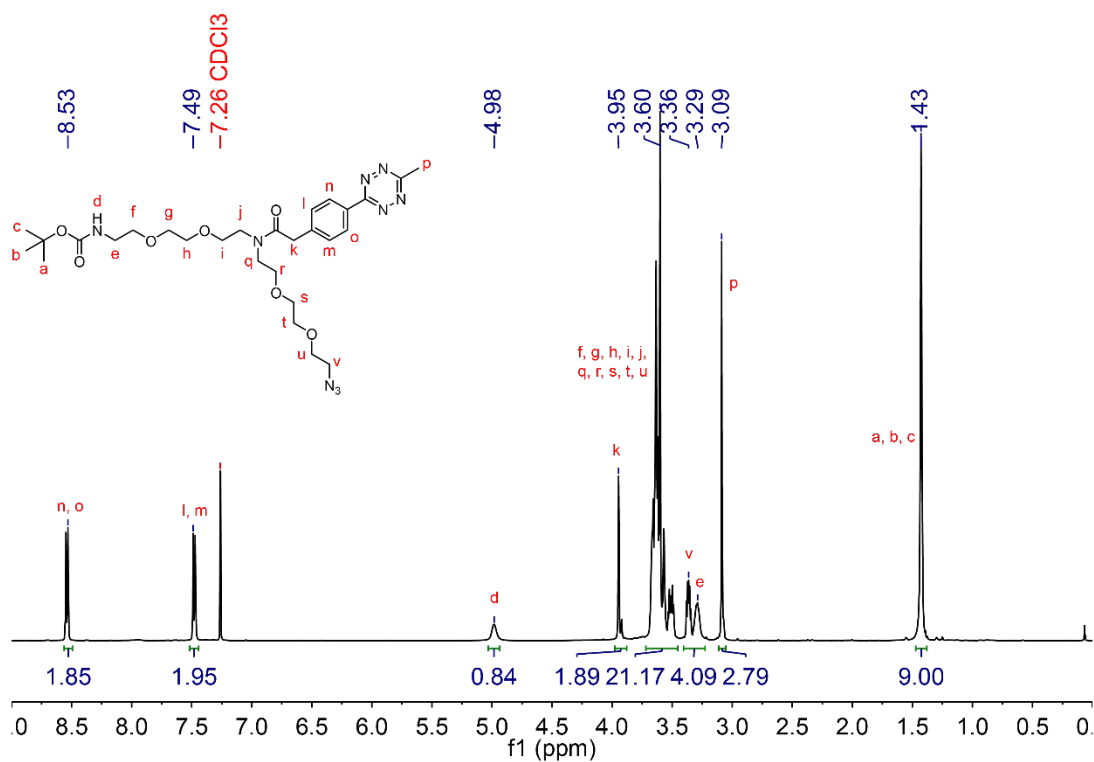
Figure A2. 20. ¹H NMR (500 MHz, CDCl₃) of compound **(16)**.

Figure A2. 21. ^{1}H NMR (500 MHz, CDCl$_3$) of compound **(17)**.

Synthesis of DBCO-PEG5K (Compound 18)

Figure A2. 22. Synthesis scheme for DBCO-PEG5K.

Figure A2. 23. MALDI-MS of compound **(18)**. Center of the distribution for the unmodified PEG5K (*) was at 5,036 Da. Center of the distribution for the DBCO-modified PEG5K (**) was at 5,481 Da. Observed difference: 445 Da, Expected Difference: 408 Da.

Synthesis of TCO-PEG5K (Compound 19)

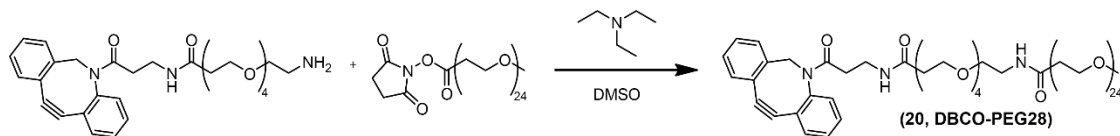**Figure A2. 24.** Synthesis scheme for TCO-PEG5K.

Figure A2. 25. MALDI-MS of compound **(19)**. Center of the distribution for the unmodified PEG5K (*) was at 5,036 Da. Center of the distribution for the TCO-modified PEG5K (**) was at 5,143 Da. Observed difference: 107 Da, Expected Difference: 111 Da.

Synthesis of DBCO-PEG28 (Compound 20)

Figure A2. 26. Synthesis scheme for DBCO-PEG28.

Fragmentation 1 (F1), Exact Mass: 1621.91 Da   Fragmentation 2 (F2), Exact Mass: 205.09 Da
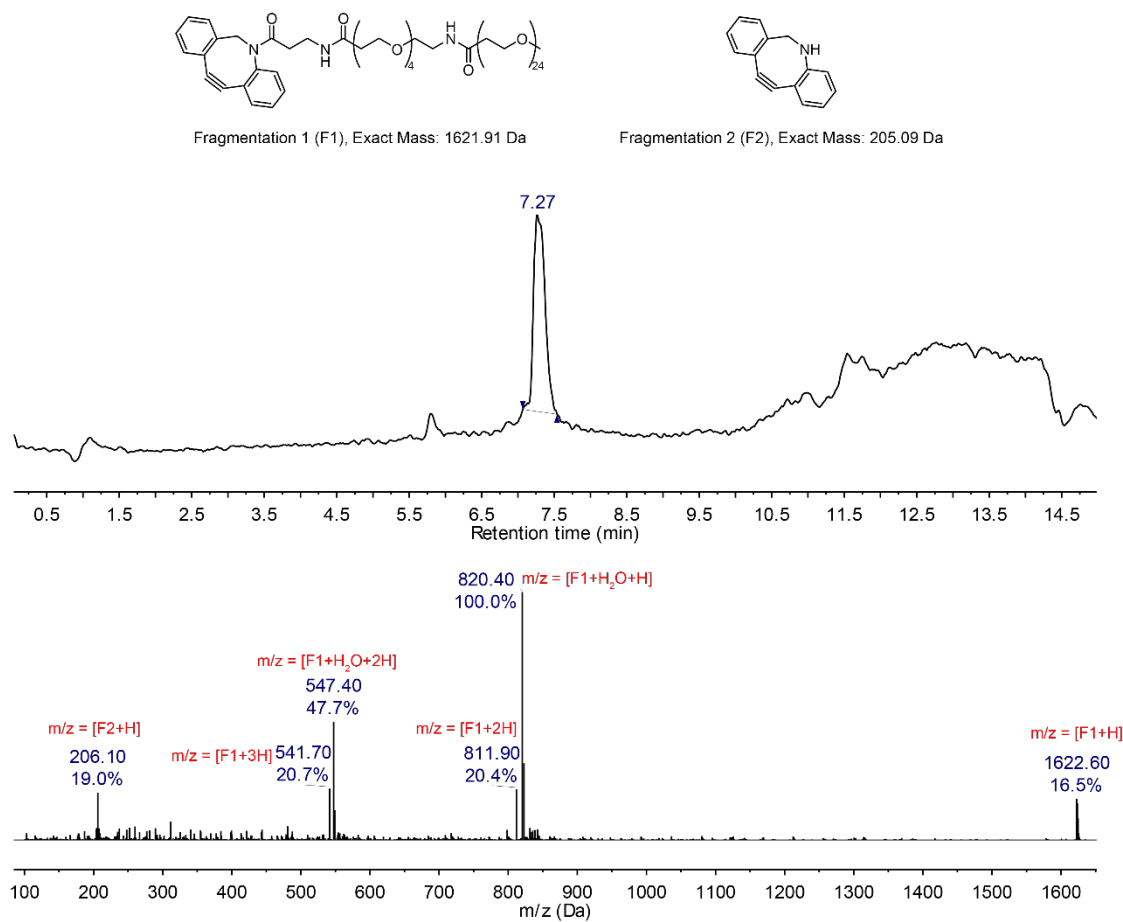
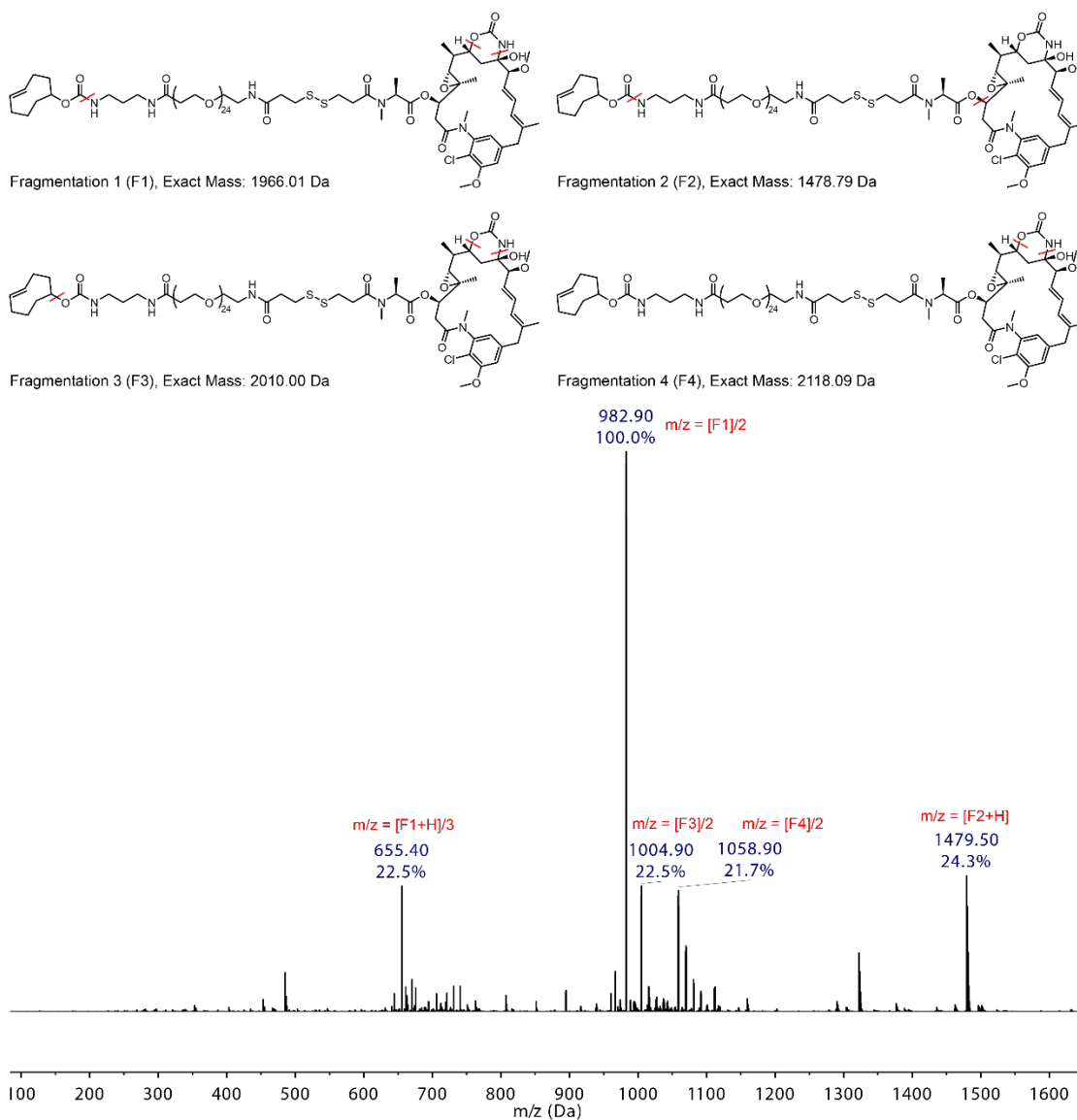**Figure A2. 27.** LC-MS of compound **(20)**.

Synthesis of TCO-PEG24-DM1 (Compound 21)
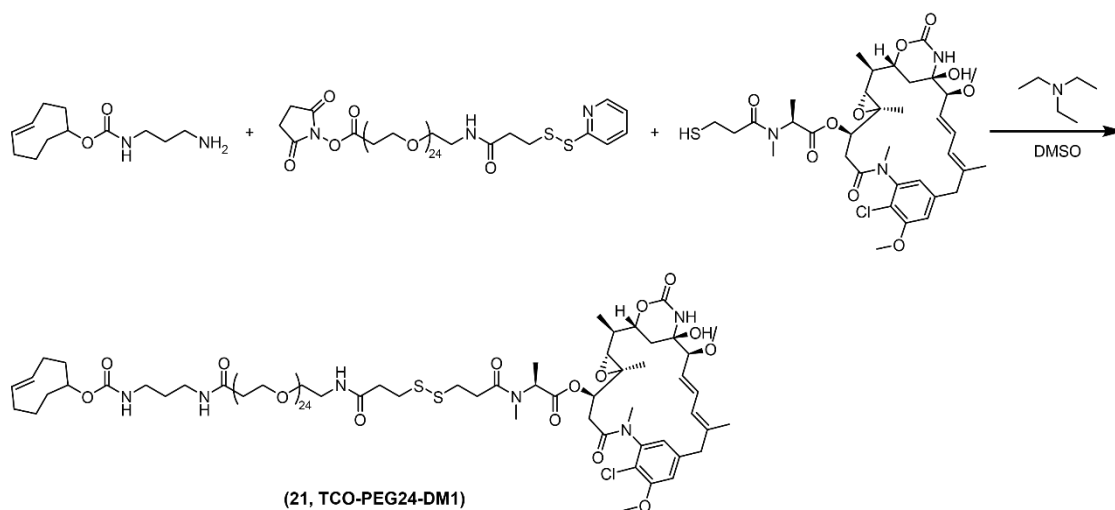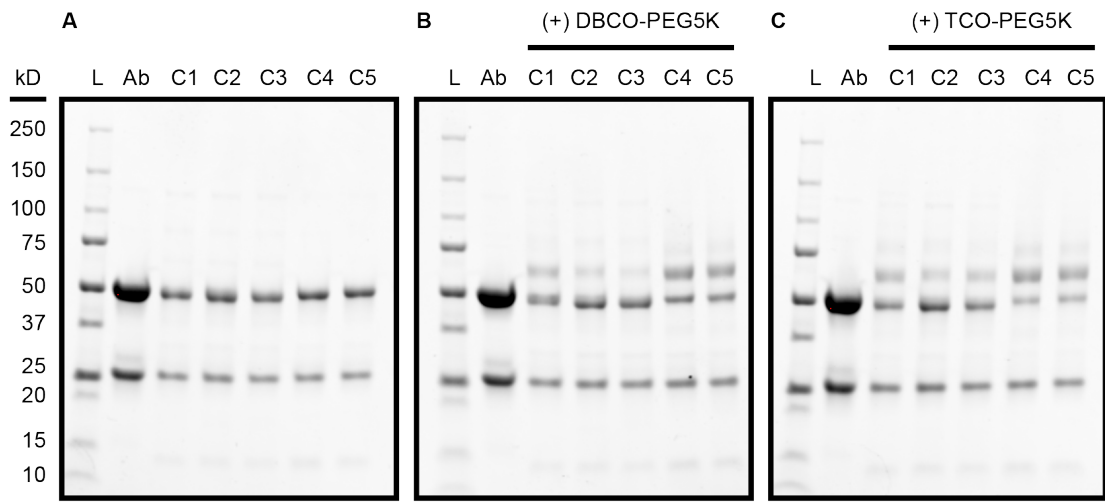

Figure A2. 28. Synthesis scheme for TCO-PEG24-DM1.

Fragmentation 1 (F1), Exact Mass: 1966.01 Da

Fragmentation 2 (F2), Exact Mass: 1478.79 Da

Fragmentation 3 (F3), Exact Mass: 2010.00 Da

Fragmentation 4 (F4), Exact Mass: 2118.09 Da

Figure A2. 29. LC-MS of compound **(21)**.

Expression and Purification of Microbial Transglutaminase

Table A2. 1. Sequencing information for microbial transglutaminase. Underlined text indicates the N-terminal pro-sequence.

	Sequence
Forward Primer (T7)	TAATACGACTCACTATAGGG
Reverse Primer (T7)	GCTAGTTATTGCTCAGCGG
DNA Sequence	<u>ATGGACAATGGCGCGGGGGAAGAGACGAAGTCCTACGCCG</u> <u>AAACCTACCGCCTCACGGCGGATGACGTCGCGAACATCAAC</u> <u>GCGCTCAACGAAAGCGCTCCGGCCGCTTCGAGCGCCGGCC</u> <u>CGTCGTTCCGGGCCCCC</u>GACTCCGACGACAGGGTCACCCC TCCCGCCGAGCCGCTCGACAGGATGCCCGACCCGTACCGT CCCTCGTACGGCAGGGCCGAGACGGTCGTCAACAACTACA TACGCAAGTGGCAGCAGGTCTACAGCCACCGCGACGGCAG GAAGCAGCAGATGACCGAGGAGCAGCGGGAGTGGCTGTCC TACGGCTGCGTCGGTGTCACCTGGGTCAATTCGGGTCAGTA CCCGACGAACAGACTGGCCTTCGCGTCCTTCGACGAGGAC AGGTTCAAGAACGAGCTGAAGAACGGCAGGCCCCGGTCCG GCGAGACGCGGGCGGAGTTCGAGGGCCGCGTCGCGAAGG AGAGCTTCGACGAGGAGAAGGGCTTCCAGCGGGCGCGTGA GGTGGCGTCCGTCATGAACAGGGCCCTGGAGAACGCCCAC GACGAGAGCGCTTACCTCGACAACCTCAAGAAGGAACTGGC GAACGGCAACGACGCCCTGCGCAACGAGGACGCCCGTTCC CCGTTCTACTCGGCGCTGCGGAACACGCCGTCCTTCAAGGA GCGGAACGGAGGCAATCACGACCCGTCCAGGATGAAGGCC GTCATCTACTCGAAGCACTTCTGGAGCGGCCAGGACCGGTC GAGTTCGGCCGACAAGAGGAAGTACGGCGACCCGGACGCC TTCCGCCCCGCCCCGGGCACCGGCCTGGTCGACATGTCGA GGGACAGGAACATTCCGCGCAGCCCCACCAGTCCCGGTGA GGGATTCGTCAATTTCGACTACGGCTGGTTCGGCGCCCAGA CGGAAGCGGACGCCGACAAGACCGTCTGGACCCACGGAAA TCACTATCACGCGCCCAATGGCAGCCTGGGTGCCATGCATG TCTACGAGAGCAAGTTCCGCAACTGGTCCGAGGGTTACTCG GACTTCGACCGCGGAGCCTATGTGATCACCTTCATCCCCAA GAGCTGGAACACCGCCCCCGACAAGGTAAAGCAGGGCTGG CCGCTCGAGCACCACCACCACCACCACTGA
Amino Acid Sequence	<u>MDNGAGEETKSYAETYRLTADDVANINALNESAPAASSAGPSF</u> <u>RAP</u>DSDDRVTPPAEPLDRMPDPYRPSYGRAETVVNNYIRKWQ QVYSHRDGRKQQMTEEQREWLSYGCVGVTWVNSGQYPTNR LAFASFDEDRFKNELKNGRPRSGETRAEFEGRVAKESFDEEK GFQRAREVASVMNRALENAHDESAYLDNLKKELANGNDALRN EDARSPFYSALRNTPSFKERNGGNHDPSRMKAVIYSKHFWSG QDRSSSADKRKYGDPDAFRPAPGTGLVDMSRDRNIPRSPTSP GEGFVNFDYGWFGAQTEADADKTVWTHGNHYHAPNGSLGA MHVYESKFRNWSEGYSDFDRGAYVITFIPKSWNTAPDKVKQG WPLEHHHHHH

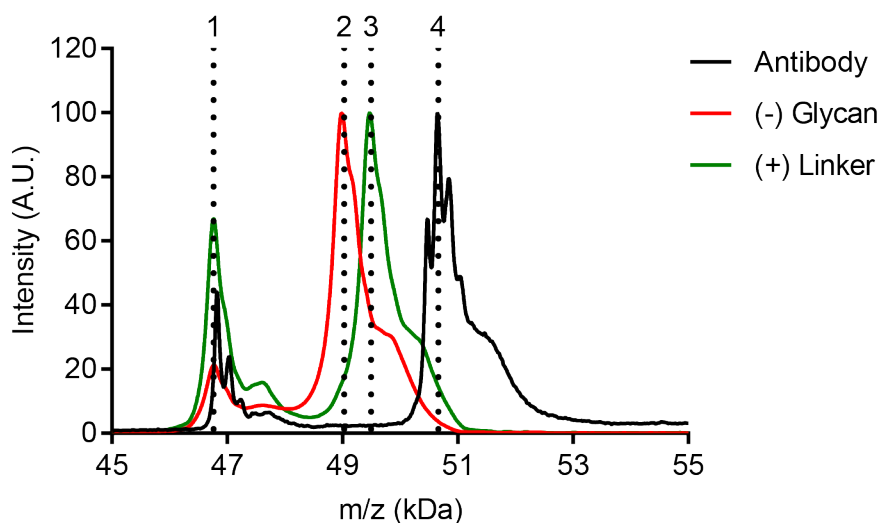**Gel Electrophoresis Analysis of Linker Conjugation Efficiency**

Figure A2. 30. SDS-PAGE analysis of conjugation efficiency. A) Linker-modified trastuzumab, B) Linker-modified trastuzumab reacted with DBCO-PEG5K, C) Linker-modified trastuzumab reacted with TCO-PEG5K.

Large Scale Purification of Conjugate 5
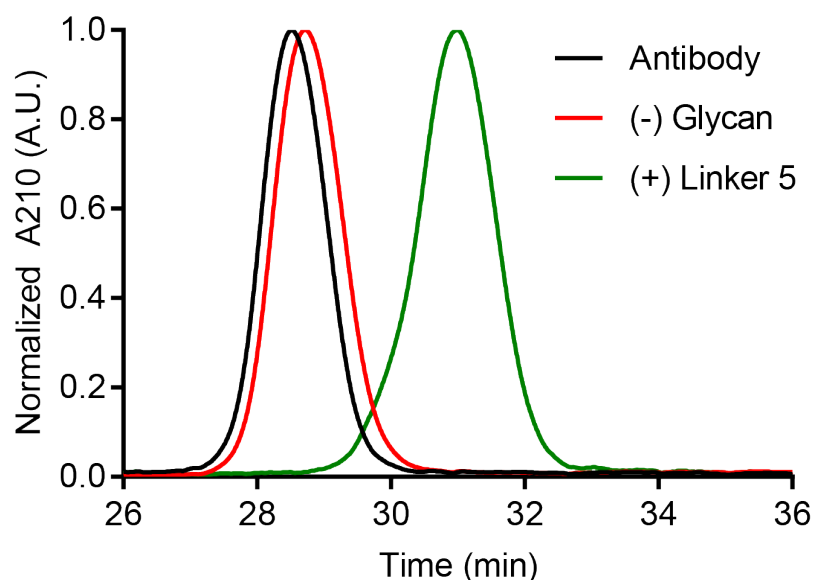
**Figure A2. 31.** HIC analysis of conjugate 5 purity.

Figure A2. 32. MALDI-MS analysis of conjugate 5 molecular weight. Conjugate was reduced before analysis to confirm attachment of linker 5 to the heavy chain of the antibody. A double mass (1) of the light chain was observed at 46,792 Da. The heavy chain of the untreated antibody (4) was observed at 50,651 Da. Upon treatment with PNGase F (2), the aglycosylated heavy chain was observed at 49,021 Da, consistent with loss of a 1,630 Da consistent with removal of the glycan at position 297. Upon treatment with MTG in the presence of linker 5 (3), the linker-modified heavy chain was observed at 49,502 Da, consistent with one addition of linker 5 to the heavy chain. Observed difference: 481 Da, Expected difference: 500 Da.

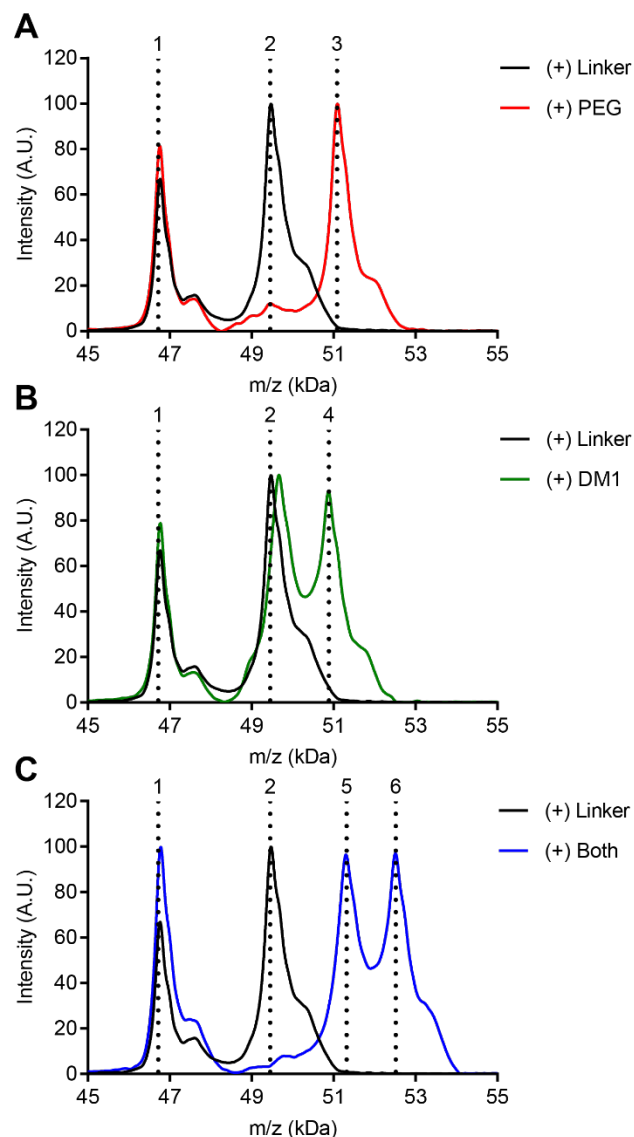**Gel Electrophoresis Analysis of Dual "Click" Modification**
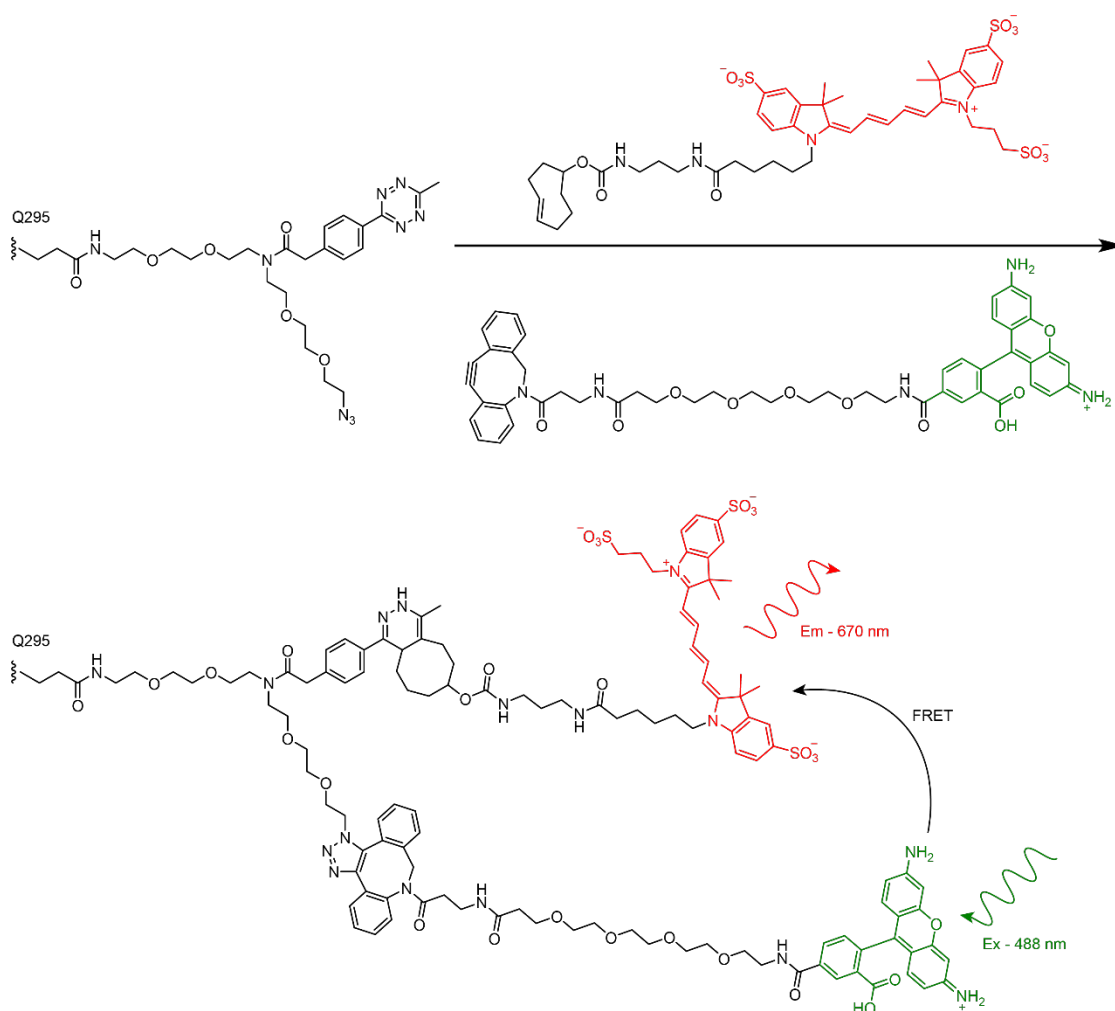
Figure A2. 33. Reaction scheme for dual "click" modification with FRET pair of fluorophores.

**One-pot Synthesis of Antibody-drug Conjugates**
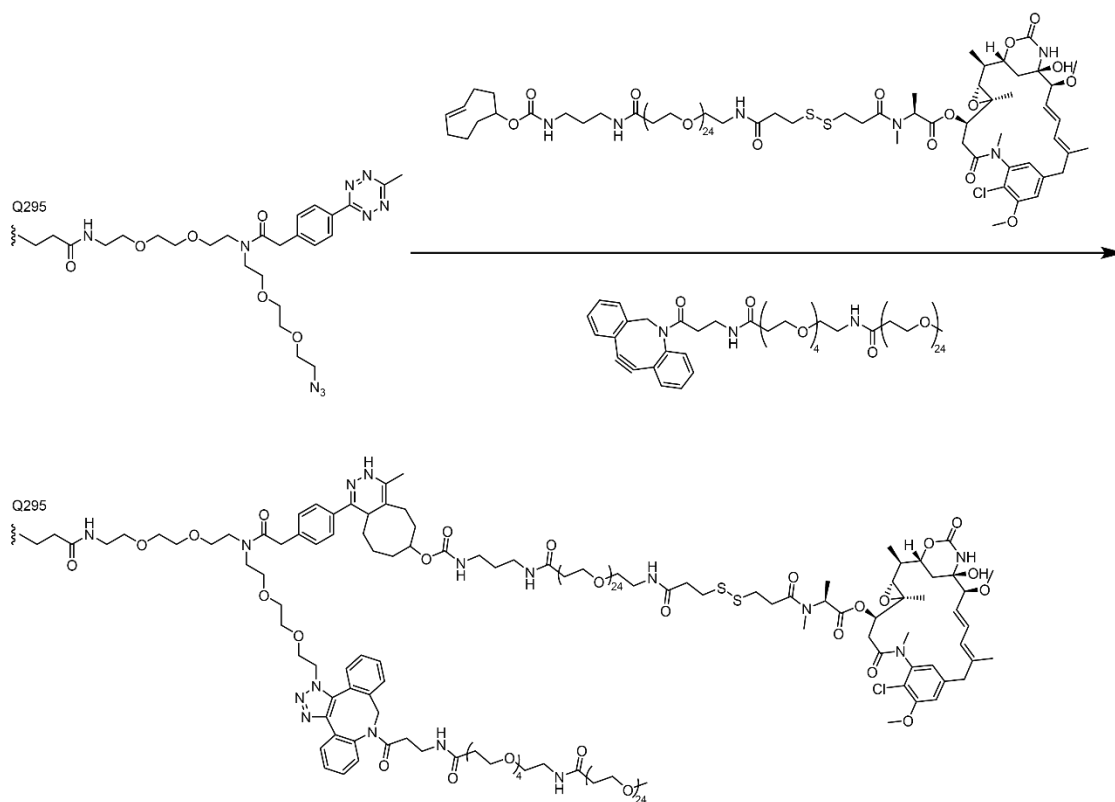
Figure A2. 34. Reaction scheme for dual "click" synthesis of antibody-drug conjugates.

Figure A2. 35. MALDI-MS analysis of antibody-drug conjugate molecular weight. Conjugates were reduced before analysis to confirm attachment to the heavy chain of the antibody. A double mass (1) of the light chain was observed at 46,786 Da in all samples. The heavy chain of the linker 5-modified antibody (2) was observed at 49,502 Da. A) Upon addition of DBCO-PEG28, complete conversion was observed with the modified heavy chain (3) appearing at 51,124 Da; Observed difference: 1,622 Da, Expected difference: 1,622 Da. B) Upon addition of TCO-PEG24-DM1, partial conversion was observed with the modified heavy chain (4) appearing at 50,900 Da; Observed difference: 1,398 Da, Expected difference: 1,414 Da. C) Upon addition of both DBCO-PEG28 and TCO-PEG24-DM1, partial conversion was observed. The first product (5) appeared at 51,331 Da corresponding to addition of DBCO-PEG28 (observed difference: 1829 Da, expected difference: 1622 Da). The second product (6) appeared at 52,536 Da corresponding to addition of both DBCO-PEG28 and TCO-PEG24-DM1 (observed difference 3,034 Da, expected difference: 3,036).

In vitro Potency of Antibody-drug Conjugates
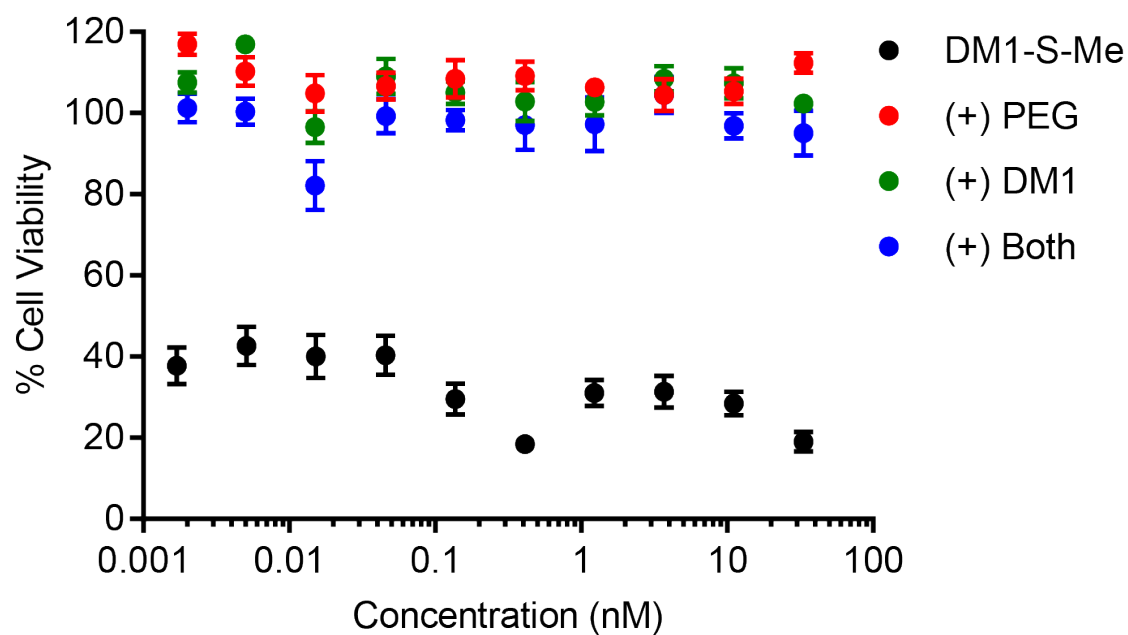
Figure A2. 36. *In vitro* potency of dual "click" antibody-drug conjugates on MCF7 cells, a Her2 negative cell line.

Chapter 2 References

1.Simpson, J. S., Campbell, A. K., Ryall, M. E. & Woodhead, J. S. A stable chemiluminescent-labelled antibody for immunological assays. *Nature* **279,** 646–647 (1979).

2.Tillberg, P. W. *et al.* Protein-retention expansion microscopy of cells and tissues labeled using standard fluorescent proteins and antibodies. *Nat Biotechnol* **34,** 987–992 (2016).

3.van Buggenum, J. A. G. L. *et al.* A covalent and cleavable antibody-DNA conjugation strategy for sensitive protein detection via immuno-PCR. *Scientific reports* **6,** 22675 (2016).

4.Atreya, R. *et al.* In vivo imaging using fluorescent antibodies to tumor necrosis factor predicts therapeutic response in Crohn's disease. *Nature medicine* **20,** 313–318 (2014).

5.Zeglis, B. M. *et al.* Enzyme-mediated methodology for the site-specific radiolabeling of antibodies based on catalyst-free click chemistry. *Bioconjugate Chemistry* **24,** 1057–1067 (2013).

6.Lehar, S. M. *et al.* Novel antibody-antibiotic conjugate eliminates intracellular S. aureus. *Nature* **527,** 323–328 (2015).

7.Lyon, R. P. *et al.* Reducing hydrophobicity of homogeneous antibody-drug conjugates improves pharmacokinetics and therapeutic index. *Nat Biotechnol* **33,** 733–735 (2015).

8.Burke, P. J. *et al.* Development of Novel Quaternary Ammonium Linkers for Antibody-Drug Conjugates. *Mol Cancer Ther* **15,** 938–945 (2016).

9.Kumar, P. *et al.* T cell-specific siRNA delivery suppresses HIV-1 infection in humanized mice. *Cell* **134,** 577–586 (2008).

10. Song, E. *et al.* Antibody mediated in vivo delivery of small interfering RNAs via cell-surface receptors. *Nat Biotechnol* **23,** 709–717 (2005).

11. Adumeau, P. *et al.* Site-Specifically Labeled Antibody-Drug Conjugate for Simultaneous Therapy and ImmunoPET. *Molecular pharmaceutics* **15,** 892–898 (2018).

12. Kazane, S. A. *et al.* Site-specific DNA-antibody conjugates for specific and sensitive immuno-PCR. *Proc Natl Acad Sci USA* **109,** 3731–3736 (2012).

13. Strop, P. *et al.* Location matters: site of conjugation modulates stability and pharmacokinetics of antibody drug conjugates. *Chem Biol* **20,** 161–167 (2013).

14. Drake, P. M. *et al.* Aldehyde tag coupled with HIPS chemistry enables the production of ADCs conjugated site-specifically to different antibody regions with distinct in vivo efficacy and PK outcomes. *Bioconjugate Chemistry* **25,** 1331–1341 (2014).

15. Huang, B. C. B. *et al.* Antibody-drug conjugate library prepared by scanning insertion of the aldehyde tag into IgG1 constant regions. *MAbs* **10,** 1182–1189 (2018).

16. Ohri, R. *et al.* High-Throughput Cysteine Scanning To Identify Stable Antibody Conjugation Sites for Maleimide- and Disulfide-Based Linkers. *Bioconjugate Chemistry* **29,** 473–485 (2018).

17. Bhakta, S., Raab, H. & Junutula, J. R. Engineering THIOMABs for site-specific conjugation of thiol-reactive linkers. *Methods Mol Biol* **1045,** 189–203 (2013).

18. Cuellar, T. L. *et al.* Systematic evaluation of antibody-mediated siRNA delivery using an industrial platform of THIOMAB-siRNA conjugates. *Nucleic Acids Res* **43,** 1189–1203 (2014).

19. Tian, F. *et al.* A general approach to site-specific antibody drug conjugates. *Proc Natl Acad Sci USA* **111,** 1766–1771 (2014).

20. Axup, J. Y. *et al.* Synthesis of site-specific antibody-drug conjugates using unnatural amino acids. *Proc Natl Acad Sci USA* **109,** 16101–16106 (2012).

21. Harmand, T. J. *et al.* One-Pot Dual Labeling of IgG 1 and Preparation of C-to-C Fusion Proteins Through a Combination of Sortase A and Butelase 1. *Bioconjugate Chemistry* **29,** 3245–3249 (2018).

22. Rabuka, D. Chemoenzymatic methods for site-specific protein modification. *Curr Opin Chem Biol* **14,** 790–796 (2010).

23. Lyon, R. P. *et al.* Self-hydrolyzing maleimides improve the stability and pharmacological properties of antibody-drug conjugates. *Nat Biotechnol* **32,** 1059–1062 (2014).

24. Nunes, J. P. M. *et al.* Functional native disulfide bridging enables delivery of a potent, stable and targeted antibody-drug conjugate (ADC). *Chem Commun (Camb)* **51,** 10624–10627 (2015).

25. Badescu, G. *et al.* Bridging disulfides for stable and defined antibody drug conjugates. *Bioconjugate Chemistry* **25,** 1124–1136 (2014).

26. Tang, F., Wang, L.-X. & Huang, W. Chemoenzymatic synthesis of glycoengineered IgG antibodies and glycosite-specific antibody-drug conjugates. *Nature protocols* **12,** 1702–1721 (2017).

27. Zhou, Q. *et al.* Site-specific antibody-drug conjugation through glycoengineering. *Bioconjugate Chemistry* **25,** 510–520 (2014).

28. Anami, Y. *et al.* Enzymatic conjugation using branched linkers for constructing homogeneous antibody-drug conjugates with high potency. *Org Biomol Chem* **15,** 5635–5642 (2017).

29.Dennler, P. *et al.* Transglutaminase-based chemo-enzymatic conjugation approach yields homogeneous antibody-drug conjugates. *Bioconjugate Chemistry* **25,** 569–578 (2014).

30.Jeger, S. *et al.* Site-specific and stoichiometric modification of antibodies by bacterial transglutaminase. *Angew Chem Int Ed Engl* **49,** 9995–9997 (2010).

31.Junutula, J. R. *et al.* Rapid identification of reactive cysteine residues for site-specific labeling of antibody-Fabs. *J Immunol Methods* **332,** 41–52 (2008).

32.Junutula, J. R. *et al.* Site-specific conjugation of a cytotoxic drug to an antibody improves the therapeutic index. *Nat Biotechnol* **26,** 925–932 (2008).

33.Zimmerman, E. S. *et al.* Production of site-specific antibody-drug conjugates using optimized non-natural amino acids in a cell-free expression system. *Bioconjugate Chemistry* **25,** 351–361 (2014).

34.Levengood, M. R. *et al.* Orthogonal Cysteine Protection Enables Homogeneous Multi-Drug Antibody-Drug Conjugates. *Angew Chem Int Ed Engl* **56,** 733–737 (2016).

35.Maruani, A. *et al.* A plug-and-play approach to antibody-based therapeutics via a chemoselective dual click strategy. *Nat Commun* **6,** 6645 (2015).

36.Knall, A.-C. & Slugovc, C. Inverse electron demand Diels-Alder (iEDDA)-initiated conjugation: a (high) potential click chemistry scheme. *Chemical Society Reviews* **42,** 5131–5142 (2013).

37.Karver, M. R., Weissleder, R. & Hilderbrand, S. A. Bioorthogonal reaction pairs enable simultaneous, selective, multi-target imaging. *Angew Chem Int Ed Engl* **51,** 920–922 (2011).

38.Strop, P. Versatility of microbial transglutaminase. *Bioconjugate Chemistry* **25,** 855–862 (2014).

39. Rachel, N. M. & Pelletier, J. N. Biotechnological applications of transglutaminases. *Biomolecules* **3,** 870–888 (2013).

40. Farias, S. E. *et al.* Mass spectrometric characterization of transglutaminase based site-specific antibody-drug conjugates. *Bioconjugate Chemistry* **25,** 240–250 (2014).

41. Anami, Y. *et al.* Glutamic acid-valine-citrulline linkers ensure stability and efficacy of antibody-drug conjugates in mice. *Nat Commun* **9,** 2512 (2018).

42. Gundersen, M. T., Keillor, J. W. & Pelletier, J. N. Microbial transglutaminase displays broad acyl-acceptor substrate specificity. *Appl Microbiol Biotechnol* **98,** 219–230 (2013).

43. Beck, A., Goetsch, L., Dumontet, C. & Corvaïa, N. Strategies and challenges for the next generation of antibody-drug conjugates. *Nat Rev Drug Discov* **16,** 315–337 (2017).

44. Dodev, T. S. *et al.* A tool kit for rapid cloning and expression of recombinant antibodies. *Scientific reports* **4,** 5885 (2014).

45. Yu, S.-F. *et al.* A Novel Anti-CD22 Anthracycline-Based Antibody-Drug Conjugate (ADC) That Overcomes Resistance to Auristatin-Based ADCs. *Clin Cancer Res* **21,** 3298–3306 (2015).

46. Shefet-Carasso, L. & Benhar, I. Antibody-targeted drugs and drug resistance--challenges and solutions. *Drug Resist Updat* **18,** 36–46 (2014).

47. Loganzo, F. *et al.* Tumor cells chronically treated with a trastuzumab-maytansinoid antibody-drug conjugate develop varied resistance mechanisms but respond to alternate treatments. *Mol Cancer Ther* **14,** 952–963 (2015).

48. Collins, D. M., Bossenmaier, B., Kollmorgen, G. & Niederfellner, G. Acquired Resistance to Antibody-Drug Conjugates. *Cancers (Basel)* **11,** (2019).

49. Loganzo, F., Sung, M. & Gerber, H.-P. Mechanisms of Resistance to Antibody-Drug Conjugates. *Mol Cancer Ther* **15,** 2825–2834 (2016).

50. Burke, P. J. *et al.* Optimization of a PEGylated Glucuronide-Monomethylauristatin E Linker for Antibody-Drug Conjugates. *Mol Cancer Ther* **16,** 116–123 (2016).

51. Lambert, J. M. & Chari, R. V. J. Ado-trastuzumab Emtansine (T-DM1): an antibody-drug conjugate (ADC) for HER2-positive breast cancer. *J Med Chem* **57,** 6949–6964 (2014).

52. Li, J. Y. *et al.* A Biparatopic HER2-Targeting Antibody-Drug Conjugate Induces Tumor Regression in Primary Models Refractory to or Ineligible for HER2-Targeted Therapy. *Cancer cell* **29,** 117–129 (2016).

53. Zhang, H. *et al.* Therapeutic potential of an anti-HER2 single chain antibody-DM1 conjugates for the treatment of HER2-positive cancer. *Signal Transduct Target Ther* **2,** 17015 (2017).

54. Schindelin, J. *et al.* Fiji: an open-source platform for biological-image analysis. *Nat Methods* **9,** 676–682 (2012).

# Chapter 3 – OligoTEA-based Substrates for Microbial Transglutaminase

3.1 – Background

Microbial transglutaminase (MTG) belongs to a family of enzymes that catalyze the formation of interprotein isopeptide bonds between glutamine and lysine residues[1,2]. MTG recognizes glutamine 295 (Q295) within the heavy chain of aglycosylated, human IgGs[3]. Co-treatment with Peptide:N-glycosidase F (PNGase F) removes the N-linked glycan at asparagine 297 (N297) and facilitates efficient bioconjugation[4]. By supplying non-natural acyl acceptor substrates, this natural function has been co-opted for site-specific, homofunctional antibody modification[5,6]. We have built on this work to design heterofunctional MTG substrates that contain both azide and methyltetrazine (mTz) functional groups. An iterative methodology for substrate synthesis, could be used to further elaborate on this work. This could enable the design of complex, heteromultifunctional antibody conjugates containing a host of functional handles, reporter molecules, and stimuli-responsive moieties that would find use in a wide range of biological applications.

We sought to adapt the oligoTEA synthesis methodology developed in our lab for the synthesis of heteromultifunctional MTG substrates. Traditional oligoTEA synthesis utilizes an orthogonally reactive *N*-allylacrylamide monomer, which can undergo alternating photoinitiated thiol−ene "click" reactions and phosphine catalyzed thiol-Michael additions[7]. OligoTEAs are built off a fluorous tag liquid support, which enables stepwise fluorous purification throughout synthesis. The fluorous purification handle is removed post synthesis by acid-catalyzed Boc deprotection. However, in this work, we employed the support-free synthesis methodology described in chapter 4 of this dissertation, "Effect of Cross-linker Sequence on Biophysical Properties of Antibody-drug Conjugates."

.3.2 – Results and Discussion

Herein, we describe our work towards elucidating structure-function relationsships for oligoTEA-based MTG substrates. These substrates, containing both azide and mTz functional handles, are functional mimetics of the substrates described in chapter 2 of this dissertation, "Site-specific Dual "Click" Modification of Native Antibodies via Microbial Transglutaminase".
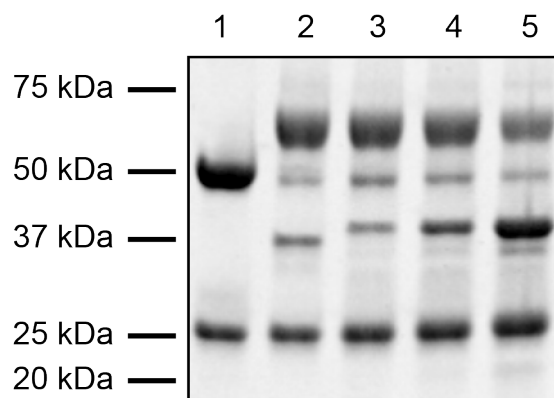
Figure 3.1. Validation of recombinant microbial transglutaminase activity. 4 – 20% Tris/Glycine Gel, 120 V for 60 minutes. Substrate: Aizde-PEG3-Amine. Lane 1: antibody control; Lane 2: 0.75 equivalencies of commercially available MTG; Lane 3: 0.75 equivalencies of recombinant MTG; Lane 4: 1.5 equivalencies of recombinant MTG; Lane 5: 3.0 equivalencies of recombinant MTG.

We first sought to validate the activity of recombinant MTG produced in our lab compared to a commercial source of MTG (**Figure 3.1**). The activity of recombinant MTG was determined using a control substrate, Azide-PEG3-Amine. Conjugation efficiency was measured via subsequent conjugation to a 5 kDa, DBCO-modified polyethylene glycol (PEG) chain (DBCO-PEG5K). Relative activity was determined by comparing conjugation efficiency at an equimolar condition (lane 2 and lane 3) as well as 2-fold (lane 4) and 4-fold (lane 5) more MTG. This experiment demonstrated that recombinant MTG produced in our lab had equal activity to that of the commercial source on a per mole basis.
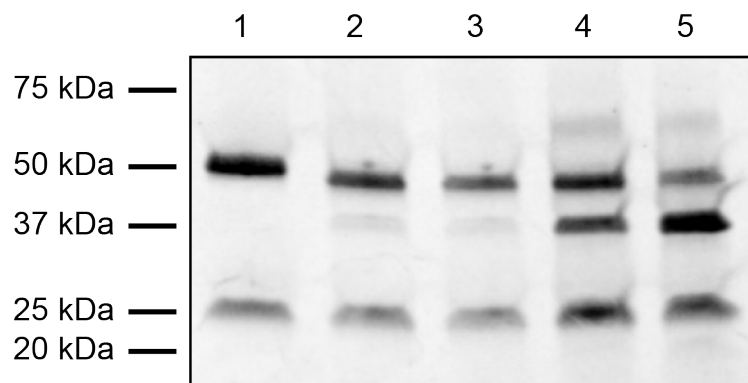
Figure 3.2. Conjugation efficiency of compound 5. 4 – 20% Tris/Glycine Gel, 120 V for 60 minutes. Antibody concentration for MTG reaction: 0.25 mg/mL. Conjugation: DBCO-PEG5K. Lane 1: antibody control; Lane 2: 0.75 equivalencies MTG, 80 equivalencies substrate; Lane 3: 0.75 equivalencies MTG, 160 equivalencies substrate; Lane 4: 3.0 equivalencies MTG, 80 equivalencies substrate; Lane 5: 3.0 equivalencies MTG, 160 equivalencies substrate.

We then tested the conjugation efficiency of compound 5 (**Figure 3.2**). Compound 5 exhibited poor solubility in PBS, pH 7.4. Therefore, conjugation was carried out at an antibody concentration of 0.25 mg/mL; 4-fold lower than the standard reaction condition. The effects of substrate (1-fold compared to 2-fold) and MTG (1-fold compared to 4-fold) equivalencies were investigated. Subsequent conjugation to DBCO-PEG5K was used as a readout of conjugation efficiency. This experiment demonstrated that increasing the equivalencies of MTG leads to a modest increase in conjugation efficiency. However, none of the tested conditions yielded efficient conjugation. From this result, we suspected that efficient MTG conjugation was at least in part concentration limited. Therefore, we aimed to increase the hydrophilic character of the oligoTEA-based substrate.
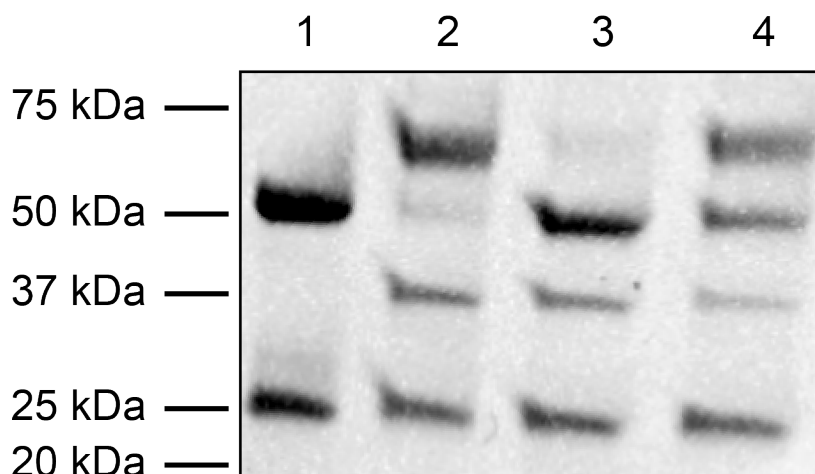
Figure 3.3. Conjugation efficiency of compound 3 and compound 8. 4 – 20% Tris/Glycine Gel, 120 V for 60 minutes. Lane 1: antibody control; Lane 2: Azide-PEG3-Amine; Lane 3: compound 3; Lane 4: compound 8.

To explore the relative importance of reaction concentration and substrate structure, we tested the conjugation efficiency of compound 3 and compound 8 (**Figure 3.3**). Compound 3 (lane 3) is a monofunctional version of compound 5 in which the mTz functional handle has been replaced by a carboxylic acid. This modification greatly improved the aqueous solubility of the substrate and enabled conjugation to take place at the standard reaction condition of 1 mg/mL. Compound 8 (lane 4) is functionally equivalent to compound 3. However, the (2,2')-ethylenedioxydiethanethiol spacer has been replaced by a more hydrophilic L-dithiothreitol spacer. Compound 8 also exhibit excellent aqueous solubility. The conjugation of these substrates was compared to a control substrate; Azide-PEG3-Amine (lane 2). Subsequent conjugation to DBCO-PEG5K was used as a readout of conjugation efficiency. This experiment demonstrated that reaction concentration alone is not enough to drive efficient MTG-based conjugation. As expected, the control substrate showed nearly complete conjugation. Compound 3 demonstrated poor conjugation efficiency, potentially indicating that the (2,2')-ethylenedioxydiethanethiol spacer alpha to the primary amine is incompatible

with MTG conjugation. Compound 8 demonstrated efficient conjugation, albeit less efficiently than the control substrate. This data indicated that there is a structural component to designing efficient MTG substrates. Compound 8 was taken as the optimal scaffold for developing a multifunctional substrate.
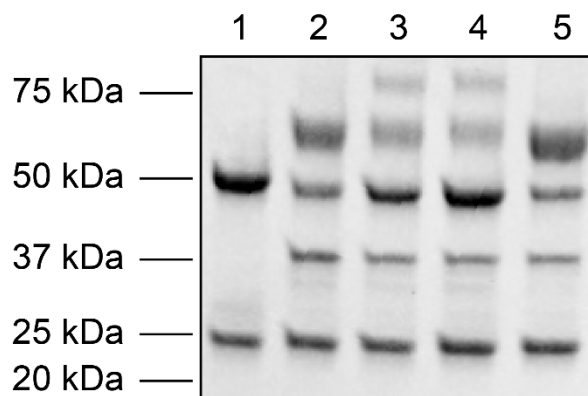
Figure 3.4. Conjugation efficiency of compound 10 and compound 12. 4 – 20% Tris/Glycine Gel, 120 V for 60 minutes. Lane 1: antibody control; Lane 2: compound 8, conjugation with DBCO-PEG5K; Lane 3: compound 10, conjugation with DBCO-PEG5K; Lane 4: compound 12, conjugation with DBCO-PEG5K; Lane 5: mTz-PEG4-Amine, conjugation with TCO-PEG5K.

Compound 8 was used to synthesize two multifunctional MTG substrates. The conjugate efficiency of these substrates, compound 10 and compound 12, was tested (**Figure 3.4**). To synthesize compound 10, mTz-Amine was coupled to the free carboxylic acid of compound 8. To synthesize compound 12, mTz-PEG4-Amine was coupled to the free carboxylic acid of compound 8. Two control substrates, Azide-PEG3-Amine and mTz-PEG4-Amine were used to evaluate conjugation efficiency. Subsequent conjugation to DBCO-PEG5K was used to monitor the conjugation efficiency of Azide-PEG3-Amine, compound 10, and compound 12. Conjugation to TCO-PEG5K was used to monitor the conjugation efficiency of mTz-PEG4-Amine. As expected, this experiment demonstrated that both control substrates, Azide-PEG3-Amine (lane 2) and mTz-PEG4-Amine (lane 5), conjugated with high efficiency. Meanwhile, compound 10 (lane 3) and compound 12 (lane 4) conjugated with slightly

lower efficiency. Interestingly, both compound 10 and compound 12 showed two higher

molecular weight bands. This was not observed in either of the control substrates. This

could be interpreted to indicate that there are multiple MTG conjugation sites within the

human IgG for compound 10 and compound 12.
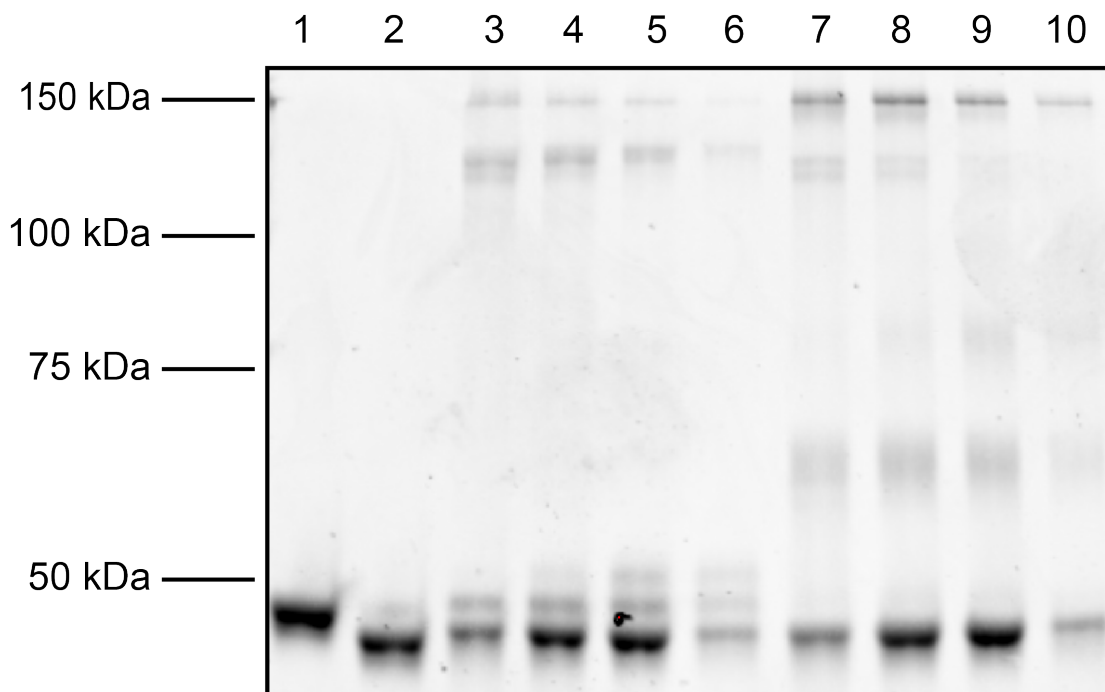
Figure 3.5. Optimization of compound 12 substrate equivalencies. 7.5% Tris/Glycine Gel, 120 V for 80 minutes. Lane 1: antibody control; Lane 2: PNGase F treatment; Lane 3: 4 equivalencies of substrate; Lane 4: 20 equivalencies of substrate; Lane 5: 80 equivalencies of substrate; Lane 6: 160 equivalencies of substrate; Lane 7: 4 equivalencies of substrate, conjugation with DBCO-PEG5K; Lane 8: 20 equivalencies of substrate, conjugation with DBCO-PEG5K; Lane 9: 80 equivalencies of substrate, conjugation with DBCO-PEG5K; Lane 10: 160 equivalencies of substrate, conjugation with DBCO-PEG5K.

Finally, we sought to investigate the source of the banding pattern observed for

compound 10 and compound 12. To this end, we tested the effect of substrate

equivalency on conjugation efficiency (**Figure 3.5**). To determine whether compound

12 could conjugate multiple times to the IgG heavy chain, substrate-modified antibody

was analyzed before (lanes 3 – 6) and after (lanes 7 – 10) conjugation to DBCO-

PEG5K. MTG conjugation was carried out with 4, 20, 80, or 160 equivalencies of

substrate. Treatment of antibody with only PNGase F (lane 2) yielded a decrease in heavy chain molecular weight corresponding to loss of the glycan. Analysis before DBCO-PEG5K conjugation revealed up to two higher molecular weight bands near the parent heavy chain (lanes 3 – 6). This result is evidence for the attachment of up to two substrates per heavy chain, giving in a mixed population overall. Further, as substrate equivalencies were increased, high molecular weight bands between 100 kDa and 150 kDa decreased, highlighting the importance of suppressing antibody-antibody cross-linking. Analysis after DBCO-PEG5K conjugation (lanes 7 – 10) revealed the expected trends. The bands near the parent heavy chain band disappeared. This indicated that the strain-promoted azide-alkyne cycloaddition proceeded to completion. As expected, two new bands appeared between 50 kDa and 100 kDa, corresponding to heavy chains species modified once and twice with DBCO-PEG5K. These data confirm that under the tested reaction conditions, compound 12 can access at least to conjugation sites within the heavy chain of the human IgG. This yields a heterogenous mixture of conjugated products, which complicates the use of oligoTEAs as MTG conjugation substrates.

3.3 – Conclusions

In conclusion, we have shown that oligoTEA-based MTG conjugation is sensitive to substrate hydrophobicity and the structure of the dithiol spacer alpha to the terminal primary amine. Substrates should have enough hydrophilic character to solubilize at approximately 500 µM in aqueous buffer. Further, a L-dithiothreitol spacer was found to be more efficient than a (2,2')-ethylenedioxydiethanethiol spacer. Finally, multifunctional substrates containing a L-dithiothreitol spacer were found to access multiple MTG conjugation sites within the heavy chain of the human IgG. This unexpected result was not observed for monofunctional Azide-PEG3-Amine or mTz-

PEG4-Amine substrates under the same reaction conditions. To the best of our knowledge, substrate-based control over the accessibility of MTG conjugation sites has not been reported. This finding warrants additional investigation. Analysis of conjugates of compound 10 or compound 12 via hydrophobic interaction chromatography (HIC) and matrix-assisted laser-desorption ionization-mass spectrometry (MALDI-MS) could confirm the existence to two conjugation sites. Further, proteolytic degradation could be used to identify reactive glutamine residues other than glutamine 295. Determining the precise nature of multisite MTG conjugation is critical to improving the design of oligoTEA-based MTG substrates. This work was an important first step towards designing heteromultifunctional MTG substrates to further expand the toolbox for site-specific antibody modification.

3.4 – Materials and Methods

Reagents for Chemical Synthesis

All chemicals were purchased from MilliporeSigma unless stated otherwise. N-(14-Amino-3,6,9,12-tetraoxatetradec-1-yl)-11,12-didehydro-γ-oxodibenz[b,f]azocine-5(6H)-butanamide (DBCO-PEG4-Amine), (E)-cyclooct-4-en-1-yl (3-aminopropyl)carbamate (TCO-Amine), 2-(2-(2-(2-azidoethoxy)ethoxy)ethoxy)ethan-1-amine (Azide-PEG3-Amine), (4-(6-methyl-1,2,4,5-tetrazin-3-yl)phenyl)methanamine (mTz-Amine), and 2-(2-(2-(2-(4-(6-methyl-1,2,4,5-tetrazin-3-yl)phenoxy)ethoxy)ethoxy)ethoxy)ethan-1-amine (mTz-PEG4-Amine) were purchased from BroadPharm. PEG5K-SVA was purchased from Laysan Bio.

Reagents for Protein Expression and Purification

The plasmid pDJ1-3 was kindly provided by Professor Joelle Pelletier (Université de Montréal, Montreal, Canada). pDJ1-3 encodes the proenzyme of microbial transglutaminase from *S. mobaraensis* with its N-terminal pro-sequence and a C-terminal hexa-histidine tag inserted between the *Nde*I and *Xho*I restriction sites of the vector pET20b. The plasmid pVITRO-Trastuzumab-IgG1/k for expressing trastuzumab was purchased from Addgene (Plasmid# 61883). Ni-NTA agarose resin was purchased from Qiagen. NAb protein A/G resin was purchased from ThermoFisher Scientific. Sequencing primers (T7 forward and reverse) were purchased from Integrated DNA Technologies (IDT). Sequencing was performed at the Cornell University Genomics Facility using the Applied Biosystems Automated 370xl DNA Analyzer using Big Dye Terminator chemistry and ApliTag-FS DNA Polymerase.

Reagents for Gel Electrophoresis, Molecular Biology, and Cell Culture

Precast protein gels (4 – 20% mini-PROTEAN® TGX™) and Bio-safe Coomassie Stain were purchased from Bio-Rad Laboratories. Peptide:N-glycosidase F (PNGase F) was

purchased from New England Biolabs. Commercially available microbial transglutaminase was purchased from Zedira.

Nuclear Magnetic Resonance (NMR) Spectroscopy

^{1}H and ^{13}C NMR spectra were recorded on an INOVA 400 MHz spectrometer. NMR data was analyzed by MestReNova software. ^{1}H and ^{13}C NMR chemical shifts are reported in units of ppm relative to chloroform.

Liquid Chromatography Mass Spectrometry (LC-MS)

LC-MS analysis was carried out on an Agilent 1100 Series LC with a Poroshell 120 EC-C18 column (100 × 3 mm, 2.7 µm, Agilent Technologies) and an Agilent G1956B Series Single Quadripole MS in positive ion mode for mass detection. The mobile phase for LC-MS (solvent A) was water with 0.1% (v/v) acetic acid, and the stationary phase (solvent B) was acetonitrile with 0.1% (v/v) acetic acid. Compounds were eluted at a flow rate of 0.6 mL/min using a gradient of 5-100% solvent B (0-10 minutes) followed by 100% solvent B (10-12 minutes) and equilibrated back to 5% solvent B (12-15 minutes).

Reverse Phase High Performance Liquid Chromatography (RP-HPLC)

HPLC purification was performed on an Agilent 1100 Series HPLC system equipped with a UV diode array detector and an 1100 Infinity fraction collector using a semi-preparative reversed-phase C18 column (Agilent Eclipse XDB-C18, 9.4 x 250 mm, 5 µm). The mobile phase for HPLC was water with 0.1% (v/v) trifluoroacetic acid (solvent A) and acetonitrile with 0.1% (v/v) trifluoroacetic acid (solvent B) unless specified otherwise. Compounds were eluted at a flow rate of 4 mL/min using a linear solvent gradient as specified below.

Standard Condition for Microbial Transglutaminase Modification

1 equivalency of trastuzumab at a concentration of 1 mg/mL in PBS buffer was treated with PNGase F (600 U/mg of antibody). The reaction was carried out at 37°C for 24 hours. Excess PNGase F was removed using a 100 kDa spin filter. 1 equivalency of aglycosylated antibody at a concentration of 1 mg/mL in PBS buffer was treated with MTG (0.75 equivalencies), and linker (80 equivalencies). The reaction was carried out at 37°C for 48 hours. Excess linker was removed using Amicon Ultra-0.5 mL centrifugal filters with a 30 kDa molecular weight cut off according to the manufacturer's instructions. The resulting conjugate (1 equivalency) was reacted with 25 equivalencies of DBCO-PEG5K, TCO-PEG5K, or both. in PBS at a concentration of 4 µM. The reaction was carried out for 24 hours at room temperature. Conjugation efficiency was analyzed via reduced and denatured SDS-PAGE.

Gel Electrophoresis of Conjugates

All samples were denatured and reduced with 2-mercaptoethanol by boiling at 100 °C for 5 minutes. A precast mini-PROTEAN® TGX™ gel was run at 120V to separate the protein samples. Protein content was visualized using Bio-Safe Coomassie Stain according to the manufacturer's instructions and imaged using a Bio-Rad ChemiDoc™ MP Imaging System.

Synthesis of Compound (1) (Figure A3. 1 and Figure A3. 2)

1 equivalency of tert-butyl allylcarbamate (255 mg, 1.62 mmol) was dissolved at 1 M in methanol. 2 equivalencies of 2,2'-(ethane-1,2-diylbis(oxy))bis(ethane-1-thiol) and 0.25 equivalencies of 2,2-dimethoxy-1,2-diphenylethan-1-one were added to this solution. The mixture was irradiated with UV light at 20 mW/cm^2 for 270 seconds. The solvent was removed under vacuum. Compound **(1)** was purified via silica gel flash chromatography. Solvent A: hexanes. Solvent B: ethyl acetate. Gradient: 0 – 40%

solvent B over 30 minutes. Yield: 42%, 230 mg, 0.68 mmol. The product was characterized by ^{1}H NMR.

Synthesis of Compound (2) (Figure A3. 3 and Figure A3. 4)

1 equivalency of compound **(1)** was dissolved at 500 mM in acetonitrile. 1 equivalency of azide-modified *N*-allylacrylamide monomer and 0.05 equivalency of DBU were added. This mixture was reacted overnight at room temperature and then dried under vacuum. The crude product was then suspended at 1 M in methanol. 2 equivalencies of 2-mercaptoacetic acid and 0.5 equivalencies of 2,2-dimethoxy-1,2-diphenylethan-1-one were added to this solution. The mixture was irradiated with UV light at 20 mW/cm^2 for 270 seconds and then purified via semi-preparative RP-HPLC. The product **(2)** was characterized via LC-MS (Calculated 722.30, Observed 722.10 [M+Na]$^+$)

Synthesis of Compound (3) (Figure A3. 5)

Removal of the Boc protecting group was achieved by dissolving compound **(2)** at 5 mM in solution of 50% (v/v) trifluoroacetic acid in dichloromethane. The reaction was stirred at room temperature for 1 hour. Excess trifluoroacetic acid was removed under vacuum. The crude product **(3)** was used without further purification or characterization.

Synthesis of Compound (4) (Figure A3. 6 and Figure A3. 7)

1 equivalency of compound **(2)** was dissolved at 33 mM in dimethyl sulfoxide. 2 equivalencies of N,N′-Diisopropylcarbodiimide, 2 equivalencies of 1-hydroxypyrrolidine-2,5-dione, 5 equivalencies of triethylamine, and 1 equivalency of mTz-Amine were added. The mixture was reacted overnight at room temperature. The product **(4)** was purified via semi-preparative RP-HPLC and characterized via LC-MS. (Calculated 905.39, Observed 905.20 [M+Na]$^+$)

Synthesis of Compound (5) (Figure A3. 8 and Figure A3. 9)

Removal of the Boc protecting group was achieved by dissolving compound **(4)** at 5 mM in solution of 50% (v/v) trifluoroacetic acid in dichloromethane. The reaction was stirred at room temperature for 1 hour. Excess trifluoroacetic acid was removed under vacuum. The crude product **(5)** was characterized via LC-MS. (Calculated 783.34, Observed 783.20 [M+H]$^+$)

Synthesis of Compound (6) (Figure A3. 10 and Figure A3. 11)

1 equivalency of tert-butyl allylcarbamate (106 mg, 0.67 mmol) was dissolved at 1.33 M in methanol. 3 equivalencies of (2R,3R)-1,4-dimercaptobutane-2,3-diol and 0.15 equivalencies of 2,2-dimethoxy-1,2-diphenylethan-1-one were added to this solution. The mixture was irradiated with UV light at 20 mW/cm^2 for 270 seconds. The solvent was removed under vacuum. Compound **(6)** was purified via silica gel flash chromatography. Solvent A: dichloromethane. Solvent B: methanol. Gradient: 0 – 2.5% solvent B over 25 minutes. Yield: 59%, 124 mg, 0.4 mmol. The product was characterized by ^{1}H NMR.

Synthesis of Compound (7) (Figure A3. 12 and Figure A3. 13)

1 equivalency of compound **(6)** was dissolved at 500 mM in acetonitrile. 1 equivalency of azide-modified *N*-allylacrylamide monomer and 0.05 equivalency of DBU were added. This mixture was reacted overnight at room temperature and then dried under vacuum. The crude product was then suspended at 1 M in methanol. 2 equivalencies of 2-mercaptoacetic acid and 0.5 equivalencies of 2,2-dimethoxy-1,2-diphenylethan-1-one were added to this solution. The mixture was irradiated with UV light at 20 mW/cm^2 for 270 seconds and then purified via semi-preparative RP-HPLC. The product **(7)** was characterized via LC-MS (Calculated 694.27, Observed 694.10 [M+Na]$^+$)

Synthesis of Compound (8) (Figure A3. 14)

Removal of the Boc protecting group was achieved by dissolving compound **(7)** at 5 mM in solution of 50% (v/v) trifluoroacetic acid in dichloromethane. The reaction was stirred at room temperature for 1 hour. Excess trifluoroacetic acid was removed under vacuum. The crude product **(8)** was used without further purification or characterization.

Synthesis of Compound (9) (Figure A3. 15 and Figure A3. 16)

1 equivalency of compound **(7)** was dissolved at 33 mM in dimethyl sulfoxide. 2 equivalencies of N,N′-Diisopropylcarbodiimide, 2 equivalencies of 1-hydroxypyrrolidine-2,5-dione, 5 equivalencies of triethylamine, and 1 equivalency of mTz-Amine were added. The mixture was reacted overnight at room temperature. The product **(9)** was purified via semi-preparative RP-HPLC and characterized via LC-MS. (Calculated 877.36, Observed 877.20 [M+Na]$^+$)

Synthesis of Compound (10) (Figure A3. 17)

Removal of the Boc protecting group was achieved by dissolving compound **(9)** at 5 mM in solution of 50% (v/v) trifluoroacetic acid in dichloromethane. The reaction was stirred at room temperature for 1 hour. Excess trifluoroacetic acid was removed under vacuum. The crude product **(10)** was used without further characterization.

Synthesis of Compound (11) (Figure A3. 18 and Figure A3. 19)

1 equivalency of compound **(7)** was dissolved at 40 mM in dimethyl sulfoxide. 2 equivalencies of N,N′-Diisopropylcarbodiimide, 2 equivalencies of 1-hydroxypyrrolidine-2,5-dione, 5 equivalencies of triethylamine, and 0.75 equivalency of mTz-PEG4-Amine were added. The mixture was reacted overnight at room temperature. The product **(11)** was purified via semi-preparative RP-HPLC and characterized via LC-MS. (Calculated 1139.45, Observed 1139.38 [M+Na]$^+$)

Synthesis of Compound (12) (Figure A3. 20)

Removal of the Boc protecting group was achieved by dissolving compound **(11)** at 5 mM in solution of 50% (v/v) trifluoroacetic acid in dichloromethane. The reaction was stirred at room temperature for 1 hour. Excess trifluoroacetic acid was removed under vacuum. The crude product **(12)** was used without further characterization.

Synthesis of DBCO-PEG5K (Compound 13, **Figure A3. 21** and **Figure A3. 22**)

1 equivalency (1.7 mg, 3.2 µmol) of DBCO-PEG4-Amine was dissolved at 100 mM in dimethyl sulfoxide in the presence of 5 equivalencies of triethylamine. To this solution, 1.25 equivalencies of PEG5K-SVA dissolved at 50 mM in dimethylsulfoxide was added. The resulting mixture was reacted at room temperature overnight and then purified via semi-preparative RP-HPLC. The reaction mixture was separated using a mobile phase of water (solvent A) and acetonitrile (solvent B) and a linear solvent gradient of 5 – 65% solvent B over 30 minutes. The product **(13)** eluted at 25 minutes and was recovered in 62% yield (10 mg, 1.8 µmol). The product was characterized by MALDI-MS.

Synthesis of TCO-PEG5K (Compound 14, Figure A3. 23 and Figure A3. 24)

1 equivalency (0.7 mg, 3.2 µmol) of TCO-Amine was dissolved at 100 mM in dimethyl sulfoxide in the presence of 5 equivalencies of triethylamine. To this solution, 1.25 equivalencies of PEG5K-SVA dissolved at 50 mM in dimethylsulfoxide was added. The resulting mixture was reacted at room temperature overnight and then purified via semi-preparative RP-HPLC. The reaction mixture was separated using a mobile phase of water (solvent A) and acetonitrile (solvent B) and a linear solvent gradient of 5 – 65% solvent B over 30 minutes. The product **(14)** eluted at 24.5 minutes and was recovered in 80% yield (12.8 mg, 2.5 µmol). The product was characterized by MALDI-MS.

Expression and Purification of Microbial Transglutaminase

Microbial transglutaminase (MTG) was expressed and purified as previously described with minor modifications[6]. Briefly, plasmid pDJ1-3 was transformed into *E. coli* BL21 (DE3), using standard procedures, and maintained with 100 µg/mL ampicillin. Before protein expression, correct plasmid sequence was confirmed (**Table A2. 1**). A 5 mL starter culture was propagated overnight at 37°C with shaking at 240 rpm in ZYP-0.8G media. The starter culture (2.5 mL) was used to inoculate 250 mL of auto-inducing ZYP-5052 medium. The expression culture was grown for 2 hours at 37°C with shaking at 240 rpm. After 2 hours, the temperature was reduced to 22°C for 20 hours. Cells were collected by centrifugation at 3,000xg at 4°C for 30 minutes. The cell pellet was suspended in 8 mL of 0.2 M Tris-HCl, pH 6.0. The cells were disrupted by sonication at 4°C (Qsonica Model CL-18, 3 cycles of 30 second pulse at 20% intensity with 60 second pause). The N-terminal MTG pro-sequence was removed by treatment for 45 minutes at 30°C with 800 µL of trypsin at a concentration of 1 mg/mL in 0.2 M Tris-HCl, pH 6.0. Activated MTG was purified using a gravity flow column charged with 0.5 mL of Ni-NTA resin. The column was equilibrated in a buffer of 50 mM phosphate, 300 mM NaCl, and 2 mM reduced glutathione, pH 7.5. His-tagged enzyme was eluted using equilibration buffer containing increasing amounts of imidazole (0 – 200 mM). Purified enzyme was concentrated and exchanged into equilibration buffer using Amicon Ultra-0.5 mL centrifugal filters with a 10 kDa molecular weight cut off according to the manufacturer's instructions. MTG yield was quantified using absorbance at 280 nm (molar extinction coefficient of 55,408 M^{-1} cm^{-1}). The average MTG yield was 10 mg/L of *E. coli* culture. Purified MTG was snap frozen as single use aliquots containing 15% (v/v) glycerol.

Expression and Purification of Trastuzumab

HEK293F suspension cells were transfected with the plasmid pVITRO-Trastuzumab-IgG1/k using FreeStyle™ MAX transfection reagent. Transfected cells were selected with 50 µg/mL hygromycin B for two weeks to establish a stably expressing cell line. Stably expressing HERK293F cells were maintained at density of approximately 1 x 10^6 cells/mL for protein production. Trastuzumab was purified from sterile-filtered, conditioned media using a gravity flow column charged with 1 mL of protein A/G resin according to the manufacturer's instructions. Purified antibody was concentrated and exchanged into PBS buffer (100 mM phosphate, 150 mM NaCl, pH 7.4) using Amicon Ultra-0.5 mL centrifugal filters with a 30 kDa molecular weight cut off according to the manufacturer's instructions. Antibody yield was quantified using absorbance at 280 nm (molar extinction coefficient of 210,000 M^{-1} cm^{-1}). The average antibody yield was 1 – 2 mg per/L of conditioned media.

Chapter 3 Appendix

OligoTEA-based Substrates for Microbial Transglutaminase

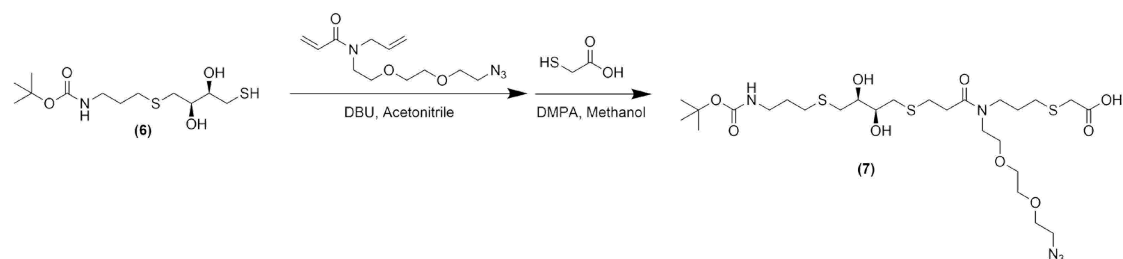**Synthesis of Compound (1)**
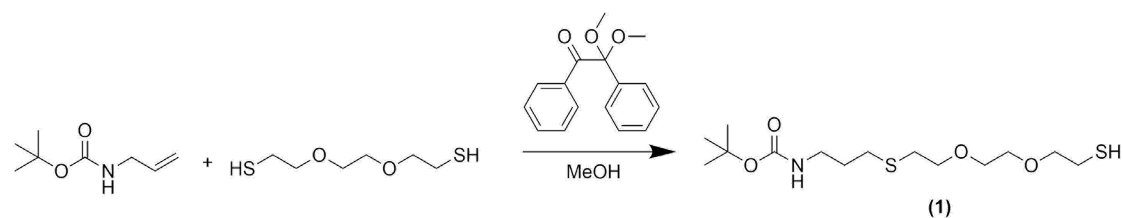
Figure A3. 1. Synthesis scheme for compound **(1)**.
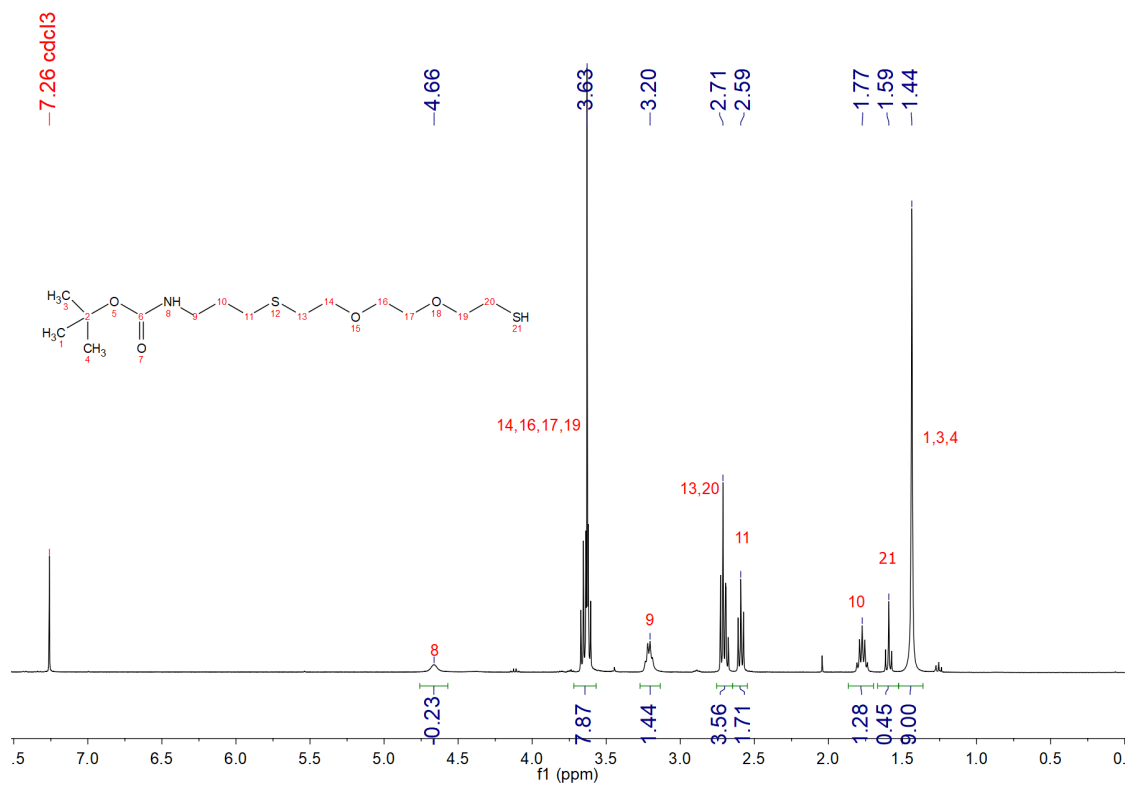
**Figure A3. 2.** ¹H NMR (400 MHz, CDCl₃) of compound **(1)**.
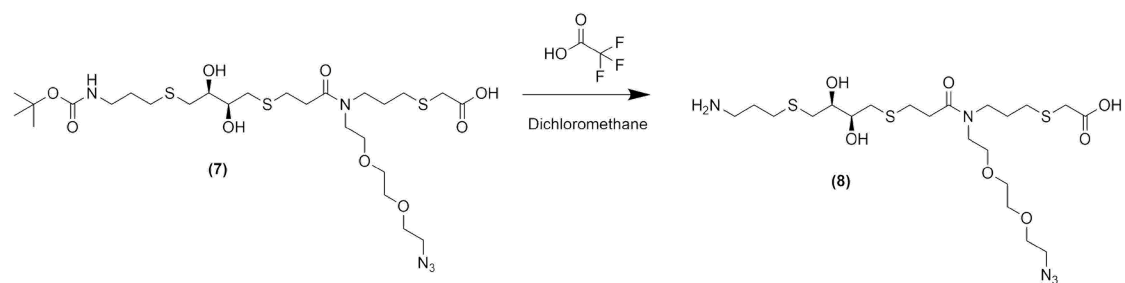
Synthesis of Compound (2)
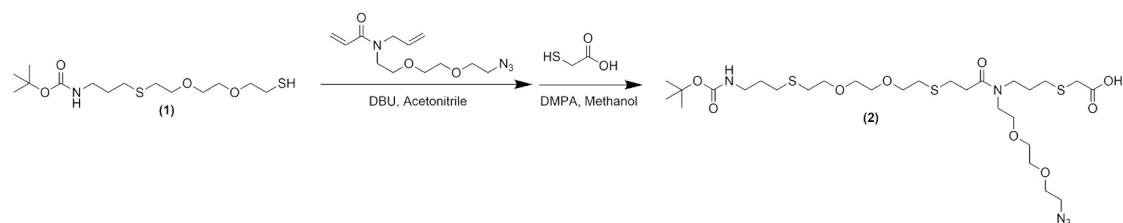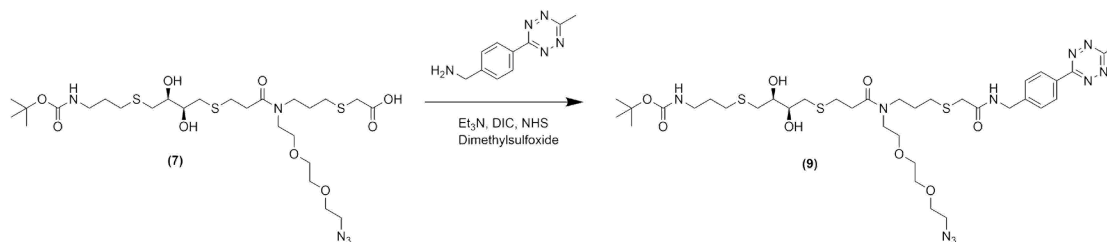

Figure A3. 3. Synthesis scheme for compound **(2)**.
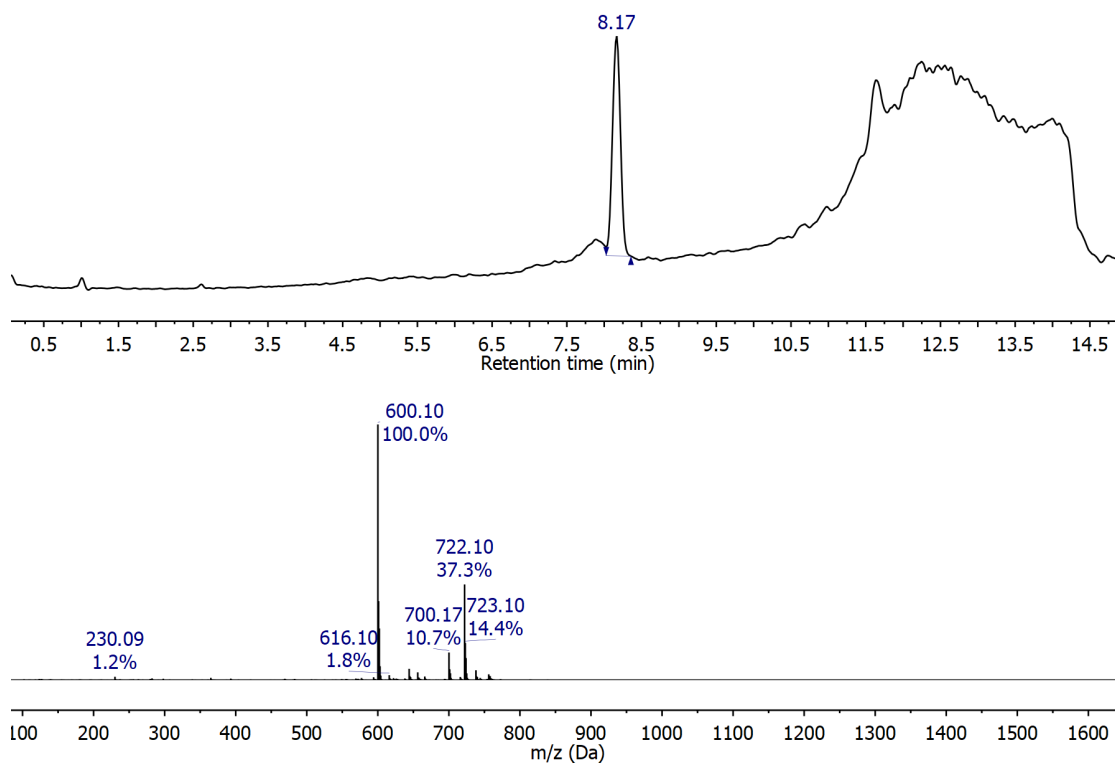
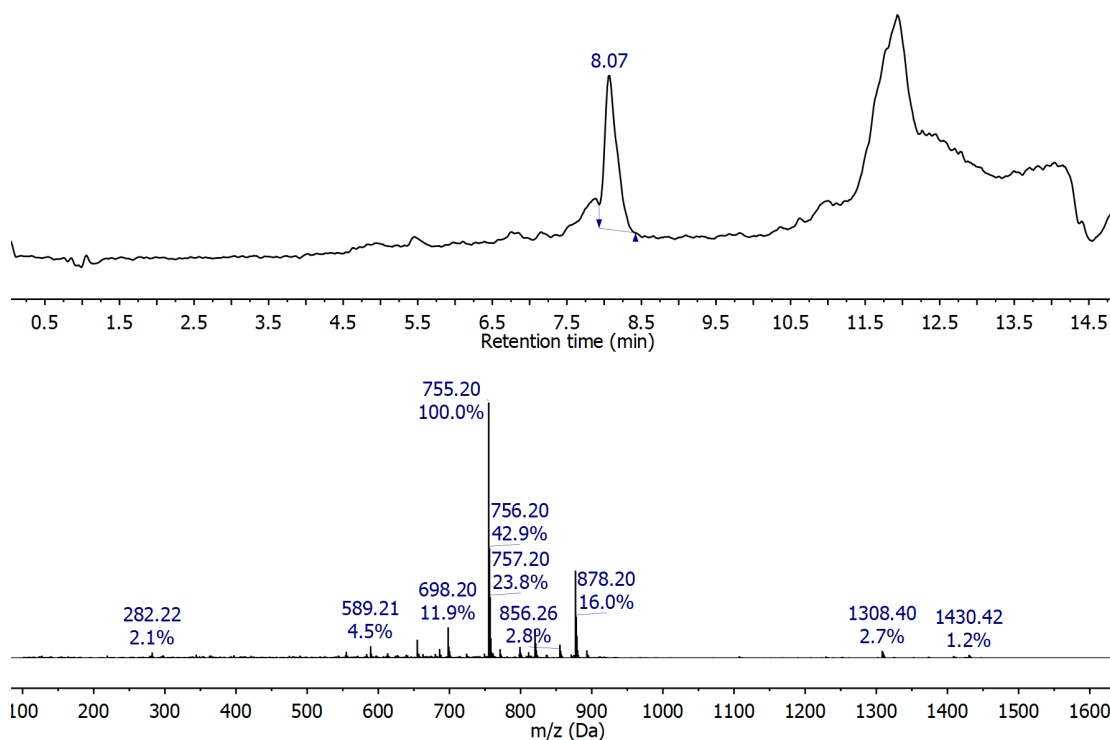**Figure A3. 4.** LC-MS analysis of compound **(2)**.

Synthesis of Compound (3)
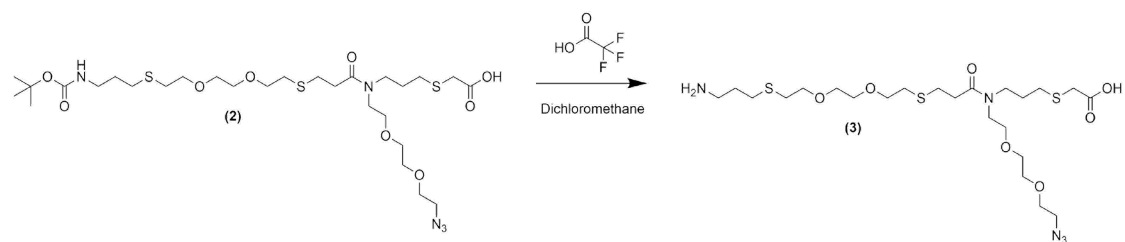
Figure A3. 5. Synthesis scheme for compound **(3)**.
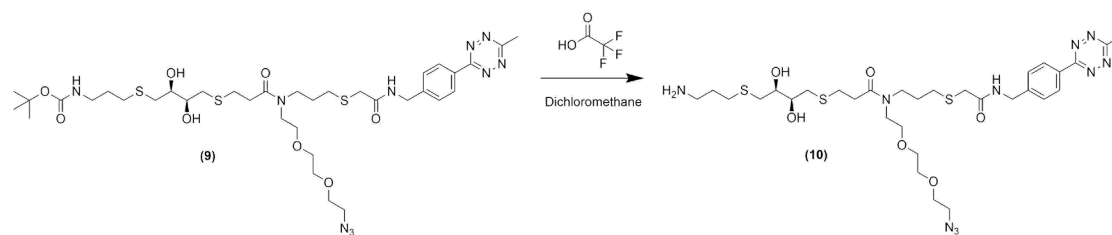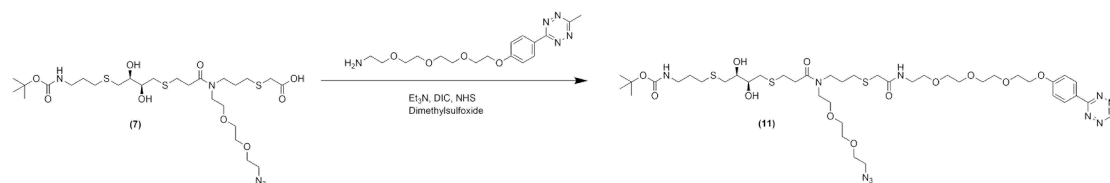
Synthesis of Compound (4)
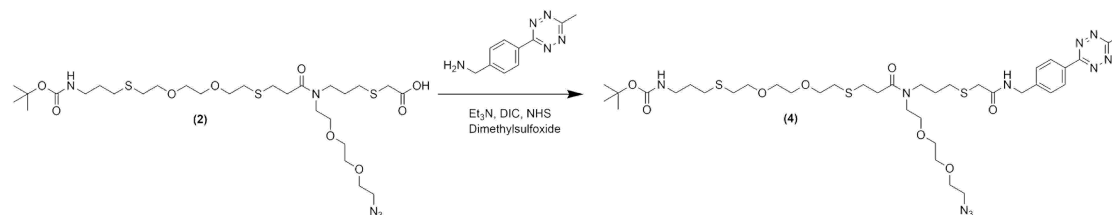
Figure A3. 6. Synthesis scheme for compound **(4)**.

t = 8.83..9.24 min
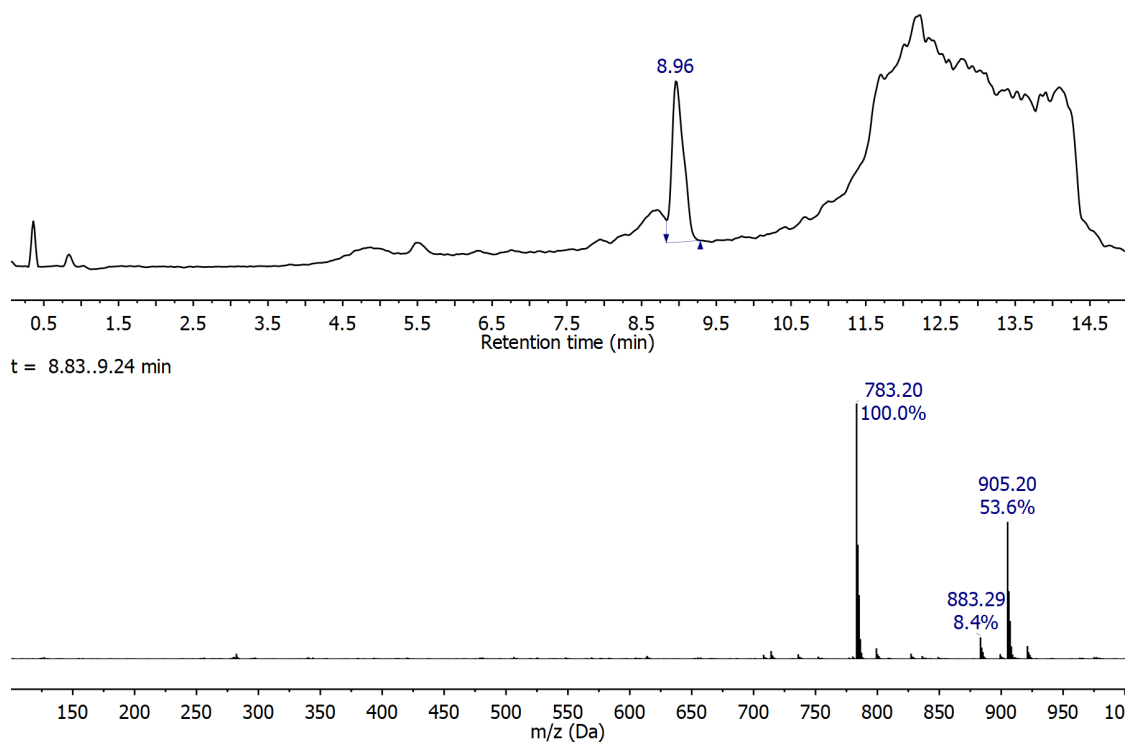
Figure A3. 7. LC-MS analysis of compound **(4)**.

Synthesis of Compound (5)

Figure A3. 8. Synthesis scheme for compound **(5)**.

t = 6.06..6.64 min

Figure A3. 9. LC-MS analysis of compound **(5)**.

Synthesis of Compound (6)
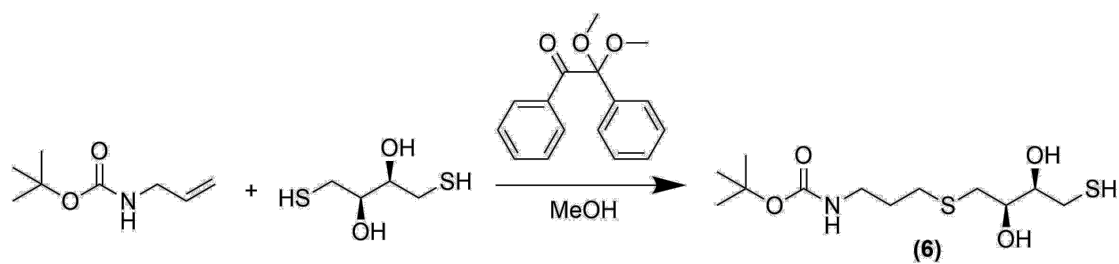
Figure A3. 10. Synthesis scheme for compound **(6)**.
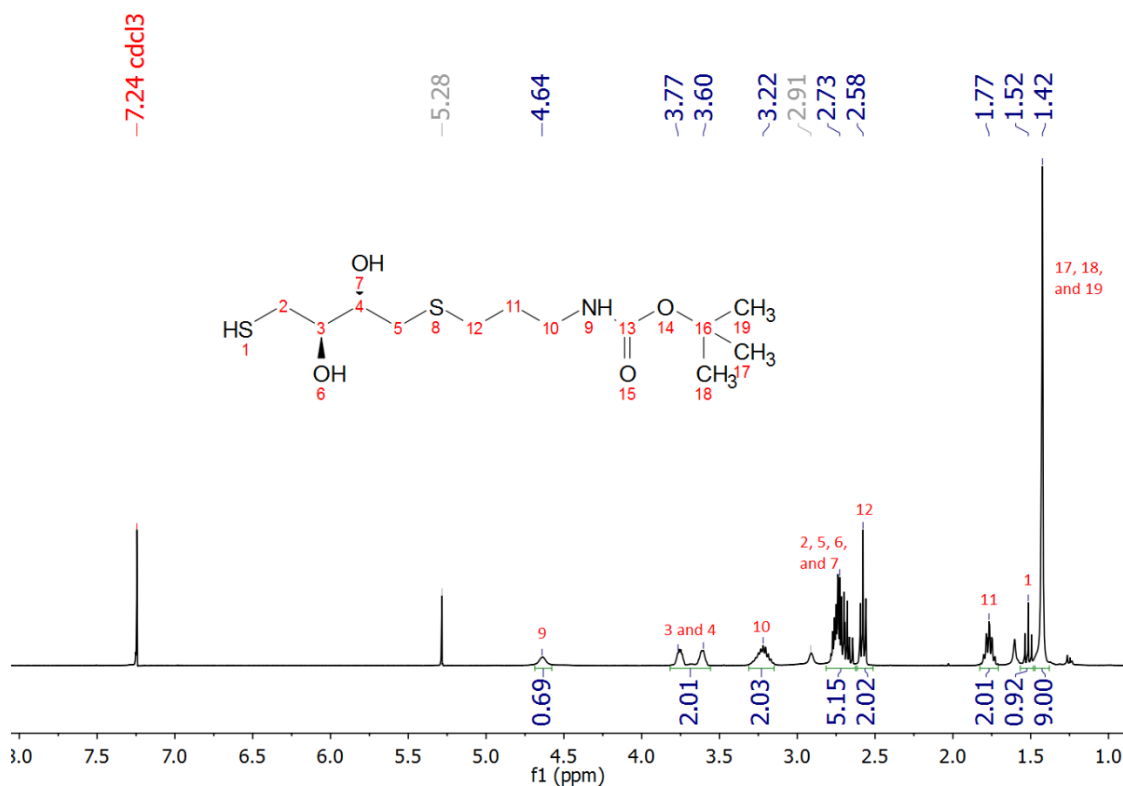
Figure A3. 11. ^{1}H NMR (400 MHz, CDCl$_3$) of compound **(6)**.

Synthesis of Compound (7)

Figure A3. 12. Synthesis scheme for compound **(7)**.
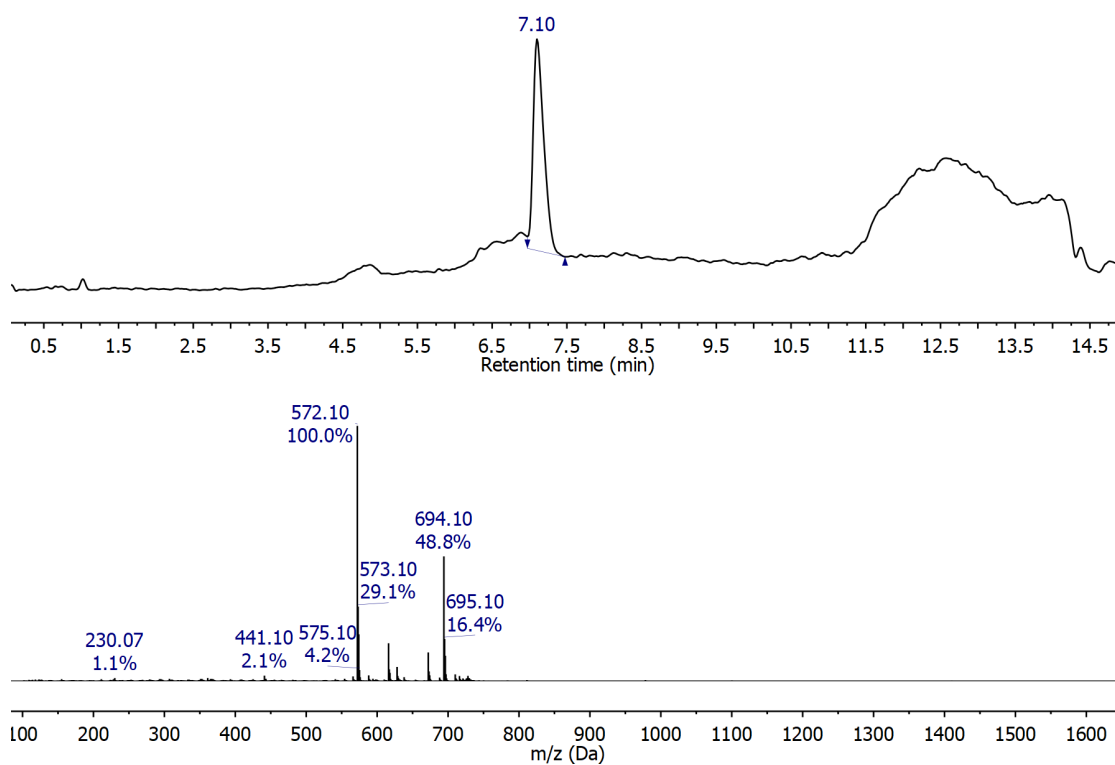
Figure A3. 13. LC-MS analysis of compound **(7)**.
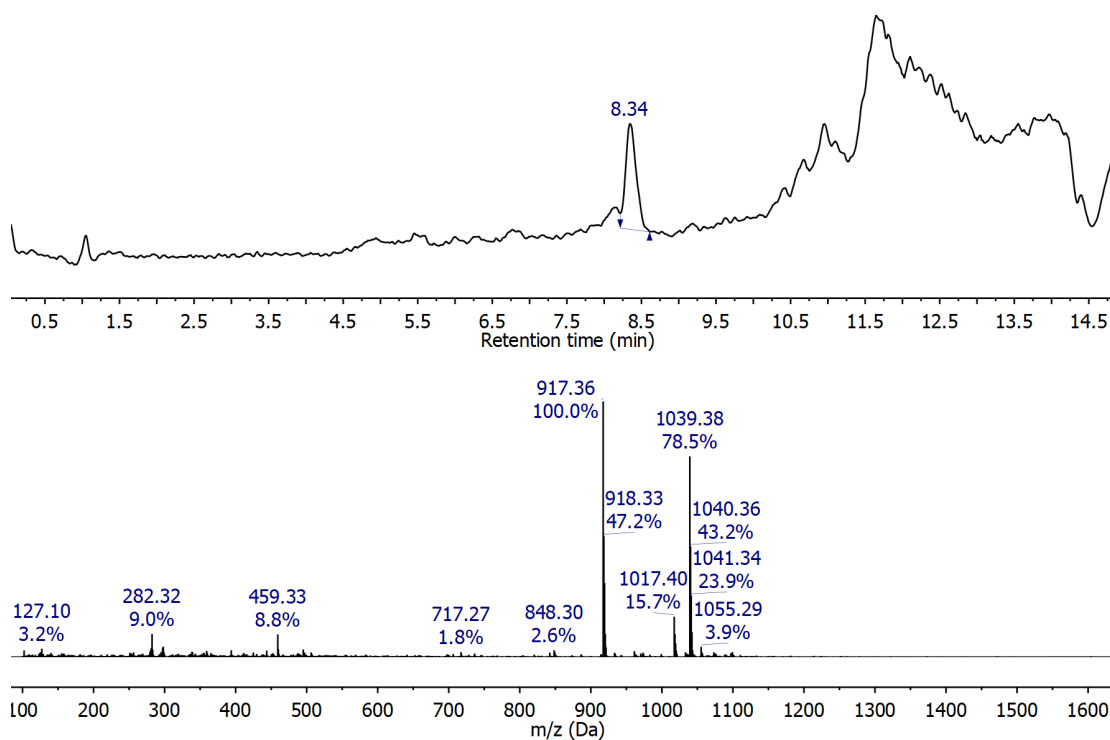
Synthesis of Compound (8)

Figure A3. 14. Synthesis scheme for compound **(8)**.

Synthesis of Compound (9)

Figure A3. 15. Synthesis scheme for compound **(9)**.

Figure A3. 16. LC-MS analysis of compound **(9)**.

Synthesis of Compound (10)

Figure A3. 17. Synthesis scheme for compound **(10)**.
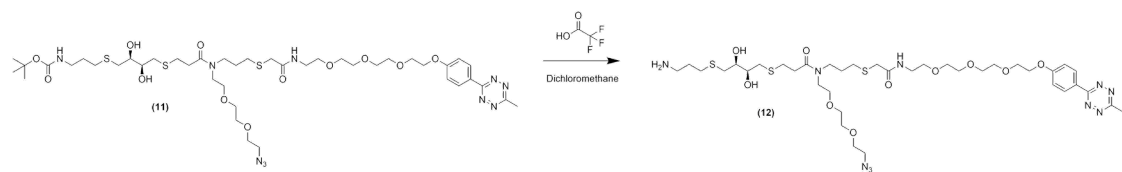
Synthesis of Compound (11)

Figure A3. 18. Synthesis scheme for compound **(11)**.
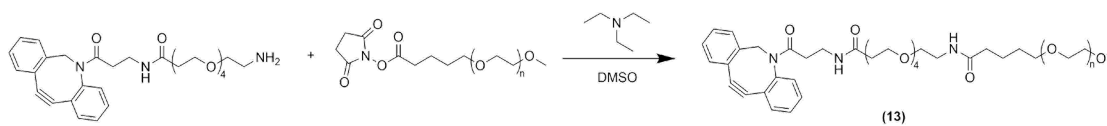

Figure A3. 19. LC-MS analysis of compound **(11)**.
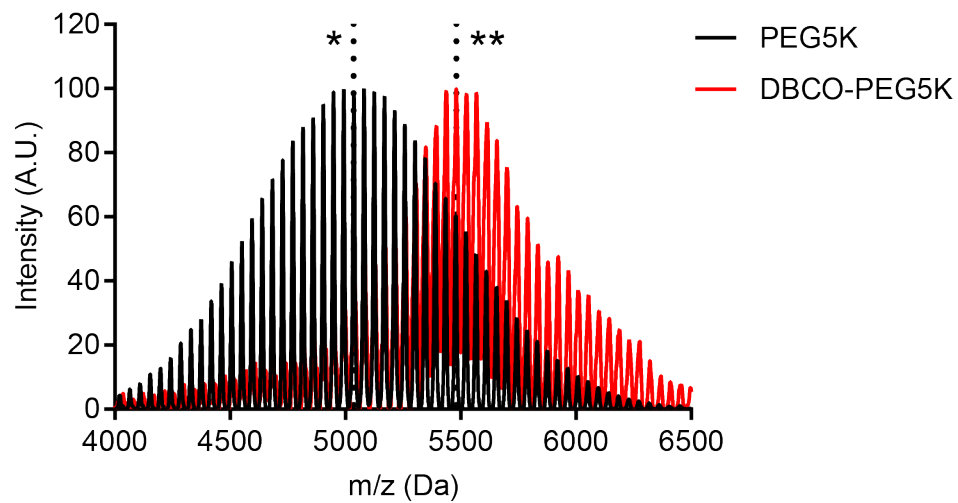
Synthesis of Compound (12)

Figure A3. 20. Synthesis scheme for compound **(12)**.

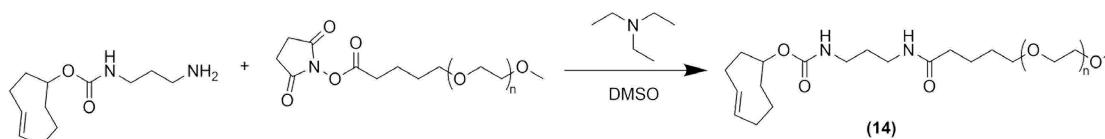**Synthesis of DBCO-PEG5K (Compound 13)**

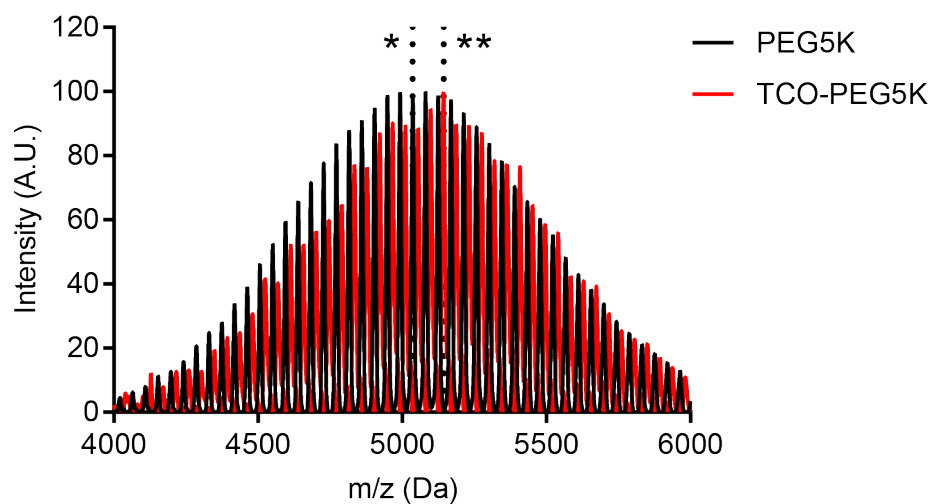**Figure A3. 21.** Synthesis scheme for compound **(13)**.

Figure A3. 22. MALDI-MS of compound **(13)**. Center of the distribution for the unmodified PEG5K (*) was at 5,036 Da. Center of the distribution for the DBCO-modified PEG5K (**) was at 5,481 Da. Observed difference: 445 Da, Expected Difference: 408 Da.

Synthesis of TCO-PEG5K (Compound 14)

Figure A3. 23. Synthesis scheme for compound **(14)**.

Figure A3. 24. MALDI-MS of compound **(14)**. Center of the distribution for the unmodified PEG5K (*) was at 5,036 Da. Center of the distribution for the TCO-modified PEG5K (**) was at 5,143 Da. Observed difference: 107 Da, Expected Difference: 111 Da.

Expression and Purification of Microbial Transglutaminase

Table A3. 1. Sequencing information for microbial transglutaminase. Underlined text indicates the N-terminal pro-sequence.

	Sequence
Forward Primer (T7)	TAATACGACTCACTATAGGG
Reverse Primer (T7)	GCTAGTTATTGCTCAGCGG
DNA Sequence	<u>ATGGACAATGGCGCGGGGGAAGAGACGAAGTCCTACGCCG</u> <u>AAACCTACCGCCTCACGGCGGATGACGTCGCGAACATCAAC</u> <u>GCGCTCAACGAAAGCGCTCCGGCCGCTTCGAGCGCCGGCC</u> <u>CGTCGTTCCGGGCCCCC</u>GACTCCGACGACAGGGTCACCCC TCCCGCCGAGCCGCTCGACAGGATGCCCGACCCGTACCGT CCCTCGTACGGCAGGGCCGAGACGGTCGTCAACAACTACA TACGCAAGTGGCAGCAGGTCTACAGCCACCGCGACGGCAG GAAGCAGCAGATGACCGAGGAGCAGCGGGAGTGGCTGTCC TACGGCTGCGTCGGTGTCACCTGGGTCAATTCGGGTCAGTA CCCGACGAACAGACTGGCCTTCGCGTCCTTCGACGAGGAC AGGTTCAAGAACGAGCTGAAGAACGGCAGGCCCCGGTCCG GCGAGACGCGGGCGGAGTTCGAGGGCCGCGTCGCGAAGG AGAGCTTCGACGAGGAGAAGGGCTTCCAGCGGGCGCGTGA GGTGGCGTCCGTCATGAACAGGGCCCTGGAGAACGCCCAC GACGAGAGCGCTTACCTCGACAACCTCAAGAAGGAACTGGC GAACGGCAACGACGCCCTGCGCAACGAGGACGCCCGTTCC CCGTTCTACTCGGCGCTGCGGAACACGCCGTCCTTCAAGGA GCGGAACGGAGGCAATCACGACCCGTCCAGGATGAAGGCC GTCATCTACTCGAAGCACTTCTGGAGCGGCCAGGACCGGTC GAGTTCGGCCGACAAGAGGAAGTACGGCGACCCGGACGCC TTCCGCCCCGCCCCGGGCACCGGCCTGGTCGACATGTCGA GGGACAGGAACATTCCGCGCAGCCCCACCAGTCCCGGTGA GGGATTCGTCAATTTCGACTACGGCTGGTTCGGCGCCCAGA CGGAAGCGGACGCCGACAAGACCGTCTGGACCCACGGAAA TCACTATCACGCGCCCAATGGCAGCCTGGGTGCCATGCATG TCTACGAGAGCAAGTTCCGCAACTGGTCCGAGGGTTACTCG GACTTCGACCGCGGAGCCTATGTGATCACCTTCATCCCCAA GAGCTGGAACACCGCCCCCGACAAGGTAAAGCAGGGCTGG CCGCTCGAGCACCACCACCACCACCACTGA
Amino Acid Sequence	<u>MDNGAGEETKSYAETYRLTADDVANINALNESAPAASSAGPSF</u> <u>RAP</u>DSDDRVTPPAEPLDRMPDPYRPSYGRAETVVNNYIRKWQ QVYSHRDGRKQQMTEEQREWLSYGCVGVTWVNSGQYPTNR LAFASFDEDRFKNELKNGRPRSGETRAEFEGRVAKESFDEEK GFQRAREVASVMNRALENAHDESAYLDNLKKELANGNDALRN EDARSPFYSALRNTPSFKERNGGNHDPSRMKAVIYSKHFWSG QDRSSSADKRKYGDPDAFRPAPGTGLVDMSRDRNIPRSPTSP GEGFVNFDYGWFGAQTEADADKTVWTHGNHYHAPNGSLGA MHVYESKFRNWSEGYSDFDRGAYVITFIPKSWNTAPDKVKQG WPLEHHHHHH

Chapter 3 References

1.Strop, P. Versatility of microbial transglutaminase. *Bioconjugate Chemistry* **25,** 855–862 (2014).

2.Rachel, N. M. & Pelletier, J. N. Biotechnological applications of transglutaminases. *Biomolecules* **3,** 870–888 (2013).

3.Farias, S. E. *et al.* Mass spectrometric characterization of transglutaminase based site-specific antibody-drug conjugates. *Bioconjugate Chemistry* **25,** 240–250 (2014).

4.Jeger, S. *et al.* Site-specific and stoichiometric modification of antibodies by bacterial transglutaminase. *Angew Chem Int Ed Engl* **49,** 9995–9997 (2010).

5.Anami, Y. *et al.* Glutamic acid-valine-citrulline linkers ensure stability and efficacy of antibody-drug conjugates in mice. *Nat Commun* **9,** 2512 (2018).

6.Gundersen, M. T., Keillor, J. W. & Pelletier, J. N. Microbial transglutaminase displays broad acyl-acceptor substrate specificity. *Appl Microbiol Biotechnol* **98,** 219–230 (2013).

7.Porel, M. & Alabi, C. A. Sequence-defined polymers via orthogonal allylacrylamide building blocks. *J Am Chem Soc* **136,** 13162–13165 (2014).

Chapter 4 – Effect of Cross-linker Sequence on the Biophysical Properties of Antibody-drug Conjugates

4.1 – Background

Antibody-drug conjugates (ADCs) are a class therapeutic bioconjugates that seek to combine the antigen specificity of antibodies with the chemotherapeutic potential of small molecule drugs. This is mediated by a chemical cross-linker that covalently links the antibody and payload. This conceptual framework has led to the development of ADCs targeted against a variety of cancer-specific antigens and carrying a wide range of therapeutic payloads. These efforts have led to the FDA approval of four ADCs with many more in the clinical pipeline[1].

Despite their clinical success, hurdles remain in the development of ADCs. Chief among these challenges is improving their therapeutic window, which is the range of doses that provide a therapeutic effect with minimal toxicity. The therapeutic window is limited by several factors broadly categorized as off-target binding, non-specific drug release, and hydrophobicity-induced aggregation. Off-target binding is dictated by the relative expression level of the target antigen in heathy and diseased tissue and can only be addressed by careful antigen selection[1]. Non-specific drug release can arise from deconjugation[2-4] or degradation of the cross-linker in circulation[5,6]. The development of new conjugation chemistries[7,8] and stimuli-responsive units[9-11] has improved cargo stability. We sought to develop methods to mitigate the third factor, hydrophobicity-induced aggregation.

Hydrophobicity is a requisite property of many small molecule drugs as it improves bioavailability by increasing membrane permeability[12,13]. However, upon chemical conjugation to an antibody, drug hydrophobicity becomes a liability. The hydrophobic nature of conjugated drugs has been shown to destabilize tertiary structure of ADCs,

leading to increased aggregation rates[14,15]. Further, studies have shown the ADC hydrophobicity decreases circulation half-life by increasing liver accumulation and subsequent premature clearance[16,17]. This results in an inverse relationship between drug loading and efficacy when the drug to antibody ratio (DAR) is greater than ~4[18].

A variety of approaches have been pursued to decrease the hydrophobicity of ADCs. Researchers at Astellas Pharm Inc. sought to address the problem by developing hydrophilic auristatin derivatives[19]. This approach is intriguing but requires time intensive synthesis of chemically complex payloads and risks negatively impacting the bioavailability and/or bioactivity of the therapeutic compound. Researchers at both Catalent Biologics[20] and Genentech[21] have adapted their respective site-specific conjugation strategies for unbiased screening and identification of stable conjugation sites. These techniques enable the identification non-intuitive conjugation sites and may help identify the structural features of antibodies that mitigate aggregation. Researcher as Seattle Genetics have pioneered a third approach in which the hydrophobicity of the conjugated payload is masked by modifying the chemical cross-linker with hydrophilic polyethylene glycol (PEG) chains[22,23]. This work has identified both the placement and length of PEG chains as tunable features to increase the circulation half-life and efficacy of ADCs. In collaboration with Catalent Biologics, we sought to build upon this body of literature by exploring the effect of cross-linker sequence on the functional and biophysical properties of ADCs.

## 4.2 – Results and Discussion
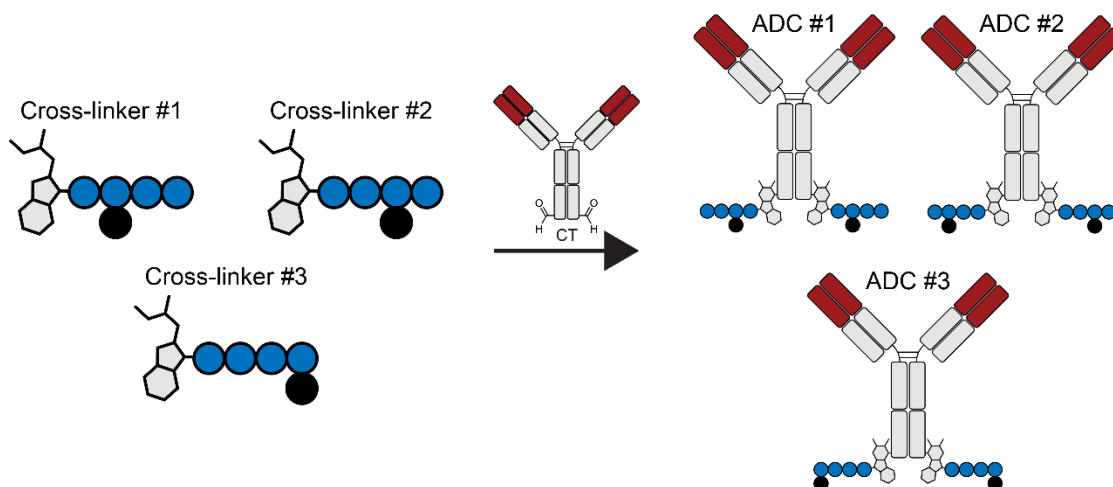
Figure 4.1. Design of sequence-defined antibody-drug conjugates. Constitutionally isomeric cross-linkers containing hydrophilic PEG-based side chains (blue circles) are used to control the local environment of a hydrophobic cargo (black circle)

Herein, we report the design, synthesis, and characterization of three constitutionally isomeric antibody-drug conjugates (**Figure 4.1**). These ADCs are comprised of trastuzumab, a Her2-targeted carrier protein, and monomethyl auristatin e (MMAE), a potent anti-mitotic drug[24]. Conjugation of the active payload is directed to the C-terminal of the IgG heavy chain through the Hydrazino-*iso*-Pictet-Spengler (HIPS) ligation using an aldehyde-tagged antibody provided by Catalent Biologics[7,25-28]. HIPS ligation was mediated through three constitutionally isomeric, sequence-defined chemical cross-linkers. These cross-linkers, based on the oligothioetheramide (oligoTEA) synthesis methodology developed by our lab, control the relative placement of the cytotoxic payload and hydrophilic polyethylene glycol side chains. We present the biophysical characterization of this library of ADCs. Specifically, the effect of cross-linker sequence has been correlated to conjugate hydrophilicity, conjugate aggregation, antigen binding, and *in vitro* efficacy.

As a first step, we sought to adapt the oligoTEA synthesis methodology to the scalable synthesis of branched, hydrophilic oligomers for bioconjugation. Traditional oligoTEA synthesis utilizes an orthogonally reactive *N*-allylacrylamide monomer, which can undergo alternating photoinitiated thiol−ene "click" reactions and phosphine catalyzed thiol-Michael additions[29]. OligoTEAs are built off a fluorous tag liquid support, which enables stepwise fluorous purification throughout synthesis. The fluorous purification handle is removed post synthesis by acid-catalyzed Boc deprotection. OligoTEA synthesis has been used as a platform to discover synthetic antibacterial agents[30] and cell penetrating oligomers[31] as well as to synthesize model systems to study the solution phase structure of polymers[32].

Previously, we have demonstrated that oligoTEAs can be used to synthesize cleavable, multifunctional chemical cross-linkers for bioconjugation[33]. However, the unique structural and synthetic requirements of PEG-modified chemical cross-linkers necessitate a new synthetic approach. First, fluorous tag purification relies on selective partitioning out of the mobile phase onto the fluorinated solid phase mediated by the fluorous tag. Chemical properties of the growing oligomer chain, specifically polyethylene glycol and azide groups, can reduce affinity for the fluorinated solid phase relative to the mobile phase. Ultimately, this reduces the synthetic yield. Further, chemical cross-linkers require only two or three pendant functional groups. This limits the utility of using the fluorous tag to achieve stepwise purification. Finally, bioconjugation applications require several post synthesis modifications to install attachment chemistries, cytotoxic drugs, nucleic acids, PEGylation, dyes, and targeting ligands. This imposes an additional synthetic burden, which necessitates the synthesis of chemical cross-linkers on the 10 − 100 mg scale. Meanwhile, traditional oligoTEA synthesis is more comfortably applied for library style synthesis at the 1 − 10 mg scale.
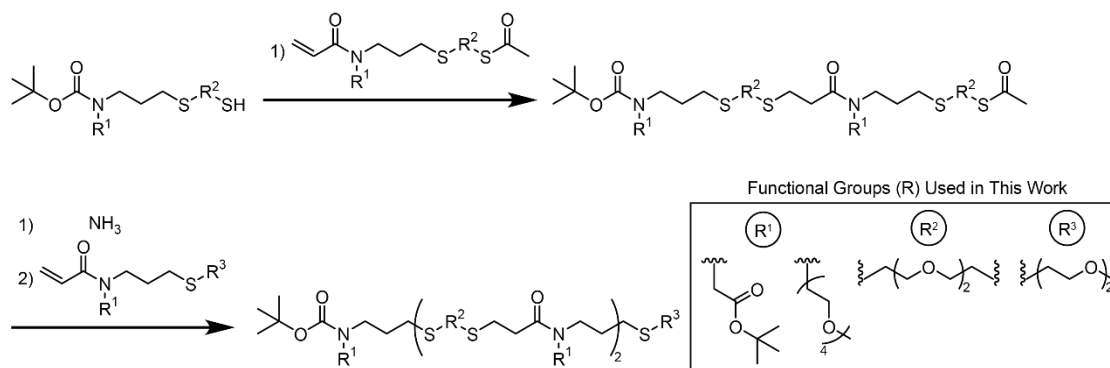
Figure 4.2. Methodology for support-free synthesis of oligoTEAs. A bifunctional monomer containing an acrylamide functional handle and acetylated thiol is used to extend the oligomer. A monofunctional monomer containing an acrylamide functional handle is used to cap the oligomer.

We envisioned a support-free strategy to synthesize oligoTEAs containing up to three pendant functional groups (**Figure 4.2**). The first pendant group is incorporated through a starting material containing both a Boc-protected secondary amine and a terminal thiol. The second pendant group is installed through a thiol-Michael addition of this starting material with a bi-functional monomer containing an acrylamide and an acetylated thiol. Treatment of this intermediate with ammonia is used to liberate the terminal thiol to elongate of the oligomer chain. An acrylamide monomer is used to add the third pendant group. This approach was used to synthesize constitutionally isomeric oligomers containing PEG and *tert*-butyl protected carboxylic acid pendant groups.
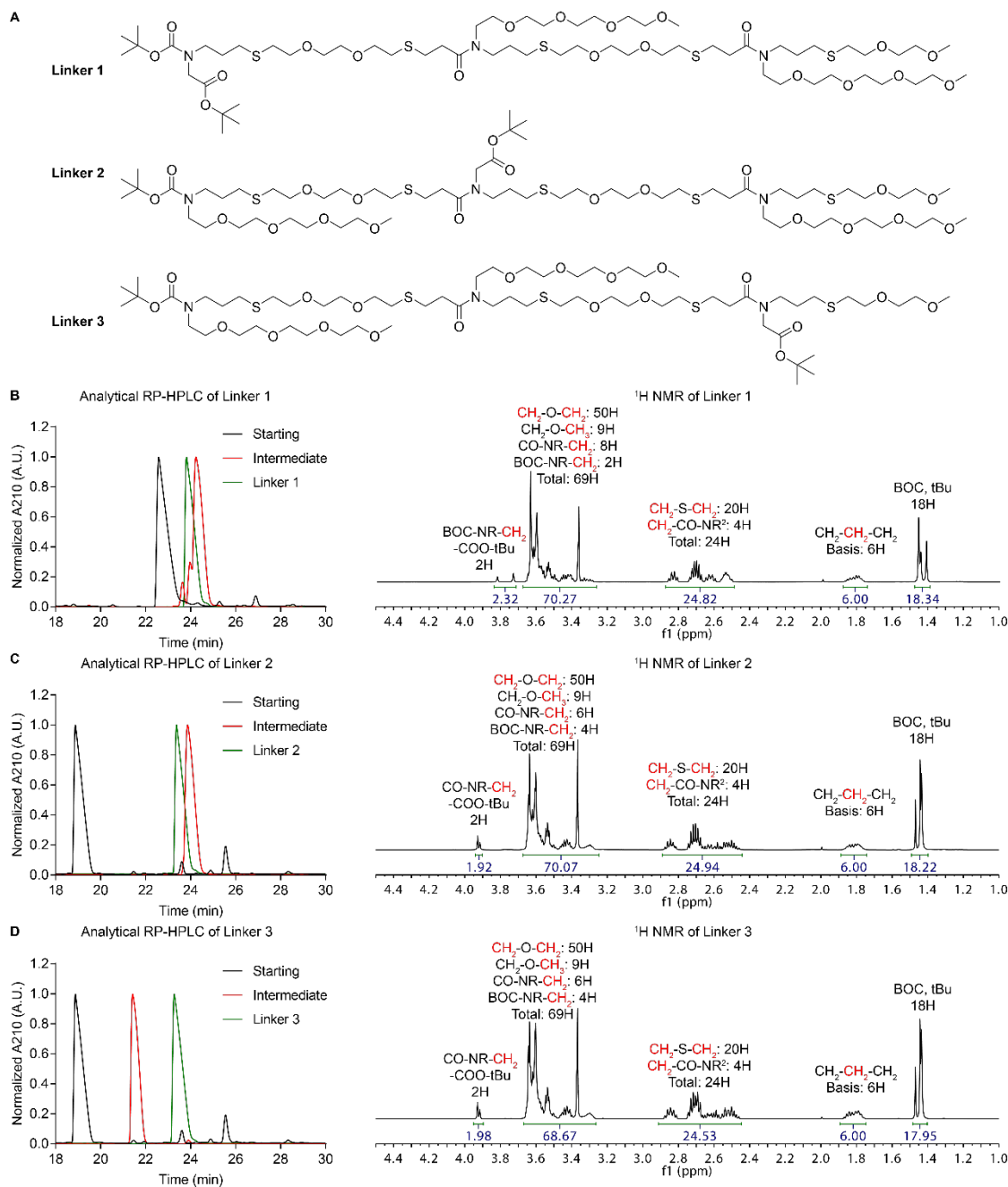
Figure 4.3. Synthesis and characterization of PEGylated oligoTEAs. A) Structure of sequence-defined, PEGylated oligoTEAs, B) RP-HPLC (left) and ^{1}H NMR (right) for synthesis of oligomer 1, C) RP-HPLC (left) and ^{1}H NMR (right) for synthesis of oligomer 2, and D). RP-HPLC (left) and ^{1}H NMR (right) for synthesis of oligomer 3.

These structures contain protected- amine and carboxylic acid functional groups for bioconjugation (**Figure 4.3**). Meanwhile the hydrophilic PEG side chains can be used to mask the hydrophobicity of cytotoxic payloads. In the absence of a fluorous

tag support, reverse phase high pressure liquid chromatography (RP-HPLC) was used for purification after each synthetic step. After each synthetic step, the desired product was isolated in high purity except for the intermediate for oligomer 1. The predominated impurity for the oligomer 1 intermediate was deprotection of the acetylated thiol under the thiol-Michael reaction conditions. However, this impurity does not interfere with subsequent synthetic steps. The purity of each oligomer was confirmed via ^{1}H NMR. Each oligomer was isolated in high purity as indicated by the accurate integration of the characteristic peaks. Further each oligomer was isolated in the 10 – 100 mg scale (oligomer 1: 50 mg, oligomer 2: 70 mg, and oligomer 3: 35 mg).
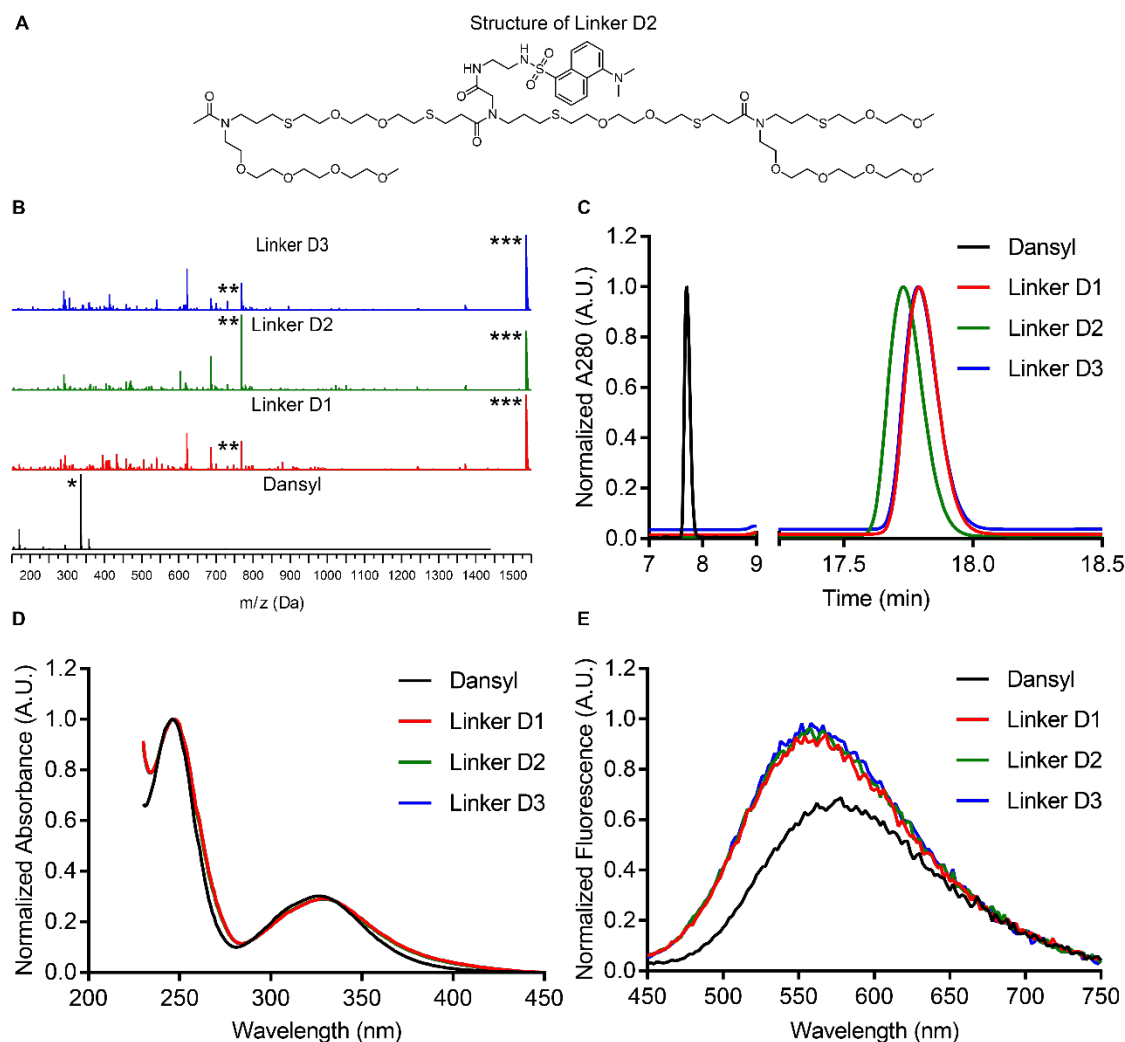
Figure 4.4. Synthesis and characterization of dansyl-modified, PEGylated cross-linkers. A) Example structure of linker D2 with dansyl placed in "2 position", B) LC-MS characterization of dansyl control and linkers D1 – D3. (*) represents [M+H]$^+$ of dansyl control (336.10 Da); (**) represents [M+2H]$^{2+}$ of dansyl-modified cross-linkers (768.40 Da); (***) represents [M+H]$^+$ of dansyl-modified cross-linkers (1,535.70 Da), C) RP-HPLC characterization of dansyl compounds, D) Absorbance spectra of dansyl compounds, and E) Fluorescence emission spectra of dansyl compounds (excitation at 327 nm).

We sought to validate the ability of these cross-linkers to modulate the local environment of attached cargo in a sequence-specific manner. To monitor changes in local environment, we synthesized cross-linkers modified with the environmentally sensitive fluorophore dansyl (**Figure 4.4**). Dansyl is known to exhibit blue shifted fluorescence emission and increased fluorescence quantum yield as the surrounding

environment becomes more non-polar[34]. This property has been used to develop peptide-based sensors for divalent zinc ions[35], fluorescent probes for the binding of small molecules to cyclodextrins[36], and to study molecule interactions between biological membranes and pore-forming peptides[37]. To synthesize dansyl-modified linkers (linkers D1 – D3), the terminal secondary amine was first acetylated. This was done to mimic the tertiary amide that will be present when these structures are attached to a protein carrier. The pendant carboxylic acid was used as the attachment site for the dansyl probe. A control dansyl probe containing an acetylated amine was prepared to determine the effect of the attached cross-linker (**Figure A4. 74**).

LC-MS and RP-HPLC were used to validate the identity and purity of the dansyl-modified cross-linkers (**Figure 4.4**). LC-MS analysis showed identical ionization patterns for each of the dansyl-modified cross-linkers. This was to be expected due to the constitutionally isomeric nature of the cross-linkers. RP-HPLC indicated that each compound was isolated in high purity. Further, RP-HPLC can be used as a measure of compound hydrophobicity. RP-HPLC analysis demonstrated that linker D2, which places the dansyl probe in the central position of the cross-linker, was more hydrophilic than linkers D1 and D3. To further probe structural effects, the absorbance and fluorescence spectrum of each dansyl compound was determined. The absorbance spectrum of each compound showed a dansyl-specific absorbance at 327 nm. The fluorescence emission curves of the dansyl-modified cross-linkers were identical. However, clear differences were observed in comparison to the acetylated dansyl control. The dansyl-modified cross-linkers (peak at 560 nm) displayed a Stokes shift of approximately 20 nm compared to the dansyl control (peak at 580 nm). Further, the peak fluorescence intensity of the dansyl control was approximately 70% relative to the dansyl-modified cross-linkers. While there are no detectable sequence-specific effects,

these spectral observations indicate that the PEGylated cross-linkers place the dansyl probe in a non-polar environment relative to the control. This could be understood as the amphipathic PEG side chains providing shielding from the surrounding aqueous environment. Compared to the RP-HPLC measurements, spectral measurements did not demonstrate sequence-specific effects. This could speak to the relative resolution of the techniques used or the importance of measuring structural effects in a physically relevant, solution-phase format.
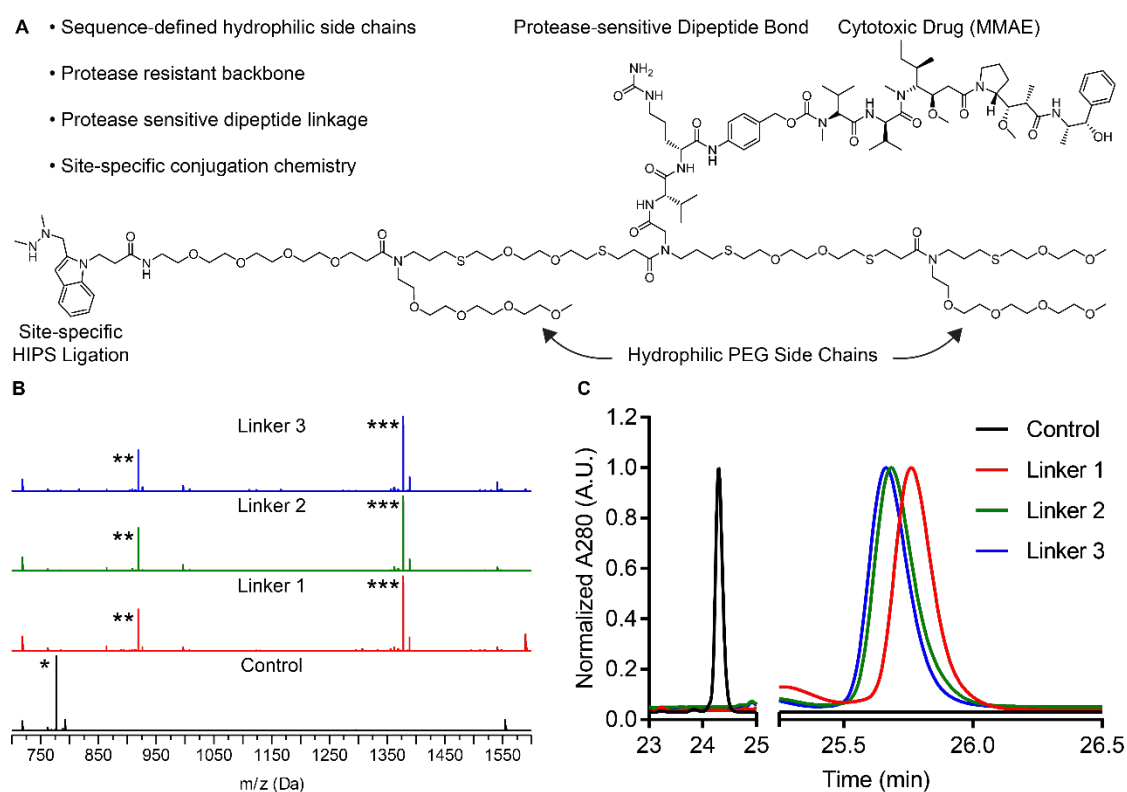
Figure 4.5. Synthesis and characterization of drug-loaded, PEGylated cross-linkers. A) Example structure of linker 2 with MMAE placed in "2 position", B) LC-MS characterization of the MMAE-loaded cross-linkers. (*) represents $[M+H]^{2+}$ of the control cross-linker fragmented alpha to the hydrazide functional group (777.46 Da); (**) represents $[M+2H]^{3+}$ of the PEGylated cross-linkers fragmented alpha to the hydrazide functional group (918.50 Da); (***) represents $[M+H]^{2+}$ of the PEGylated cross-linkers fragmented alpha to the hydrazide functional group (1,377.25 Da), C) RP-HPLC characterization of the drug-loaded cross-linkers.

These oligomers were used to synthesize a series of drug-loaded cross-linkers (**Figure 4.5**). The terminal secondary amine was used to attach a HIPS functional group

for bioconjugation to aldehyde-tagged antibodies. The pendant carboxylic acid functional group was used as an attachment site for MMAE, a potent anti-mitotic drug. The cytotoxic payload was attached via a protease-sensitive dipeptide linkage. The relative placement of hydrophilic PEG side chains was controlled by placing the payload on pendant position 1, 2, or 3. Location of the payload was used to differentiate the cross-linkers as linker 1, 2, and 3 corresponding to position 1, 2, and 3 respectively. As an example, the structure of linker 2 is shown. A control cross-linker was synthesized wherein the payload is directly attached to a HIPS functional group for bioconjugation (**Figure A4. 70**). Liquid-chromatography mass spectrometry (LC-MS) was used to confirm the isomeric nature of the linkers. RP-HPLC was used to assess the purity and hydrophobicity of the isolated cross-linkers. RP-HPLC indicated that each linker was isolated in high purity. Additionally, linker 1 was shown to be more hydrophobic than linkers 2 and 3, which were nearly indistinguishable via RP-HPLC. Interestingly, this is different from the trend that was observed for the dansyl-modified cross-linkers. This result highlights the influence of cross-linker modifications such as cargo and conjugation chemistry on the sequence-specific properties of chemical cross-linkers.
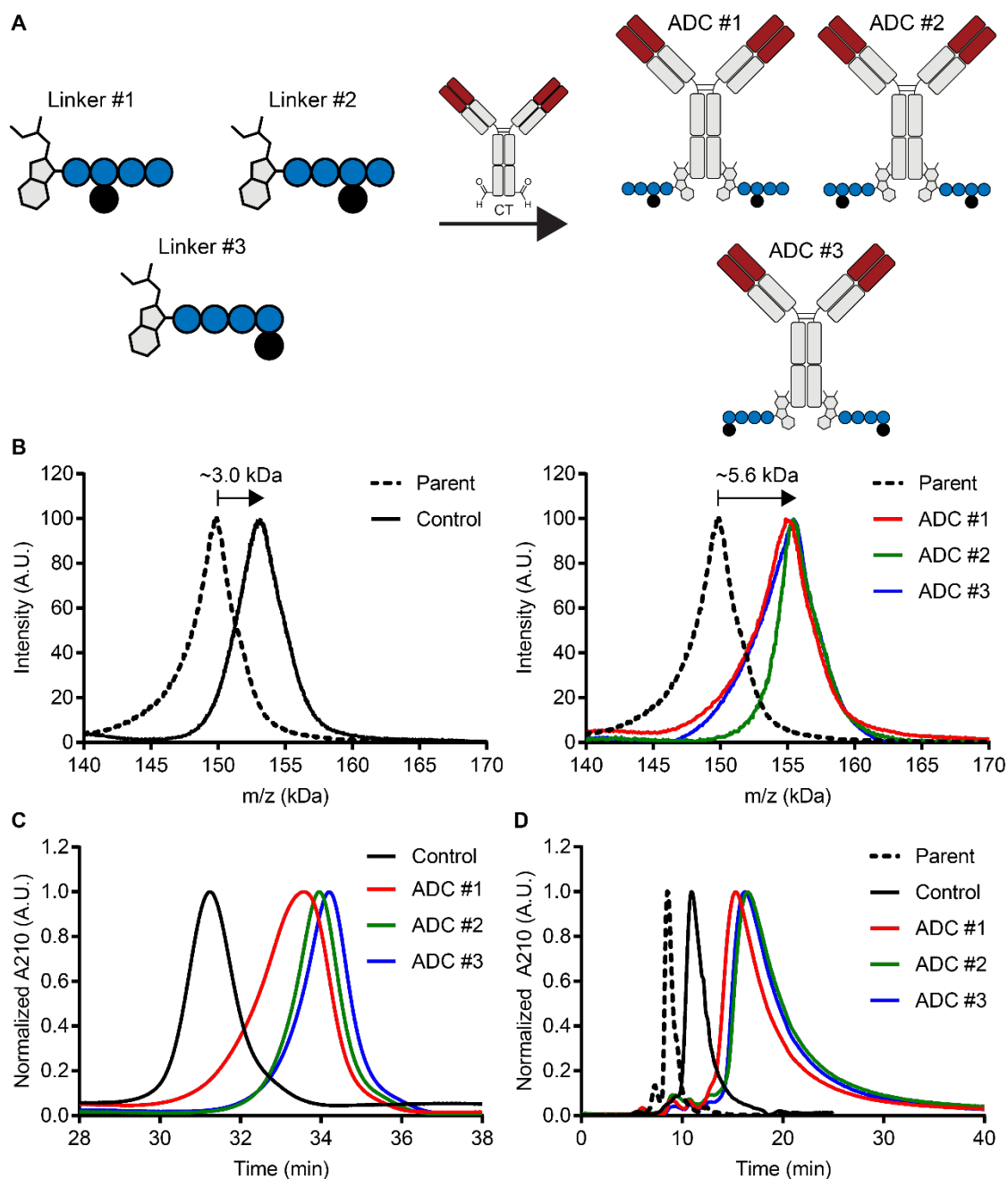
Figure 4.6. Synthesis and characterization of sequence-defined antibody-drug conjugates (ADCs). A) Synthesis scheme for sequence-defined ADCs, B) MALDI-MS characterization of control ADC (left) and sequence-defined ADCs (right), C) HIC characterization of ADCs, and D) SEC characterization of ADCs.

To assess how cross-linker properties translate to antibody-drug conjugate properties, we conjugated each cross-linker to C-terminally aldehyde-tagged trastuzumab (**Figure 4.6**). Conjugate molecular weight was confirmed by MALDI-MS

analysis. Conjugation of trastuzumab with the control cross-linker and PEGylated cross-linkers gave increases of 3 kDa and 5.6 kDa respectively in the apparent molecular weight, as expected. The global hydrophobicity of each antibody-drug conjugate was analyzed via HIC. When analyzed via RP-HPLC, the control cross-linker was noticeably more hydrophilic than the PEGylated cross-linkers. Consistent with this result, the control ADC was more hydrophilic than the PEGylated ADCs when analyzed via HIC. Analysis of the PEGylated ADCs via HIC reveals that RP-HPLC analysis does not directly translate. When analyzed via RP-HPLC, linker 1 was found to be more hydrophobic than linkers 2 and 3. However, HIC analysis showed that ADC #1, which places the payload closest to the antibody, was most hydrophilic. As the hydrophobic payload was placed further away from the antibody the overall hydrophobicity of the ADC increased. This result indicates that hydrophobic screening is most efficient when PEGylation is placed distally from the payload. Further, this result highlights the importance of analyzing cross-linker properties within the context of the conjugated antibody.

Size exclusion chromatography (SEC) was used to analyze the aggregation propensity of the ADCs (**Figure 4.6**). Each of the ADCs eluted later than the parent antibody. This is consistent with increased hydrophobic interactions with the underlying solid phase. Interestingly, hydrophobic retention via SEC confirms that ADC #1 is the most hydrophilic of the PEGylated ADCs. The control ADC showed no noticeable signs of aggregation. However, each of the PEGylated ADCs showed a small degree of aggregation as quantified via area under the curve (ADC #1: 3.0%, ADC #2: 3.0%, and ADC #3: 1.7%). ADC #1 was measured to be the most hydrophilic of the PEGylated ADCs whereas ADC #3 was determined to have the smallest aggregated fraction. However, overall, none of the ADCs showed a significant degree of aggregation.
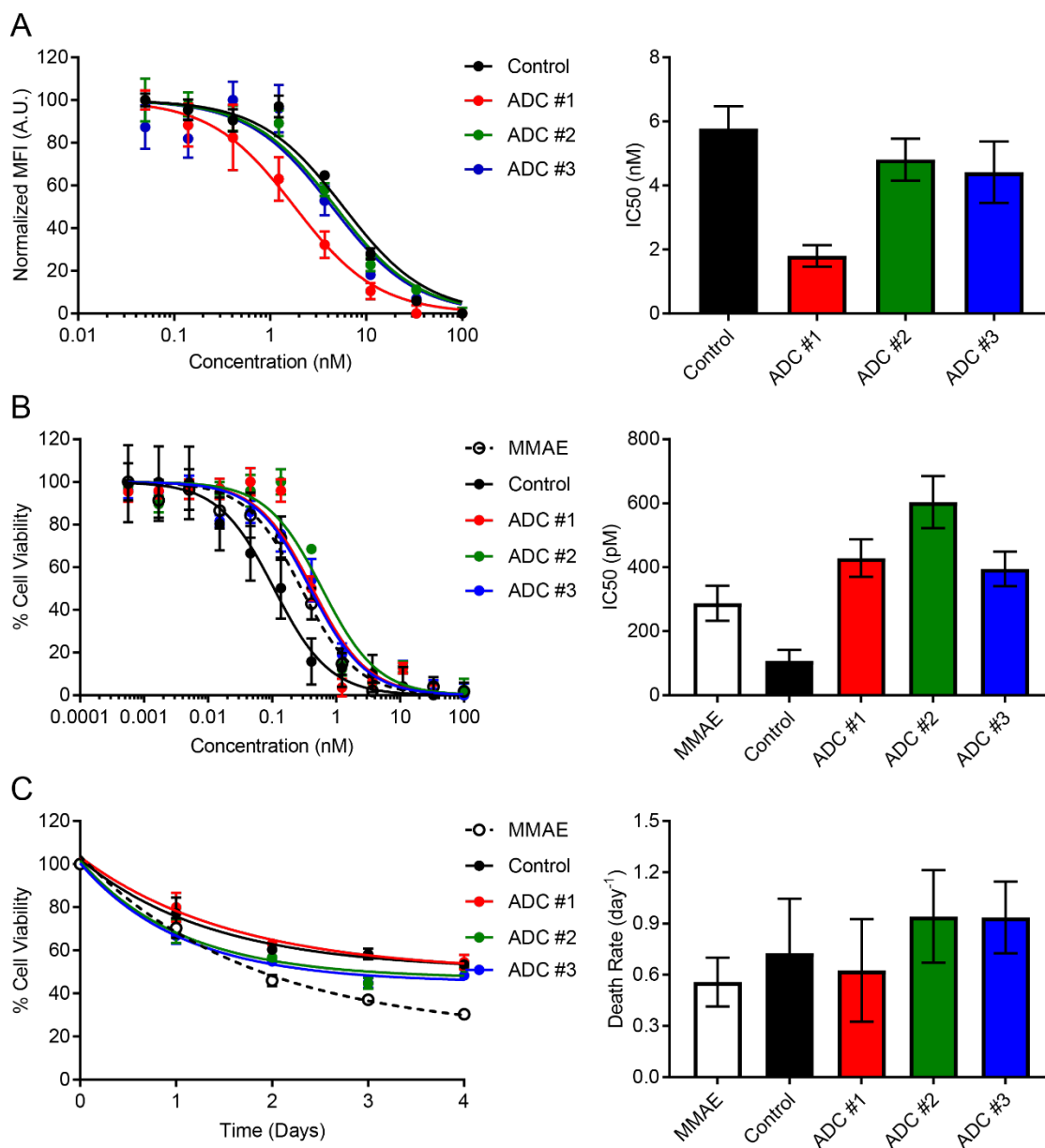
Figure 4.7. Functional testing of antibody-drug conjugates using SKOV3 cells. A) Characterization of receptor binding affinity (2 biological replicates measured in duplicate), B) Characterization of ADC potency (3 biological replicates measured in triplicate) C) Kinetic measurement of ADC potency (3 biological replicates measured in triplicate.

Antigen binding was assessed via a competition binding experiment with a fluorescein-modified trastuzumab (**Figure 4.7**). Fluorescein is a relatively small modification and therefore should minimally impact antigen binding. Analysis via flow cytometry showed that the fluorescein conjugate binds to SKOV3 cells, a Her2 positive

cell line, with an apparent affinity of 2.4 nM. Competition binding was performed in which a constant amount of fluorescein-modified antibody was mixed with an increasing amount of each ADC. This experiment yields a binding inhibition curve from which the concentration required to inhibit 50% of binding can be determined. The control ADC bound to the Her2 receptor with an IC50 value of 5.8 nM. ADC #2 and ADC #3 bound with IC50 values of 4.8 nM and 4.4 nM respectively, which were statistically indistinguishable from the binding of the control ADC. However, ADC #1 displayed an IC50 value of 1.8 nM, which was statistically distinguishable from all other ADCs tested ($p < 0.05$)

To evaluate the effect of cross-linker sequence on intracellular processing, *in vitro* potency of the ADCs was analyzed using SKOV3 cells, a model Her2 positive cell line (**Figure 4.7**). A positive control of the free drug (MMAE) showed and IC50 values of 288 pM, in line with literature reports. The control ADC, ADC #1, ADC #2, and ADC #3 displayed IC50 values of 108 pM, 429 pM, 604 pM, and 395 pM respectively. ADCs #1 – 3 all performed worse than the control ADC ($p < 0.001$). When compared to each other, ADC #2 performed ($p < 0.05$) worse than ADC #1 and ADC #3, which were statistically indistinguishable. This data suggests that cross-linker PEGylation and sequence may influence the intracellular processing of ADCs. This may be due to steric hindrance near the protease-sensitive dipeptide bond. Steric hindrance may inhibit the activity of intracellular proteases towards cleaving the dipeptide bond that links MMAE to the cross-linker. We reasoned that differential release inside cells may lead to differences in the rate of cell death upon treatment with our library of ADCs. To test this, we carried out a kinetic measurement of cell viability at a constant ADC concentration of 1 nM. Qualitatively, there appear to be some subtle differences in the measured death curves. However, the degree of uncertainty in the death rates

extracted from the data yielded statistically insignificant difference. Careful analysis of the intracellular degradation rate of these bonds would be needed to ascertain the functional basis for this decrease in potency.

4.3 – Conclusions

In conclusion, we have developed a support-free methodology for the synthesis of oligoTEA-based chemical cross-linkers. This methodology was successfully applied to the synthesis three constitutionally isomeric oligomers containing amine and carboxylic acid functional groups for bioconjugation as well as hydrophilic PEG side chains. We employed these sequence-defined oligomers to explore the effect of cross-linker sequence on the solution-phase shielding of dansyl, an environmentally sensitive dye. PEGylated oligomers were found to shield the attached dye from the polar aqueous environment. However, spectrally, sequence-specific effects were not observed. Further, we sought to investigate the effect of cross-linker sequence on biophysical properties and performance of antibody-drug conjugates. To this end, we designed, synthesized, and characterized three ADCs, comprised of trastuzumab and monomethyl auristatin e (MMAE), which differed in the placement of the drug payload relative to two hydrophilic PEG side chains. We took a holistic approach to characterizing these ADCs and their interactions with cells. Oligomer sequence was found to affect the apparent hydrophobicity of cross-linkers loaded with payload and a HIPS functional group for bioconjugation. Upon attachment to the antibody, placement of PEG side chains distally from the antibody (ADC #1) was found to increase the hydrophilicity of the resulting ADC. Aggregation analysis via SEC indicated that none of the ADCs displayed significant amounts of aggregation. Placement of payload was shown to influence antigen binding with ADC #1 displaying the tightest binding to the Her2 receptor expressed on SKOV3 cells. Finally, PEGylation was shown to influence

148

the potency of the ADCs towards SKOV3 cells, with each PEGylated ADC performing worse than the control ADC. Taken together, these data highlight the subtle and unexpected ways in which cross-linker sequence can affect the biophysical and *in vitro* functional properties of antibody-drug conjugates. However, *in vivo* studies will be needed to determine if this collection of in vitro differences translates to differences in efficacy. Studies of the influence of cross-linker sequence on other *in vivo* parameters such as circulation time and non-specific drug release are another important next step. The support-free synthesis methodology presented here can be used to explore the influence of other features such as different payloads, multiple payloads, variable PEG length, or antibody conjugation site. In this way, cross-linker sequence will emerge as a novel handle to fine tune the properties of antibody-drug conjugates.

4.4 – Alternative Approaches

The support-free synthesis methodology developed here (**Figure 4.2** and **Figure 4.3**) proved to be a convenient and effective route to synthesizing PEGylated cross-linkers for antibody-drug conjugates. However, the use of a bi-functional monomer limits the utility of this approach as a general platform for oligoTEA synthesis. The use of bifunctional monomers couples the selection of pendant group functionality and backbone chemistry. This negates two advantages of traditional oligoTEA synthesis. By taking a co-monomer approach, traditional oligoTEA synthesis decouples the selection of pendant group and backbone chemistry. This enables the modulation of oligomer properties using a variety of commercially available dithiol building block. Further, *N*-allylacrylamide monomers typically required two synthetic steps as compared to six steps required to synthesize a bifunctional acrylamide-acetylated thiol.
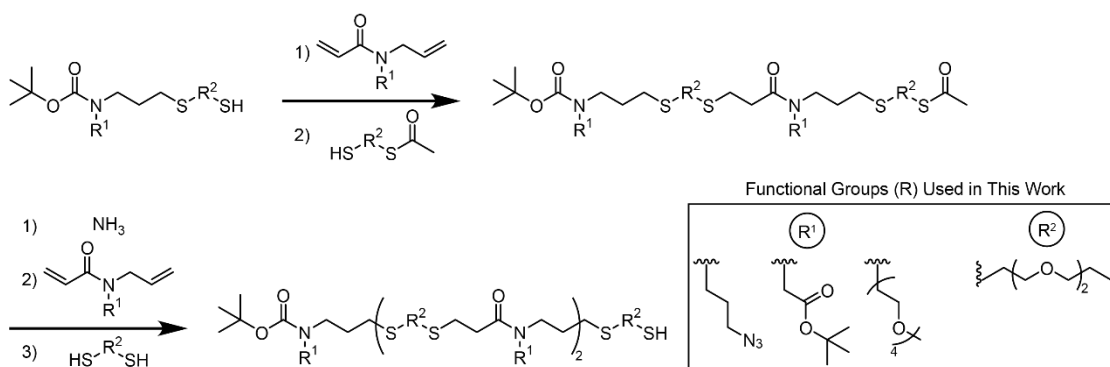
Figure 4.8. Alternative methodology for support-free synthesis of oligoTEAs. One-pot, sequential addition of a bifunctional *N*-allylacrylamide monomer and a monoacetylated dithiol monomer is used to extend the oligomer.

To address these shortcomings, we envisioned an alternative support-free strategy to synthesize oligoTEAs (**Figure 4.8**). In this approach, the first pendant group is incorporated through a starting material containing both a Boc-protected secondary amine and a terminal thiol. The second pendant group is installed through sequential, one-pot thiol-Michael and thiol-ene reactions using an *N*-allylacrylamide monomer and

a monoacetylated dithiol co-monomer. Treatment of this intermediate with ammonia is used to liberate the terminal thiol to elongate of the oligomer chain. A second synthetic cycle using an *N*-allylacrylamide monomer and an unprotected dithiol is used to install the third functional group. This terminal thiol can be used for directly for bioconjugation or to elongate the oligomer chain. To demonstrate the feasibility of this alternative approach we synthesized three constitutionally isomeric oligomers containing a variety of functional groups relevant in bioconjugation.
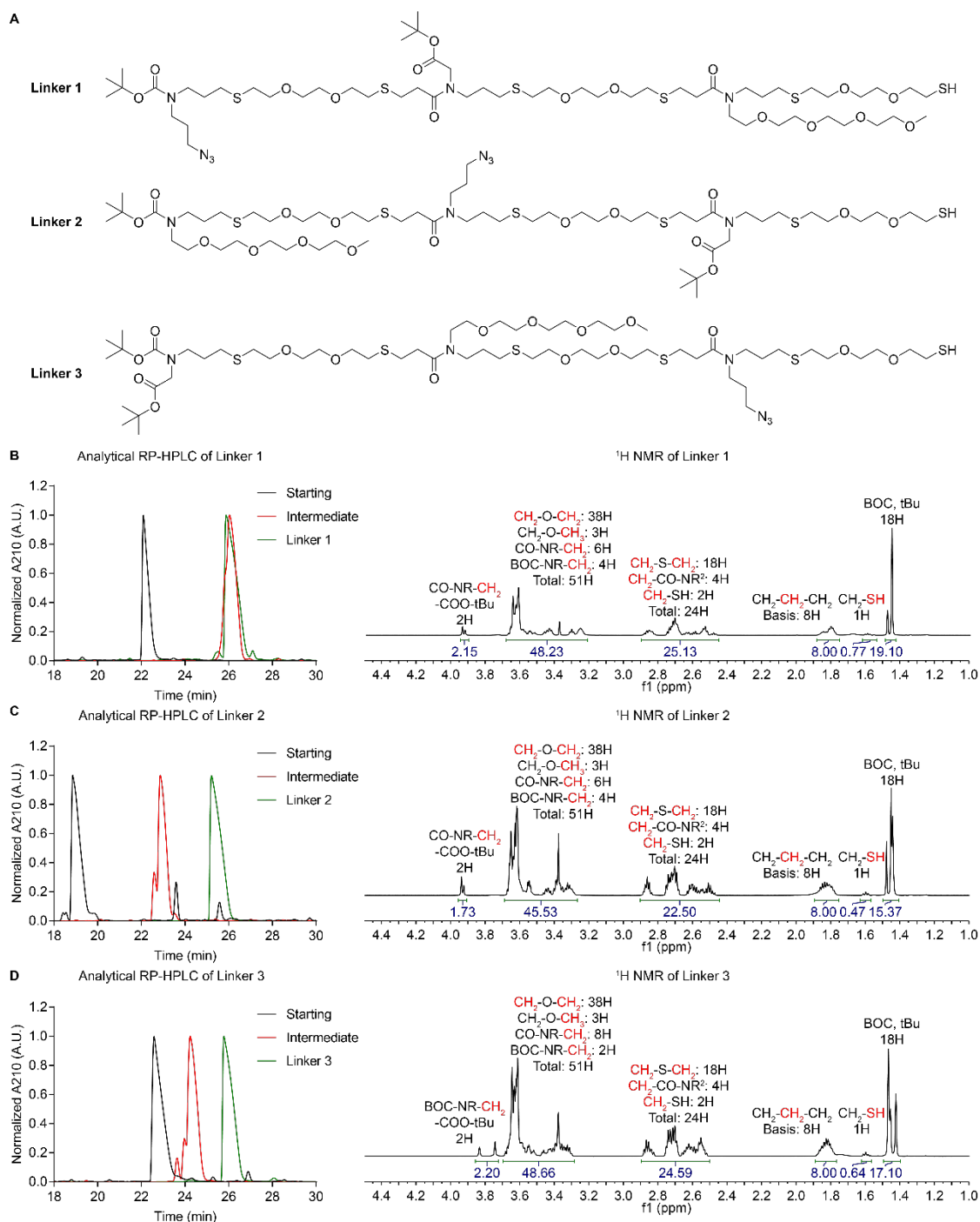
Figure 4.9. Synthesis and characterization of multifunctional oligoTEAs. A) Structure of sequence-defined, multifunctional oligoTEAs, B) RP-HPLC (left) and ^{1}H NMR (right) for synthesis of oligomer 1, C) RP-HPLC (left) and ^{1}H NMR (right) for synthesis of oligomer 2, and D). RP-HPLC (left) and ^{1}H NMR (right) for synthesis of oligomer 3.

152

These structures contain four functional groups for bioconjugation (Boc protected amine, *tert*-butyl protected carboxylic acid, azide, and thiol) and a hydrophilic PEG side chain (**Figure 4.9**). Reverse phase high pressure liquid chromatography (RP-HPLC) was used for purification after each synthetic step. Each intermediate product was isolated in reasonable. The predominated impurity for the intermediates was deprotection of the acetylated thiol due to the presence of catalytic amounts of base required for the thiol-Michael reaction. However, this impurity does not interfere with subsequent synthetic steps. The purity of each oligomer was confirmed via ^{1}H NMR. Each oligomer was isolated in high purity as indicated by the accurate integration of the characteristic peaks. Further each oligomer was isolated at a near 10 mg scale (oligomer 1: 10.4 mg, oligomer 2: 8.5 mg, and oligomer 3: 9.0 mg). This data presents the sequential reaction approach as a viable alternative that will provide greater structural flexibility compared to complex, bi-functional monomers.

Materials and Methods

Reagents for Chemical Synthesis

All chemicals were purchased from MilliporeSigma unless stated otherwise.

Reagents for Molecular Biology and Cell Culture

All cell culture reagents were purchased from ThermoFisher Scientific unless stated otherwise. SKOV3 and MCF7 cells were cultured in Dulbecco's Modified Eagle Medium (DMEM) and DMEM supplemented with insulin (0.01 mg/mL), respectively. CellTiter 96® AQ$_{ueous}$ One Solution Cell Proliferation Assay (MTS) was purchased from Promega.

Flash Chromatography

Flash chromatography was performed on a Teledyne ISCO CombiFlash Rf-200i chromatography system equipped with UV-Vis and evaporative light scattering detectors (ELSD).

Nuclear Magnetic Resonance (NMR) Spectroscopy

^{1}H and ^{13}C NMR spectra were recorded on either an INOVA 400 MHz or 500 MHz spectrometer as specified. NMR data was analyzed by MestReNova software. ^{1}H and ^{13}C NMR chemical shifts are reported in units of ppm relative to chloroform.

Liquid Chromatography Mass Spectrometry (LC-MS)

LC-MS analysis was carried out on an Agilent 1100 Series LC with a Poroshell 120 EC-C18 column (100 × 3 mm, 2.7 μm, Agilent Technologies) and an Agilent G1956B Series Single Quadripole MS in positive ion mode for mass detection. The mobile phase for LC-MS (solvent A) was water with 0.1% (v/v) acetic acid, and the stationary phase (solvent B) was acetonitrile with 0.1% (v/v) acetic acid. Compounds were eluted at a flow rate of 0.6 mL/min using a gradient of 5-100% solvent B (0-10 minutes) followed

by 100% solvent B (10-12 minutes) and equilibrated back to 5% solvent B (12-15 minutes).

Reverse Phase High Performance Liquid Chromatography (RP-HPLC)

HPLC purification was performed on an Agilent 1100 Series HPLC system equipped with a UV diode array detector and an 1100 Infinity fraction collector. Semi-preparative RP-HPLC was performed with a C18 column (Agilent Eclipse XDB-C18, 9.4 x 250 mm, 5 μm). Analytical RP-HPLC was performed with a C18 column (Agilent Eclipse Plus C18, 4.6 x 150 mm, 5 μm). The mobile phase for HPLC was water with 0.1% (v/v) trifluoroacetic acid (solvent A) and acetonitrile with 0.1% (v/v) trifluoroacetic acid (solvent B) unless specified otherwise. Compounds were eluted at a flow rate of either 4 mL/min (semi-preparative) or 1 mL/min (analytical) using a linear solvent gradient as specified below.

Hydrophobic Interaction Chromatography (HIC)

HIC was performed on an Agilent 1100 Series HPLC system equipped with a UV diode array detector and an 1100 Infinity fraction collector using a Tosoh Biosciences TSKgel SuperSW3000 column (4.6 x 300 mm, 4 μm). The mobile phase for SEC was 100 mM Na_2SO_4, 100 mM phosphate, pH 6.7. Compounds were eluted isocratic at a flow rate of 0.35 mL/min.

Size Exclusion Chromatography (SEC)

SEC was performed on an Agilent 1100 Series HPLC system equipped with a UV diode array detector and an 1100 Infinity fraction collector using a reversed-phase phenyl column (Tosoh Biosciences LLC, TSKgel Phenyl-5PW, 7.5 x 75 mm, 10 μm). The mobile phase for HIC was 25 mM phosphate, 1.5 M ammonium sulfate, pH 7.0 (solvent A) and 18.75 mM phosphate, 25% (v/v) isopropyl alcohol, pH 7.0 (solvent B).

Compounds were eluted at a flow rate of 1 mL/min using a linear solvent gradient as specified below.

Flow Cytometry Quantification of Binding Affinity (K$_D$)

One day prior to the experiment, SKOV3 cells were plated at 60,000 cells/well in a 24-well plate. The next day, the media was removed, the cells were washed with PBS, and then incubated at 37°C for 1 hour with dilutions of fluorescein-modified antibody starting at a concentration of 10 nM. After incubation, the cells were washed with PBS, trypsinized, pelleted, and suspended in PBS for flow cytometry analysis. Green fluorescence was measured on a BD FACS Calibur with BD FACS Calibur with the following instrument settings: FSC detector: E-1 Voltage, 3 Amp Gain, SSC detector: 400 Voltage, 1 Amp Gain, FL1 detector: 600 Voltage, 1 Amp Gain. Data processing was performed using FlowJo software.

Flow Cytometry Analysis of Competitive Binding

One day prior to the experiment, SKOV3 cells were plated at 60,000 cells/well in a 24-well plate. The next day, the media was removed, the cells were washed with PBS, and then incubated at 37°C for 1 hour with a mixture of 1 nM of fluorescein-modified antibody and three-fold serial dilutions of the conjugate to be tested starting at a concentration of 100 nM. After incubation, the cells were washed with PBS, trypsinized, pelleted, and suspended in PBS for flow cytometry analysis. Green fluorescence was measured on a BD FACS Calibur with BD FACS Calibur with the following instrument settings: FSC detector: E-1 Voltage, 3 Amp Gain, SSC detector: 400 Voltage, 1 Amp Gain, FL1 detector: 600 Voltage, 1 Amp Gain. Data processing was performed using FlowJo software.

In Vitro Potency of Antibody-drug Conjugates

SKOV3 and MCF7 cells were plated at 6,000 and 1,500 cells/well, respectively, and allowed to adhere overnight. After overnight incubation, three-fold serial dilutions of the conjugates or MMAE control starting at 100 nM were added. Treated cells were then incubated for 4 days. Cell viability was measured using MTS according to the manufacturer's instructions using a Tecan Infinite M1000 Pro microplate reader. Percent viability was calculated by comparison to untreated cells and media alone. Potency data for MCF7, a Her2 negative cell line, is provided.

Synthesis of Compound (1) (*Figure A4. 1* **and** *Figure A4. 2***)**

1 equivalency of acetyl chloride (400 mg, 5.3 mmol) was dissolved at 1.7 M in tetrahydrofuran. Separately, 2 equivalencies of 2,2'-(ethane-1,2-diylbis(oxy))bis(ethane-1-thiol) was dissolved at 150 mM in tetrahydrofuran in the presence of 6 equivalencies of triethylamine and stirred on ice for 15 minutes. The acetyl chloride solution was then added dropwise on ice over one hour. The reaction mixture was removed to room temperature for one hour. Then the reaction was quenched with 50 mL of water and extracted with ethyl acetate (40 mL, 3x). The combined organic layers were dried with sodium sulfate and concentrated under vacuum. Compound **(1)** was purified via silica gel flash chromatography. Solvent A: hexanes. Solvent B: ethyl acetate. Gradient: 0 – 30% solvent B over 40 minutes. Elution: 15% ethyl acetate. Yield: 60%, 740 mg, 3.3 mmol. The product was characterized by ^{1}H NMR.

Synthesis of Compound (2) (*Figure A4. 3* **and** *Figure A4. 4***)**

1 equivalency of tert-butyl 2-bromoacetate (1 g, 5.2 mmol) was added dropwise to a stirred solution of 10 equivalencies of prop-2-en-1-amine and 1.1 equivalencies of potassium carbonate. The mixture was reacted at room temperature overnight. The

mixture was then filtered through celite and recovered by washing with a copious amount of dichloromethane. The filtered product was collected and concentrated under vacuum. The crude product **(2)** was used without further purification. Yield: 95%, 840 mg, 4.9 mmol. The product was characterized by ^{1}H NMR.

Synthesis of Compound (3) (*Figure A4. 5*** and *Figure A4. 6***)**

1 equivalency of **(2)** (920 mg, 5.4 mmol) was dissolved at 214 mM in dichloromethane. Triethylamine (1.1 equivalencies) was added to the solution. The resulting mixture was stirred on ice for 5 minutes. Separately, 1.1 equivalency of di-tert-butyl dicarbonate was dissolved at 550 mM in dichloromethane. The di-tert-butyl dicarbonate solution was added to the stirred solution over 5 minutes. The mixture was reacted on ice for 1 hour. The mixture was then removed to room temperature and react at room temperature overnight. The reaction was quenched with 150 mL of saturated sodium bicarbonate and extracted with dichloromethane (50 mL, 3x). The combined organic layers were dried with sodium sulfate and concentrated under vacuum. The crude product **(3)** was used without further purification. Yield: 97%, 1430 mg, 5.3 mmol. The product was characterized by ^{1}H NMR.

Synthesis of Compound (4) (*Figure A4. 7*** and *Figure A4. 8***)**

1 equivalency of **(3)** (800 mg, 3 mmol) was dissolved at 1 M in methanol. 3 equivalencies of 2,2'-(ethane-1,2-diylbis(oxy))bis(ethane-1-thiol) and 0.6 equivalencies of 2,2-dimethoxy-1,2-diphenylethan-1-one were added to this solution. The mixture was irradiated with UV light at 20 mW/cm^2 for 270 seconds. The solvent was removed under vacuum. Compound **(4)** was purified via silica gel flash chromatography. Solvent A: hexanes. Solvent B: ethyl acetate. Gradient: 0 – 30% solvent B over 30 minutes. Elution: 25% ethyl acetate. Yield: 48%, 640 mg, 1.4 mmol. The product was characterized by ^{1}H NMR and LC-MS (calculated: 476.22, observed: 476.20 [M+Na]$^+$).

Synthesis of Compound (5) (*Figure A4. 9* **and** *Figure A4. 10***)**

1 equivalency of **(3)** (800 mg, 3 mmol) was dissolved at 1 M in methanol. 1.1 equivalencies of **(1)** and 0.22 equivalencies of 2,2-dimethoxy-1,2-diphenylethan-1-one were added to this solution. The mixture was irradiated with UV light at 20 mW/cm^2 for 270 seconds. The solvent was removed under vacuum. Compound **(5)** was purified via silica gel flash chromatography. Solvent A: hexanes. Solvent B: ethyl acetate. Gradient: 0 – 30% solvent B over 30 minutes. Elution: 25% ethyl acetate. Yield: 63%, 920 mg, 1.9 mmol. The product was characterized by ^{1}H NMR and LC-MS (calculated: 518.23, observed: 518.20 [M+Na]$^+$).

Synthesis of Compound (6) (Figure A4. 11 and Figure A4. 12)

Selective removal of the Boc protecting group was achieved by dissolving 1 equivalency (660 mg, 1.3 mmol) of **(5)** at 200 mM in ethyl acetate in the presence of 5 equivalencies of hydrochloric acid. Boc deprotection was carried out at room temperature for 4 hours. The reaction was then place on ice and the hydrochloric acid was neutralized with triethylamine. 2 equivalencies of triethylamine were added to the neutralized reaction mixture and stirred on ice for 5 minutes. Separately, 1.5 equivalencies of acryloyl chloride were dissolved at 1.1 M in ethyl acetate. The acryloyl chloride solution was added dropwise over 1 hour on ice. The reaction was then removed to room temperature for 1 hour. The reaction was quenched with 150 mL of water and extracted with ethyl acetate (25 mL, 3x). The combined organic layers were dried with sodium sulfate and the solvent was removed under vacuum. The crude product **(6)** was purified via silica gel flash chromatography. Solvent A: hexanes. Solvent B: ethyl acetate. Gradient: 0 – 100% solvent B over 40 minutes. Elution: 67% ethyl acetate. Yield: 33%, 183 mg, 0.4 mmol. The product was characterized by ^{1}H NMR and LC-MS (calculated: 472.19, observed: 472.10 [M+Na]$^+$).

Synthesis of Compound (7) (Figure A4. 13 and Figure A4. 14)

1 equivalency of **(3)** (670 mg, 2.5 mmol) was dissolved at 1 M in methanol. 1.2 equivalencies of 2-(2-methoxyethoxy)ethane-1-thiol and 0.24 equivalencies of 2,2-dimethoxy-1,2-diphenylethan-1-one were added to this solution. The mixture was irradiated with UV light at 20 mW/cm^2 for 270 seconds. The solvent was removed under vacuum. Compound **(7)** was purified via silica gel flash chromatography. Solvent A: hexanes. Solvent B: ethyl acetate. Gradient: 0 – 40% solvent B over 40 minutes. Elution: 20% ethyl acetate. Yield: 64%, 640 mg, 1.6 mmol. The product was characterized by ^{1}H NMR and LC-MS (calculated: 430.23, observed: 430.20 [M+Na]$^+$).

Synthesis of Compound (8) (Figure A4. 15 and Figure A4. 16)

Removal of the Boc protecting group was achieved by dissolving 1 equivalency (640 mg, 1.6 mmol) of **(7)** at 500 mM in solution of 50% (v/v) trifluoroacetic acid in dichloromethane. The reaction was stirred at room temperature for 1 hour. Excess trifluoroacetic acid was removed under vacuum. The crude product was then dissolved at 214 mM in dichloromethane and residual trifluoroacetic acid was neutralized with triethylamine. 1.2 equivalencies of triethylamine were added to the neutralized reaction mixture and stirred on ice for 5 minutes. Separately, 1.5 equivalencies of acryloyl chloride were dissolved at 750 mM in dichloromethane. The acryloyl chloride solution was added dropwise over 1 hour on ice. The reaction was then removed to room temperature for 1 hour. The reaction was quenched with 150 mL of water and extracted with dichloromethane (40 mL, 3x). The combined organic layers were dried with sodium sulfate and the solvent was removed under vacuum. The crude product **(8)** was purified via silica gel flash chromatography. Solvent A: hexanes. Solvent B: ethyl acetate. Gradient: 0 – 100% solvent B over 30 minutes. Elution: 65% ethyl acetate. Yield: 15%,

86 mg, 0.24 mmol. The product was characterized by ^{1}H NMR and LC-MS (calculated: 384.19, observed: 384.15 [M+Na]$^+$).

Synthesis of Compound (9) (Figure A4. 17 and Figure A4. 18)

1 equivalency of 13-bromo-2,5,8,11-tetraoxatridecane (1 g, 3.7 mmol) was added dropwise to a stirred solution of 10 equivalencies of prop-2-en-1-amine and 1.1 equivalencies of potassium carbonate. The mixture was reacted at room temperature overnight. The mixture was then filtered through celite and recovered by washing with a copious amount of dichloromethane. The filtered product was collected and concentrated under vacuum. The crude product **(9)** was used without further purification. Yield: 93%, 940 mg, 3.8 mmol. The product was characterized by ^{1}H NMR.

Synthesis of Compound (10) (Figure A4. 19 and Figure A4. 20)

1 equivalency of **(9)** (940 mg, 3.8 mmol) was dissolved at 214 mM in dichloromethane. Triethylamine (1.1 equivalencies) was added to the solution. The resulting mixture was stirred on ice for 5 minutes. Separately, 1.1 equivalency of di-tert-butyl dicarbonate was dissolved at 550 mM in dichloromethane. The di-tert-butyl dicarbonate solution was added to the stirred solution over 5 minutes. The mixture was reacted on ice for 1 hour. The mixture was then removed to room temperature and react at room temperature overnight. The reaction was quenched with 150 mL of saturated sodium bicarbonate and extracted with dichloromethane (50 mL, 3x). The combined organic layers were dried with sodium sulfate and concentrated under vacuum. The crude product **(3)** was used without further purification. Yield: 95%, 1250 mg, 3.6 mmol. The product was characterized by ^{1}H NMR.

Synthesis of Compound (11) (Figure A4. 21 and Figure A4. 22)

1 equivalency of **(10)** (660 mg, 1.9 mmol) was dissolved at 1 M in methanol. 3 equivalencies of 2,2'-(ethane-1,2-diylbis(oxy))bis(ethane-1-thiol) and 0.6 equivalencies

of 2,2-dimethoxy-1,2-diphenylethan-1-one were added to this solution. The mixture was irradiated with UV light at 20 mW/cm^2 for 270 seconds. The solvent was removed under vacuum. Compound **(11)** was purified via silica gel flash chromatography. Solvent A: hexanes. Solvent B: ethyl acetate. Gradient: 0 – 100% solvent B over 30 minutes. Elution: 80% ethyl acetate. Yield: 58%, 580 mg, 1.1 mmol. The product was characterized by ^{1}H NMR and LC-MS (calculated: 552.27, observed: 552.20 [M+Na]$^+$).

Synthesis of Compound (12) (Figure A4. 23 and Figure A4. 24)

1 equivalency of **(10)** (870 mg, 2.5 mmol) was dissolved at 1 M in methanol. 1.1 equivalencies of **(1)** and 0.22 equivalencies of 2,2-dimethoxy-1,2-diphenylethan-1-one were added to this solution. The mixture was irradiated with UV light at 20 mW/cm^2 for 270 seconds. The solvent was removed under vacuum. Compound **(12)** was purified via silica gel flash chromatography. Solvent A: hexanes. Solvent B: ethyl acetate. Gradient: 0 – 100% solvent B over 30 minutes. Elution: 80% ethyl acetate. Yield: 67%, 950 mg, 1.7 mmol. The product was characterized by ^{1}H NMR and LC-MS (calculated: 594.28, observed: 594.20 [M+Na]$^+$).

Synthesis of Compound (13) (Figure A4. 25 and Figure A4. 26)

Removal of the Boc protecting group was achieved by dissolving 1 equivalency (615 mg, 1.1 mmol) of **(12)** at 500 mM in solution of 50% (v/v) trifluoroacetic acid in dichloromethane. The reaction was stirred at room temperature for 1 hour. Excess trifluoroacetic acid was removed under vacuum. The crude product was then dissolved at 214 mM in dichloromethane and residual trifluoroacetic acid was neutralized with triethylamine. 1.2 equivalencies of triethylamine were added to the neutralized reaction mixture and stirred on ice for 5 minutes. Separately, 1.5 equivalencies of acryloyl chloride were dissolved at 750 mM in dichloromethane. The acryloyl chloride solution was added dropwise over 1 hour on ice. The reaction was then removed to room

temperature for 1 hour. The reaction was quenched with 100 mL of water and extracted with dichloromethane (25 mL, 3x). The combined organic layers were dried with sodium sulfate and the solvent was removed under vacuum. The crude product was purified via silica gel flash chromatography. Solvent A: dichloromethane. Solvent B: methanol. Gradient: 0 – 10% solvent B over 30 minutes. Elution: 2.5% methanol. Yield: 70%, 400 mg, 0.75 mmol. The product was characterized by ^{1}H NMR and LC-MS (calculated: 526.24, observed: 526.20 [M+H]$^+$).

Synthesis of Compound (14) (Figure A4. 27 and Figure A4. 28)

1 equivalency of **(10)** (390 mg, 1.1 mmol) was dissolved at 1 M in methanol. 1.2 equivalencies of 2-(2-methoxyethoxy)ethane-1-thiol and 0.24 equivalencies of 2,2-dimethoxy-1,2-diphenylethan-1-one were added to this solution. The mixture was irradiated with UV light at 20 mW/cm^2 for 270 seconds. The solvent was removed under vacuum. Compound **(14)** was purified via silica gel flash chromatography. Solvent A: dichloromethane. Solvent B: methanol. Gradient: 0 – 5% solvent B over 30 minutes. Elution: 2.5% methanol. Yield: 76%, 410 mg, 0.85 mmol. The product was characterized by ^{1}H NMR and LC-MS (calculated: 506.29, observed: 506.20 [M+Na]$^+$).

Synthesis of Compound (15) (Figure A4. 29 and Figure A4. 30)

Removal of the Boc protecting group was achieved by dissolving 1 equivalency (410 mg, 0.85 mmol) of **(14)** at 500 mM in solution of 50% (v/v) trifluoroacetic acid in dichloromethane. The reaction was stirred at room temperature for 1 hour. Excess trifluoroacetic acid was removed under vacuum. The crude product was then dissolved at 214 mM in dichloromethane and residual trifluoroacetic acid was neutralized with triethylamine. 1.2 equivalencies of triethylamine were added to the neutralized reaction mixture and stirred on ice for 5 minutes. Separately, 1.5 equivalencies of acryloyl chloride were dissolved at 750 mM in dichloromethane. The acryloyl chloride solution

was added dropwise over 1 hour on ice. The reaction was then removed to room temperature for 1 hour. The reaction was quenched with 100 mL of water and extracted with dichloromethane (25 mL, 3x). The combined organic layers were dried with sodium sulfate and the solvent was removed under vacuum. The crude product **(15)** was purified via silica gel flash chromatography. Solvent A: dichloromethane. Solvent B: methanol. Gradient: 0 – 10% solvent B over 30 minutes. Elution: 3.5% methanol. Yield: 63%, 230 mg, 0.53 mmol. The product was characterized by ^{1}H NMR and LC-MS (calculated: 438.24, observed: 438.20 $[M+H]^+$).

Synthesis of Compound (16) (Figure A4. 31 – Figure A4. 33)

1 equivalency of 3-bromopropan-1-ol (4470 mg, 32.4 mmol) was dissolved at 950 mM in water. 2 equivalencies of sodium azide were added to this solution. The resulting mixture was heated to near reflux (90°C) and stirred overnight. Then the reaction mixture was extracted with dichloromethane (35 mL, 4x). The combined organic layer was dried with sodium sulfate and the solvent was removed under vacuum. The crude product **(16)** was used without further purification. Yield: 80%, 2630 mg, 26 mmol. The product was characterized by ^{1}H NMR and ^{13}C NMR.

Synthesis of Compound (17) (Figure A4. 34 – Figure A4. 36)

1 equivalency (1430 mg, 14 mmol) of (16) was dissolved at 340 mM in dry chloroform. 2 equivalencies of phosphorus tribromide were added to this solution slowly. The resulting mixture was refluxed at 50°C overnight. Then the reaction mixture was removed from reflux and placed in an ice bath. The reaction was quenched by the slow addition of 125 mL of saturated sodium bicarbonate and extracted with chloroform (50 mL, 4x). The combined organic layers were dried with sodium sulfate and the solvent was removed under vacuum. The crude product **(17)** was used without further

purification. Yield: 63%, 1450 mg, 8.9 mmol. The product was characterized by ^{1}H NMR and ^{13}C NMR.

Synthesis of Compound (18) (Figure A4. 37 and Figure A4. 38)

1 equivalency (1450 mg, 8.9 mmol) of **(17)** was added dropwise to a stirred solution of 10 equivalencies of prop-2-en-1-amine and 1.1 equivalencies of potassium carbonate. The mixture was reacted at room temperature overnight. The mixture was then filtered through celite and recovered by washing with a copious amount of dichloromethane. The filtered product was collected and concentrated under vacuum. The crude product **(18)** was used without further purification. Yield: 78%, 980 mg, 7 mmol. The product was characterized by ^{1}H NMR.

Synthesis of Compound (19) (Figure A4. 39)

1 equivalency of **(18)** (500 mg, 3.6 mmol) was dissolved at 214 mM in dichloromethane. Triethylamine (1.1 equivalencies) was added to the solution. The resulting mixture was stirred on ice for 5 minutes. Separately, 1.1 equivalency of di-tert-butyl dicarbonate was dissolved at 550 mM in dichloromethane. The di-tert-butyl dicarbonate solution was added to the stirred solution over 5 minutes. The mixture was reacted on ice for 1 hour. The mixture was then removed to room temperature and react at room temperature overnight. The reaction was quenched with 100 mL of saturated sodium bicarbonate and extracted with dichloromethane (80 mL, 4x). The combined organic layers were dried with sodium sulfate and concentrated under vacuum. The crude product **(19)** was used without further purification or characterization. Yield: 90%, 770 mg, 3.2 mmol.

Synthesis of Compound (20) (Figure A4. 40 and Figure A4. 41)

1 equivalency of **(19)** (494 mg, 2.1 mmol) was dissolved at 1 M in methanol. 3 equivalencies of 2,2'-(ethane-1,2-diylbis(oxy))bis(ethane-1-thiol) and 0.6 equivalencies of 2,2-dimethoxy-1,2-diphenylethan-1-one were added to this solution. The mixture

was irradiated with UV light at 20 mW/cm^2 for 270 seconds. The solvent was removed under vacuum. Compound **(20)** was purified via silica gel flash chromatography. Solvent A: hexanes. Solvent B: ethyl acetate. Gradient: 0 – 50% solvent B over 30 minutes. Elution: 33% ethyl acetate. Yield: 31%, 580 mg, 0.64 mmol. The product was characterized by ^{1}H NMR and LC-MS (calculated: 445.20, observed: 445.10 [M+Na]$^+$).

Synthesis of Compound (21) (Figure A4. 42 and Figure A4. 43)

1 equivalency (375 mg, 2.7 mmol) of **(18)** was dissolved at 214 mM in dichloromethane. 1.2 equivalencies of triethylamine were added to this solution and stirred on ice for 5 minutes. Separately, 1.2 equivalencies of acryloyl chloride were dissolved at 750 mM in dichloromethane. The acryloyl chloride solution was added dropwise over 1 hour on ice. The reaction was then removed to room temperature for 1 hour. The reaction was quenched with 10 mL of water and extracted with dichloromethane (50 mL, 3x). The combined organic layers were dried with sodium sulfate and the solvent was removed under vacuum. The crude product **(21)** was purified via silica gel flash chromatography. Solvent A: hexanes. Solvent B: ethyl acetate. Gradient: 0 – 100% solvent B over 30 minutes. Elution: 33% ethyl acetate. Yield: 30%, 156 mg, 0.80 mmol. The product was characterized by ^{1}H NMR.

Synthesis of Compound (22) (Figure A4. 44 and Figure A4. 45)

1 equivalency (890 mg, 5.2 mmol) of **(2)** was dissolved at 214 mM in dichloromethane. 1.2 equivalencies of triethylamine were added to this solution and stirred on ice for 5 minutes. Separately, 1.2 equivalencies of acryloyl chloride were dissolved at 750 mM in dichloromethane. The acryloyl chloride solution was added dropwise over 1 hour on ice. The reaction was then removed to room temperature for 1 hour. The reaction was quenched with 100 mL of water and extracted with dichloromethane (50 mL, 3x). The combined organic layers were dried with sodium sulfate and the solvent was removed

under vacuum. The crude product **(22)** was purified via silica gel flash chromatography. Solvent A: hexanes. Solvent B: ethyl acetate. Gradient: 0 – 50% solvent B over 30 minutes. Elution: 25% ethyl acetate. Yield: 72%, 848 mg, 3.8 mmol. The product was characterized by ^{1}H NMR.

Synthesis of Compound (23) (Figure A4. 46 and Figure A4. 47)

1 equivalency (890 mg, 3.6 mmol) of **(9)** was dissolved at 214 mM in dichloromethane. 1.2 equivalencies of triethylamine were added to this solution and stirred on ice for 5 minutes. Separately, 1.2 equivalencies of acryloyl chloride were dissolved at 750 mM in dichloromethane. The acryloyl chloride solution was added dropwise over 1 hour on ice. The reaction was then removed to room temperature for 1 hour. The reaction was quenched with 100 mL of water and extracted with dichloromethane (50 mL, 3x). The combined organic layers were dried with sodium sulfate and the solvent was removed under vacuum. The crude product **(23)** was purified via silica gel flash chromatography. Solvent A: dichloromethane. Solvent B: methanol. Gradient: 0 – 5% solvent B over 15 minutes. Elution: 2.5% methanol. Yield: 79%, 860 mg, 2.86 mmol. The product was characterized by ^{1}H NMR.

Synthesis of PEGylated Oligomers (Compounds 24 – 29) (Figure A4. 48 – Figure A4. 54)

Step 1: 1 equivalency of thiol-containing starting material **(compound 4 or 11)** was dissolved at 500 mM in acetonitrile. 1 equivalency of mono-protected acrylamide monomer **(compound 6 or 13)** and 1 equivalency of triethylamine were added. This mixture was reacted overnight at room temperature and then purified via semi-preparative RP-HPLC. The reaction mixture was separated using a linear solvent gradient of 5 – 95% solvent B over 30 minutes and characterized via LC-MS.

Compound **(24):** eluted at 28.4 min. Calculated 1001.46, Observed 1001.40 [M+Na]$^+$

Compound **(25):** eluted at 28.0 min. Calculated 1001.46, Observed 1001.36 [M+Na]$^+$

Compound **(26):** eluted at 24.8 min. Calculated 1077.52, Observed 1077.30 [M+Na]$^+$

Step 2: Removal of the thioester protecting group was achieved by dissolving 1 equivalency of step 1 product **(compound 24, 25, or 26)** at 175 mM in methanol containing 7 M ammonia. Deprotection was performed for 1 hour at room temperature. After deprotection, methanol and ammonia were removed under vacuum. The deprotected product was then dissolved at 500 mM in acetonitrile. 1.2 equivalency of acrylamide monomer **(compound 8 or 15)** and 0.1 equivalencies of DBU were added. The mixture was reacted overnight at room temperature and then purified via semi-preparative RP-HPLC. The reaction mixture was separated using a linear solvent gradient of 5 – 95% solvent B over 30 minutes and characterized via ^{1}H NMR and LC-MS.

Compound **(27):** eluted at 26.0 min. Calculated 1396.70, Observed 1396.50 [M+Na]$^+$

Compound **(28):** eluted at 25.8 min. Calculated 1396.70, Observed 1396.40 [M+Na]$^+$

Compound **(29):** eluted at 25.6 min. Calculated 1396.70, Observed 1396.60 [M+Na]$^+$

Synthesis of Multifunctional Oligomers (Compounds 30 – 35) (Figure A4. 55 – Figure A4. 61)

Step 1: 1 equivalency of thiol-containing starting material **(compound 4, 11, 20)** was dissolved at 500 mM in acetonitrile. 1.1 equivalency of *N*-allylacrylamide monomer **(compound 21, 22, or 23)** and 0.1 equivalency of DBU were added. This mixture was reacted overnight at room temperature and then dried under vacuum. The crude product was then suspended at 1 M in methanol. 3 equivalencies of compound **(1)** and 0.6 equivalencies of 2,2-dimethoxy-1,2-diphenylethan-1-one were added to this solution. The mixture was irradiated with UV light at 20 mW/cm^2 for 270 seconds and then purified via semi-preparative RP-HPLC. The reaction mixture was separated using

a linear solvent gradient of 5 – 95% solvent B over 30 minutes followed by 5 minutes of isocratic 95% solvent B and characterized via LC-MS.

Compound **(30):** eluted at 30.4 minutes. Calculated 894.39, Observed 894.20 [M+Na]$^+$

Compound **(31):** eluted at 27.0 minutes. Calculated 970.45, Observed 970.30 [M+Na]$^+$

Compound **(32):** eluted at 28.6 minutes. Calculated 1001.46, Observed 1001.30 [M+Na]$^+$

Step 2: Removal of the thioester protecting group was achieved by dissolving 1 equivalency of step 1 product **(compound 30, 31, or 32)** at 175 mM in methanol containing 7 M ammonia. Deprotection was performed for 1 hour at room temperature. After deprotection, methanol and ammonia were removed under vacuum. The deprotected product was then dissolved at 500 mM in acetonitrile. 1.1 equivalency of *N*-allylacrylamide monomer **(compound 21, 22, or 23)** and 0.1 equivalencies of DBU were added. The mixture was reacted overnight at room temperature and then dried under vacuum. The crude product was then suspended at 1 M in methanol. 3 equivalencies of 2,2'-(ethane-1,2-diylbis(oxy))bis(ethane-1-thiol) and 0.6 equivalencies of 2,2-dimethoxy-1,2-diphenylethan-1-one were added to this solution. The mixture was irradiated with UV light at 20 mW/cm^2 for 270 seconds and then purified via semi-preparative RP-HPLC. The reaction mixture was separated using a linear solvent gradient of 5 – 95% solvent B over 30 minutes followed by 5 minutes of isocratic 95% solvent B and characterized via ^{1}H NMR and LC-MS.

Compound **(33):** eluted at 30.2 minutes. Calculated 1335.61, Observed 1335.40 [M+Na]$^+$

Compound **(34):** eluted at 29.2 minutes. Calculated 1335.61, Observed 1335.50 [M+Na]$^+$

Compound **(35):** eluted at 30.0 minutes. Calculated 1335.61, Observed 1335.40 [M+Na]$^+$

Synthesis of Dipeptide-modified MMAE (Compound 36) (Figure A4. 62)

1 equivalency (11.6 mg, 16 μmol) of monomethyl auristatin e (MMAE) was dissolved at 250 mM in dimethylformamide. 2 equivalencies of Fmoc-Val-Cit-PAB-PNP ester, 0.2 equivalencies of HOBt, and 8 equivalencies of pyridine were added. The mixture was reacted for 2 days at 37°C. The Fmoc protecting group was removed by treatment with 20% (v/v) piperidine for 1 hour. The product **(36)** was purified via semi-preparative RP-HPLC. The reaction mixture was separated using a linear solvent gradient of 5 – 65% solvent B over 30 minutes Elution: 23.5 minutes. Yield: 87%, 15.7 mg, 14 μmol. The product was characterized via LC-MS (calculated: 1123.71, observed: 1123.50 [M+H]$^+$).

Synthesis of MMAE-loaded, PEGylated Cross-linkers (Compounds 37 – 45) (Figure A4. 63 – Figure A4. 69)

Step 1: Removal of the Boc and tert-butyl protecting groups was achieved by dissolving the oligomer **(Compound 27, 28, or 29)** at 50 mM in solution of 50% (v/v) trifluoroacetic acid in dichloromethane. The reaction was stirred at room temperature for 1 hour. Excess trifluoroacetic acid was removed under vacuum. The crude product was used without further purification or characterization.

Step 2: 1 equivalency of crude product from step 1 was dissolved at 50 mM in dimethyl sulfoxide. 3 equivalencies of triethylamine and 1 equivalency of Fmoc-PEG4-TFP ester was added. The mixture was reacted for 5 hours at room temperature. The product **(compound 37, 40, or 43)** was purified via semi-preparative RP-HPLC. The reaction mixture was separated using a linear solvent gradient of 5 – 95% solvent B over 30

minutes. The product **(compound 37, 40, or 43)** eluted at 23 minutes and was characterized via LC-MS.

Compound **(37):** Calculated 844.40, Observed 844.50 [M+2H]$^{2+}$

Compound **(40):** Calculated 844.40, Observed 844.50 [M+2H]$^{2+}$

Compound **(43):** Calculated 844.40, Observed 844.60 [M+2H]$^{2+}$

Step 3: 1 equivalency of product from step 2 **(compound 37, 40, or 43)** was dissolved at 20 mM in dimethyl sulfoxide. 3 equivalencies of N,N′-Diisopropylcarbodiimide, 3 equivalencies of 1-hydroxypyrrolidine-2,5-dione, 2 equivalencies of triethylamine, and 1 equivalency of compound **(36)** were added. The mixture was reacted overnight at room temperature. The Fmoc protecting group was removed by treatment with 5% (v/v) piperidine for 1 hour. The product **(compound 38, 41, or 44)** was purified via semi-preparative RP-HPLC. The reaction mixture was separated using a linear solvent gradient of 5 – 95% solvent B over 30 minutes. The product **(compound 38, 41, or 44)** eluted at 21 minutes and was characterized via LC-MS.

Compound **(38):** Calculated 857.50, Observed 857.80 [M+3H]$^{3+}$

Compound **(41):** Calculated 857.50, Observed 857.70 [M+3H]$^{3+}$

Compound **(44):** Calculated 857.50, Observed 857.90 [M+3H]$^{3+}$

Step 4: 1 equivalency of product from step 3 **(compound 38, 41, or 44)** was dissolved at 10 mM in dimethyl sulfoxide. 2 equivalencies of triethylamine and 1.25 equivalencies of Fmoc-HIPS-PFP ester were added. The mixture was reacted overnight at room temperature. The product **(compound 39, 42, or 45)** was purified via semi-preparative RP-HPLC. The reaction mixture was separated using a linear solvent gradient of 5 – 95% solvent B over 45 minutes. The product **(compound 39, 40, or 45)** eluted at 38.5 minutes and was characterized via LC-MS, observing fragmentation alpha to the hydrazide.

Compound **(39):** Calculated 1377.30, Observed 1377.70 [M+H]$^{2+}$

Compound **(42):** Calculated 1377.30, Observed 1377.70 [M+H]$^{2+}$

Compound **(45):** Calculated 1377.30, Observed 1377.70 [M+H]$^{2+}$

Synthesis of MMAE-loaded, Non-PEGylated Cross-linker (Compounds 46 – 47) (Figure A4. 70)

Synthesis of Compound (46): 1 equivalency (2.9 mg, 4.5 µmol) of **(36)** was dissolved at 33 mM in dimethyl sulfoxide. 2 equivalencies of triethylamine and 1 equivalency of Fmoc-PEG4-TFP ester were added. The mixture was reacted overnight at room temperature. The Fmoc protecting group was removed by treatment with 20% (v/v) piperidine for 1 hour. The product **(46)** was purified via semi-preparative RP-HPLC. The reaction mixture was separated using a linear solvent gradient of 5 – 95% solvent B over 30 minutes Elution: 17.5 minutes. Yield: 81%, 5 mg, 3.7 µmol. The product was characterized via LC-MS (calculated: 1370.85, observed: 1370.60 [M+H]$^+$).

Synthesis of Compound (47): 1 equivalency (5 mg, 3.7 µmol) of **(46)** was dissolved at 10 mM in dimethyl sulfoxide. 2 equivalencies of triethylamine and 1.25 equivalencies of Fmoc-HIPS-PFP ester were added. The mixture was reacted overnight at room temperature. The product **(47)** was purified via semi-preparative RP-HPLC. The reaction mixture was separated using a linear solvent gradient of 5 – 95% solvent B over 30 minutes Elution: 26.5 minutes. Yield: 49%, 3.3 mg, 1.8 µmol. The product was characterized via LC-MS, observing fragmentation alpha to the Fmoc-protected hydrazide (calculated: 1553.92, observed: 1553.80 [M]$^+$).

Synthesis of Fluorescein-modified Cross-linker (Compounds 48 – 49) (Figure A4. 71)

Synthesis of Compound (48): 1 equivalency (2 mg, 4.2 µmol) of fluorescein-NHS ester was dissolved at 57 mM in dimethyl sulfoxide. 2 equivalencies of triethylamine and 5

equivalencies of 2,2'-(ethane-1,2-diylbis(oxy))bis(ethan-1-amine) were added. The mixture was reacted overnight at room temperature. The product **(48)** was purified via semi-preparative RP-HPLC. The reaction mixture was separated using a linear solvent gradient of 5 – 95% solvent B over 30 minutes Elution: 10.5 minutes. Yield: 95%, 2 mg, 4 μmol. The product was characterized via LC-MS (calculated: 507.12, observed: 507.10 $[M+H]^+$).

Synthesis of Compound (49): 1 equivalency (2 mg, 4 μmol) of **(48)** was dissolved at 10 mM in dimethyl sulfoxide. 2 equivalencies of triethylamine and 1.25 equivalencies of Fmoc-HIPS-PFP ester were added. The mixture was reacted overnight at room temperature. The product **(49)** was purified via semi-preparative RP-HPLC. The reaction mixture was separated using a linear solvent gradient of 5 – 95% solvent B over 30 minutes Elution: 23.5 minutes. Yield: 49%, 2 mg, 1 μmol. The product was characterized via LC-MS (calculated: 972.37, observed: 972.20 $[M+H]^+$).

Synthesis of Dansyl-NH-Boc and Dansyl-NH$_2$ (Compound 50 and 51) (Figure A4. 72 and Figure A4. 73)

Synthesis of Compound (50): 1 equivalency (250 mg, 0.93 mmol) of 5-(dimethylamino)naphthalene-1-sulfonyl chloride was dissolved at 125 mM in dichloromethane. 1 equivalency of triethylamine and 3 equivalencies of tert-butyl (2-aminoethyl)carbamate were added to this solution and stirred on ice for 1 hour. The reaction was then removed to room temperature for 1 hour. The reaction was quenched with 5 mL of saturated sodium bicarbonate and extracted with dichloromethane (50 mL, 3x). The combined organic layers were dried with sodium sulfate and the solvent was removed under vacuum. The crude product **(50)** was purified via silica gel flash chromatography: Solvent A: dichloromethane. Solvent B: methanol. Gradient 0 – 2.5% solvent B over 20 minutes. Elution: 1.5% methanol. Yield: 69%, 250 mg, 0.64 mmol.

The product was characterized by ^{1}H NMR and LC-MS (calculated: 416.17, observed: 416.10 [M+Na]$^+$).

Synthesis of Compound (51): Removal of the Boc protecting group was achieved by dissolving 88 µmol of **(50)** at 50 mM in solution of 50% (v/v) trifluoroacetic acid in dichloromethane. The reaction was stirred at room temperature for 1 hour. Excess trifluoroacetic acid was removed under vacuum. The crude product was characterized via LC-MS (calculated: 294.12, observed 294.20 [M+H]$^+$)

Synthesis of Dansyl-NH-Ac (Compound 52) (Figure A4. 74)

1 equivalency (5.2 mg, 17.6 µmol) of **(51)** was dissolved at 24 mM in dichloromethane. 5 equivalencies of triethylamine and 2 equivalencies of acetyl chloride were added to this solution. The mixture was reacted for 1 hour at room temperature. The solvent was then removed under vacuum. The product **(52)** was purified via semi-preparative RP-HPLC. The reaction mixture was separated using a linear solvent gradient of 5 – 95% solvent B over 30 minutes Elution: 9 minutes. Yield: 95%, 5.6 mg, 16.7 µmol. The product was characterized via LC-MS (calculated: 336.13, observed: 336.10 [M+H]$^+$).

Synthesis of Dansyl-modified, PEGylated Cross-linkers (Compounds 53 – 58) (Figure A4. 75 – Figure A4. 79)

Step 1: Removal of the Boc and tert-butyl protecting groups was achieved by dissolving the oligomer **(Compound 27, 28, or 29)** at 50 mM in solution of 50% (v/v) trifluoroacetic acid in dichloromethane. The reaction was stirred at room temperature for 1 hour. Excess trifluoroacetic acid was removed under vacuum. The crude product was used without further purification or characterization.

Step 2: 1 equivalency of crude product from step 1 was dissolved at 24 mM in dichloromethane. 5 equivalencies of triethylamine and 2 equivalencies of acetyl chloride were added to this solution. The mixture was reacted for 1 hour at room

temperature. The solvent was then removed under vacuum. The product **(compound 53, 55, or 57)** was purified via semi-preparative RP-HPLC. The reaction mixture was separated using a linear solvent gradient of 5 – 95% solvent B over 30 minutes. The product **(compound 53, 55, or 57)** eluted at 18.2 minutes and was characterized via LC-MS.

Compound **(53):** Calculated 1260.59, Observed 1260.50 $[M+H]^{1+}$

Compound **(54):** Calculated 1260.59, Observed 1260.40 $[M+H]^{1+}$

Compound **(55):** Calculated 1260.59, Observed 1260.40 $[M+1H]^{1+}$

Step 3: 1 equivalency of product from step 2 **(compound 53, 55, or 57)** was dissolved at 33 mM in dimethyl sulfoxide. 4 equivalencies of N,N′-Diisopropylcarbodiimide, 4 equivalencies of 1-hydroxypyrrolidine-2,5-dione, 4 equivalencies of triethylamine, and 2 equivalency of compound **(51)** were added. The mixture was reacted for 2 hours at room temperature. The product **(compound 54, 56, or 58)** was purified via semi-preparative RP-HPLC. The reaction mixture was separated using a linear solvent gradient of 5 – 95% solvent B over 30 minutes. The product **(compound 54, 56, or 58)** eluted at 18.8 minutes and was characterized via LC-MS.

Compound **(56):** Calculated 1535.70, Observed 1535.60 $[M+H]^+$

Compound **(57):** Calculated 1535.70, Observed 1535.60 $[M+H]^+$

Compound **(58):** Calculated 1535.70, Observed 1535.70 $[M+H]^+$

Spectral Characterization of Dansyl-modified, PEGylated Cross-linkers

For absorbance measurements, compound 52, 56, 57, and 58 were dissolved at 2.5 mM in PBS buffer, pH 7.4. The absorbance spectrum of each compound was measured from 230 nm to 450 nm in increments of 1 nm. The peak absorbance wavelength of 327 nm was used for fluorescence measurements. To measure fluorescence, each compound was dissolved at 10 µM in PBS buffer, pH 7.4. Upon excitation with 327 nm

light, fluorescence emission was measured from 400 nm to 800 nm in increments of 2 nm with a bandwidth of 5 nm.

Synthesis of Antibody-drug and Antibody-fluorescein Conjugates

HIPS-modified cross-linkers were stored in their Fmoc-protected form prior to conjugation. The Fmoc protecting group was removed by dissolving the cross-linker **(compound 39, 42, 45, 47, or 49)** at 40 mM in dimethylacetamide containing 200 mM piperidine. Deprotection was carried out at room temperature for 1 hour. Deprotected cross-linker (20 equivalencies) was added to aldehyde-tagged antibody (1 equivalencies) at a final antibody concentration of 100 μM. The composition of the reaction solvent was 18.5% (v/v) dimethylacetamide in citrate buffer (20 mM citrate, 50 mM NaCl, pH 5.5). The mixture was reacted for 2 days at 37°C then purified via analytical HIC using a linear solvent gradient of 0 – 100% solvent B over 30 minutes followed by 5 minutes of isocratic 100% solvent B. The conjugates were concentrated and exchanged into PBS buffer, pH 7.4 using Amicon Ultra-0.5 mL centrifugal filters with a 30 kDa molecular weight cut off according to the manufacturer's instructions. Conjugate molecular weight and degree-of-labeling was characterized via MALDI-MS. Elution times for the conjugates in this work are as follows: Parent Antibody (17 minutes), Fluorescein-modified Antibody (22 minutes), Control Antibody-drug Conjugate (31.2 minutes), Antibody-drug Conjugate #1 (33.5 minutes), Antibody-drug Conjugate #2 (34 minutes), and Antibody-drug Conjugate #3 (34.3 minutes).

Chapter 4 Appendix

Effect of Cross-linker Sequence on the Biophysical Properties of Antibody-drug

Conjugates

Synthesis of Compound (1)
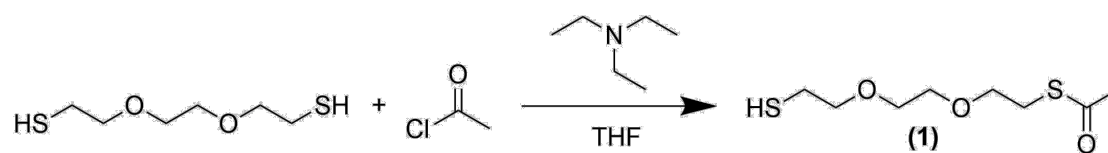
Figure A4. 1. Synthesis scheme for compound **(1)**.
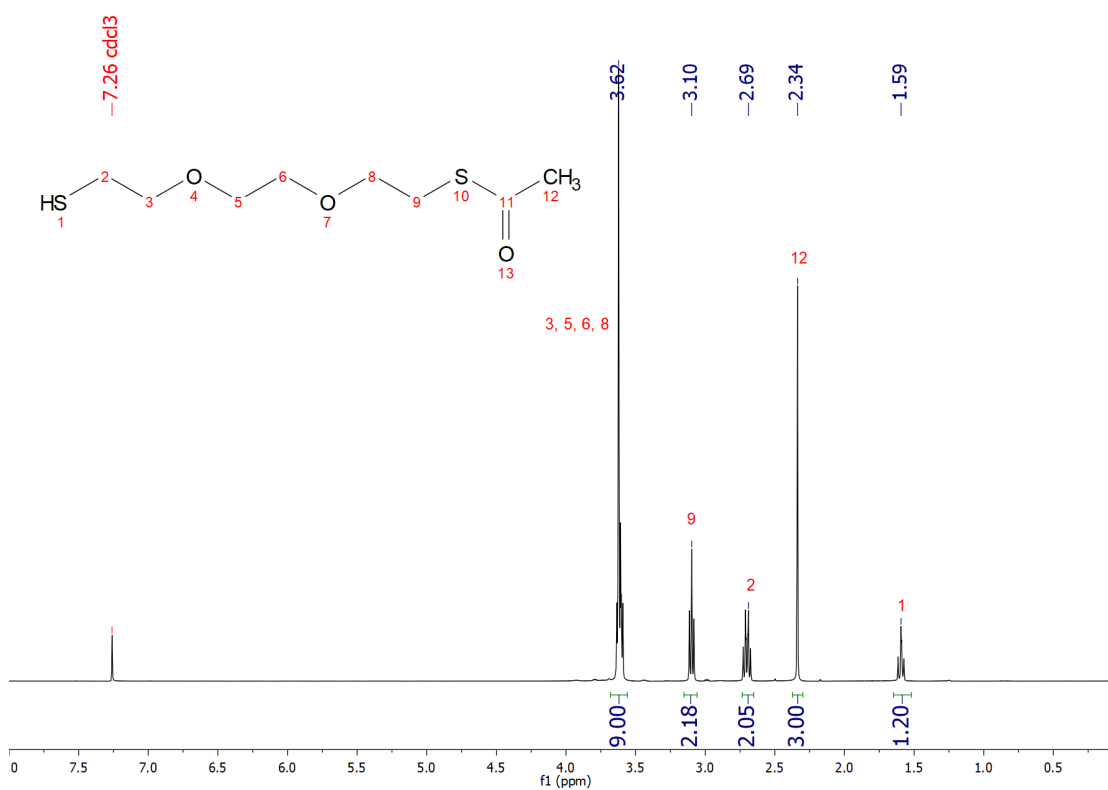
Figure A4. 2. ^{1}H NMR (400 MHz, CDCl$_3$) of compound **(1)**.

Synthesis of Compound (2)
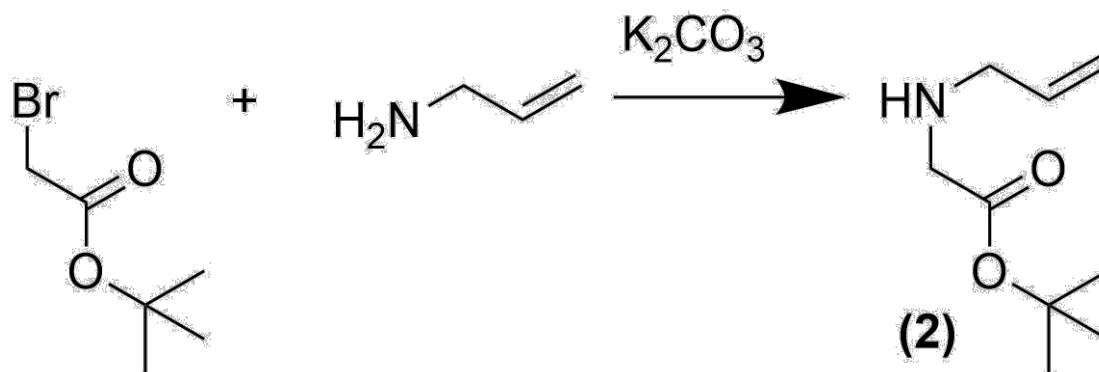
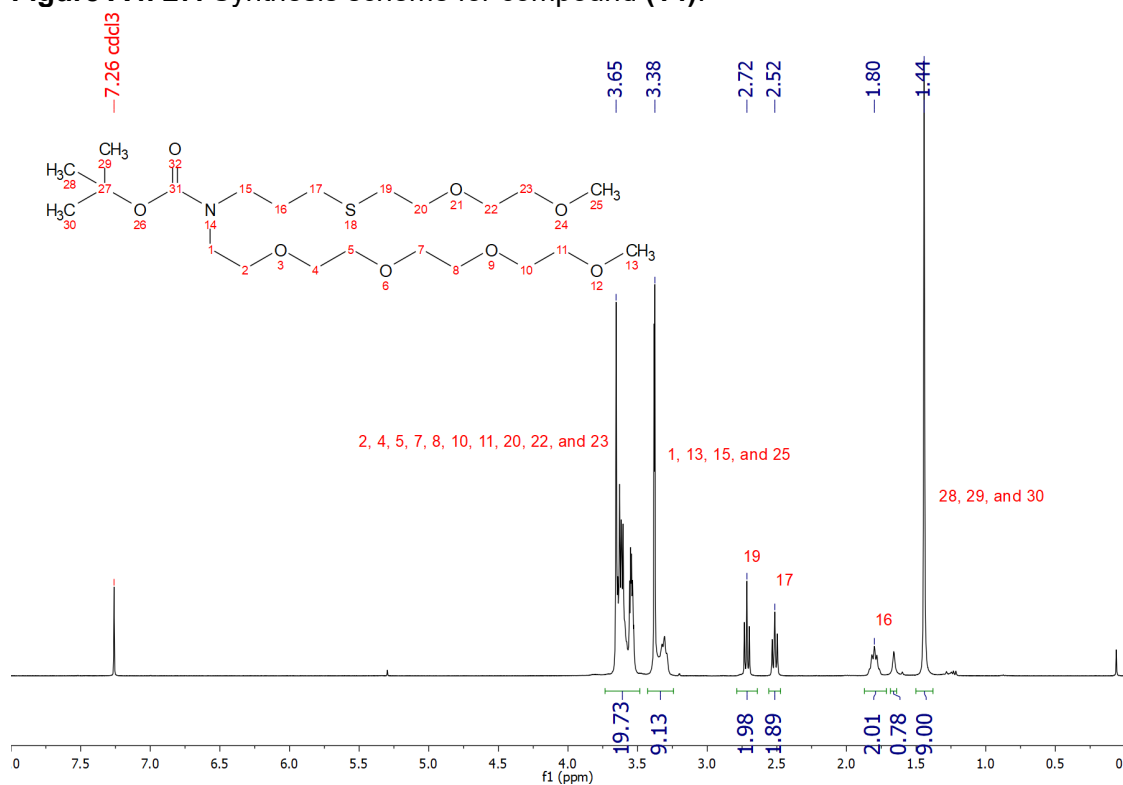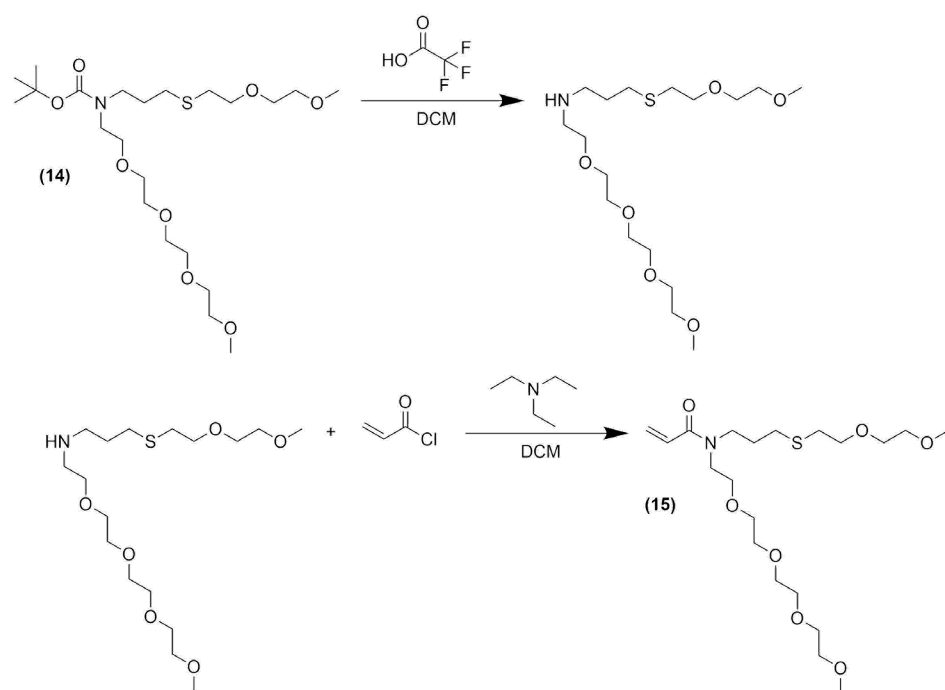**Figure A4. 3.** Synthesis scheme for compound **(2)**.
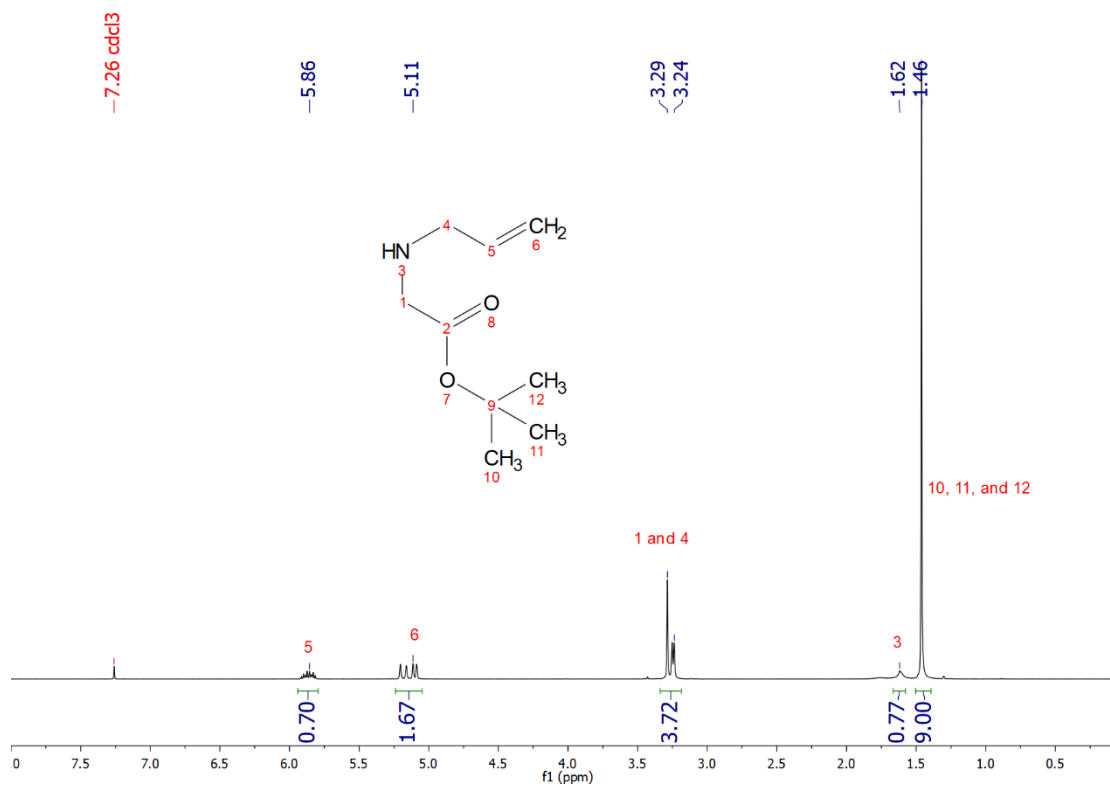
Figure A4. 4. ^1H NMR (400 MHz, CDCl$_3$) of compound **(2)**.

Synthesis of Compound (3)
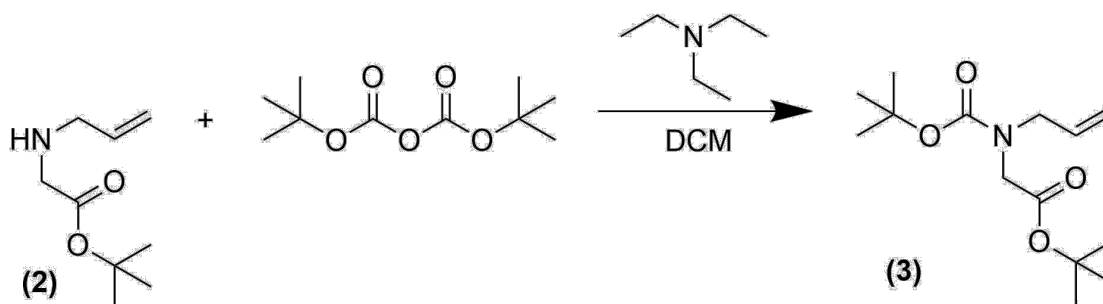
Figure A4. 5. Synthesis scheme for compound **(3)**.
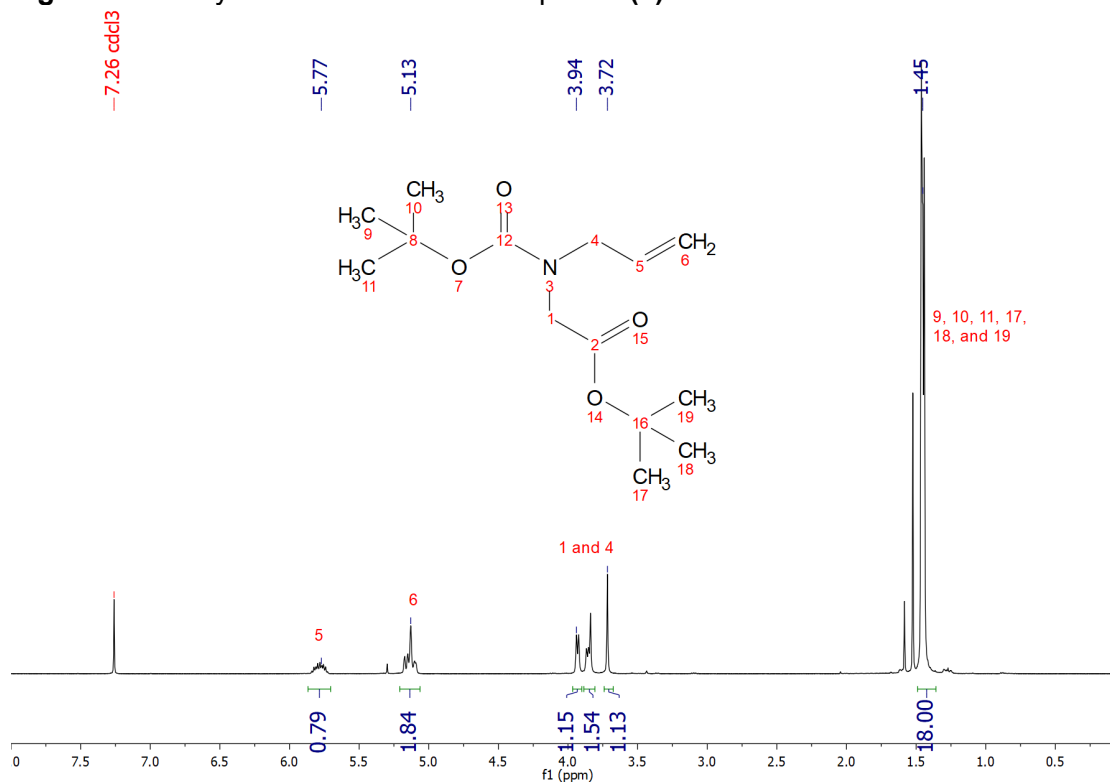
Figure A4. 6. ¹H NMR (400 MHz, CDCl$_3$) of compound **(3)**.

Synthesis of Compound (4)
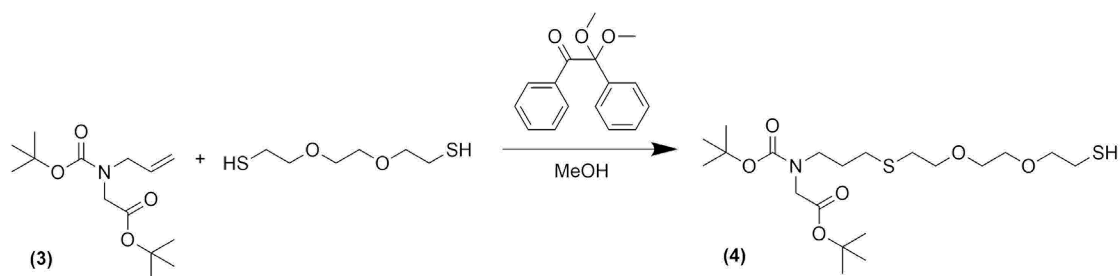
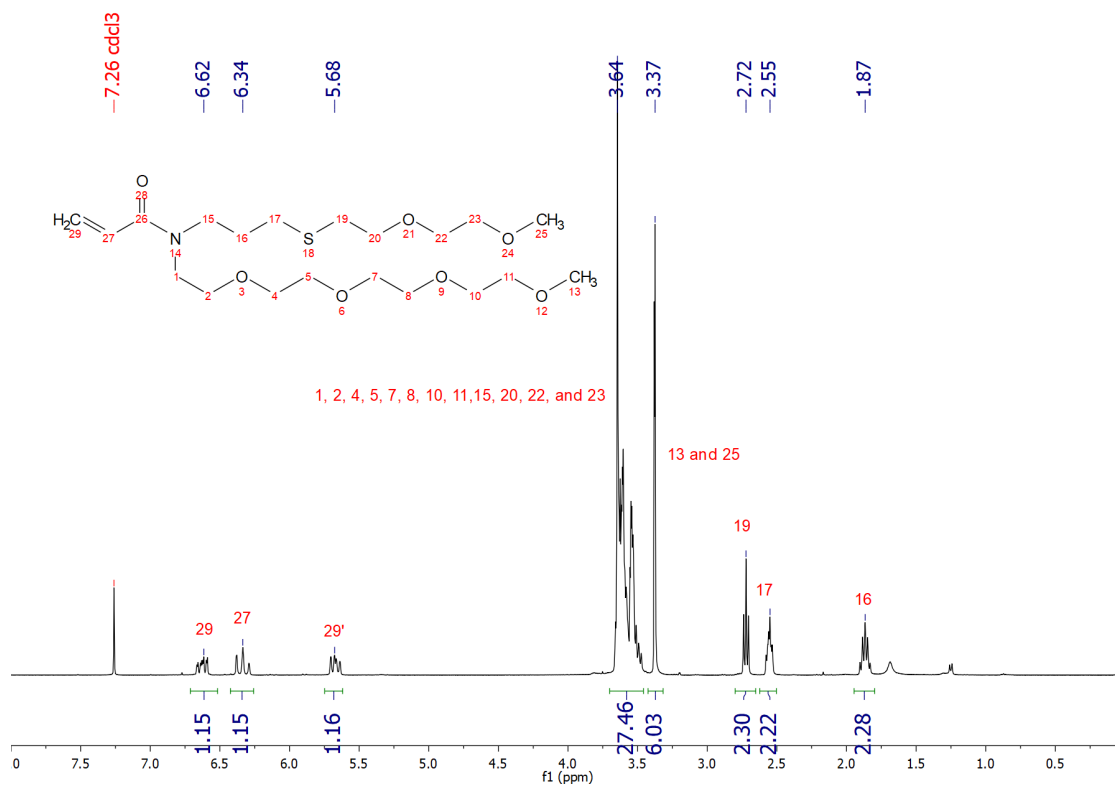**Figure A4. 7.** Synthesis scheme for compound **(4)**.
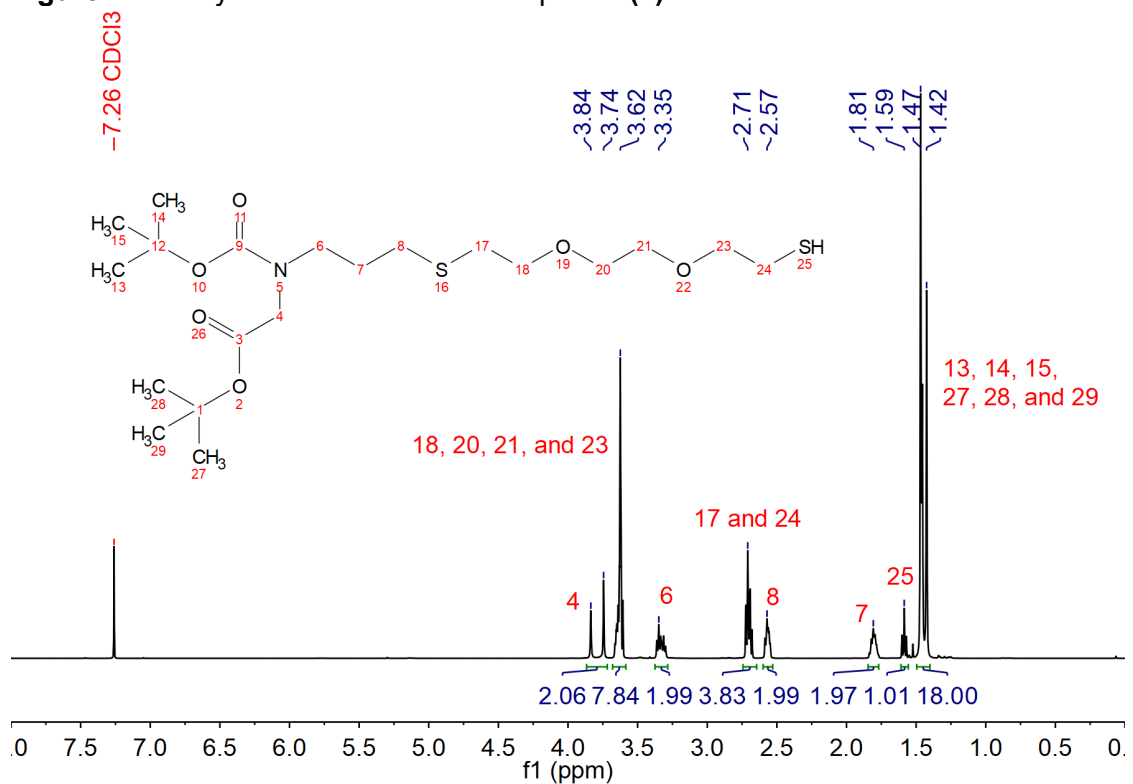
Figure A4. 8. ¹H NMR (500 MHz, CDCl₃) of compound **(4)**.

Synthesis of Compound (5)
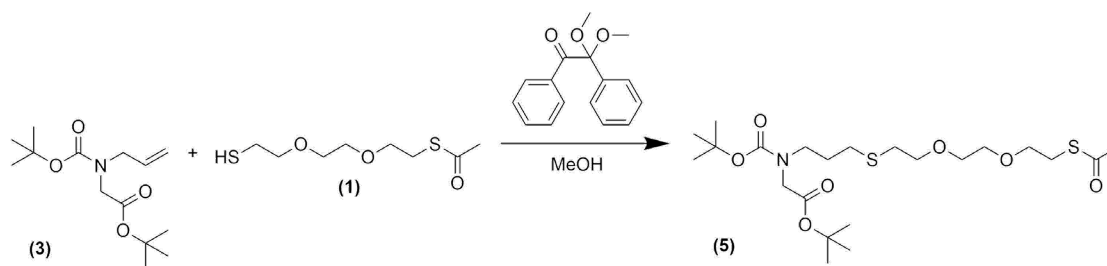
Figure A4. 9. Synthesis scheme for compound **(5)**.
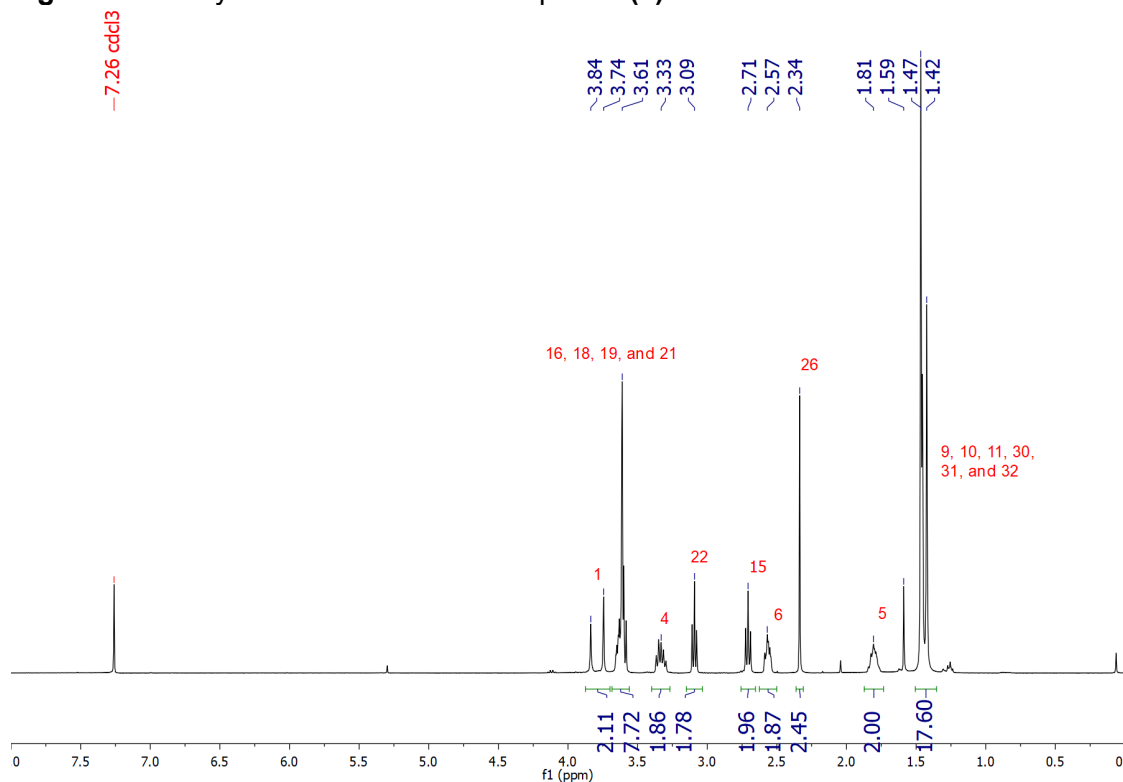
Figure A4. 10. ¹H NMR (400 MHz, CDCl₃) of compound **(5)**.

Synthesis of Compound (6)
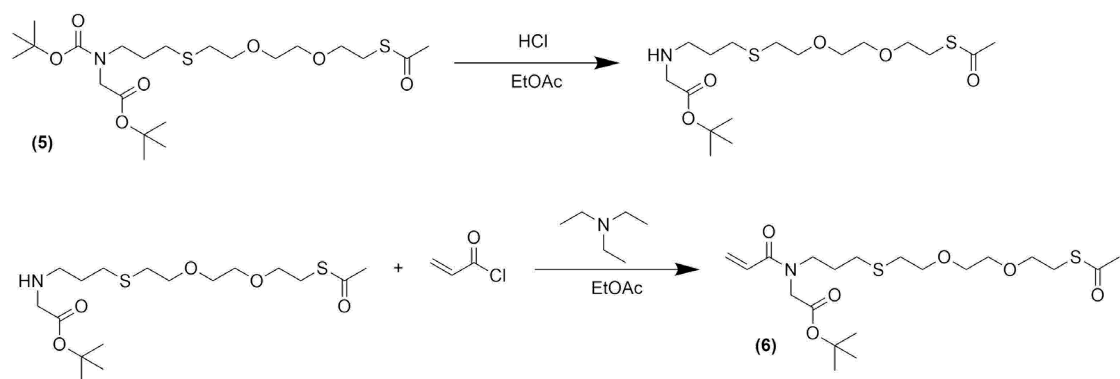
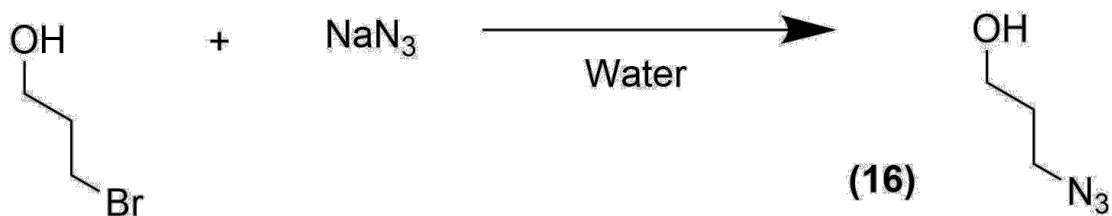**Figure A4. 11.** Synthesis scheme for compound **(6)**.
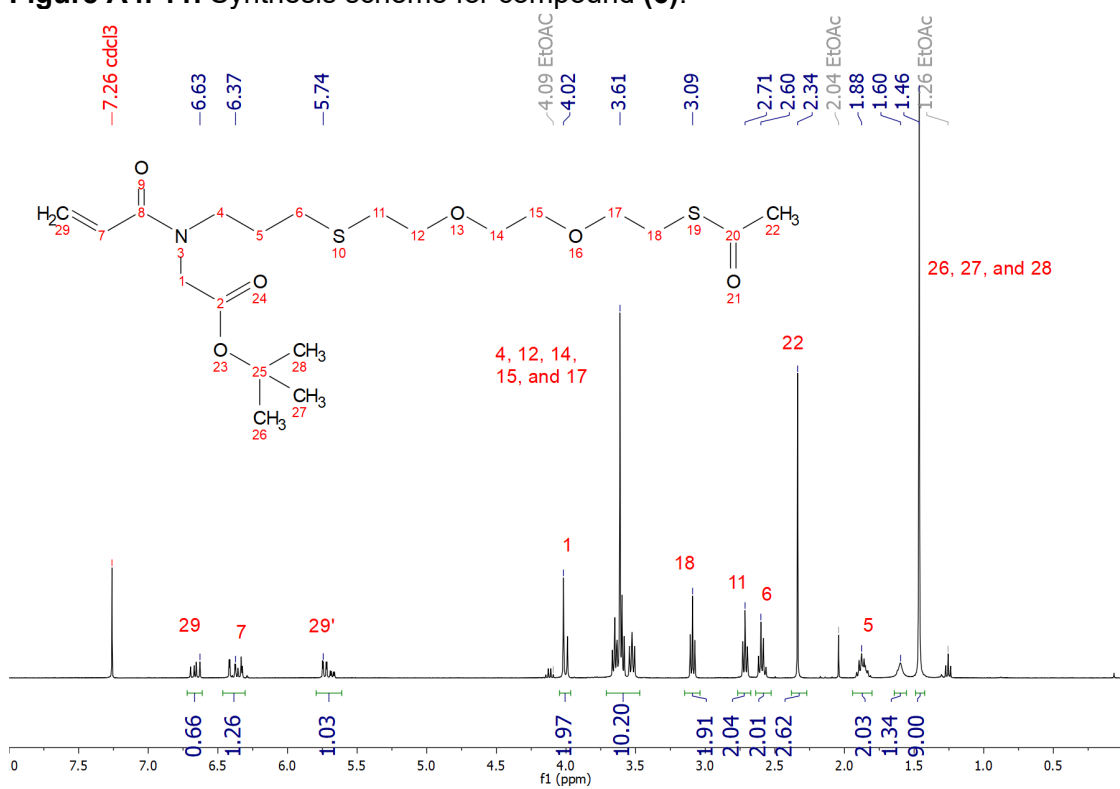
Figure A4. 12. ¹H NMR (400 MHz, CDCl₃) of compound **(6)**.

Synthesis of Compound (7)
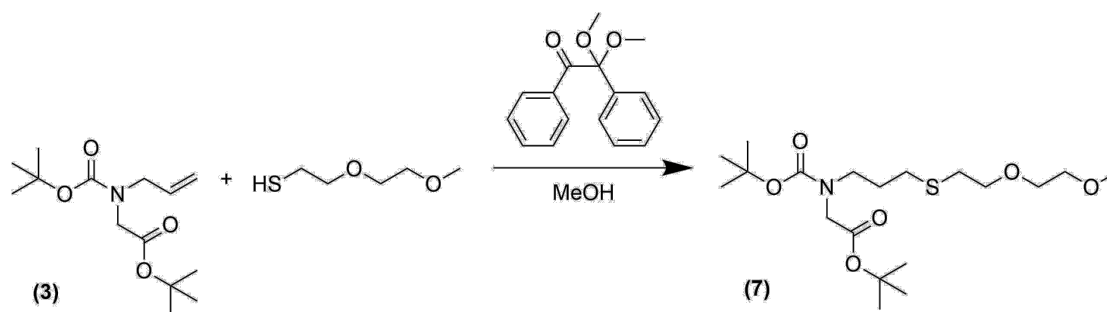
Figure A4. 13. Synthesis scheme for compound **(7)**.
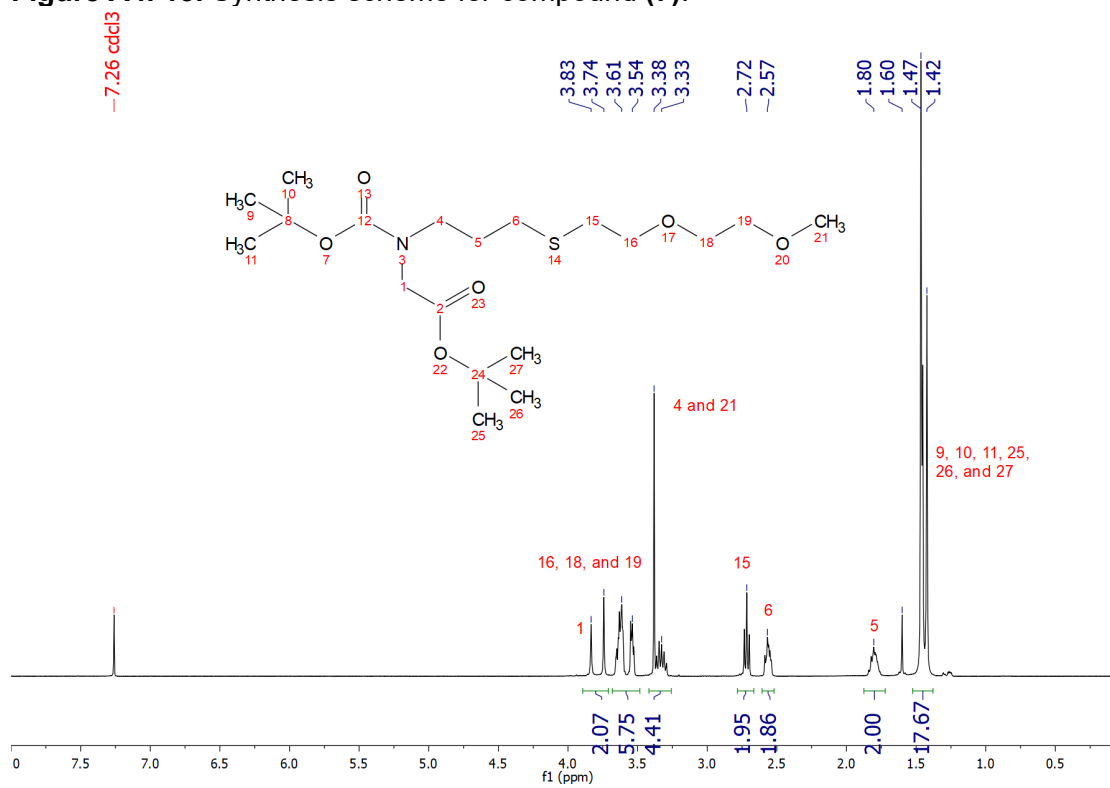
Figure A4. 14. 1H NMR (400 MHz, CDCl3) of compound **(7)**.

Synthesis of Compound (8)
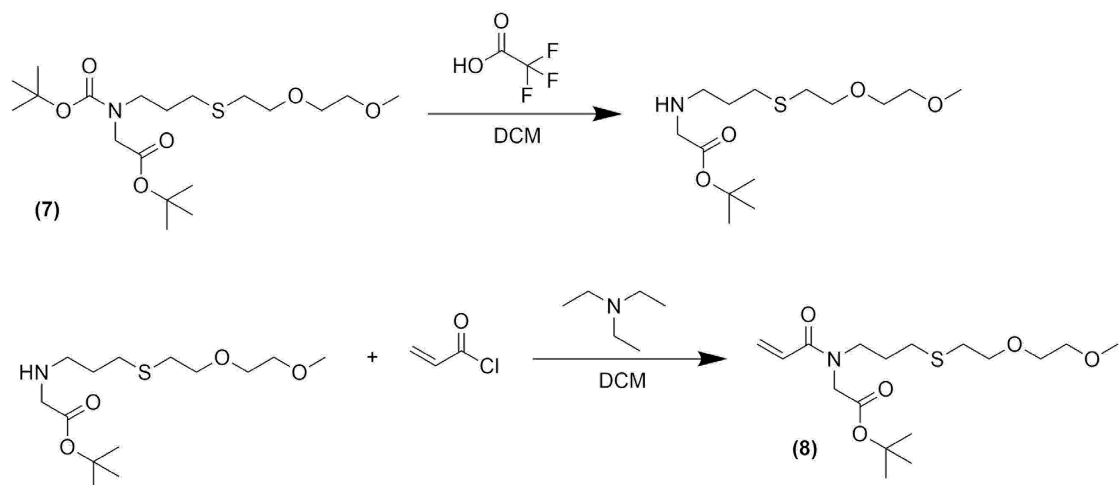
Figure A4. 15. Synthesis scheme for compound **(8)**.
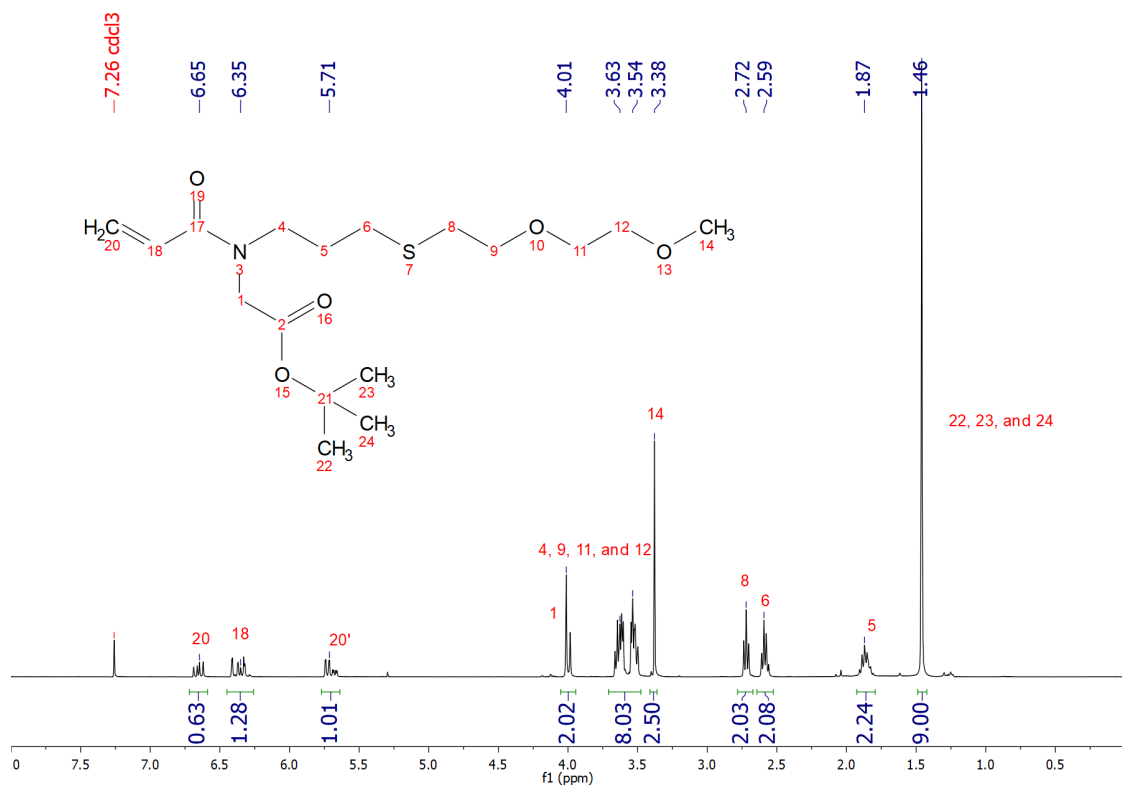
Figure A4. 16. ^{1}H NMR (400 MHz, CDCl$_3$) of compound **(8)**.

Synthesis of Compound (9)
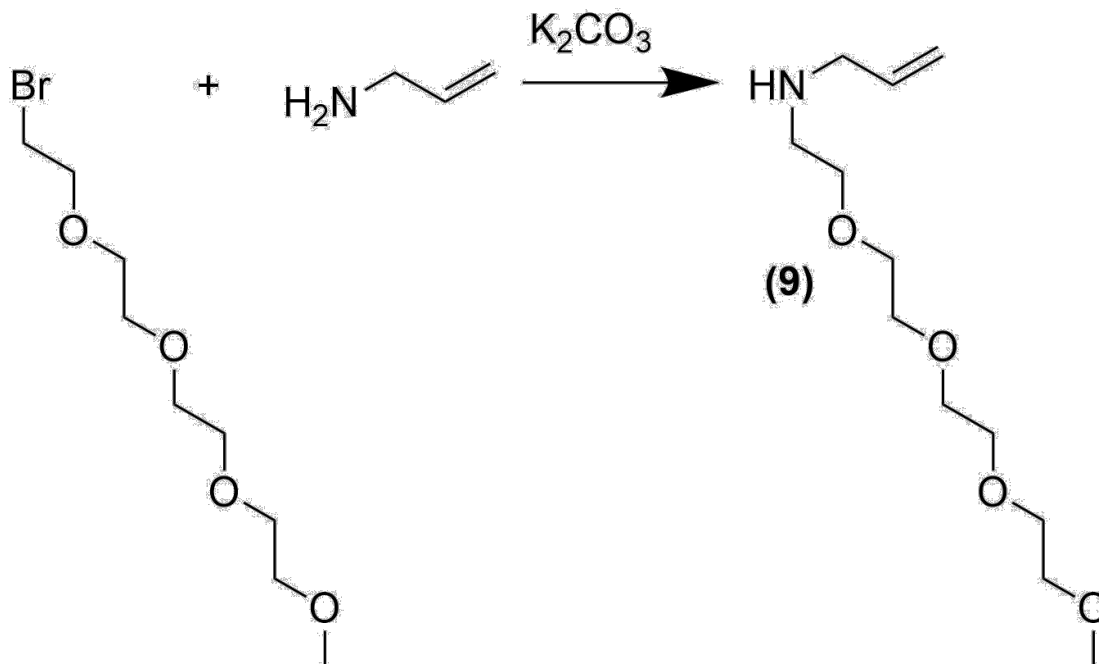
Figure A4. 17. Synthesis scheme for compound **(9)**.
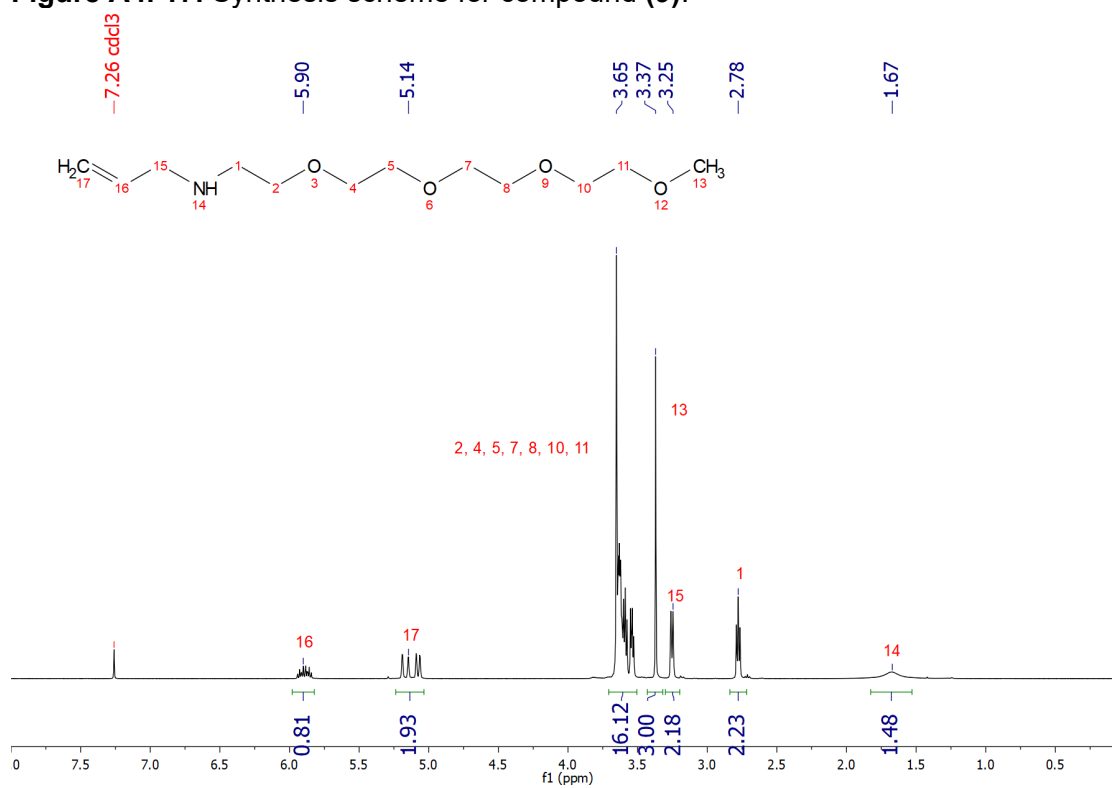
Figure A4. 18. ^{1}H NMR (400 MHz, CDCl$_3$) of compound **(9)**.

Synthesis of Compound (10)
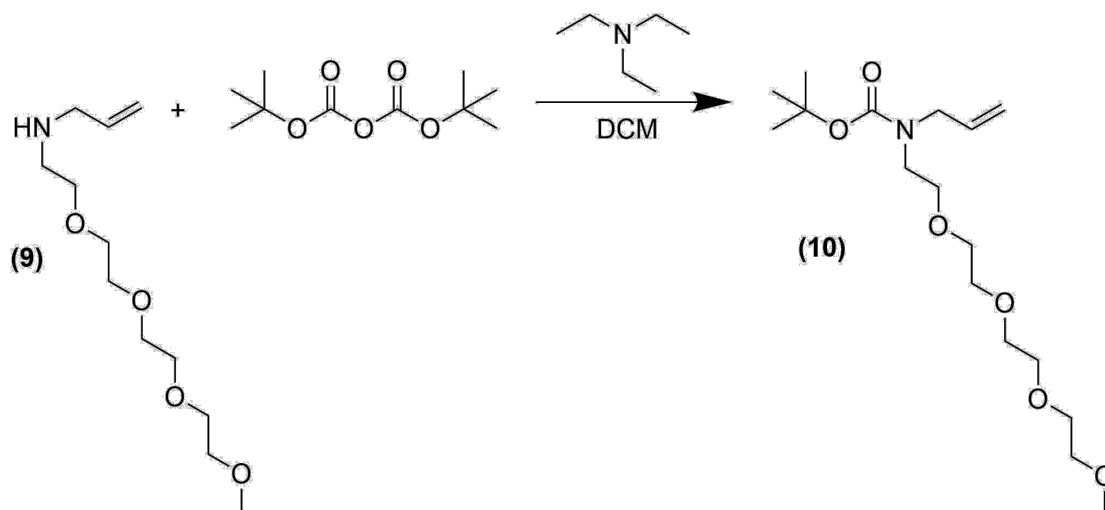
Figure A4. 19. Synthesis scheme for compound **(10)**.
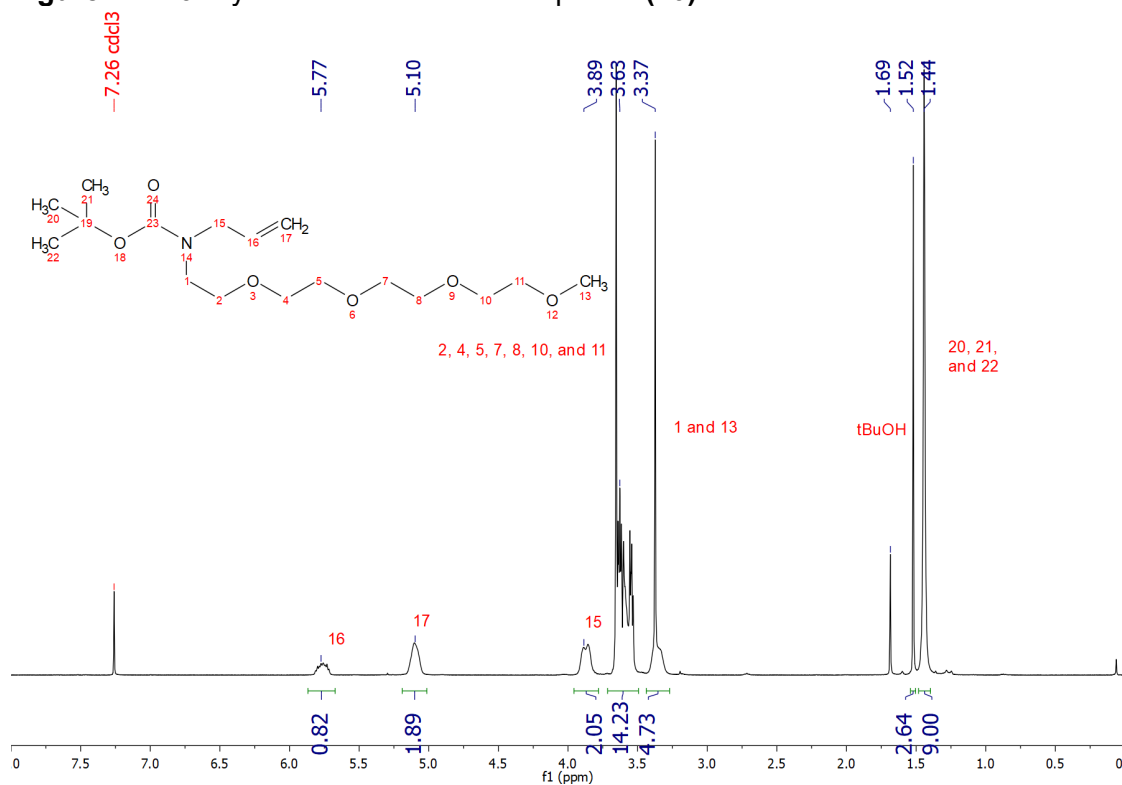
Figure A4. 20. ¹H NMR (400 MHz, CDCl₃) of compound **(10)**.

Synthesis of Compound (11)
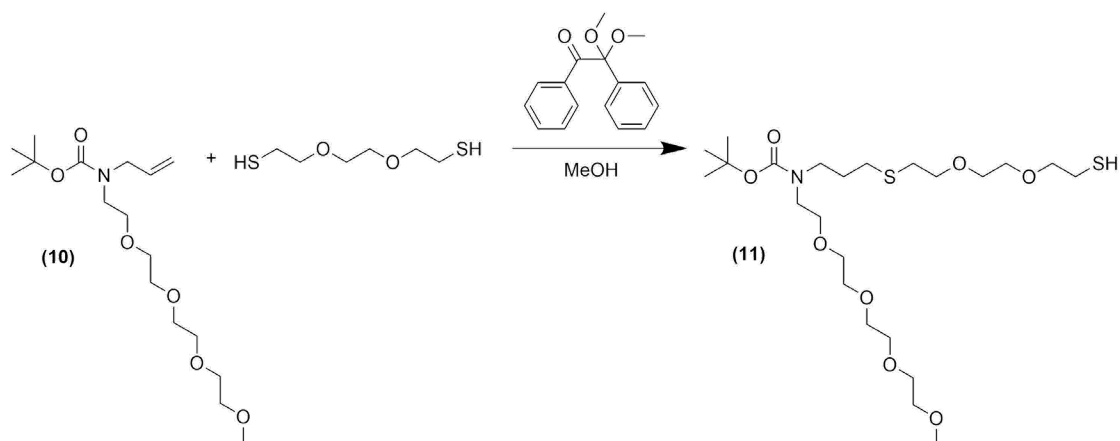
Figure A4. 21. Synthesis scheme for compound **(11)**.
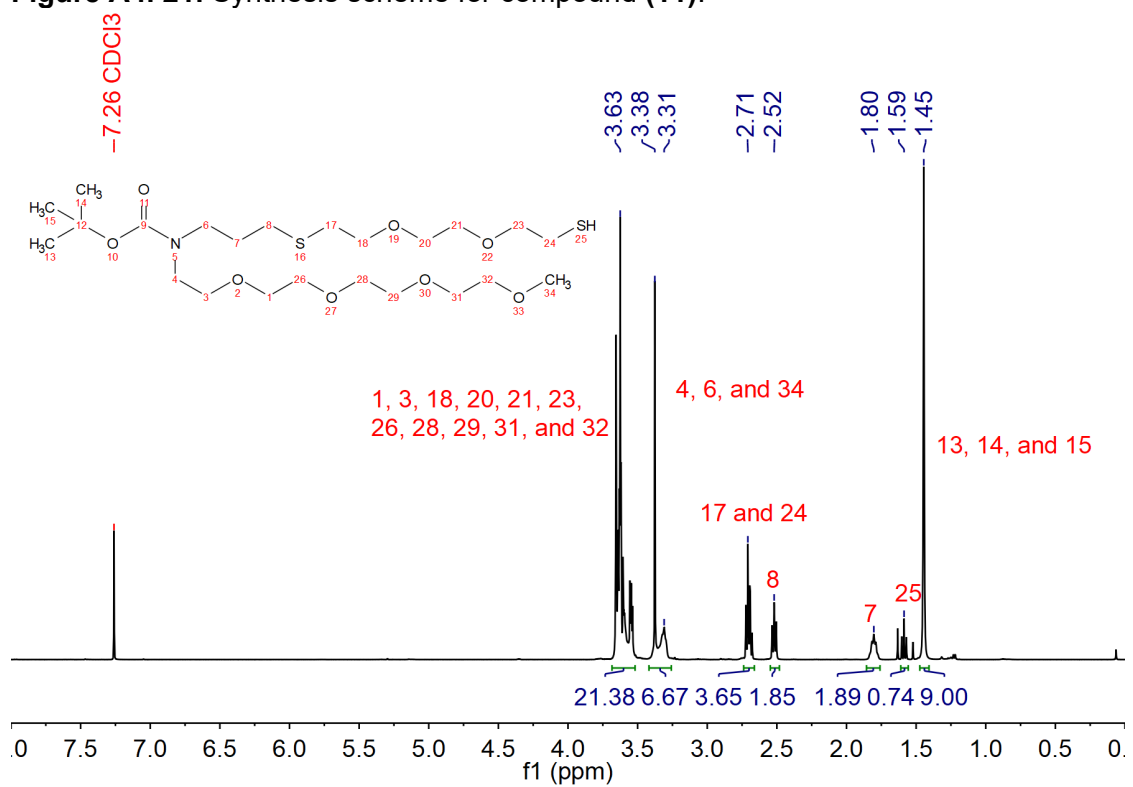
Figure A4. 22. ¹H NMR (500 MHz, CDCl₃) of compound **(11)**.

Synthesis of Compound (12)
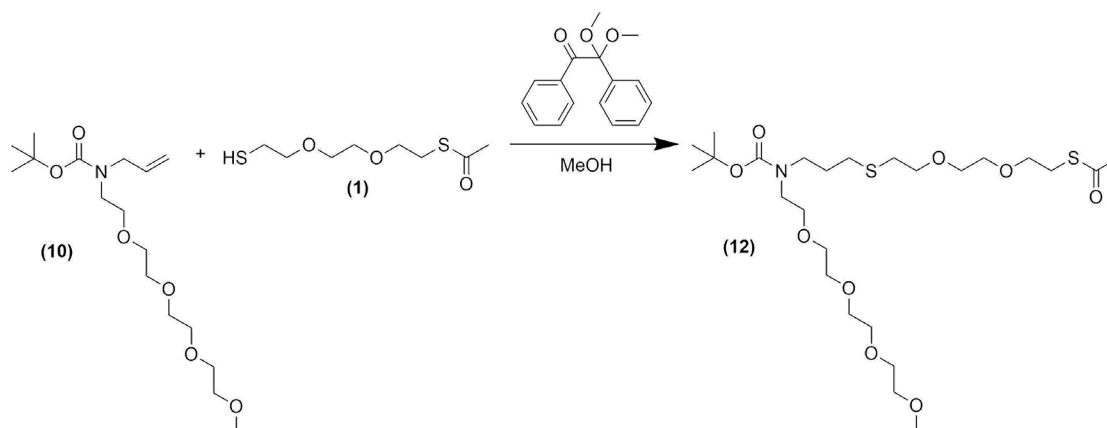
Figure A4. 23. Synthesis scheme for compound **(12)**.
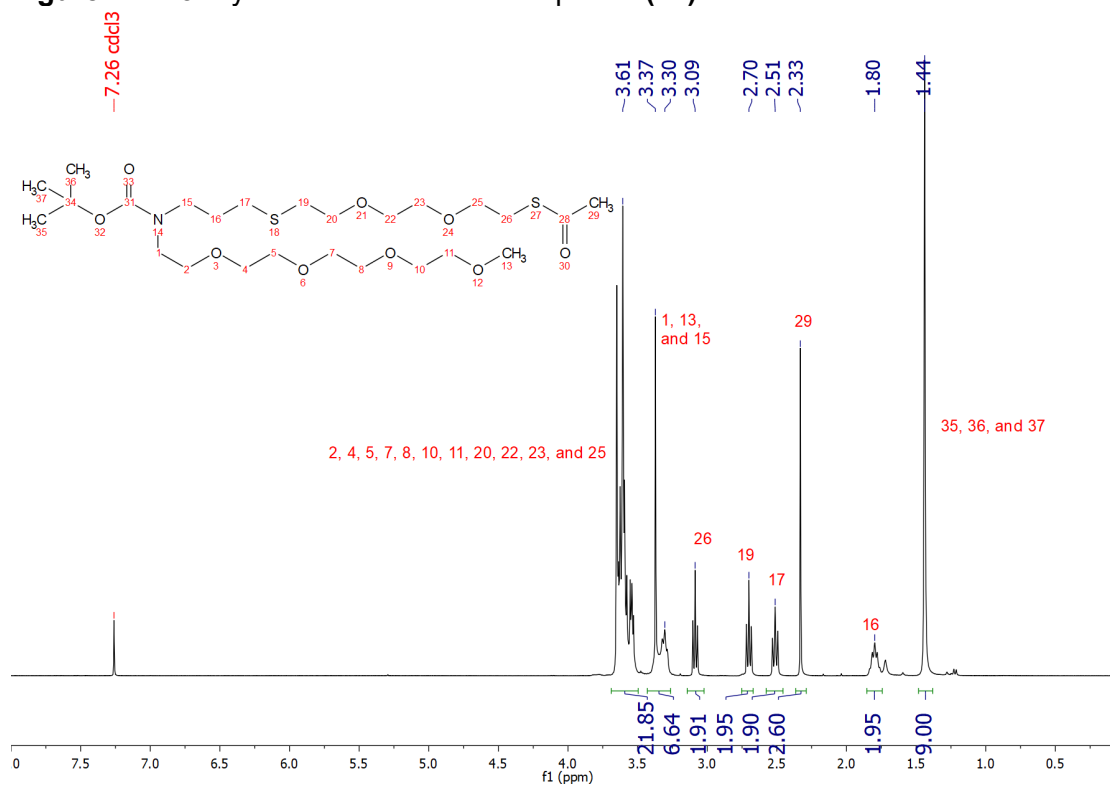
Figure A4. 24. ¹H NMR (400 MHz, CDCl₃) of compound **(12)**.

Synthesis of Compound (13)
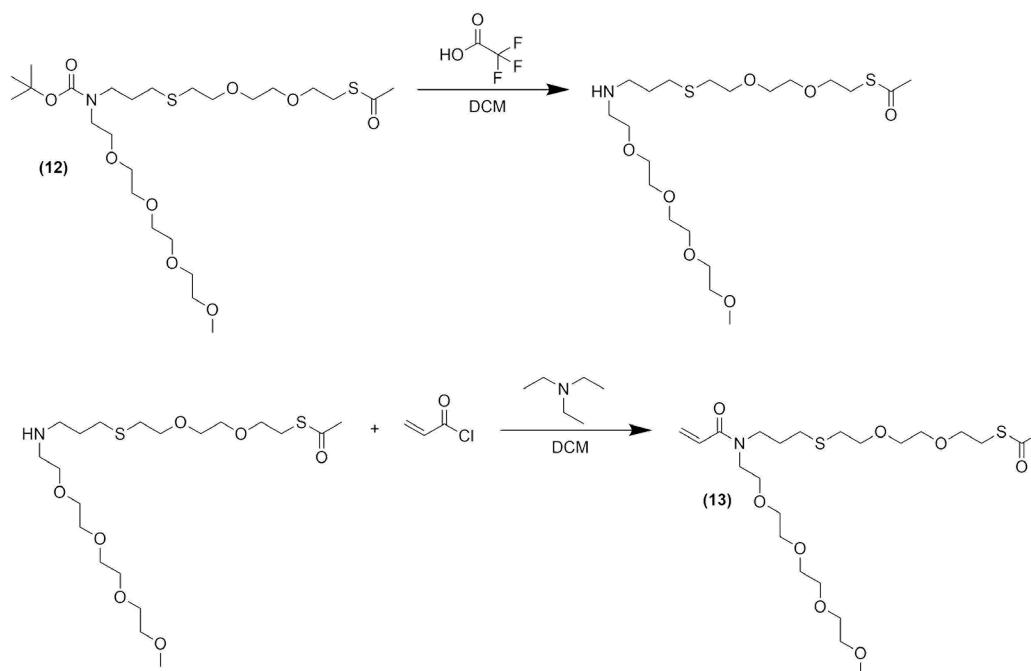
Figure A4. 25. Synthesis scheme for compound **(13)**.
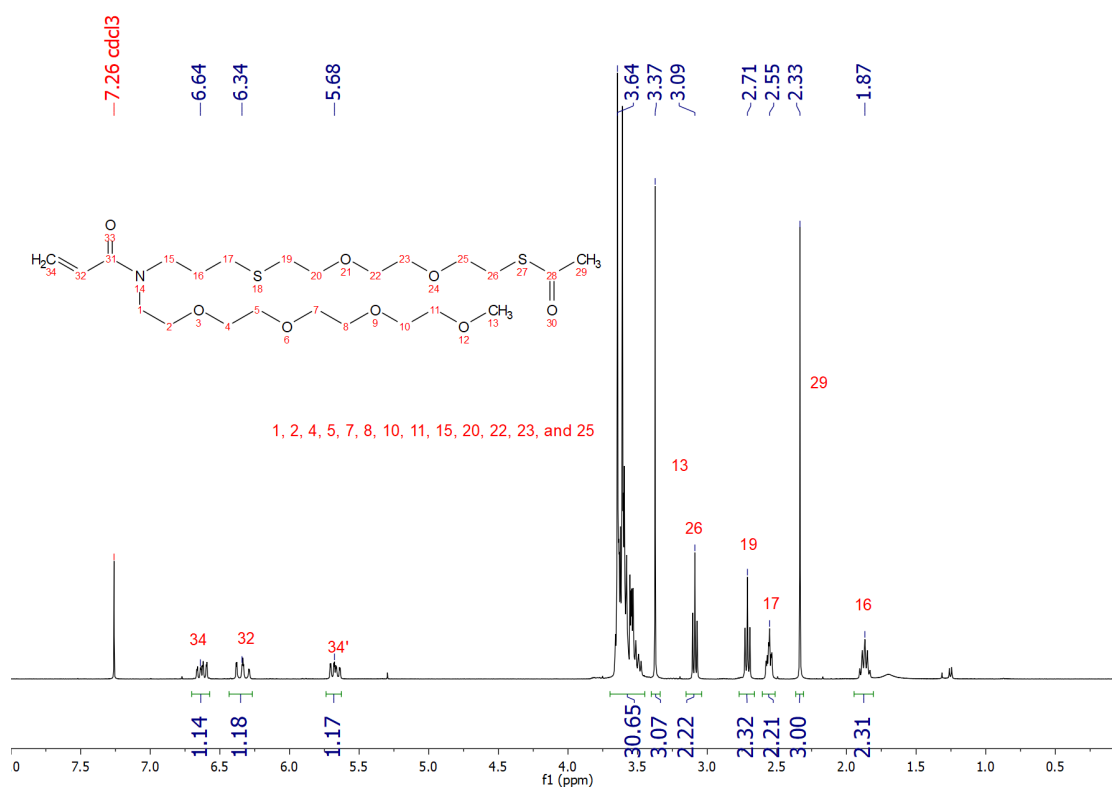
Figure A4. 26. ¹H NMR (400 MHz, CDCl₃) of compound **(13)**.

Synthesis of Compound (14)
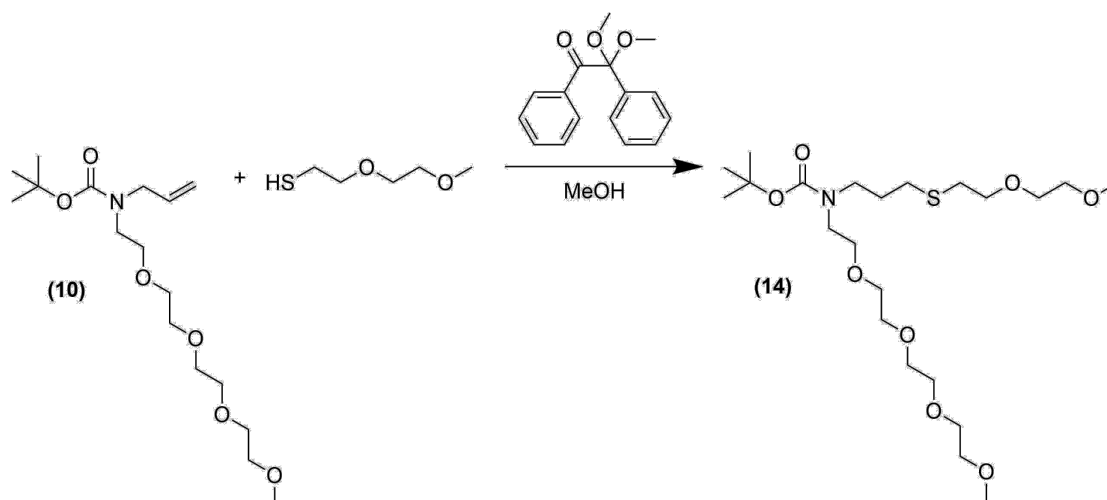
Figure A4. 27. Synthesis scheme for compound **(14)**.

Figure A4. 28. ^{1}H NMR (400 MHz, CDCl$_3$) of compound **(14)**.

Synthesis of Compound (15)

Figure A4. 29. Synthesis scheme for compound **(15)**.

Figure A4. 30. ^{1}H NMR (400 MHz, CDCl$_3$) of compound **(15)**.

Synthesis of Compound (16)

Figure A4. 31. Synthesis scheme for compound **(16)**.
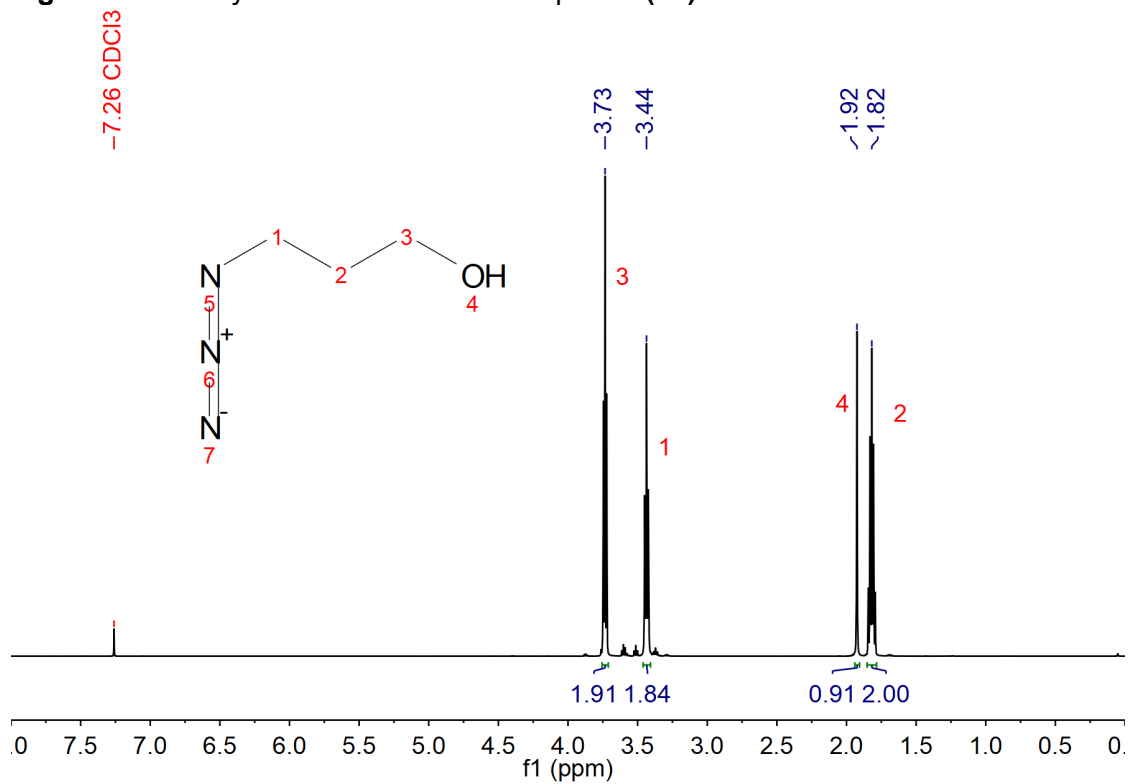
Figure A4. 32. ^{1}H NMR (500 MHz, CDCl$_3$) of compound **(16)**.
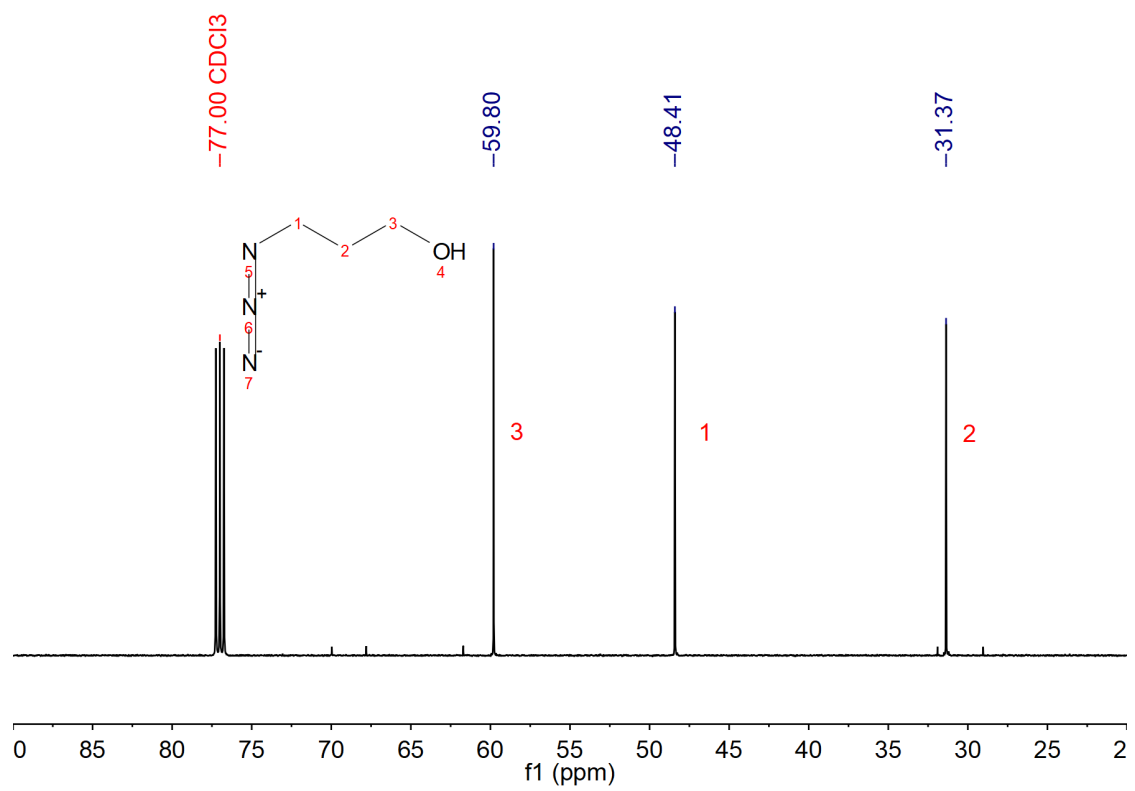
Figure A4. 33. ^{13}C NMR (500 MHz, CDCl$_3$) of compound **(16)**.

Synthesis of Compound (17)
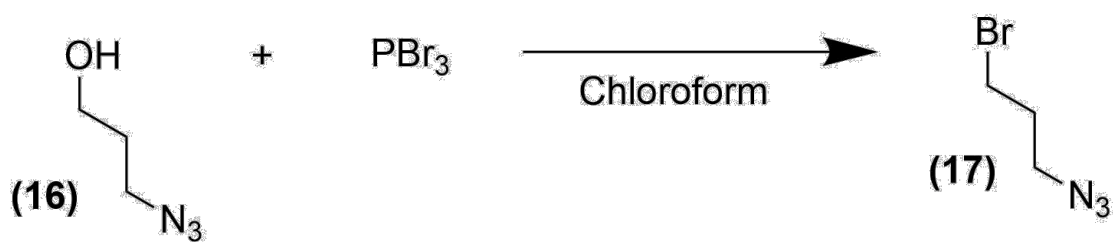
Figure A4. 34. Synthesis scheme for compound **(17)**.
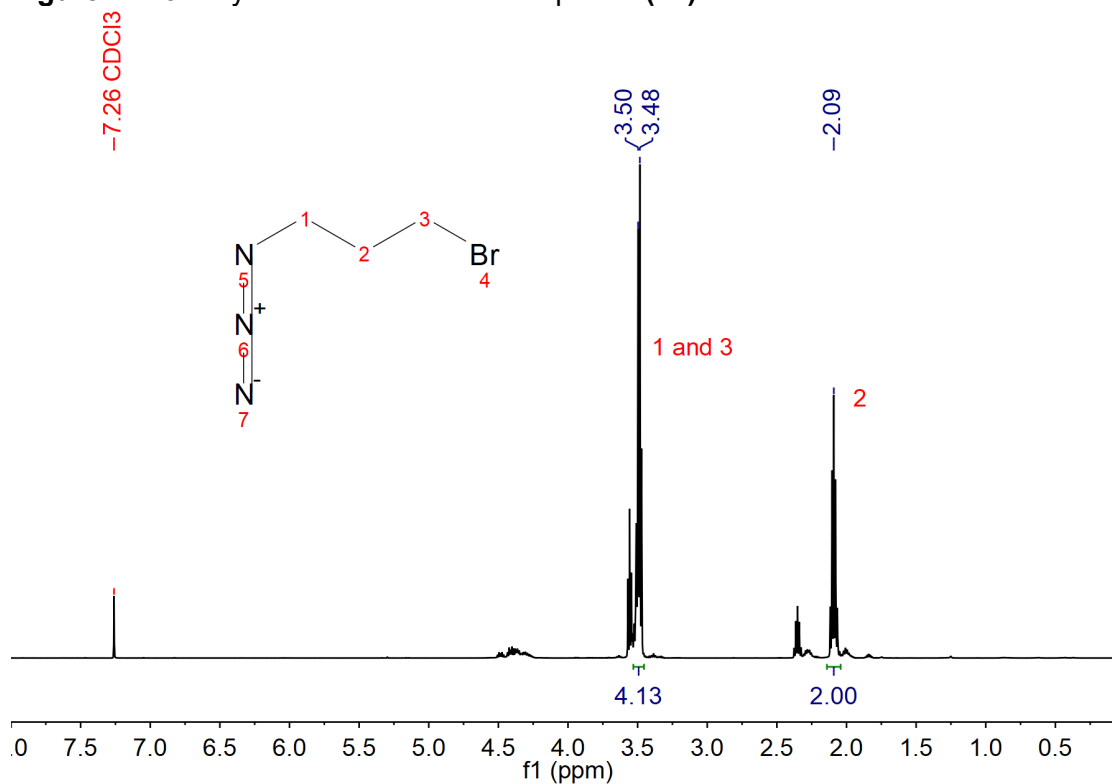
Figure A4. 35. ^{1}H NMR (500 MHz, CDCl$_3$) of compound **(17)**.
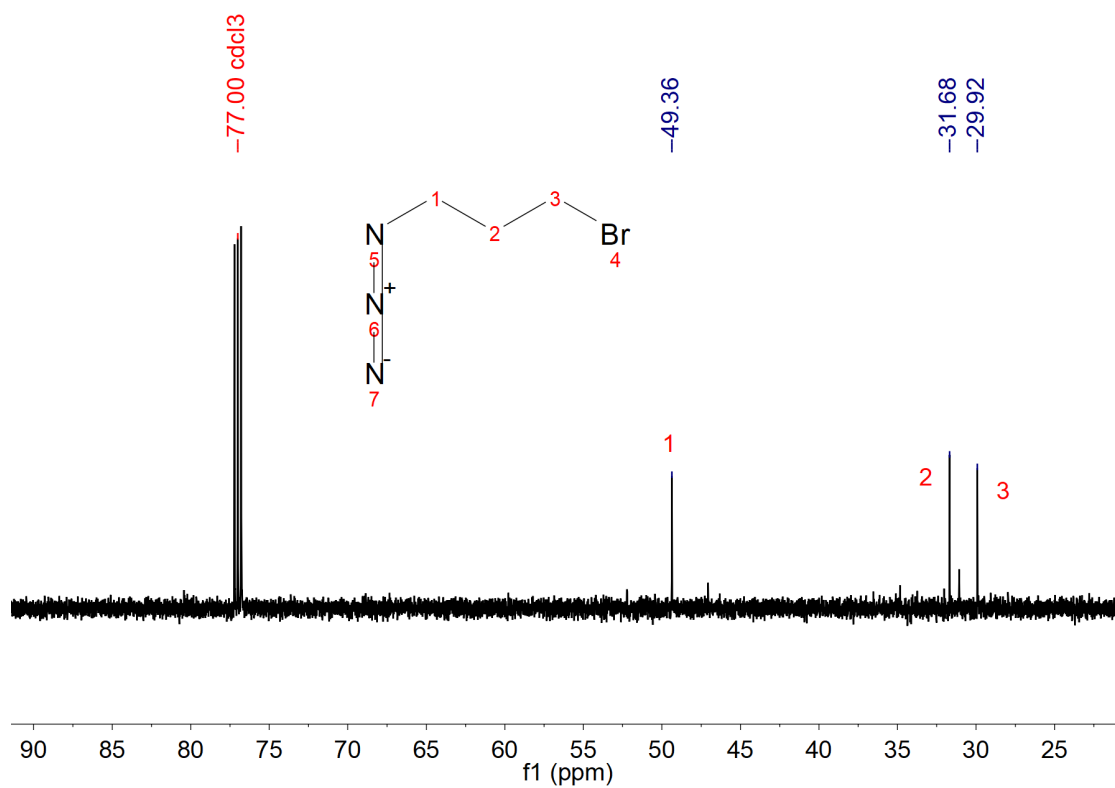
Figure A4. 36. ^{13}C NMR (500 MHz, CDCl$_3$) of compound **(17)**.

Synthesis of Compound (18)
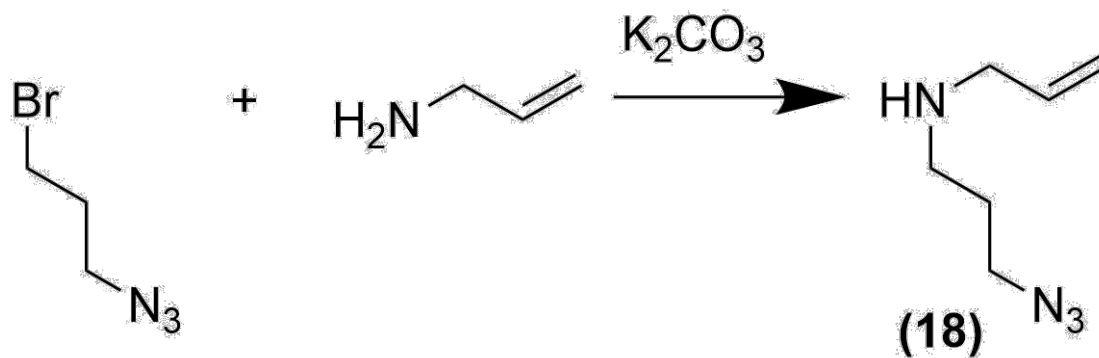
Figure A4. 37. Synthesis scheme for compound **(18)**.
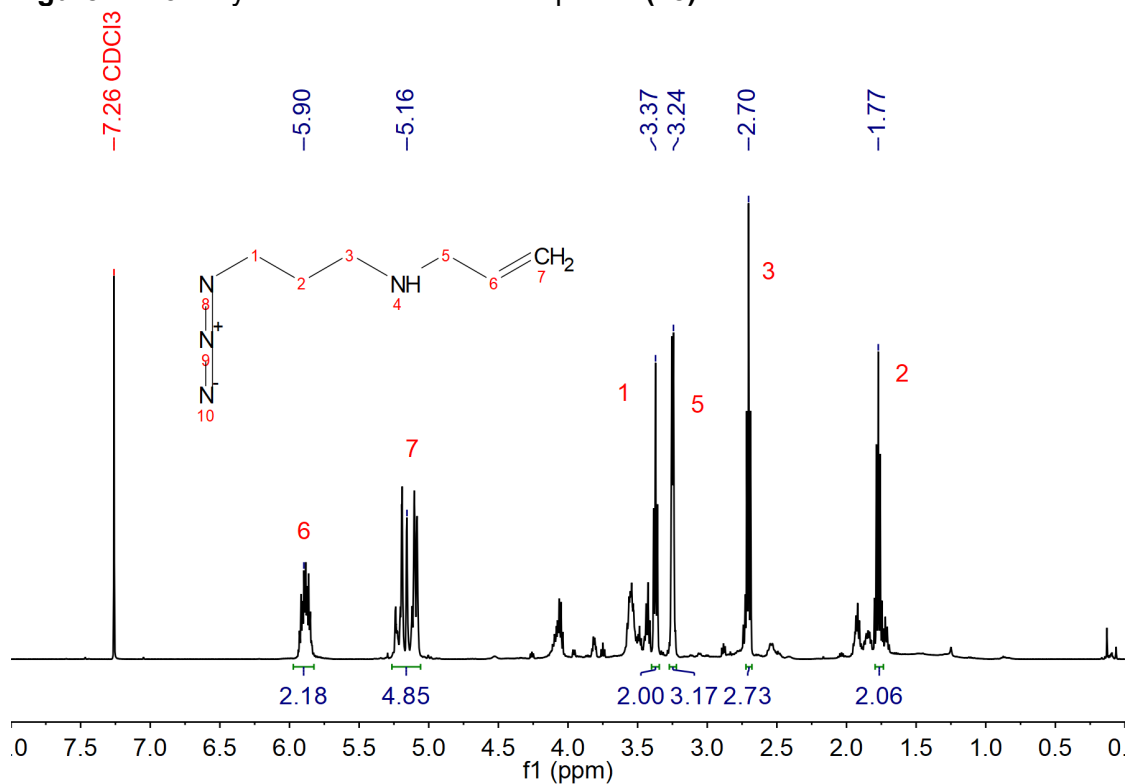
Figure A4. 38. ^{1}H NMR (500 MHz, CDCl$_3$) of compound **(18)**.

Synthesis of Compound (19)
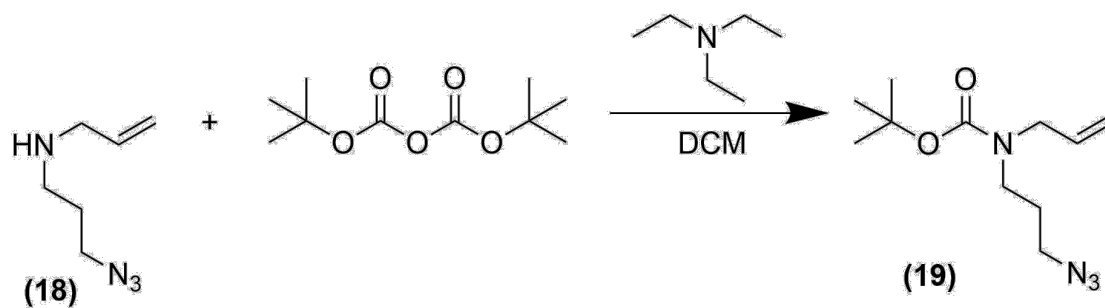
Figure A4. 39. Synthesis scheme for compound **(19)**.

Synthesis of Compound (20)
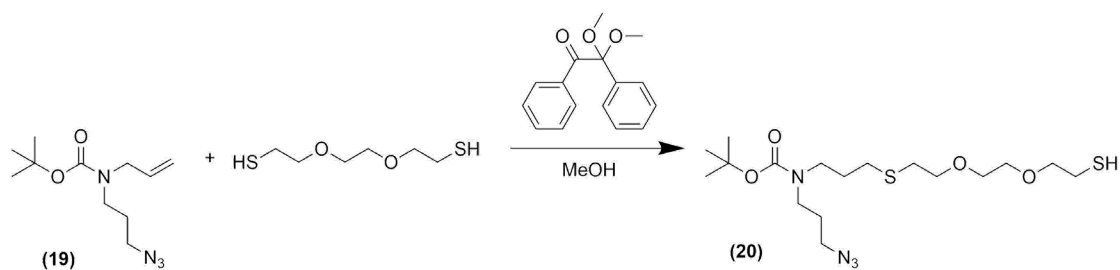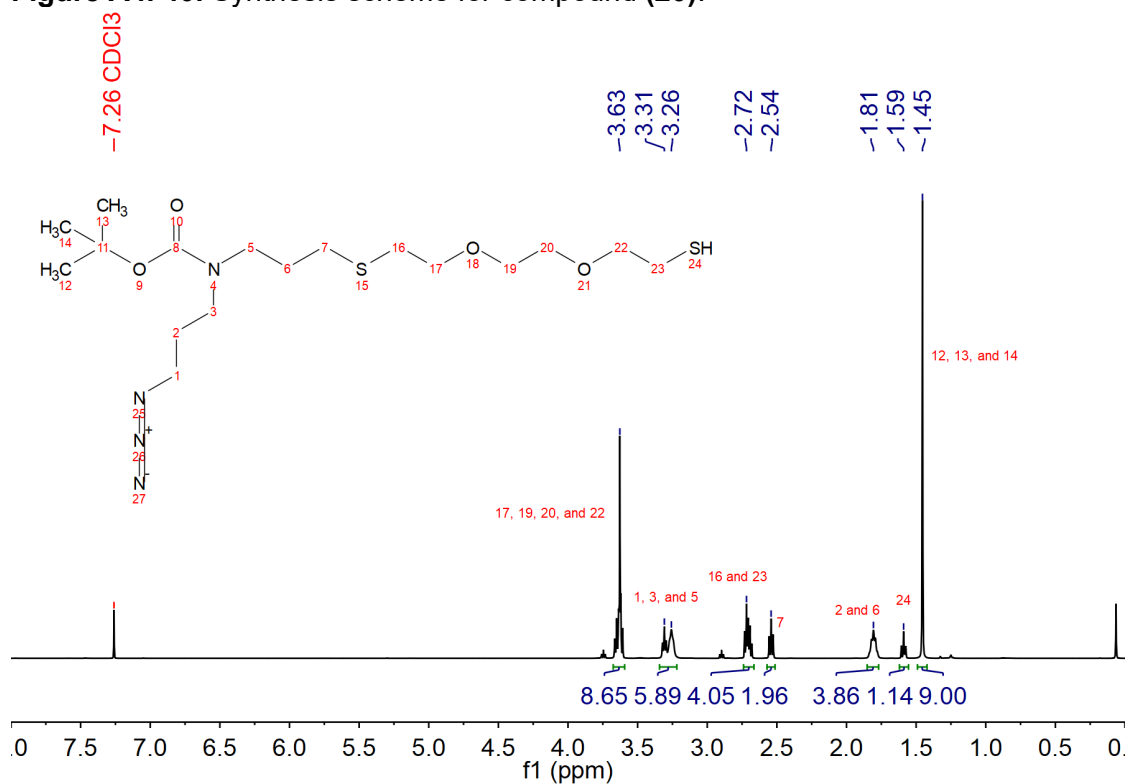

Figure A4. 40. Synthesis scheme for compound **(20)**.

Figure A4. 41. ¹H NMR (500 MHz, CDCl₃) of compound **(20)**.
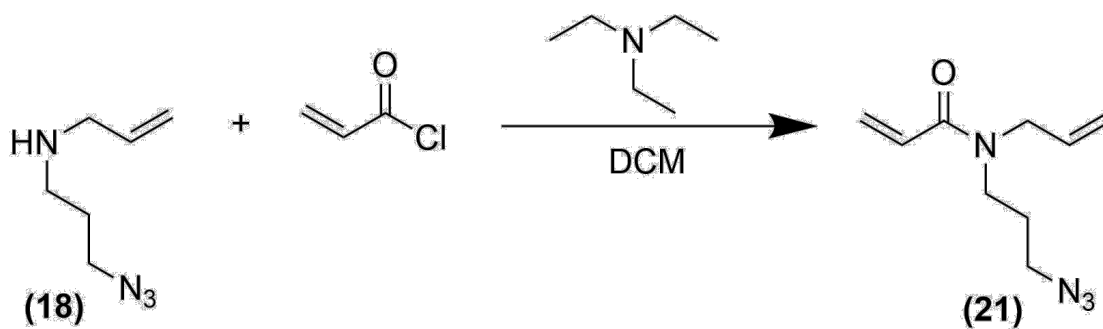
Synthesis of Compound (21)
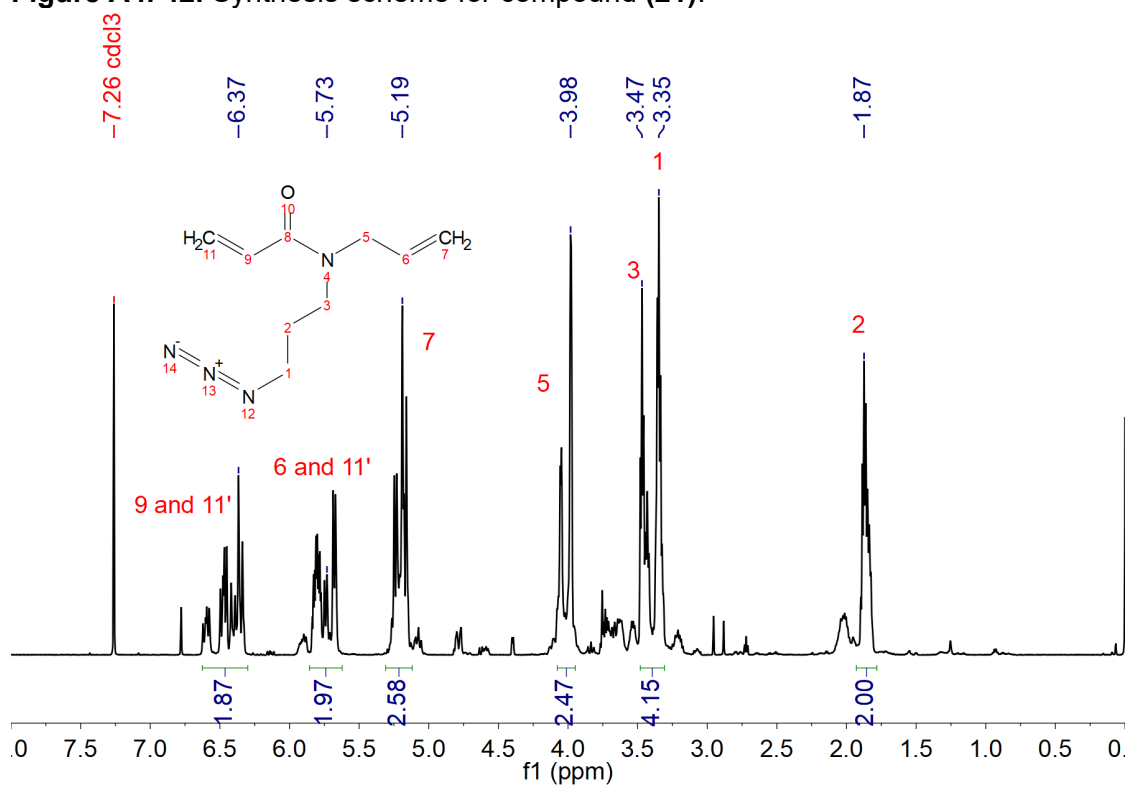

Figure A4. 42. Synthesis scheme for compound **(21)**.

Figure A4. 43. ¹H NMR (500 MHz, CDCl₃) of compound **(21)**.

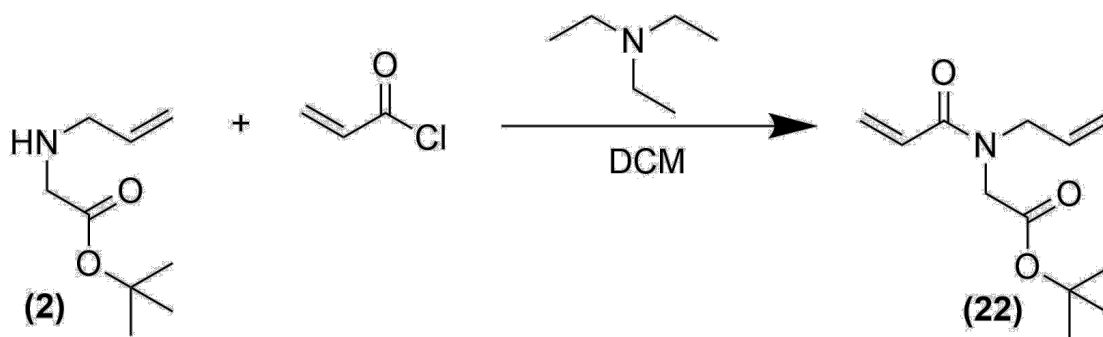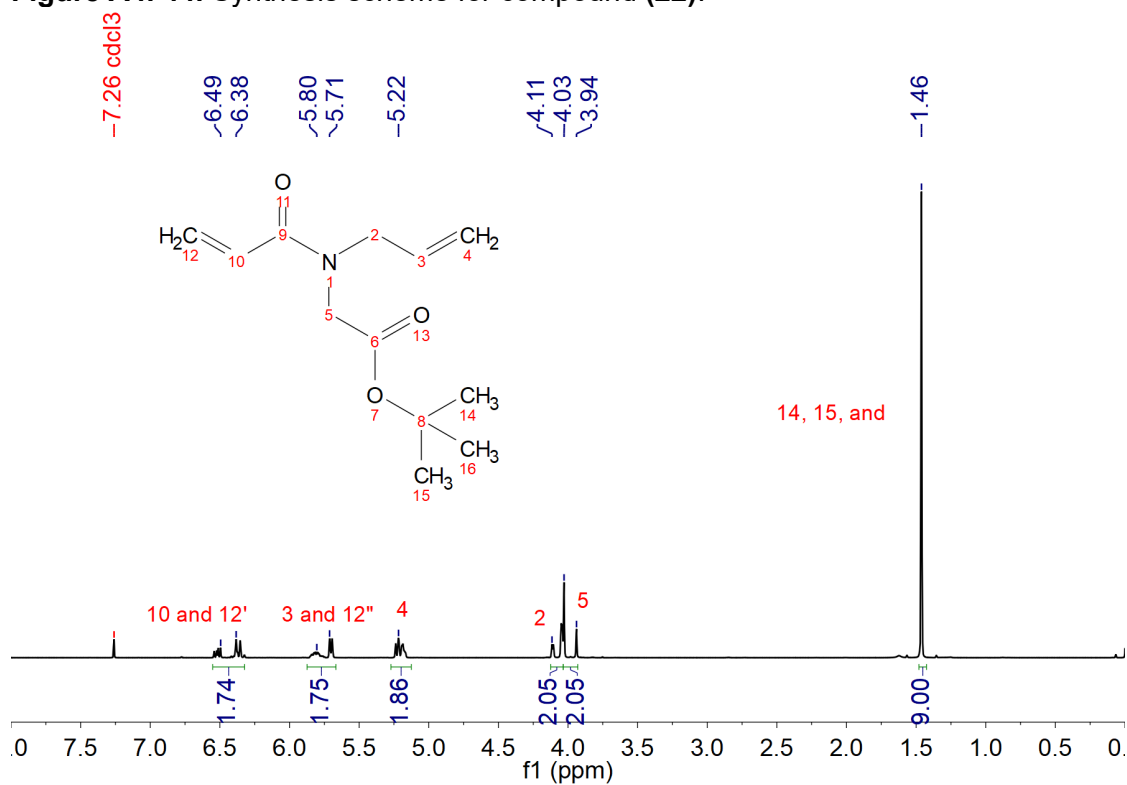**Synthesis of Compound (22)**

Figure A4. 44. Synthesis scheme for compound **(22)**.

Figure A4. 45. ^{1}H NMR (500 MHz, CDCl$_3$) of compound **(22)**.
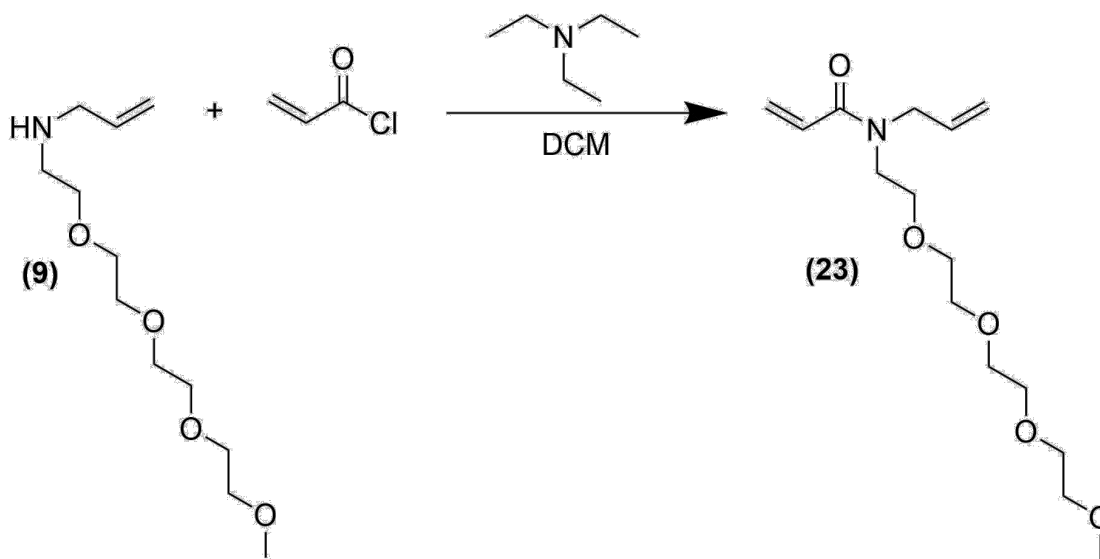
Synthesis of Compound (23)

Figure A4. 46. Synthesis scheme for compound **(23)**.
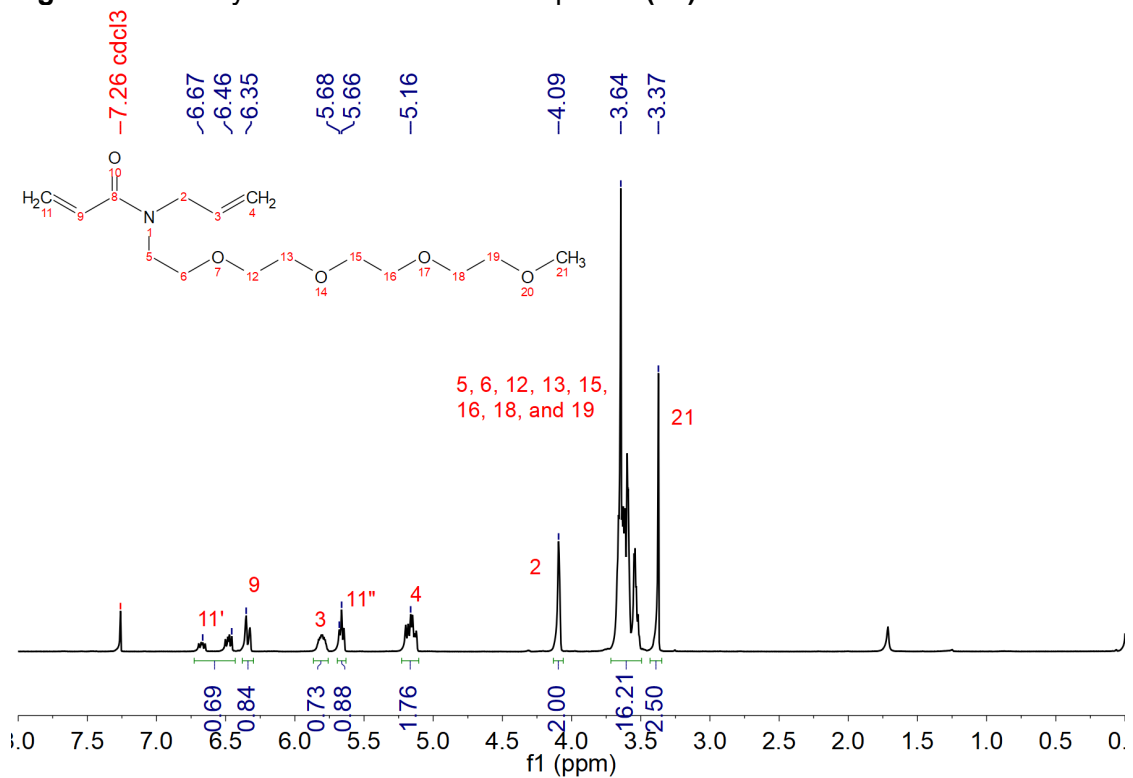

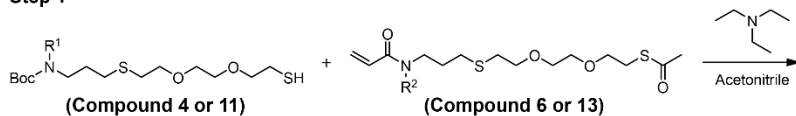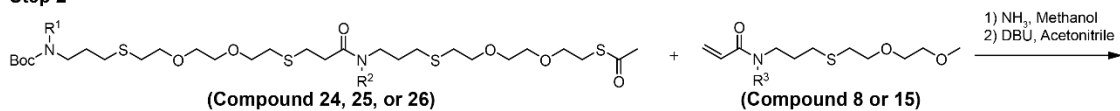**Figure A4. 47.** ^{1}H NMR (500 MHz, CDCl$_3$) of compound **(23)**.

Synthesis of PEGylated Oligomers

Step 1

(Compound 4 or 11)   +   (Compound 6 or 13)   Acetonitrile →

Step 2

(Compound 24, 25, or 26)   +   (Compound 8 or 15)   1) NH₃, Methanol 2) DBU, Acetonitrile →

Final Oligomer

(Compound 27, 28, or 29)
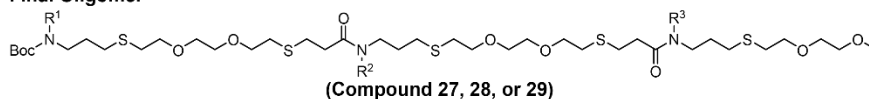
Figure A4. 48. Overview of PEGylated oligomer synthesis.
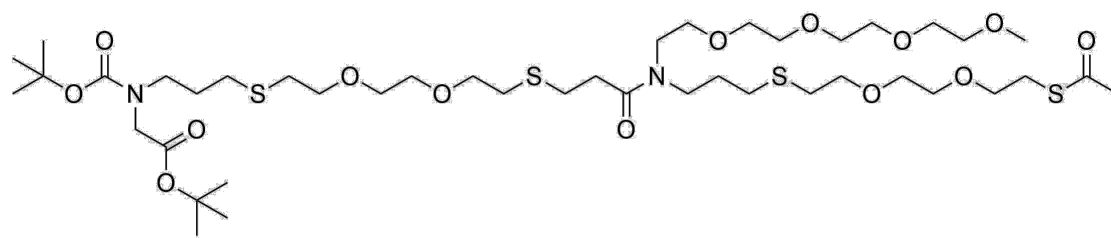
Figure A4. 49. Structure of PEGylated oligomer 1 intermediate, compound **(24)**.
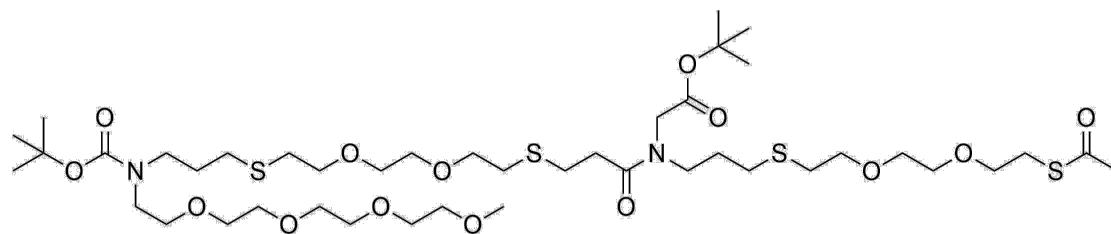
Figure A4. 50. Structure of PEGylated oligomer 2 intermediate, compound **(25)**.
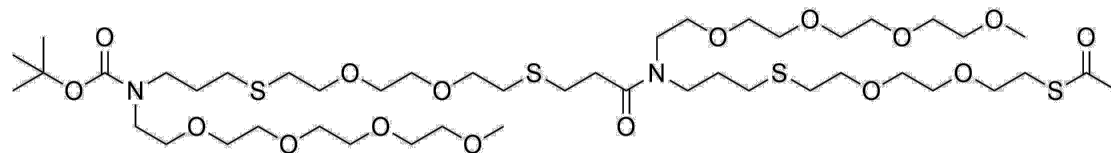
Figure A4. 51. Structure of PEGylated oligomer 3 intermediate, compound **(26)**.

Figure A4. 52. Structure of PEGylated oligomer 1, compound **(27)**.
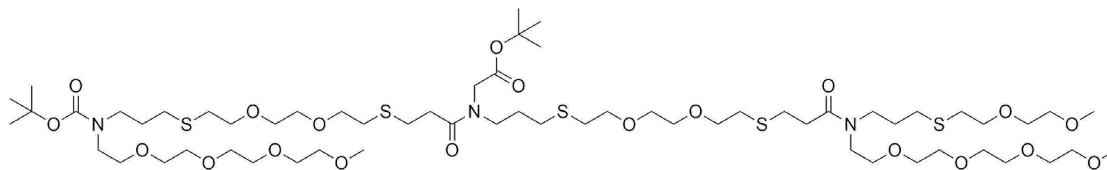
Figure A4. 53. Structure of PEGylated oligomer 2, compound **(28)**.
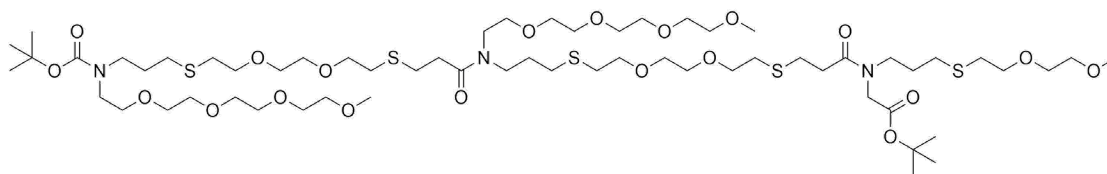
Figure A4. 54. Structure of PEGylated oligomer 3, compound **(29)**.

Synthesis of Multifunctional Oligomers

Step 1

(Compound 21, 22, or 23) (Compound 1)

(Compound 4, 11, or 20)

DBU, Acetonitrile DMPA, Methanol

Step 2

(Compound 21, 22, or 23)

(Compound 30, 31, or 32)

1) NH$_3$, Methoanol
2) DBU, Acetonitrile

DMPA, Methanol

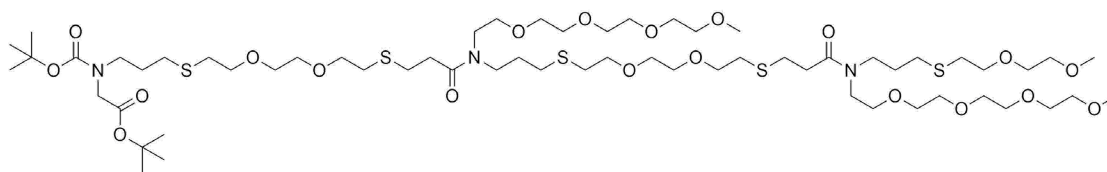**Final Oligomer**

(Compound 33, 34, or 35)
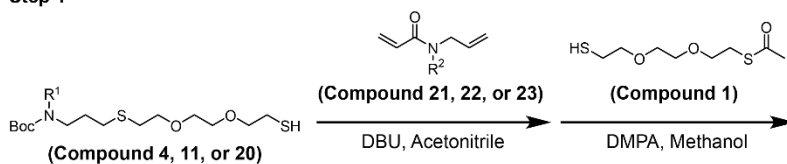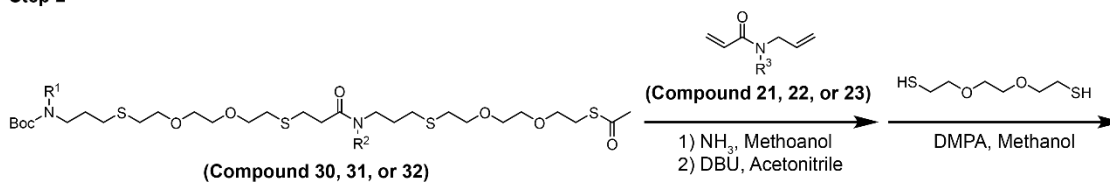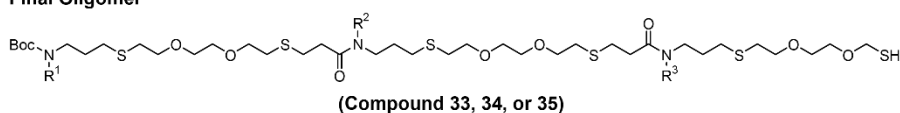
Figure A4. 55. Overview of multifunctional oligomer synthesis.
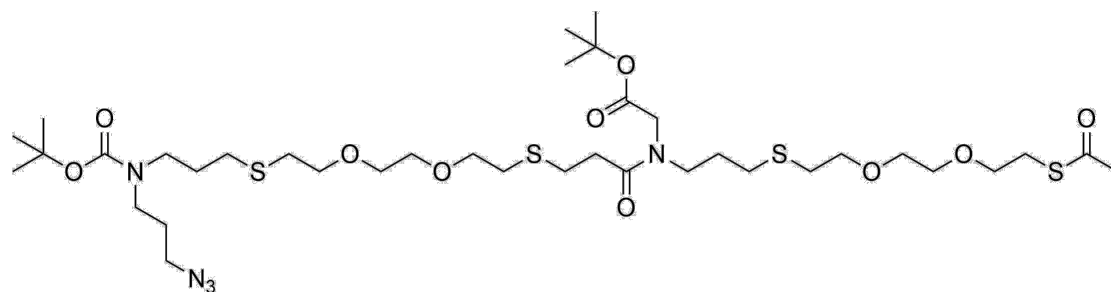
Figure A4. 56. Structure of multifunctional oligomer 1 intermediate, compound **(30)**.
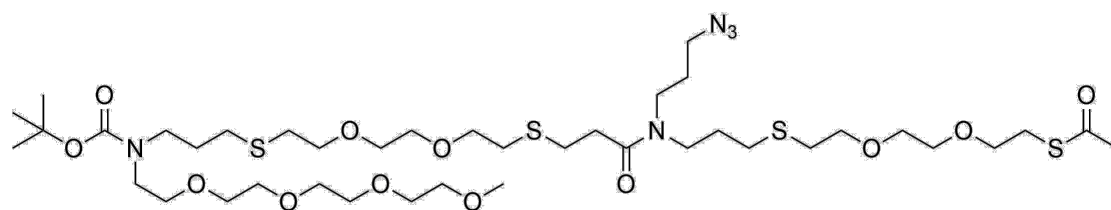
Figure A4. 57. Structure of multifunctional oligomer 2 intermediate, compound **(31)**.
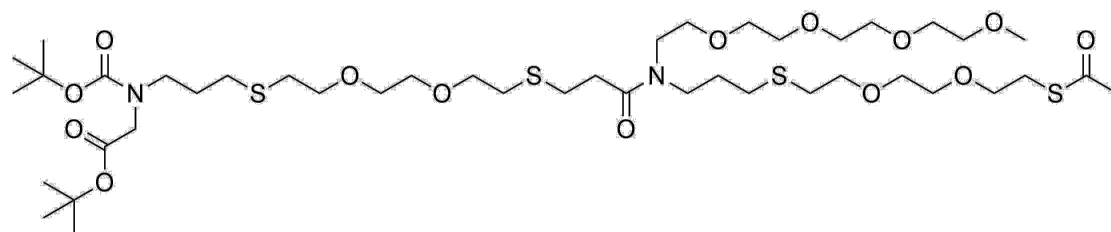
Figure A4. 58. Structure of multifunctional oligomer 3 intermediate, compound **(32)**.

205
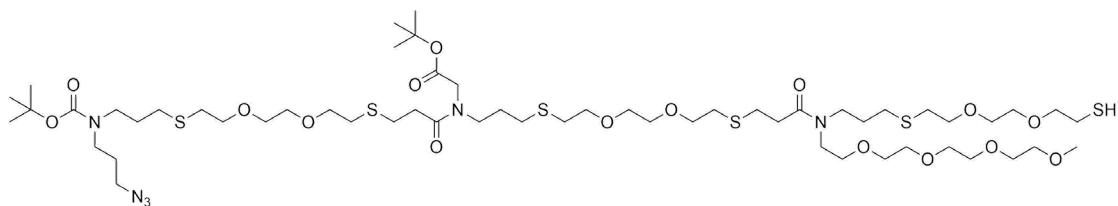
Figure A4. 59. Structure of multifunctional oligomer 1, compound **(33)**.
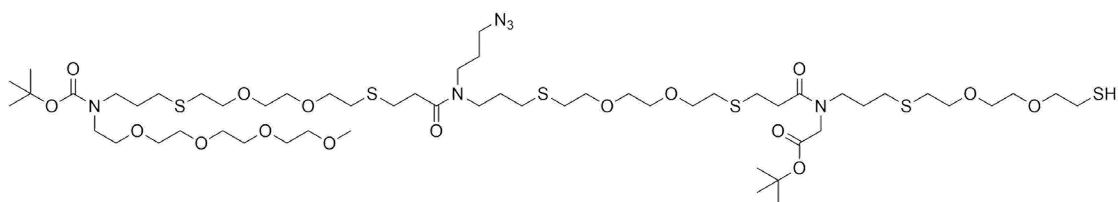
Figure A4. 60. Structure of multifunctional oligomer 2, compound **(34)**.
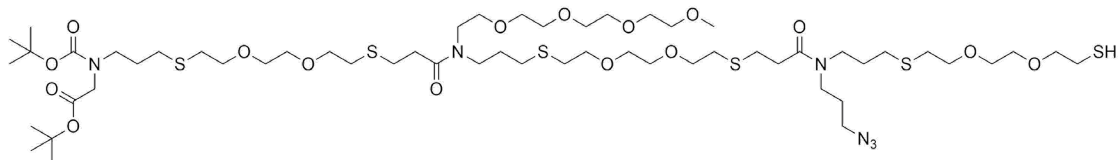
Figure A4. 61. Structure of multifunctional oligomer 3, compound **(35)**.

Synthesis of Dipeptide-modified MMAE (Compound 36)
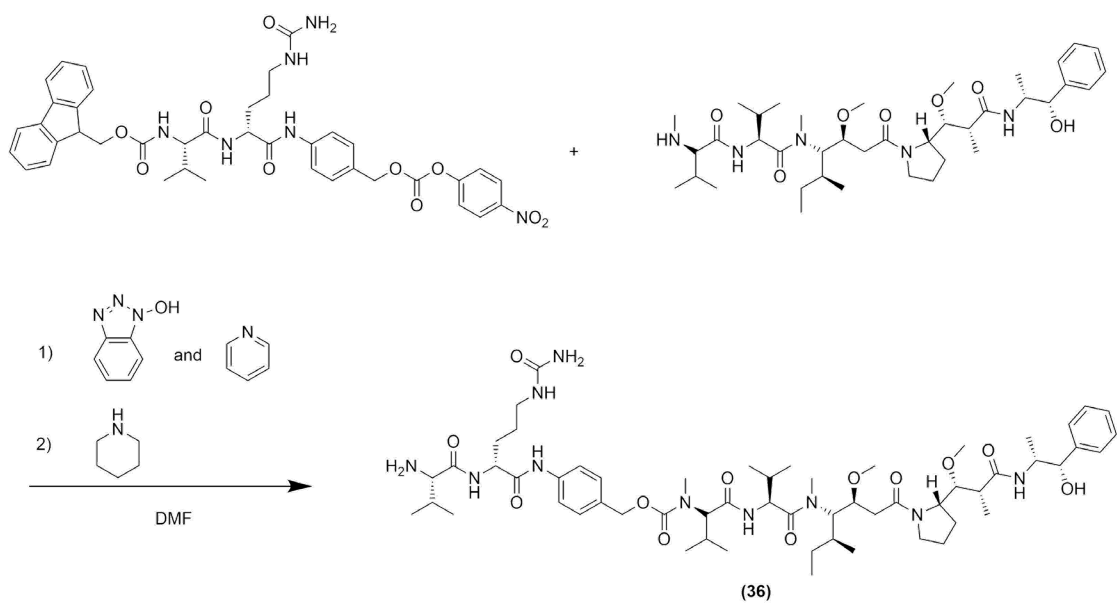
Figure A4. 62. Synthesis scheme for compound **(36)**.

Synthesis of MMAE-loaded, PEGylated Cross-linkers (Compounds 37 – 45)
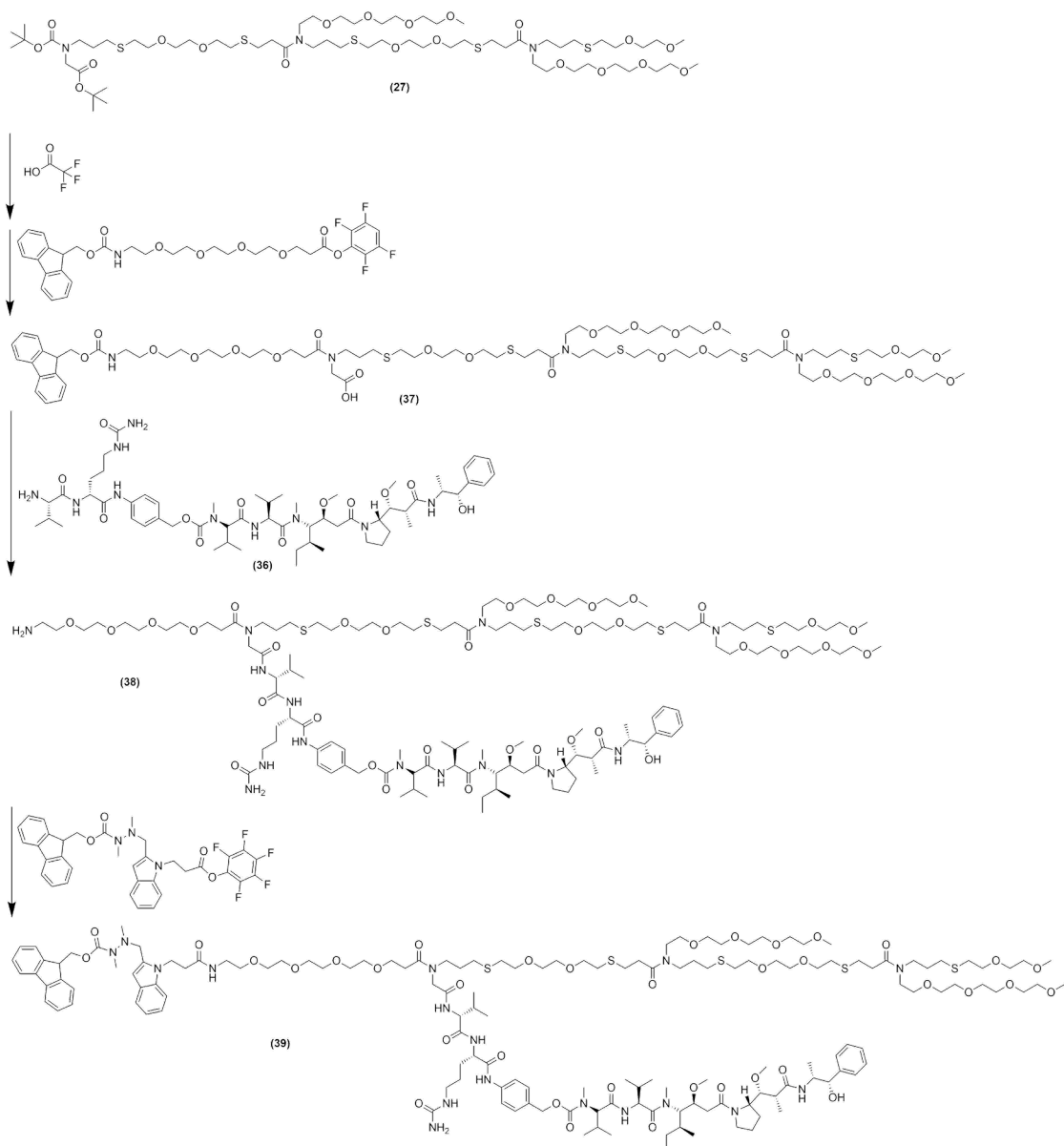
Figure A4. 63. Synthesis scheme for compounds **(37 – 39)**.
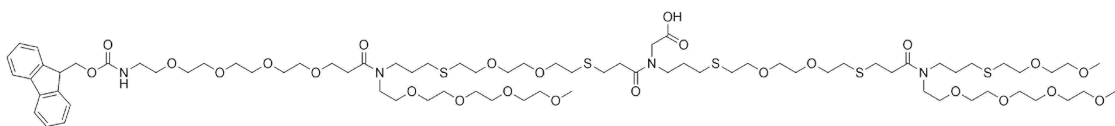
Figure A4. 64. Structure of compound **(40)**.
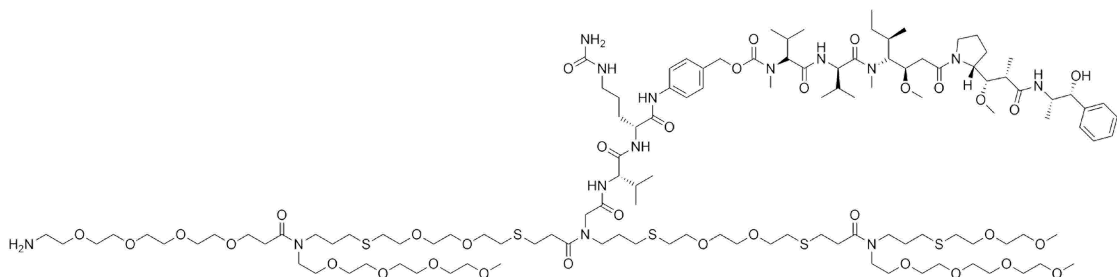
Figure A4. 65. Structure of compound **(41)**.
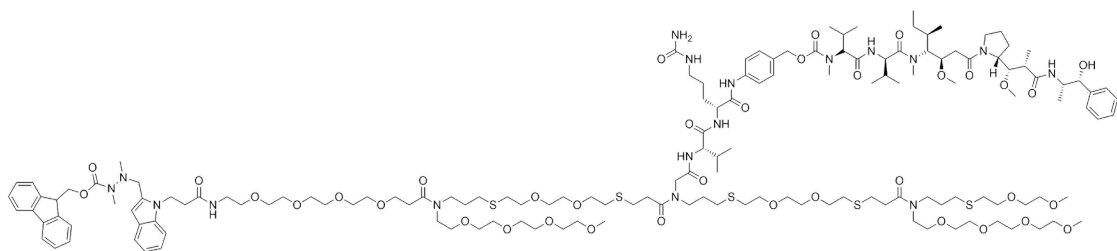
Figure A4. 66. Structure of compound **(42)**.
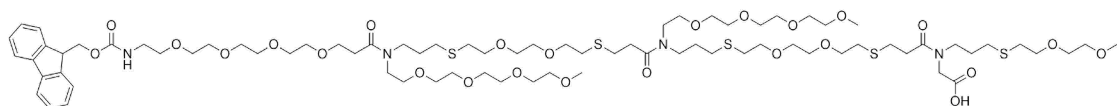
Figure A4. 67. Structure of compound **(43)**.
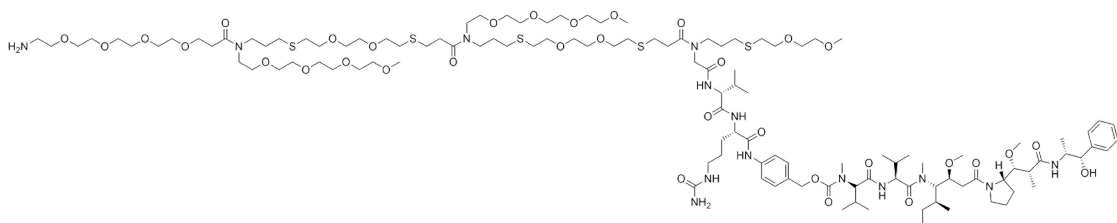
Figure A4. 68. Structure of compound **(44)**.
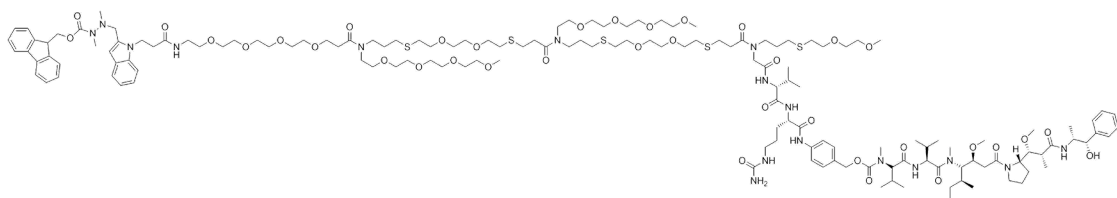
Figure A4. 69. Structure of compound **(45)**.

Synthesis of MMAE-loaded, Non-PEGylated Cross-linker (Compounds 46 – 47)

(36)

(46)

(47)
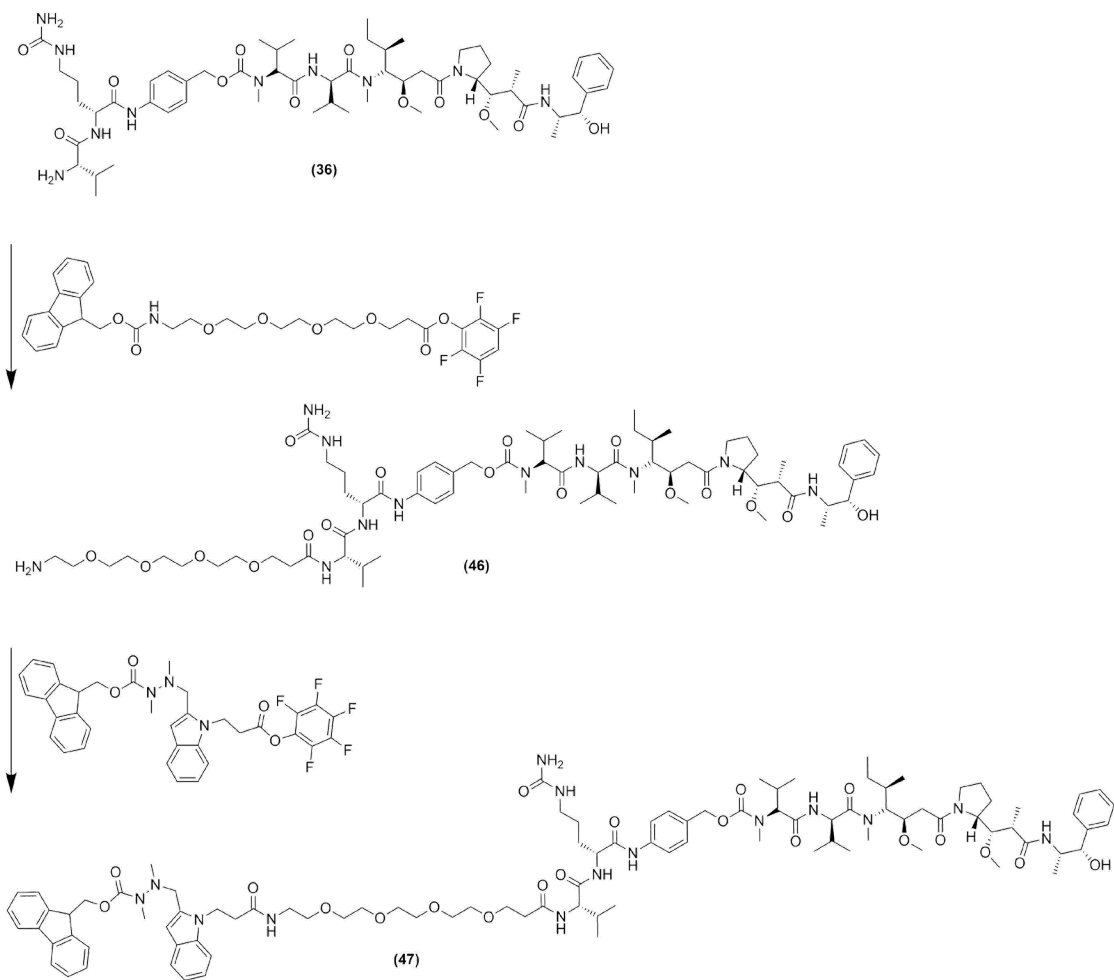
Figure A4. 70. Synthesis scheme for compounds **(46 and 47)**.

Synthesis of Fluorescein-modified Cross-linker (Compounds 48 – 49)
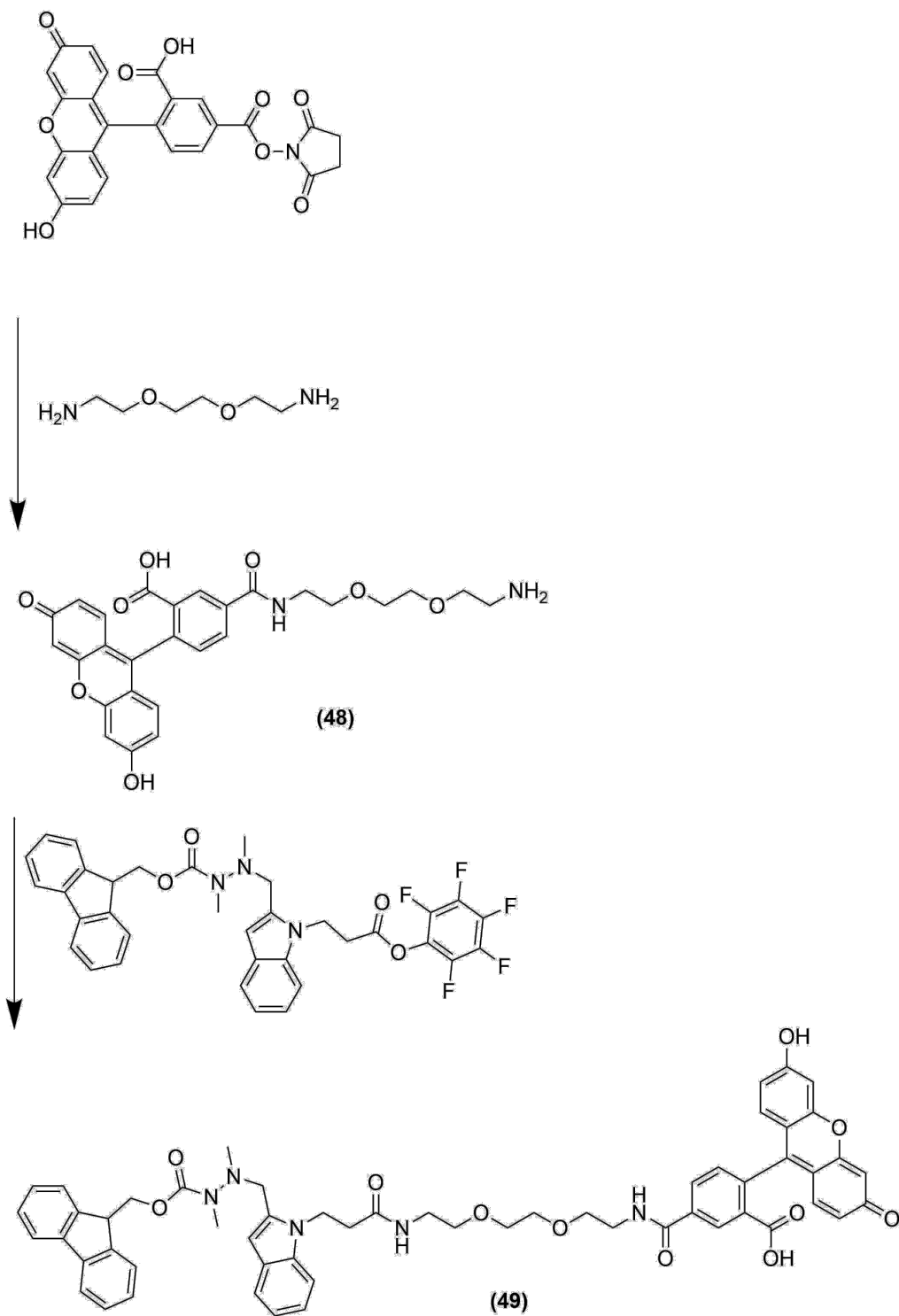
Figure A4. 71. Synthesis scheme for compounds **(48 and 49)**.

Synthesis of Dansyl-NH-Boc and Dansyl-NH₂ (Compound 50 and 51)
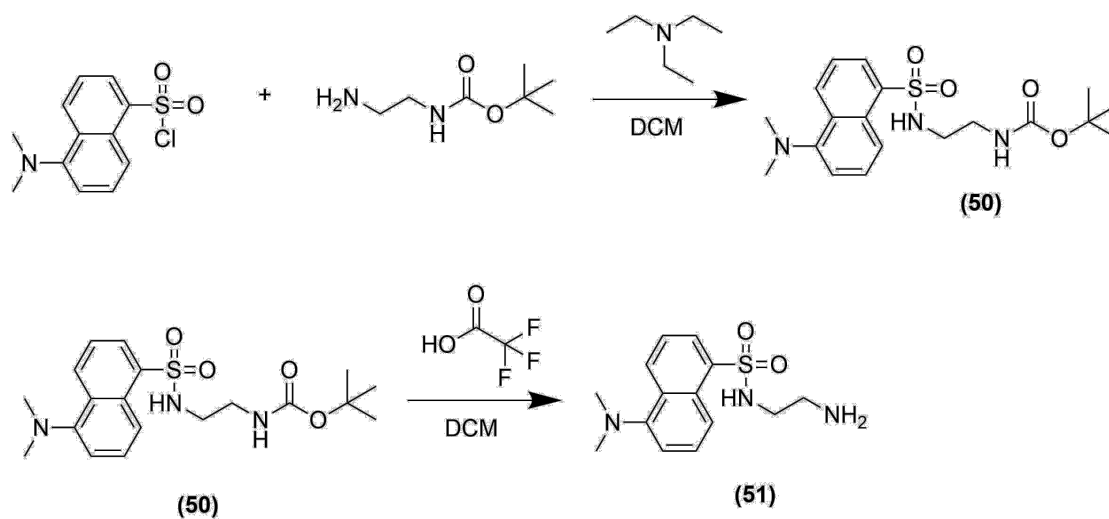
Figure A4. 72. Synthesis scheme for compounds **(50 and 51)**.
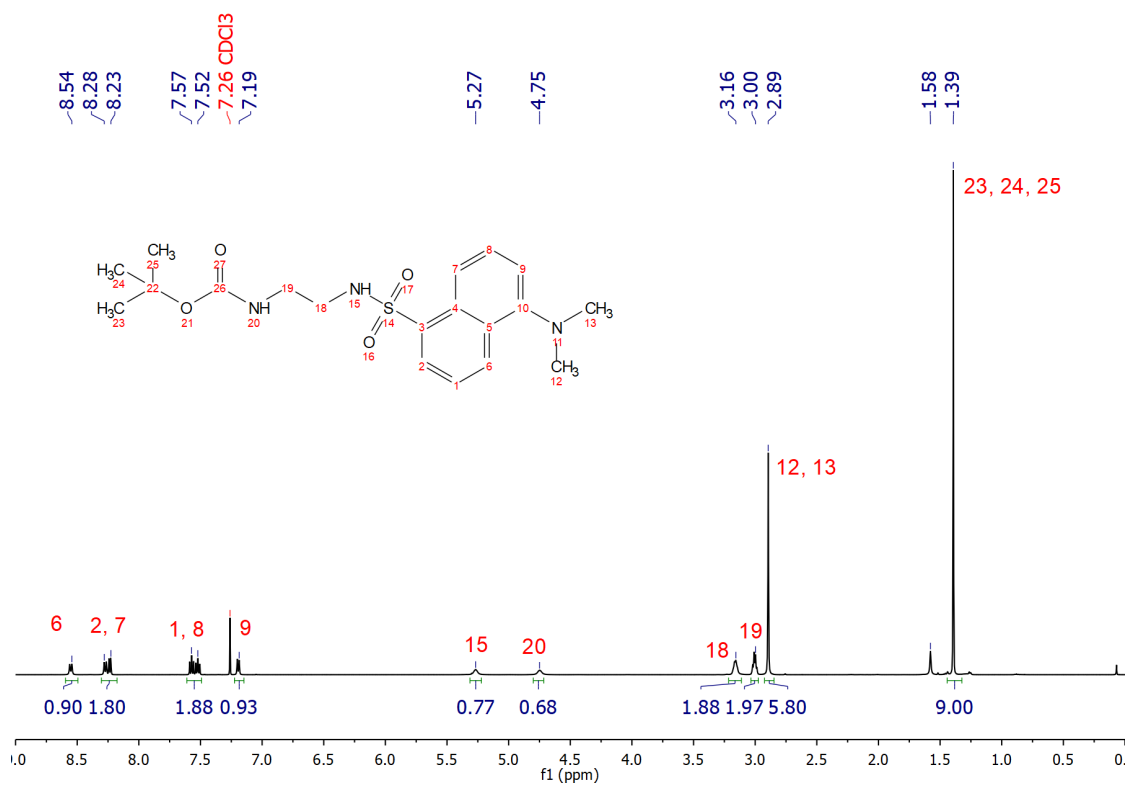
Figure A4. 73. ¹H NMR (400 MHz, CDCl₃) of compound **(50)**.

Synthesis of Dansyl-NH-Ac (Compound 52)
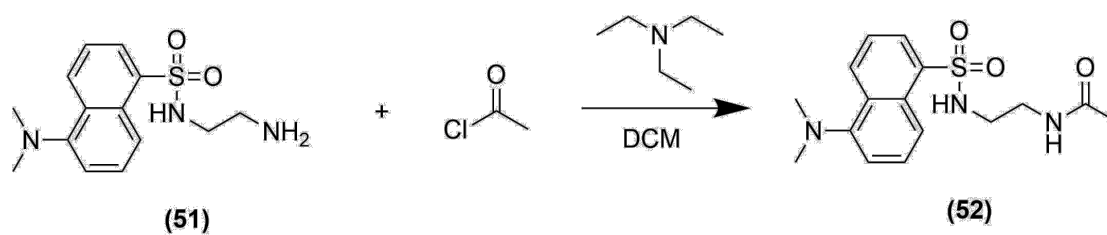
Figure A4. 74. Synthesis scheme for compound **(52).**

Synthesis of Dansyl-modified, PEGylated Cross-linkers (Compounds 53 – 58)
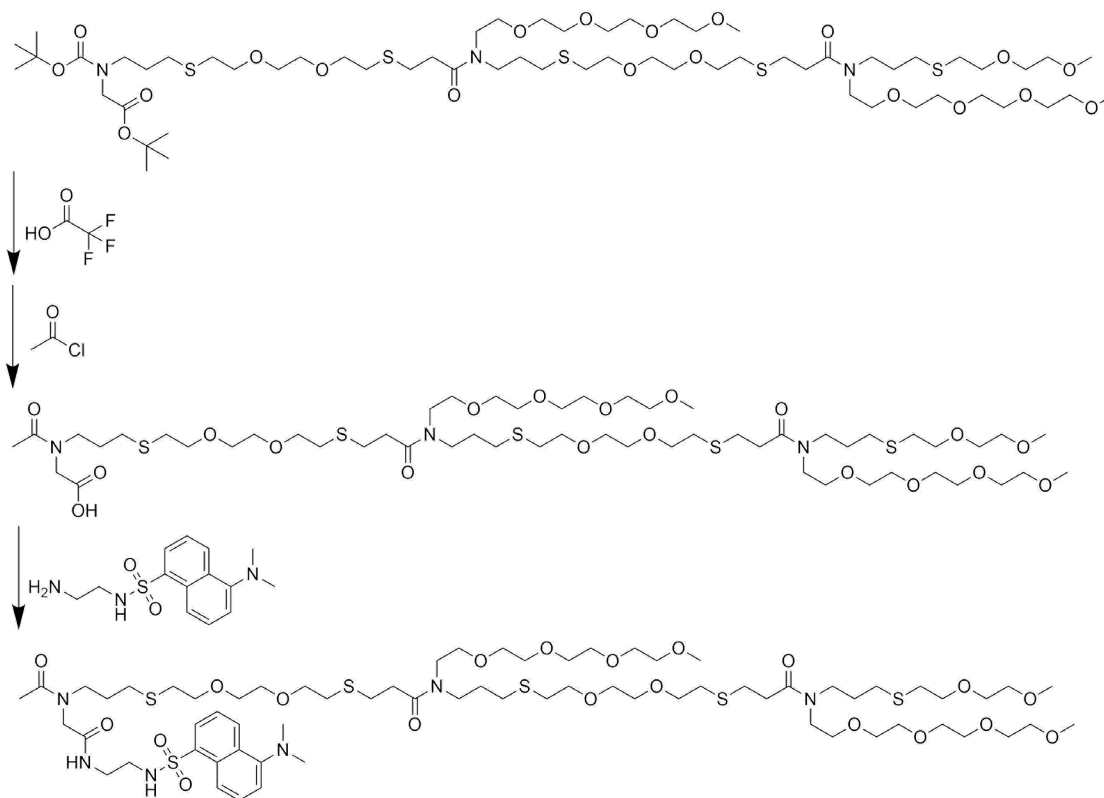
Figure A4. 75. Synthesis scheme for compounds **(53 and 54)**.
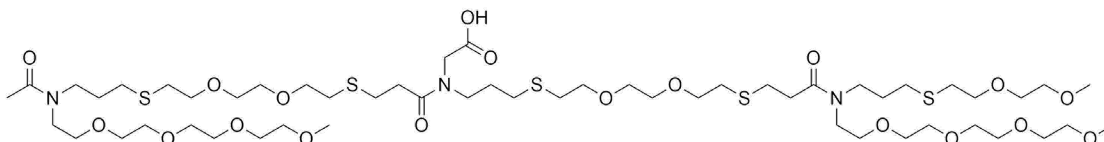
Figure A4. 76. Structure of compound **(55)**.
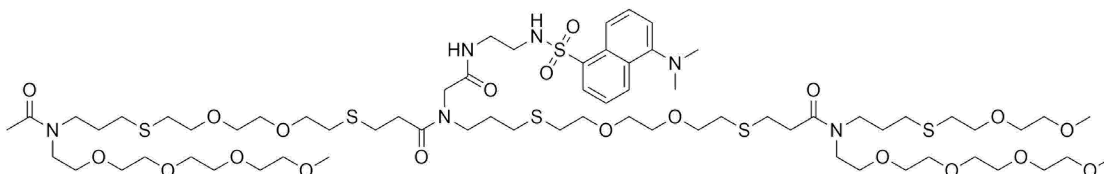
Figure A4. 77. Structure of compound **(56)**.
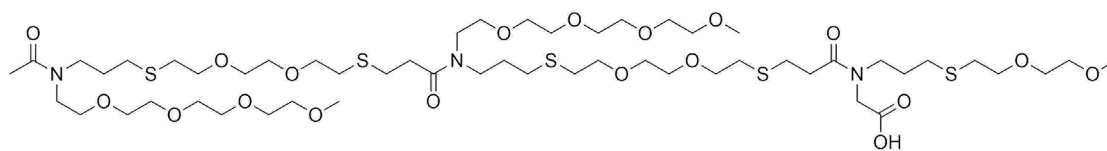
Figure A4. 78. Structure of compound **(57)**.
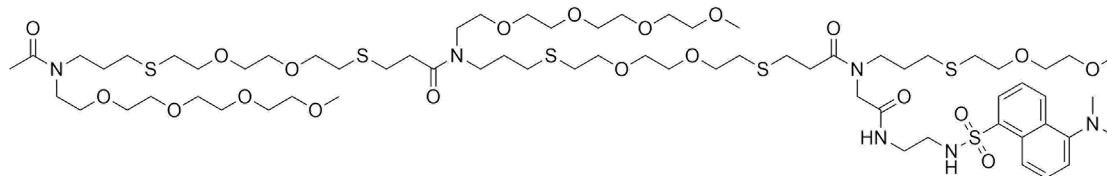
Figure A4. 79. Structure of compound **(58)**.

Characterization of Antibody-fluorescein Conjugate
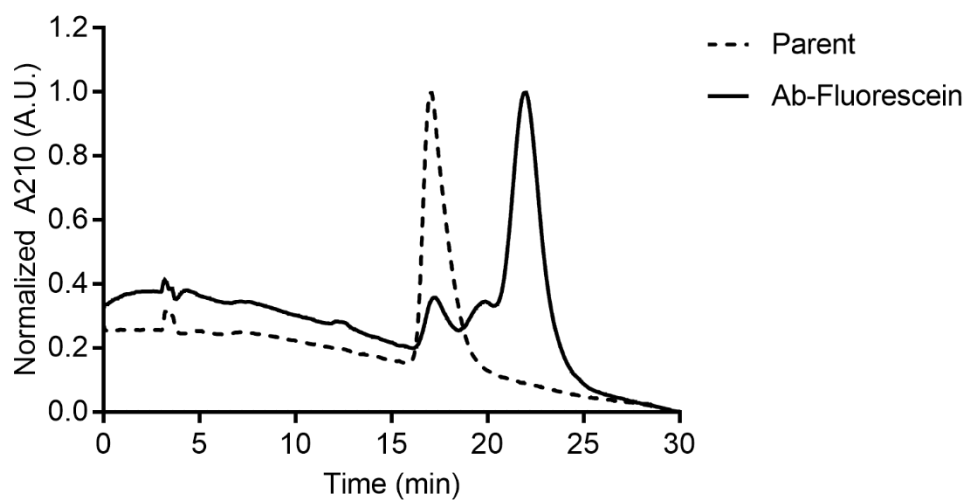
Figure A4. 80. HIC analysis of antibody-fluorescein conjugate.
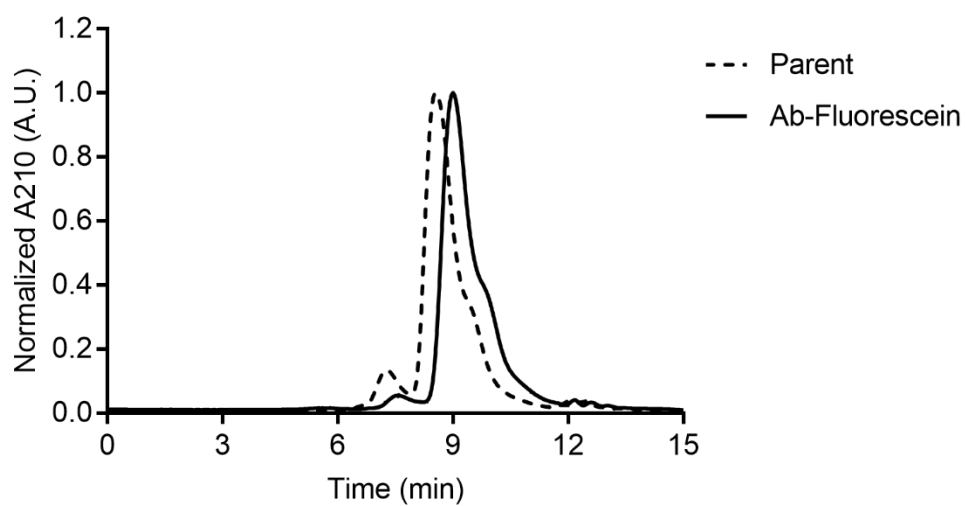
Figure A4. 81. SEC analysis of antibody-fluorescein conjugate.
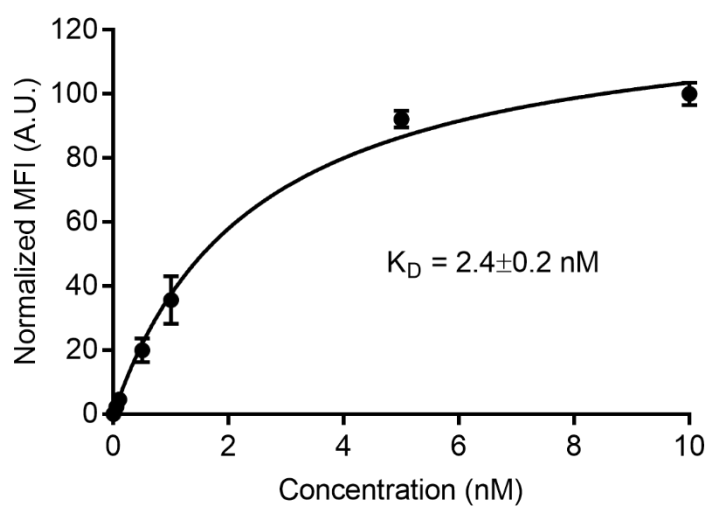
Figure A4. 82. Binding curve for fluorescein-modified antibody on SKOV3 cells.

In vitro Potency of Antibody-drug Conjugates
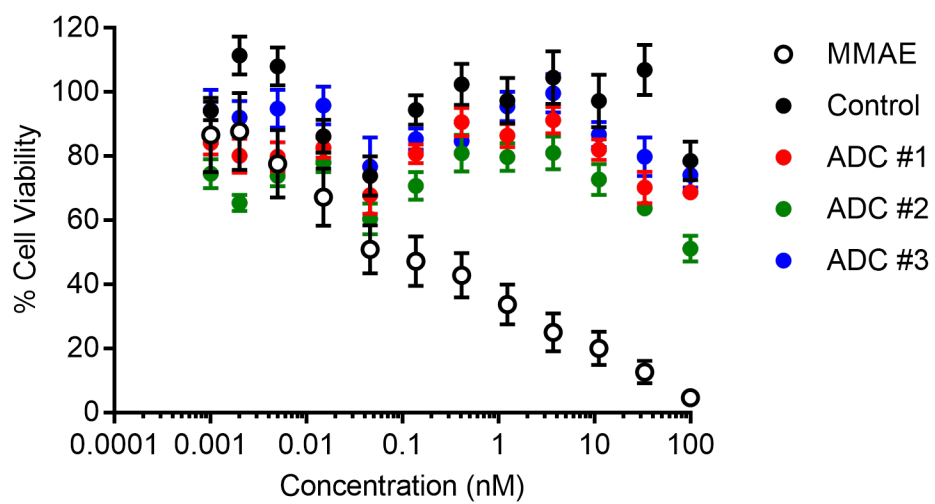
Figure A4. 83. *In vitro* potency of conjugates on MCF7 cells.

Chapter 4 References

1.Beck, A., Goetsch, L., Dumontet, C. & Corvaïa, N. Strategies and challenges for the next generation of antibody-drug conjugates. *Nat Rev Drug Discov* **16,** 315–337 (2017).

2.Hamann, P. R. *et al.* An Anti-CD33 Antibody−Calicheamicin Conjugate for Treatment of Acute Myeloid Leukemia. Choice of Linker. *Bioconjugate Chemistry* **13,** 40 (2002).

3.Shen, B.-Q. *et al.* Conjugation site modulates the in vivo stability and therapeutic activity of antibody-drug conjugates. *Nat Biotechnol* **30,** 184–189 (2012).

4.Alley, S. C. *et al.* Contribution of linker stability to the activities of anticancer immunoconjugates. *Bioconjugate Chemistry* **19,** 759–765 (2008).

5.Erickson, H. K. *et al.* Tumor delivery and in vivo processing of disulfide-linked and thioether-linked antibody-maytansinoid conjugates. *Bioconjugate Chemistry* **21,** 84–92 (2009).

6.Sanderson, R. J. *et al.* In vivo drug-linker stability of an anti-CD30 dipeptide-linked auristatin immunoconjugate. *Clin Cancer Res* **11,** 843–852 (2005).

7.Agarwal, P., van der Weijden, J., Sletten, E. M., Rabuka, D. & Bertozzi, C. R. A Pictet-Spengler ligation for protein chemical modification. *Proc Natl Acad Sci USA* **110,** 46–51 (2012).

8.Lyon, R. P. *et al.* Self-hydrolyzing maleimides improve the stability and pharmacological properties of antibody-drug conjugates. *Nat Biotechnol* **32,** 1059–1062 (2014).

9.Widdison, W. C. *et al.* Semisynthetic maytansine analogues for the targeted treatment of cancer. *J Med Chem* **49,** 4392–4408 (2006).

10.Thorpe, P. E. *et al.* New coupling agents for the synthesis of immunotoxins containing a hindered disulfide bond with improved stability in vivo. *Cancer Res* **47,** 5924–5931 (1987).

11. Anami, Y. *et al.* Glutamic acid-valine-citrulline linkers ensure stability and efficacy of antibody-drug conjugates in mice. *Nat Commun* **9,** 2512 (2018).

12. Menichetti, R., Kanekal, K. H. & Bereau, T. Drug-Membrane Permeability across Chemical Space. *ACS Cent Sci* **5,** 290–298 (2019).

13. Hansch, C., Steward, A. R., Anderson, S. M. & Bentley, D. L. Parabolic dependence of drug action upon lipophilic character as revealed by a study of hypnotics. *J Med Chem* **11,** 1 (1968).

14. Beckley, N. S., Lazzareschi, K. P., Chih, H.-W., Sharma, V. K. & Flores, H. L. Investigation into temperature-induced aggregation of an antibody drug conjugate. *Bioconjugate Chemistry* **24,** 1674–1683 (2013).

15. Buecheler, J. W., Winzer, M., Tonillo, J., Weber, C. & Gieseler, H. Impact of Payload Hydrophobicity on the Stability of Antibody-Drug Conjugates. *Molecular pharmaceutics* **15,** 2656–2664 (2018).

16. Strop, P. *et al.* Site-specific conjugation improves therapeutic index of antibody drug conjugates with high drug loading. *Nat Biotechnol* **33,** 694–696 (2015).

17. Sun, X. *et al.* Effects of Drug-Antibody Ratio on Pharmacokinetics, Biodistribution, Efficacy, and Tolerability of Antibody-Maytansinoid Conjugates. *Bioconjugate Chemistry* **28,** 1371–1381 (2017).

18. Hamblett, K. J. *et al.* Effects of drug loading on the antitumor activity of a monoclonal antibody drug conjugate. *Clin Cancer Res* **10,** 7063–7070 (2004).

19. Mendelsohn, B. A. *et al.* Investigation of Hydrophilic Auristatin Derivatives for Use in Antibody Drug Conjugates. *Bioconjugate Chemistry* **28,** 371–381 (2017).

20. Huang, B. C. B. *et al.* Antibody-drug conjugate library prepared by scanning insertion of the aldehyde tag into IgG1 constant regions. *MAbs* **10,** 1182–1189 (2018).

21. Ohri, R. *et al.* High-Throughput Cysteine Scanning To Identify Stable Antibody Conjugation Sites for Maleimide- and Disulfide-Based Linkers. *Bioconjugate Chemistry* **29,** 473–485 (2018).

22. Burke, P. J. *et al.* Optimization of a PEGylated Glucuronide-Monomethylauristatin E Linker for Antibody-Drug Conjugates. *Mol Cancer Ther* **16,** 116–123 (2016).

23. Lyon, R. P. *et al.* Reducing hydrophobicity of homogeneous antibody-drug conjugates improves pharmacokinetics and therapeutic index. *Nat Biotechnol* **33,** 733–735 (2015).

24. Senter, P. D. & Sievers, E. L. The discovery and development of brentuximab vedotin for use in relapsed Hodgkin lymphoma and systemic anaplastic large cell lymphoma. *Nat Biotechnol* **30,** 631–637 (2012).

25. Kudirka, R. A. *et al.* Site-Specific Tandem Knoevenagel Condensation-Michael Addition To Generate Antibody-Drug Conjugates. *ACS Med Chem Lett* **7,** 994–998 (2016).

26. Kudirka, R. *et al.* Generating site-specifically modified proteins via a versatile and stable nucleophilic carbon ligation. *Chem Biol* **22,** 293–298 (2015).

27. Barfield, R. M. & Rabuka, D. Leveraging Formylglycine-Generating Enzyme for Production of Site-Specifically Modified Bioconjugates. *Methods Mol Biol* **1728,** 3–16 (2018).

28. Drake, P. M. *et al.* Aldehyde tag coupled with HIPS chemistry enables the production of ADCs conjugated site-specifically to different antibody regions with distinct in vivo efficacy and PK outcomes. *Bioconjugate Chemistry* **25,** 1331–1341 (2014).

29. Porel, M. & Alabi, C. A. Sequence-defined polymers via orthogonal allylacrylamide building blocks. *J Am Chem Soc* **136,** 13162–13165 (2014).

30.Porel, M., Thornlow, D. N., Phan, N. N. & Alabi, C. A. Sequence-defined bioactive macrocycles via an acid-catalysed cascade reaction. *Nat Chem* **8,** 590–596 (2016).

31.Phan, N. N., Li, C. & Alabi, C. A. Intracellular Delivery via Noncharged Sequence-Defined Cell-Penetrating Oligomers. *Bioconjugate Chemistry* **29,** 2628–2635 (2018).

32.Brown, J. S. *et al.* Synthesis and Solution-Phase Characterization of Sulfonated Oligothioetheramides. *Macromolecules* **50,** 8731–8738 (2017).

33.Sorkin, M. R., Walker, J. A., Brown, J. S. & Alabi, C. A. Versatile Platform for the Synthesis of Orthogonally Cleavable Heteromultifunctional Cross-Linkers. *Bioconjugate Chemistry* **28,** 907–912 (2017).

34.Lakowicz, J. R. *Principles of Fluorescence Spectroscopy*. (Springer, 2006).

35.Walkup, G. K. & Imperiali, B. Design and Evaluation of a Peptidyl Fluorescent Chemosensor for Divalent Zinc. *J Am Chem Soc* **118,** 3053 (1996).

36.Wang, Y., Ikeda, T., Ikeda, H., Ueno, A. & Toda, F. Dansyl-β-cyclodextrins as Fluorescent Sensors Responsive to Organic Compounds. *Bulletin of the Chemical Society of Japan* **67,** 1598 (1994).

37.Haldar, S., Raghuraman, H. & Chattopadhyay, A. Monitoring orientation and dynamics of membrane-bound melittin utilizing dansyl fluorescence. *J Phys Chem B* **112,** 14075–14082 (2008).

Chapter 5 – DNA- and Polymer-Protein Conjugates to Characterize Extracellular Vesicles

5.1 – Background

Extracellular vesicles (EVs), the portion of the cellular secretome comprised of exosomes and microvesicles, are known to activate cell surface receptors[1,2] as well as deliver their cargo of proteins[3-6] and nucleic acids[7-10] into the cytosol of target cells. Studies of these endogenous functions have implicated EVs in the regulation of fundamental biological processes such as stem cell differentiation[11], tissue repair[12-14], and immune response[7,10,15-17]. Pathologically, EVs have been proposed to stimulate tumor progression[2,18-20], participate in viral infection[17,21-24] and aid the spread of neurodegenerative diseases[25,26]. Taken together, these functions have stoked intense interest in adapting EVs as platforms for disease diagnostics and patient-derived therapeutics[27-30].

Despite these preliminary demonstrations of their broad utility, a precise molecular definition of EVs has remained elusive. Consequently, physical properties such as particle diameter and density have been used to differentiate and purify exosomes from microvesicles via the use of differential centrifugation[31]. However, the success of this approach has been reported to be dependent on the initial purity of the particle suspension, a highly variable and unpredictable parameter[32-34]. Recent studies have highlighted the importance of efficiently separating heterogeneous EV samples. For example, Kanada et al. identified crucial differences between exosomes and microvesicles with respect to their capacity for exogenous loading of nucleic acids and subsequent delivery of cargo[35]. Furthermore, a study by Chivellet et al., which compared the stoichiometry of miRNA copy number and particle count, revealed that

in a sample of exosomes considered to be "pure", less than 1% of the particles contained a single copy of the miRNA of interest[36].

These studies and others illustrate the inherent heterogeneity of EV samples isolated from both cultured cell lines and clinically relevant bodily fluids[37,38]. This heterogeneity obfuscates the properties of particle subpopulations, limiting our understanding of fundamental EV biology. This in turn stymies their development as both disease diagnostics and patient-derived therapeutics. Measurements of EV particle diameter and density alone are not enough to resolve this heterogeneity. To overcome these issues, a new definition amenable to identifying particle subpopulations is needed. As such, we proposed to develop a molecular definition of the EV surface based on differential protein-protein clustering on the particle surface. We hypothesized that this definition would enable the design of capture agents capable of isolating particle subpopulations. EV subpopulations would be analyzed by ELISA and flow cytometry-based surface protein characterization as well as protein and nucleic acid sequencing. In this way, a holistic view of each particle subpopulation would be developed. By correlating this data set with biological activity data, the first EV structure-content-function relationships would be identified, allowing for the design of smarter EV-based diagnostics and therapeutics.

To study differential properties of EV subpopulations, we drew inspiration from the field of target-guided synthesis (TGS) to develop a methodology for the bottom-up design of particle-specific capture agents. The concept of TGS was introduced by Sharpless in 2002 as a method for the *in situ* design of bivalent, small molecule protein inhibitors[39]. This approach utilizes the enzyme active site as a selective template to accelerate the reaction rate between small molecule building blocks that bind near one another. Application of this methodology by Sharpless and others has led to the

discovery of a host of novel small molecule enzyme inhibitors[39-43]. Recent work has sought to extend the application of TGS beyond the confines of the enzyme active site. Specifically, the Heath group has utilized protein tertiary structure as a template for the combinatorial design of peptide-based, protein-specific capture agents[44-46] and allosteric inhibitors[47]. In other work, the Bertozzi group has combined the concepts of TGS with metabolic labeling and copper-free click chemistry to enable live-cell labeling of protein glycoforms. These works present TGS as a technique able to probe multivalent interactions across multiple length scales. Thus, we propose the nanometer length scale of biological membranes as the next frontier of TGS templates. Specifically, we aim to extend the concepts of TGS to probe protein-protein interactions on the surface of EVs. We sought to demonstrate the feasibility of this idea in two ways: 1) bifunctional, cleavable DNA-streptavidin conjugates containing both "click" handles and fluorescent reporters and 2) polymer-streptavidin conjugates containing oligoTEA-based molecular barcodes[48].

5.2 – Results and Discussion

Consideration of Solution Phase Reaction Kinetics

TGS relies on bioorthogonal chemistry and slow solution phase reaction kinetics to prevent non-specific reactivity and confounding false positives. Selecting reactive pairs with appropriate reaction kinetics requires careful consideration of the binding affinity of the targeting ligand. When designing protein inhibitors and capture agents, the relevant affinity is that of small molecule fragments and monovalent peptides. These ligands typically bind to their target with affinities in the micromolar range. Thus, the reactive pair must be inert in solution at micromolar concentrations. To satisfy this criterion, researchers have turned to the uncatalyzed cycloaddition between an azide and linear alkyne. The kinetics of this reaction are unmeasurable in

solution and therefore minimizes false positives. In work that was concurrent with our work presented here, the Bertozzi lab utilized glycoprotein-specific aptamers which have nanomolar binding affinities. An increase in binding affinity enables saturation of the target a lower solution phase concentration. Therefore, a more reactive pair can be used while minimizing solution phase reaction. This led the Bertozzi group to employ a strain-promoted cycloaddition between an azide and a cyclooctyne (SPAAC), which occurs readily in solution at micromolar concentrations.

In our work, we sought to demonstrate the concept of TGS on the EV surface by using a synthetic system of biotinylated nanoparticles and a streptavidin-based targeting ligand. As a first step, we looked to verify that the SPAAC reaction would be inert in solution at nanomolar concentrations.
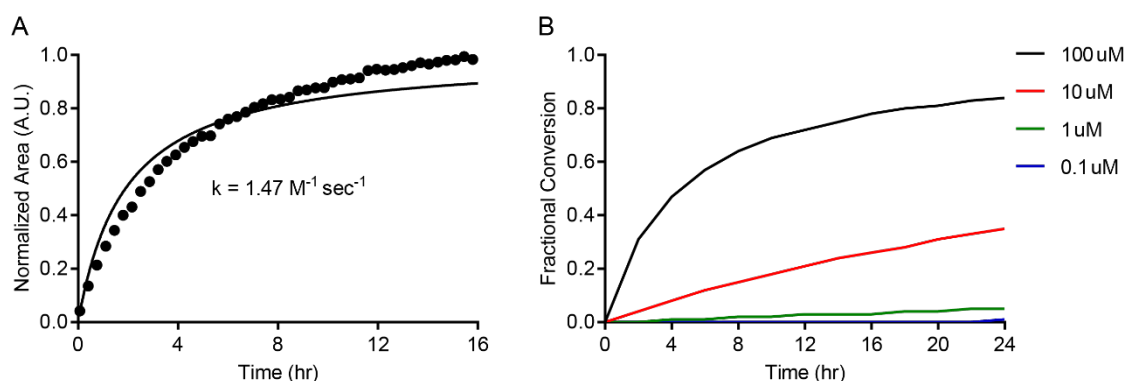
Figure 5.1. Solution phase kinetics of SPAAC reaction. A) LC-MS quantification of rate constant. B) Prediction of solution phase reaction kinetics.

Quantification of the rate constant for the SPAAC reaction at room temperature in aqueous solution confirmed that the SPAAC reaction be inert at nanomolar concentrations for at least 24 hours (**Figure 5.1**). This conclusion is validated by the glycoprotein work from Carolyn Bertozzi's lab.

DNA-based Target-guided Synthesis Probes
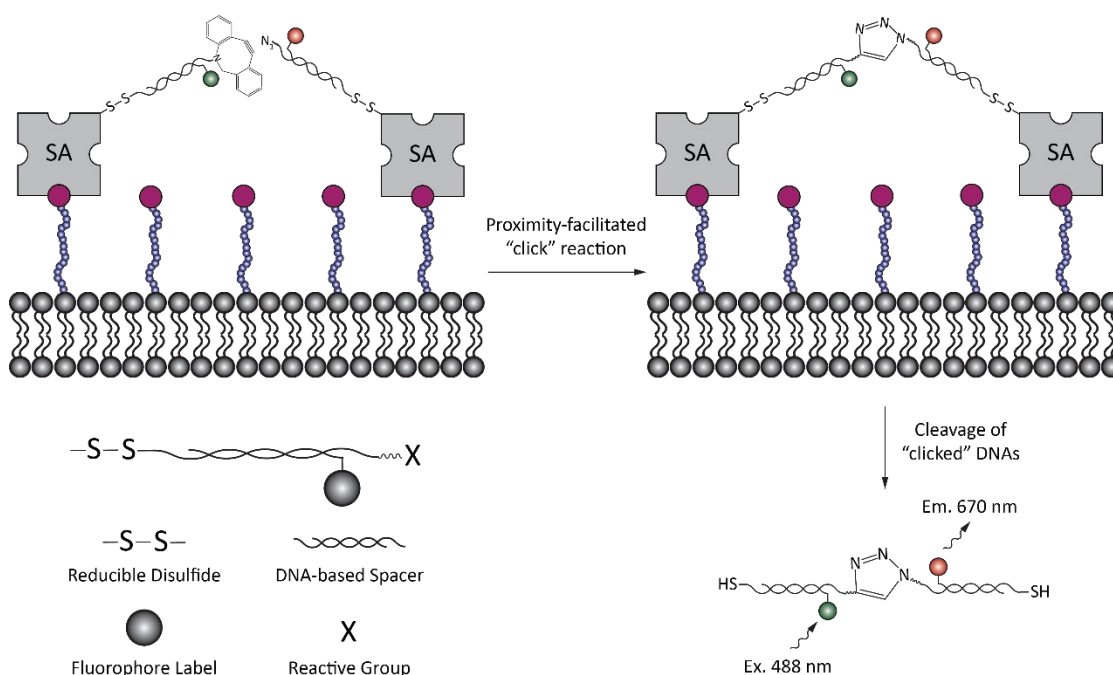
Figure 5.2. Design of DNA-based TGS probes. Cross-linkers are attached to a model protein, streptavidin, via a reduction sensitive disulfide bond. Terminal fluorophore modifications report on the surface-bound proximity of TGS probes. Terminal DBCO and azide modifications undergo proximity facilitated SPAAC reaction. Reduction of the disulfide bond leads to a solution phase FRET readout upon successful SPAAC reaction.

With solution-phase reactivity confirmed we designed a set of fluorescently labeled, DNA-based probes to demonstrate TGS on the surface of biotinylated lipid nanoparticles (LNPs) (**Figure 5.2**). The use of biotinylated LNPs allowed us to tune the density of binding target (biotin) without affecting particle size. This would allow us to probe the effect of inter-ligand distance without introducing confounding effects of particle curvature. The choice of biotin as our target led to the selection of streptavidin as our targeting ligand due to its exceptional binding affinity and commercial availability. Our TGS probes utilized 20mer single-stranded DNA (ssDNA) as a chemical cross-linker. We saw multiple benefits to using a DNA-based system. Short, double stranded DNA (dsDNA) adopts a "rigid rod" structure that would enable us to use DNA length as

227

a molecular ruler to approximate the distance between ligands on the particle surface. Further, the highly charged nature of dsDNA would minimize the solution-phase kinetics of the SPAAC reaction. Finally, in future designs, DNA-based probes could be adapted for ultrasensitive, multiplexed detection via DNA sequencing.

The DNA-based probes were comprised two complimentary strands of chemically modified ssDNA. The first strand was modified on the 3' end via NHS ester chemistry to contain either an azide- or DBCO-functional group. These strands serve as the site for SPAAC reaction between the two probes. The second strand was modified through a three-step synthesis to contain a reducible 3' transcyclooctene (TCO) functionality and a 5' Alexa Fluor 488 or 647. The TCO functional group enables conjugation via the inverse electron demand diels-alder (IEDDA) reaction to a methyltetrazine-modified streptavidin. Alexa Fluor 488 and 647 form a Förster resonance energy transfer (FRET) pair. Therefore, when bound in proximity, the TGS probes should display a characteristic FRET signal, which can be monitored in real time. After the probes bind to the particle surface and react, the reduction sensitive disulfide bond is used to liberate the probes from the particle surface. Conjugated probes display a characteristic FRET signal in solution, while unconjugated probes display no FRET signal.
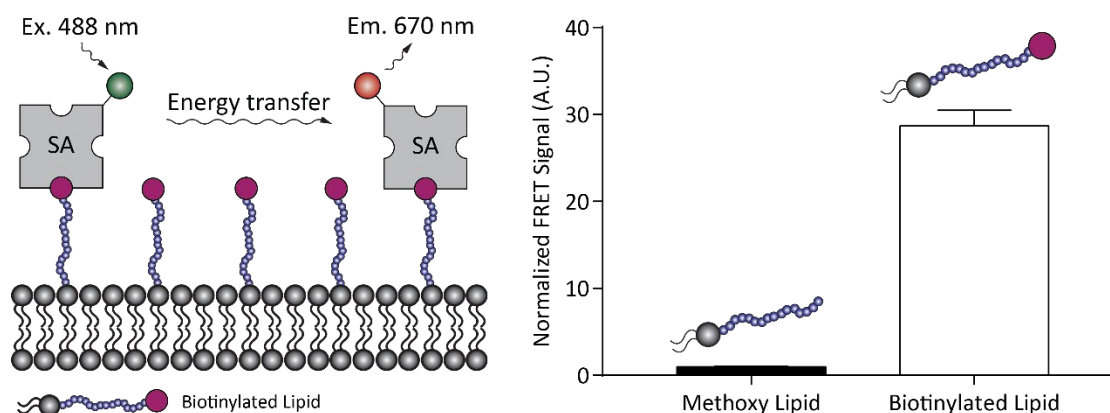
Figure 5.3. FRET of Alexa Fluor-labeled streptavidin on the surface of LNPs. A biotin-specific FRET signal is observed in the presence of Alexa Fluor-488 and Alexa Fluor-647 labeled streptavidin.

To validate the ability of biotinylated LNPs to generate a FRET signal, commercially available Alexa Fluor-labeled streptavidin was mixed with biotinylated LNPs (**Figure 5.3**). An equimolar mixture of Alexa Fluor 488 and 647-labeled streptavidin generated a significant FRET signal in comparison to unlabeled LNPs. The control of unlabeled LNPs accounts for any signal generated as a result of non-specific binding. This result indicates that proteins-sized targeting ligands can pack onto the particle surface at reasonable density.
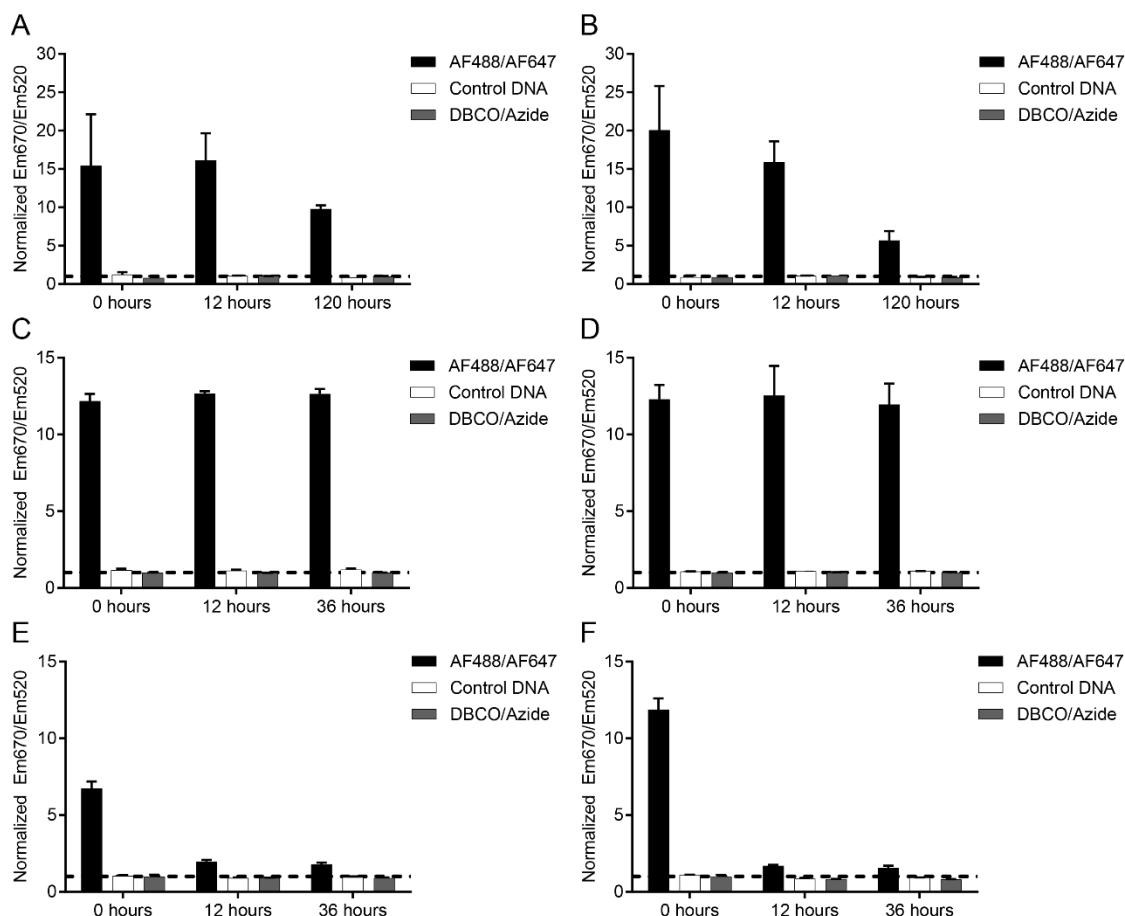
Figure 5.4. FRET-based readout of TGS on the LNP surface. A) LNPs containing 5% biotinylated lipid diluted 1:100, B) LNPs containing 10% biotinylated lipid diluted 1:100, C) LNPs containing 5% biotinylated lipid diluted 1:10, D) LNPs containing 10% biotinylated lipid diluted 1:10, E) LNPs containing 5% biotinylated lipid diluted 1:1000, F) LNPs containing 10% biotinylated lipid diluted 1:1000. The dashed line represents the threshold for positive FRET signal. Equimolar mixture of streptavidin at 10 nM.

After confirming that streptavidin can bind in proximity on the LNP surface, we sought to demonstrate particle-based the concept of TGS (**Figure 5.4**). In every condition, FRET was observed for the positive control of a pair of Alexa Fluor-labeled streptavidin. However, at low particle concentrations, the FRET signal was unstable and dissipated over the course of 12 hours. In every condition tested, the azide- and DBCO-modified streptavidin probes showed no FRET signal. This was confirmed by two controls. The first control was a sample of non-biotinylated LNP that controls for

non-specific binding. Every data point was normalized such that signal greater than 1 is interpreted as FRET signal in excess of FRET due to non-specific binding. The second control is a sample of streptavidin conjugates lacking the azide and DBCO functionalities (labeled as "Control DNA"). This control would account for FRET signal that arises from close binding. Signal above this control would indicate FRET signal arising from the SPAAC reaction between streptavidin probes. These experiments proved that FRET was not occurring between the TGS probes on the particle surface.
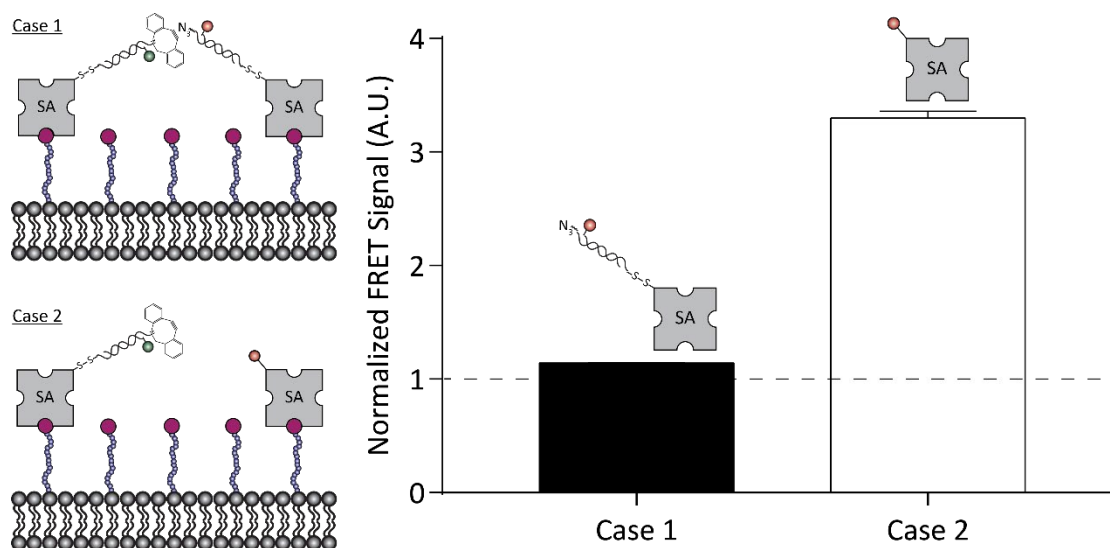
Figure 5.5. FRET on LNP surface using mixture of streptavidin probes. Case 1 using two DNA-modified streptavidin probes yielded no detectable FRET signal. Case 2 using a mixture of DNA-modified and fluorophore-modified streptavidin yielded a detectable FRET signal.

We considered two possible causes of the lack of FRET signal generated by our TGS probes on the LNP surface. First, a non-specific conjugation strategy was used to conjugate the DNAs to streptavidin. This could negatively impact binding affinity if attachment occurred near the biotin-streptavidin binding site. Second, dsDNA is a rigid, highly charged structure. This could make it unfavorable for two TGS probes to bind in proximity. Alternatively, TGS probes may bind in proximity but orient the DNA modifications in a way that minimizes electrostatic repulsion. To address these issues,

we carried out an experiment wherein an equimolar mixture of TGS probes was compared to an equimolar mixture of one TGS probe with an Alexa Fluor-labeled streptavidin (**Figure 5.5**). As expected, this experiment showed FRET in the case of the two TGS probes. However, a detectable FRET signal was observed when one DNA-modified streptavidin was exchanged for an Alexa Fluor-modified streptavidin. This result supports the interpretation that the TGS probes do maintain their ability to bind biotin. However, they do not bind in proximity to one another. This could be caused by electrostatic repulsion between the dsDNA probes. Therefore, we identified strong charge as a design feature to be avoided in TGS probes.

OligoTEA-based Target-guided Synthesis Probes
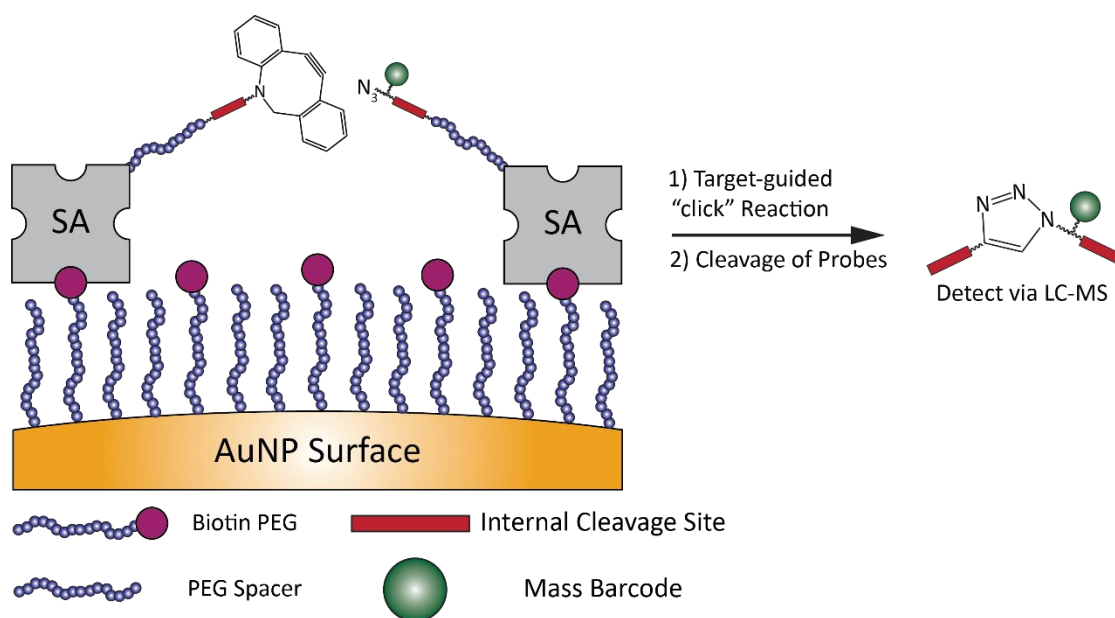
Figure 5.6. Design of oligoTEA-based TGS probes. Probes are attached to streptavidin via PEG-based cross-linkers and an internal, oxidation sensitive cis-1,2-diol. Terminal DBCO and azide modifications undergo proximity facilitated SPAAC reaction. Oxidation of the cis-1,2-diol liberates a unique mass fragment that can be detected via LC-MS.

To resolve the issue of inefficient proximity binding of two charged bioconjugates on the particle surface, we designed TGS probes that utilize uncharged, polyethylene glycol (PEG)-based cross-linkers (**Figure 5.6**). In this test system,

biotinylated gold nanoparticles are used as a surrogate for biologically derived vesicles and streptavidin is used a model targeting ligand. By switching to PEG-based cross-linkers we lost the ability to leverage multiplexed detection via DNA sequencing. Therefore, we envisioned incorporating a molecular weight barcode into the TGS probes. Upon cleavage of the conjugated probes, a fragment of the probe would be release into solution for detection via liquid-chromatography mass-spectrometry (LC-MS). A molecular barcode would generate a unique mass signature for each TGS probe. This would enable simultaneous analysis of a particle reacted with a mixture differentially targeted TGS probes.
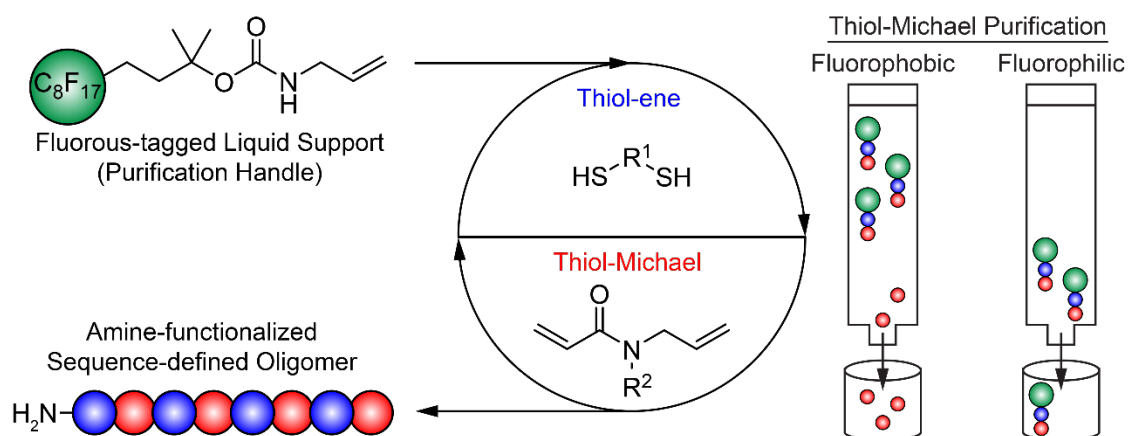
Figure 5.7. Overview of oligothioetheramide synthesis. Iterative synthesis scheme (left) and fluorous phase extraction (right).

To design synthesize molecular barcodes, we turned to the sequence-defined oligothioetheramide (oligoTEA) synthesis methodology developed in our lab (**Figure 5.7**). OligoTEA synthesis utilizes an orthogonally reactive *N*-allylacrylamide monomer, which can undergo alternating photoinitiated thiol−ene "click" reactions and phosphine catalyzed thiol-Michael additions[48]. OligoTEAs are built off a fluorous tag liquid support, which enables stepwise fluorous purification throughout synthesis. The fluorous purification handle is removed post synthesis by acid-catalyzed Boc deprotection.

OligoTEA synthesis has been used as a platform to discover synthetic antibacterial agents[49] and cell penetrating oligomers[50] as well as to synthesize model systems to study the solution phase structure of polymers[51].
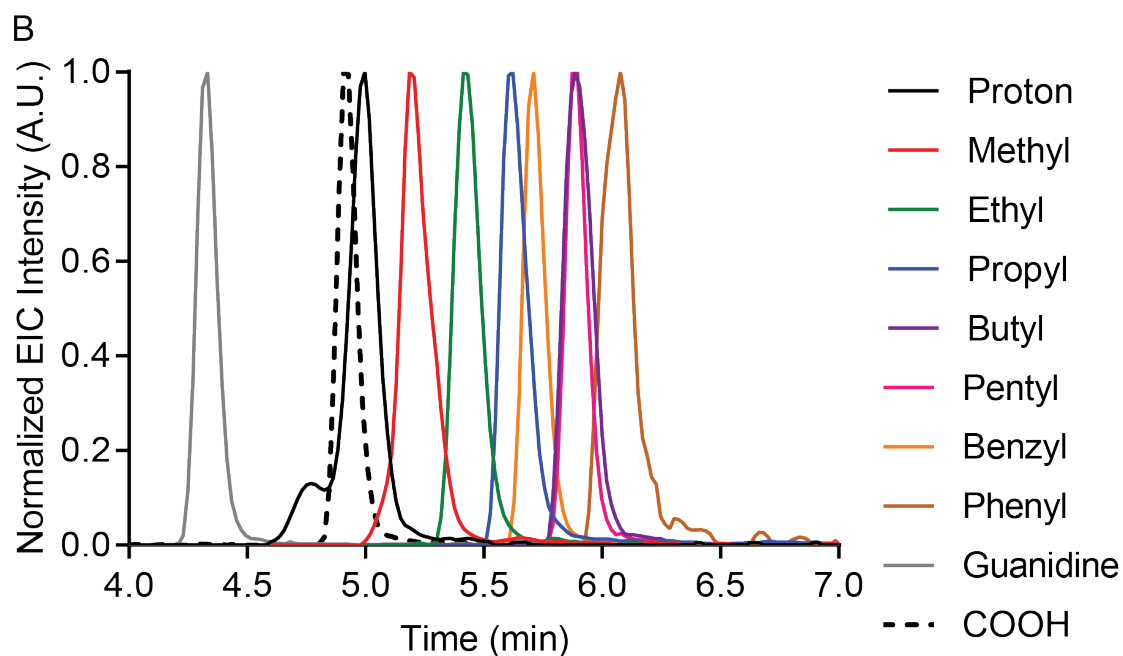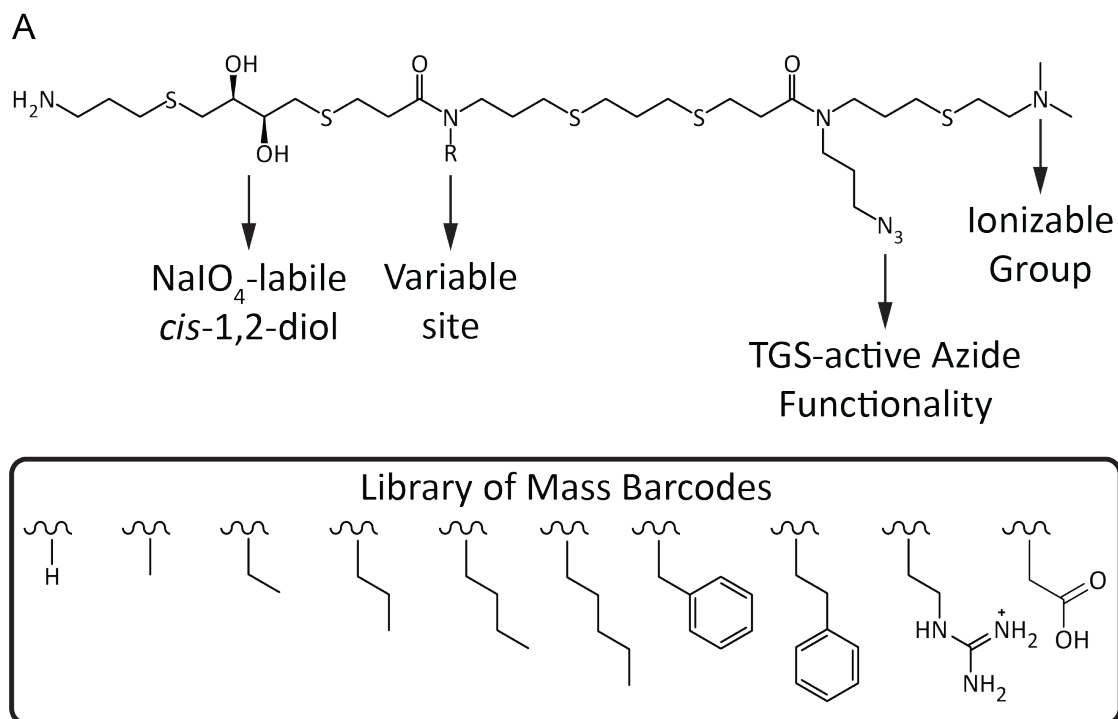
Figure 5.8. Synthesis of oligoTEA-based molecular barcodes. A) Structural features of molecular barcodes. B) Oligomer confirmation via extracted ion elution profiles collected via LC-MS.

Our oligoTEA-based TGS probes contained a several important structural features (**Figure 5.8**). The terminal primary amine enabled attachment of the probe to a variety of PEG-based cross-linkers. Commercial PEG-based cross-linkers are available in a wide range of sizes. Performing a TGS experiment with a variety of different length PEGs could be used to approximate the distance between target sites. Each oligomer contained an internal *cis*-1,2-diol, which can be cleaved by treatment with sodium periodate to liberate the probe from the particle surface for detection via LC-MS. A library of *N*-allylacrylamide monomers were used to install a molecular weight barcode within the oligomer. Alternatively, this site was used to install a carboxylic acid functional group. The carboxylic acid could be used as a site to derivatize this structure with isolation handles or reporter molecules. An azide-modified *N*-allylacrylamide monomer provided a "click" handle for the SPAAC reaction. A terminally tertiary amine was used to cap the oligomer. This is a highly ionizable group and therefore, provides a means of sensitive detection via LC-MS. Each oligomer was synthesized via oligoTEA synthesis, purified via RP-HPLC, and characterized via LC-MS (**Figure 5.8**).
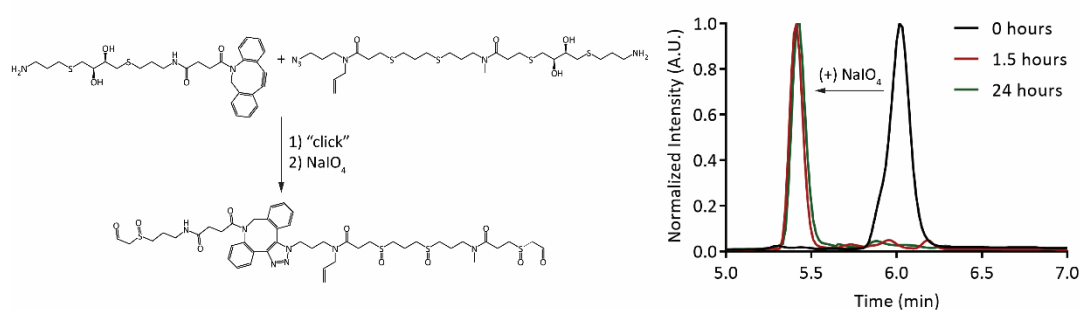
Figure 5.9. Sodium periodate oxidation of TGS probes. Structure of "clicked", singly oxidized TGS probe (left) and LC-MS based detection of TGS probe (right).

The efficiency of sodium periodate oxidation was tested using a version of the oligoTEA probe which did not contain a terminal tertiary amine (**Figure 5.9**). The LC-

MS compatible azide and DBCO probes were reacted to form the expected "clicked" product. This standard was treated with ten equivalencies of sodium periodate and monitored via LC-MS. After 1.5 hours, both *cis*-1,2-diols were cleaved and oxidation of the four thioether bonds was observed. Sodium periodate is known to oxidize thioether bonds to sulfoxides under gentle reaction conditions. Under these conditions, we observed a molecular weight indicative of a single oxidation at each of the four available thioether bonds. However, we cannot rule out a mixture of thioether, sulfoxide, and sulfone products. After 24 hours of treatment, the oxidized product remained stable to further oxidation. This result indicates that oxidation for approximately 1.5 hours was adequate to generate a homogenous mass fragment which can be reliably detected via LC-MS.
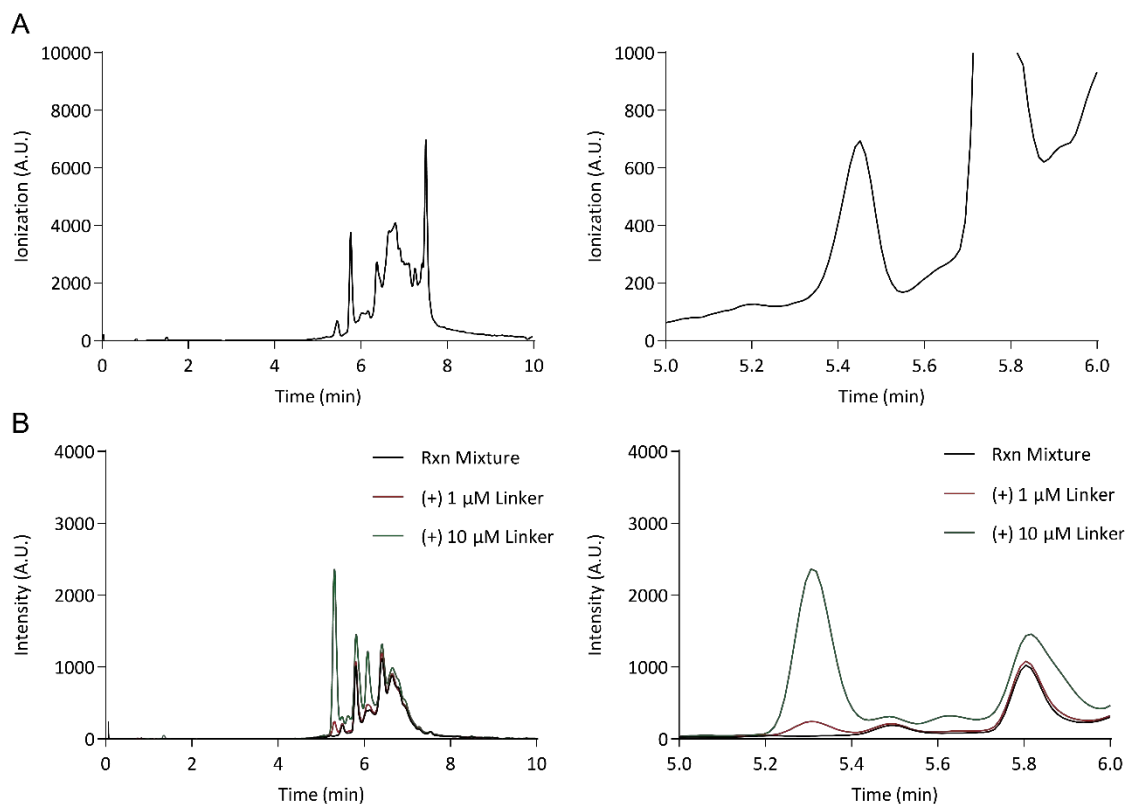
Figure 5.10. Detection limit of TGS product via LC-MS. A) TGS experiment without internal control. Substantial noise was observed from 5 – 8 minutes. B) TGS experiment with internal control. Internal control demonstrated a detection limit of 1 µM and no observable reaction.

The azide- and DBCO-modified TGS probes were conjugated to streptavidin via 5,000 g/mol polydisperse PEG chain. These conjugates were then used to detect TGS on the surface of biotinylated gold nanoparticles (**Figure 5.10**). After incubation with gold nanoparticles, the mixture was centrifuged and washed repeatedly to remove unbound TGS probes and concentrate the nanoparticle solution for LC-MS analysis. The concentrated particle mixture was treated with sodium periodate using the optimized conditions and analyzed via LC-MS using selective ion monitoring. An initial experiment demonstrated that the treatment protocol results in a large amount of noisy signal from approximately 5 – 8 minutes. Closer inspection of the LC-MS results

238

showed a small peak at approximately 5.4 minutes. This result was promising as a standard of the "clicked" product (**Figure 5.9**) was shown to elute form the column at a similar time. To validate this result, we sought to replicate this experiment with additional controls. After reaction, purification, and sodium periodate treatment, we analyzed the cleavage product directly as well as mixed with known amounts of the "clicked" product standard. This internal control accounted for subtle differences in the LC-MS mobile phase, which may have caused shifts in the retention time for the desired product. Further, the internal standard was used to determine the approximate detection limit of LC-MS analysis. Upon addition of 1 µM of standard, a low intensity peak was observed at approximately 5.3 minutes. This peak grew in intensity upon addition of 10 µM of standard. This result suggested that no product was detected from the TGS reaction on the particle surface. This could be interpreted to mean that no reaction had occurred or that the detection limit of the product was not reached. The internal controls indicated that 1 µM of product would have been detected. Therefore, given the concentration of particles used, approximately 500 reactions per particle would be needed to reach the detection limit. At this condition, the concentrated particle solution was essentially dry (i.e. no solvent remaining). Therefore, it was not feasible to use more particles to overcome the detection limit. We reasoned that a probe with a higher potential for ionization would lower the detection limit. To test this hypothesis, we generated a "clicked" product standard using the guanidine modified TGS probe. However, upon treatment with sodium periodate numerous unidentified side reactions occurred. This yielded a highly heterogeneous product in which no characteristic ions could be identified (data not shown).

5.3 – Conclusions

In conclusion, with an eye towards studying EVs, we sought to apply the principles of target-guided synthesis to probe inter-ligand distances on the surface of nanoparticles. In one approach, we pursued DNA-based cross-linkers with a FRET-based readout of reaction conversion. This system was not functional, which we attributed to the repulsive electrostatic interactions between the dsDNA probes. To remedy this issue, we pursued a second approach which utilized multifunctional PEG-based cross-linkers and an LC-MS-based readout of reaction conversion. We successfully synthesized and library of molecular barcodes using the oligoTEA synthesis methodology developed in our lab. However, the sensitivity of LC-MS-based detection was shown to be insufficient to detect successful ligation of TGS product. Despite the negative results from our studies, work carried out concurrently in Carolyn Bertozzi's lab[52] confirms that TGS using the SPAAC reaction and affinity reagents with nanomolar affinity is feasible. To address the shortcomings of this work, new reaction detection strategies should be considered. Specifically, an enzymatic readout would provide signal amplification. This would likely improve the detection limit of the TGS experiments. Further, enzymatic assays can be readily quantified and adapted to a high throughput microplate format. Alternatively, a biotin handle could be used in a pull-down assay format to directly isolate and characterize particle subpopulations.

5.4 – Materials and Methods

Flash Chromatography

Flash chromatography was performed on a Teledyne ISCO CombiFlash Rf-200i chromatography system equipped with UV-Vis and evaporative light scattering detectors (ELSD).

Nuclear Magnetic Resonance (NMR) Spectroscopy

^{1}H and ^{13}C NMR spectra were recorded on an INOVA 400 MHz spectrometer. NMR data was analyzed by MestReNova software. ^{1}H and ^{13}C NMR chemical shifts are reported in units of ppm relative to chloroform.

Liquid Chromatography Mass Spectrometry (LC-MS)

LC-MS analysis was carried out on an Agilent 1100 Series LC with a Poroshell 120 EC-C18 column (100 × 3 mm, 2.7 µm, Agilent Technologies) and an Agilent G1956B Series Single Quadripole MS in positive ion mode for mass detection. The mobile phase for LC-MS (solvent A) was water with 0.1% (v/v) acetic acid, and the stationary phase (solvent B) was acetonitrile with 0.1% (v/v) acetic acid. Compounds were eluted at a flow rate of 0.6 mL/min using a gradient of 5-100% solvent B (0-10 minutes) followed by 100% solvent B (10-12 minutes) and equilibrated back to 5% solvent B (12-15 minutes).

Reverse Phase High Performance Liquid Chromatography (RP-HPLC)

HPLC purification was performed on an Agilent 1100 Series HPLC system equipped with a UV diode array detector and an 1100 Infinity fraction collector. Semi-preparative RP-HPLC was performed with a C18 column (Agilent Eclipse XDB-C18, 9.4 x 250 mm, 5 µm). Analytical RP-HPLC was performed with a C18 column (Agilent Eclipse Plus C18, 4.6 x 150 mm, 5 µm). The mobile phase for HPLC was water with 0.1% (v/v) trifluoroacetic acid (solvent A) and acetonitrile with 0.1% (v/v) trifluoroacetic acid

(solvent B) unless specified otherwise. Compounds were eluted at a flow rate of either 4 mL/min (semi-preparative) or 1 mL/min (analytical) using a linear solvent gradient as specified below.

LC-MS Analysis of SPAAC Reaction Kinetics

An equimolar mixture of DBCO-PEG4-COOH and Azide-PEG4-COOH was prepared at 100 μM in water. The reaction was carried out at room temperature and analyzed every 15 minutes via LC-MS using selective ion monitoring (SIM) to identify the expected product mass. For each time point, area under the curve (AUC) was quantified and used as a surrogate for reaction conversion. A plot of normalized AUC versus time was fit in GraphPad Prism using an equimolar bimolecular rate law to extract the rate constant for the reaction.

Purification of Modified DNAs

HPLC purification was performed on an Agilent 1100 Series HPLC system equipped with a UV diode array detector and an 1100 Infinity fraction collector. Purification of modified DNAs was performed using an analytical RP-HPLC with a C18 column (Agilent Eclipse Plus C18, 4.6 x 150 mm, 5 μm). The mobile phase for HPLC was TEAA buffer (100 mM triethylamine, 100 mM acetic acid, pH 7.2, solvent A) and acetonitrile (solvent B). Compounds were eluted at a flow rate of either 1 mL/min using a linear solvent gradient as specified below.

Synthesis of "Click"-modified DNAs

1 equivalency of (50 μg, 7 nmol) of monofunctional DNA (3' C6 spacer, Amine) was reacted with 50 equivalencies of NHS ester activated Azide or DBCO (Azide-PEG4-NHS or DBCO-PEG4-NHS) at a DNA concentration of 100 μM. The solvent for the reaction was 40% (v/v) dimethyl sulfoxide in borate buffered saline (BBS), pH 8.2 (100 mM borate, 150 mM NaCl). The reaction was carried out at room temperature

overnight. The product was dialyzed against water to remove excess NHS ester and concentrated under vacuum. The crude product was purified via analytical RP-HPLC and dried under vacuum to yield the final product. The pure azide- and DBCO-modified DNAs were isolated in 87% and 39% yield, respectively.

Synthesis of Cleavable, Fluorophore-modified DNAs for IEDDA Conjugation

Step 1: Acylation of 5' Amine Modification

1 equivalency (50 µg, 7 nmol) of bifunctional DNA (3' C9 spacer, SS-OH; 5' C6 spacer, Amine) was reacted with 50 equivalencies of NHS ester activated Alexa Fluor 488 or 647 at a DNA concentration of 100 µM. The solvent for the reaction was 40% (v/v) dimethyl sulfoxide in borate buffered saline (BBS), pH 8.2 (100 mM borate, 150 mM NaCl). The reaction was carried out at room temperature overnight. The product was dialyzed against water to remove excess dye and concentrated under vacuum. The product was used without further characterization or purification.

Step 2: Thiol-disulfide Exchange of 3' Thiol Modification

Liberation of the 3' thiol modification was achieved by suspending the crude step 1 product in 5 µL of a 100 mM solution of dithiothreitol (DTT) in BBS, pH 8.2. Reduction was carried out for 1 hour at room temperature. Excess DTT was removed by extractions with ethyl acetate (3x, 100 µL). Residual ethyl acetate was removed by placing the product under vacuum for 10 minutes. 1 equivalency of the deprotection product was capped with 50 equivalencies of 2-(pyridin-2-yldisulfaneyl)ethan-1-amine (PDA) in BBS, pH 8.2 at a DNA concentration of 150 µM. The reaction was carried out at room temperature overnight. The product was dialyzed against water to remove excess PDA and concentrated under vacuum. The product was used without further characterization or purification.

Step 3: Acylation of Reducible 3' Amine Modification

Modification of the reducible 3' amine modification was achieved by reacting 1 equivalency of crude step 2 product with 50 equivalencies of NHS ester activated transcyclooctene (TCO-PEG4-NHS) at a DNA concentration of 100 μM. The reaction solvent was 40% (v/v) dimethyl sulfoxide in BBS, pH 8.2. The reaction was carried out at room temperature overnight. The product was dialyzed against water to remove excess NHS ester and concentrated under vacuum. The crude product was purified via analytical RP-HPLC and dried under vacuum to yield the final product. The pure product was typically isolated in 35% yield.

Synthesis of Lipid "A10"

Step 1: Aza-Michael Addition

1 equivalency of diethylaminoproylamine (365 μmol) was added to 2.5 equivalencies of propargyl acrylate. The reaction was carried out neat at 45°C overnight. Excess propargyl acrylate was then removed under vacuum. The product was characterized by ^{1}H NMR and used without further purification.

Step 2: Thiol-yne Reaction

5.6 equivalencies of decane-1-thiol was added to 1 equivalency (26 mg, 75 μmol) of step 1 product. DMPA catalyst was added at 4% by weight. The mixture was irradiated with 10 mW/cm^2 UV for 270 seconds. The crude product was suspended in 4 mL of a 9:1 mixture of methanol and water. The suspended product was sonicated for 5 minutes before lipid precipitation via centrifugation at 3,000xg for 10 minutes. The supernatant was decanted, and the precipitation was repeated four times. The purified product was dried under vacuum to remove residual solvent. The product "A10" lipid was characterized via ^{1}H NMR. The product was isolated in 91% yield (71 mg, 69 μmol).

Synthesis of Biotinylated Lipid-nanoparticles

Biotinylated lipid nanoparticles were synthesized as previously described[53]. Briefly, a lipid mixture (basis: 100 µg of "A10" lipid) in 25 µL of ethanol was prepared. The mixture was composed of the "A10 Lipid" (50 mol%), DSPC (10 mol%), cholesterol (30 mol%), non-functionalized, PEGylated lipid, and biotin-functionalized, PEGylated lipid. The total amount of PEGylated lipid was 10 mol%. The lipid solution was rapidly and vigorously mixed with 25 µL of 10 mM sodium citrate, pH 3.0. Then 50 µL of PBS, pH 7.4 was added. The suspension of lipid nanoparticles (LNPs) was then dialyzed in against PBS, pH 7.4 in a 3.5 kDa dialysis cassette for 4 hours. Using this method, LNPs were prepared with a biotinylated lipid content of 0%, 5% and 10%. The resulting LNPs were analyzed via dynamic light scattering to determine their size distribution.

Synthesis of Streptavidin-DNA Conjugates

Step 1: Synthesis of Methyltetrazine-modified Streptavidin

1 equivalency of streptavidin (200 ug, 3.8 nmol) was reacted with 10 equivalencies of Methyltetrazine-PEG4-NHS at a streptavidin concentration of 150 µM. The solvent for the reaction was PBS, pH 7.4 with 3% (v/v) dimethyl sulfoxide. The reaction was carried out at room temperature overnight. The resulting product was dialyzed against PBS, pH 7.4 to remove excess NHS ester.

Step 2: IEDDA Reaction to Attach Alexa Fluor 488 and 647-modified DNA

1 equivalency of step 1 product (7.5 µg, 0.14 nmol) was reacted with 2.5 equivalencies of fluorophore-modified DNA at a streptavidin concentration of 4 µM. The solvent for the reaction was PBS, pH 7.4. The reaction was carried out at room temperature overnight before the conjugate was stored at 4°C. The conjugates were used without further purification or characterization.

Förster Resonance Energy Transfer on Biotinylated Lipid Nanoparticles

Streptavidin modified with single stranded, fluorophore-labeled DNA was mixed with the complimentary azide- or DBCO-modified DNA strand (1.1 equivalencies) and allowed to anneal at room temperature for 10 minutes. An equimolar mixture of Alexa Fluor 488 and 647-modified streptavidin conjugates at 10 nM were added to biotinylated LNPs diluted by 10x, 100x, or 1000x compared to the initial LNP solution. FRET was monitored by monitoring fluorescence channels for Alexa Fluor 488 Ex/Em (490 nm/520 nm), Alexa Fluor 647 Ex/Em (650 nm/670 nm), and FRET Ex/Em (490 nm/670 nm). Fluorescence signal was calculated by taking the ratio of 670 nm and 520 nm emission upon excitation with 490 nm light. This ratio was expressed as a fold increase relative to a mixture of streptavidin conjugates and non-biotinylated LNPs to account for non-specific binding. Control experiments were performed with streptavidin conjugate directly conjugated to Alexa Fluor 488 or 647 and a mixture of direct and DNA conjugates to account for DNA-DNA repulsion that may decrease FRET signal.

Synthesis of Azido *N*-allylacrylamide Monomer (compounds 1 – 3)

Synthesis of Compound (1)

Sodium azide (55 mmols in 17 mL of water) was added to a stirred solution of 3-bromopropylamine hydrobromide (16.5 mmols in 11 mL of water). The resulting mixture was then reacted under reflux conditions (98°C) for 16 hours. The reaction mixture was cooled to room temperature before removal of approximately two thirds of the solvent in vacuo. The concentrated reaction mixture was basified by the addition of sodium hydroxide pellets (79 mmols) while stirred on ice for five minutes. Diethylether (50 mL) was added to the basified mixture and stirred on ice for an additional five minutes. The resulting organic layer was separated from the aqueous layer. The aqueous layer was then extracted with diethylether (2x with 50 mL). The combined organic layers were

dried with sodium sulfate before concentration in vacuo. The product was a clear, yellow oil, which was used as is without further purification. The product (1) was isolated in 60% yield (960 mg) and characterized via ^{1}H and ^{13}C NMR.

Synthesis of Compound (2)

Triethylamine (3.75 mmol) was added to a stirred solution of compound **(1)** (3.41 mmol in 23 mL of dichloromethane) on ice and equilibrated for 10 minutes. Acryloyl chloride (4.1 mmol in 2 mL of dichloromethane) was added to the reaction dropwise for 1 hour on ice. The reaction then was carried out on ice for 1 hour and at room temperature for 1 hour. The reaction was quenched with water (3 mL) before the addition of 50 mL of dichloromethane. The organic layer was separated from the aqueous layer. The aqueous layer was then extracted with dichloromethane (2x with 50 mL). The combined organic layers were dried with sodium sulfate before concentration in vacuo. The product **(2)** without further purification. The product was isolated in 77% yield (405 mg) and characterized via ^{1}H NMR. The product is unstable and must be used immediately.

Synthesis of Compound (3)

Compound **(2)** (2.6 mmol in 7 mL of dry dimethylformamide) was added to a stirred solution of sodium hydride (3.4 mmol in 14 mL of dry dimethylformamide). The resulting solution equilibrated for 10 minutes. Allylbromide (6.6 mmol) was added to the stirred solution. The resulting mixture was reacted at room temperature for 1 hour. The reaction was quenched by the addition for 4 mL of water before the addition of 50 mL of diethyl ether. The organic layer was separated from the aqueous layer. The aqueous layer was then extracted with diethyl ether (2x with 50 mL). The combined organic layers were dried with sodium sulfate before concentration in vacuo. The crude product was purified via silica gel flash chromatography. Solvent A: hexanes. Solvent B: ethyl acetate. Gradient: 0 – 100% solvent B over 30 minutes. Elution: 40% ethyl acetate.

Yield: 42%, 215 mg, 1.1 mmol. The product (3) was characterized by ^{1}H NMR. The final product is prone to polymerization and thus was stabilized by the addition of 4-methoxyphenol at a concentration of 1 part per thousand and stored under oxygen at -20°C.

Synthesis of Fluorous Allylamine (compound 4)

1 equivalency (123 mg, 181 μmol) of fluorous-Boc-On was reacted with 2 equivalencies of allylamine in the presence of 4 equivalencies of triethylamine at a concentration of 15 mM in tetrahydrofuran. The reaction was stirred at room temperature for 4 hours. The solvent was then removed under vacuum. The crude product purified via fluorous solid phase extraction (FSPE). In short, the product was suspended in 0.5 mL of methanol and precipitated by the addition of 0.5 mL of water. The slurry was loaded onto a 2-gram, hand-packed column of fluorinated silica gel. Excess reagents were washed from the column with 20 mL of an 80:20 mixture of methanol and water. The product (4), was eluted from the column by washing with 10 mL of methanol. The solvent was removed under vacuum and the product was characterized via ^{1}H NMR.

Synthesis of oligoTEA-based Molecular Barcodes (compounds 5 – 14)

OligoTEA-based molecular barcodes were synthesized via the established method[48]. General reaction conditions and purification protocols are provided below. The synthesis of each oligomer was performed with a starting basis of 20 mg of compound (4).

General Thiol-ene Protocol

1 equivalency of fluorous-allyl was mixed with 3 equivalencies of dithiol and 0.15 equivalencies of 2,2-dimethoxy-2-phenylacetophenon (DMPA) at a final concentration of 200 mM in methanol. The mixture was irradiated with 20 mW/cm^2 UV light for 270 seconds. The product was purified by FSPE using a 500 mg column of fluorinated silica

248

gel and 3 mL of wash solution (80:20 methanol:water) per 10 mg of fluorous material. and the methanol. The product was eluted with 2 mL of methanol per 10 mg of fluorous material. Methanol was evaporated under reduced pressure to yield the fluorous-thiol product.

General Michael Addition Protocol

1 equivalency of fluorous-thiol was mixed with 2 equivalencies of *N*-allylacrylamide monomer and 0.1 equivalencies of dimethylphosphine (DMPP) at a final concentration of 200 mM in methanol. The mixture was reacted at 40°C until all thiol was consumed, as monitored by the dithiodipyridine (DTDP) assay[51]. The product was purified via FSPE using a 500 mg column of fluorinated silica gel and 3 mL of wash solution (80:20 methanol:water) per 10 mg of fluorous material. and the methanol. The product was eluted with 2 mL of methanol per 10 mg of fluorous material. Methanol was evaporated under reduced pressure to yield the fluorous-allyl product.

General Tertiary Amine Capping Protocol

Capping of the oligomers with a tertiary amine-modified thiol was performed as previously described. However, the wash solution was changed to 100 mM NaOH in an 80:20 mixture of methanol and water. This was done to improve yield by preventing protonation of the terminal tertiary amine.

General Deprotection Protocol

Fluorous oligoTEA was dissolved at 5 mM in 50% trifluoroacetic acid in dichloromethane. The reaction was carried out at room temperature for 3 hours. The solvent was removed under vacuum and the product was purified via semi-preparative RP-HPLC using a linear solvent gradient from 5 – 95% solvent B over 45 minutes. The products were characterized via LC-MS.

Summary of Elution Times and Identified Masses

(5): Proton; Elution: 15.3 minutes; Calc: 730.32 Da; Obs: 730.20 Da ([M+H]$^+$)

(6): Methyl; Elution: 16.1 minutes; Calc: 744.34 Da; Obs: 744.30 Da ([M+H]$^+$)

(7): Ethyl; Elution: 17.0 minutes; Calc: 758.35 Da; Obs: 758.20 Da ([M+H]$^+$)

(8): Propyl; Elution: 18.1 minutes; Calc: 772.37 Da; Obs: 772.20 Da ([M+H]$^+$)

(9): Butyl; Elution: 19.5 minutes; Calc: 786.39 Da; Obs: 786.30 Da ([M+H]$^+$)

(10): Pentyl; Elution: 21.1 minutes; Calc: 800.40 Da; Obs: 800.30 Da ([M+H]$^+$)

(11): Benzyl; Elution: 19.9 minutes; Calc: 820.37 Da; Obs: 820.30 Da ([M+H]$^+$)

(12): Phenyl; Elution: 20.1 minutes; Calc: 834.39 Da; Obs: 834.60 Da ([M+H]$^+$)

(13): Guanidine; Elution: 14.3 minutes; Calc: 815.39 Da; Obs: 815.30 Da ([M+H]$^+$)

(14): Carboxylic Acid; Elution: 16.3 minutes; Calc: 788.33 Da; Obs: 788.20 Da ([M+H]$^+$)

Synthesis of DBCO-L(-)DTT-Amine (compounds 15 – 17)

Synthesis of Compound (15)

1 equivalency (124 mg, 807 µmol) of L(-)DTT was dissolved at 1.6 M in methanol. 3 equivalencies of tert-butyl allylcarbamate and 0.05 equivalencies of DMPA were added. The mixture was irradiated at 20 mW/cm^2 for 270 seconds. The solvent was removed, and the product was purified via silica gel flash chromatography. Solvent A: dichloromethane. Solvent B: methanol. Gradient: 0 – 5% solvent B over 60 minutes. Elution: 2.5% methanol. Yield: 78%, 296 mg, 630 µmol. The product **(15)** was characterized by ^{1}H NMR and LC-MS (calculated: 491.23, observed: 491.20 [M+Na]$^+$).

Synthesis of Compound (16)

1 equivalency (53 mg, 114 µmol) of compound **(15)** was dissolved at 50 mM in 50% (v/v) trifluoroacetic acid in dichloromethane. The mixture was reacted at room temperature for 3 hours. The solvent was then removed under vacuum. The product was recovered in quantitative yield and characterized via LC-MS (calculated: 269.13;

observed: 269.20 [M+H]$^+$) The product **(16)** was used without further purification or characterization.

Synthesis of Compound (17)

1 equivalency (3.5 mg, 8.7 μmol) of DBCO-NHS ester was dissolved at 30 mM in dimethyl sulfoxide. 10 equivalencies of compound **(15)** and 15 equivalencies of triethylamine were added. The mixture was reacted at room temperature for 4 hours and purified via semi-preparative RP-HPLC. The reaction mixture was separated using a linear solvent gradient of 5 – 65% solvent B over 30 minutes and characterized via LC-MS. Compound **(17)** eluted at 18 minutes. Yield: 67%, 3.4 mg, 5.8 μmol, Calculated 556.22, Observed 556.10 [M+H]$^+$

Synthesis of oligoTEA-modified PEG5K (compounds 18)

1 equivalency of oligoTEA probe was dissolved at 6 mM in dimethyl sulfoxide. 5 equivalencies of SVA-PEG5K-SVA and 5 equivalencies of triethylamine were added. The mixture was reacted overnight at room temperature and the product was purified via semi-preparative RP-HPLC using a linear solvent gradient from 5 – 95% solvent B over 30 minutes. The product was isolated in 30% yield.

Synthesis of DBCO-L(-)DTT-modified PEG5K (compounds 19)

1 equivalency of compound **(17)** was dissolved at 4.75 mM in dimethyl sulfoxide. 5 equivalencies of SVA-PEG5K-SVA and 4 equivalencies of triethylamine were added. The mixture was reacted overnight at room temperature and the product was purified via semi-preparative RP-HPLC using a linear solvent gradient from 5 – 95% solvent B over 30 minutes. The product was isolated in 60% yield.

Synthesis of PEGylated Streptavidin

1 equivalency of streptavidin was reacted with 20 equivalencies of compound (18) or (19) at protein concentration of 100 μM. The solvent for the reaction was 10% (v/v)

251

dimethyl sulfoxide in PBS, pH 7.4. The reactions were carried out at room temperature overnight. The reaction mixture was dialyzed against PBS, pH 7.4 to remove excess NHS ester.

Sodium Periodate Oxidation of oligoTEA Probes

Azide- and DBCO-modified probes were mixed equimolar at a concentration of 100 µM in water. The mixture was reacted overnight at room temperature. The mixture was then treated with sodium periodate at the indicated concentrations for the indicated amount of time. Excess sodium periodate was removed using a ZipTip according to the manufacturer's instructions. The product was analyzed via LC-MS using both full scan and SIM modes to identify the reaction products.

Chapter 5 Appendix

DNA- and Polymer-Protein Conjugates to Characterize Extracellular Vesicles

Synthesis of "Click"-modified DNAs
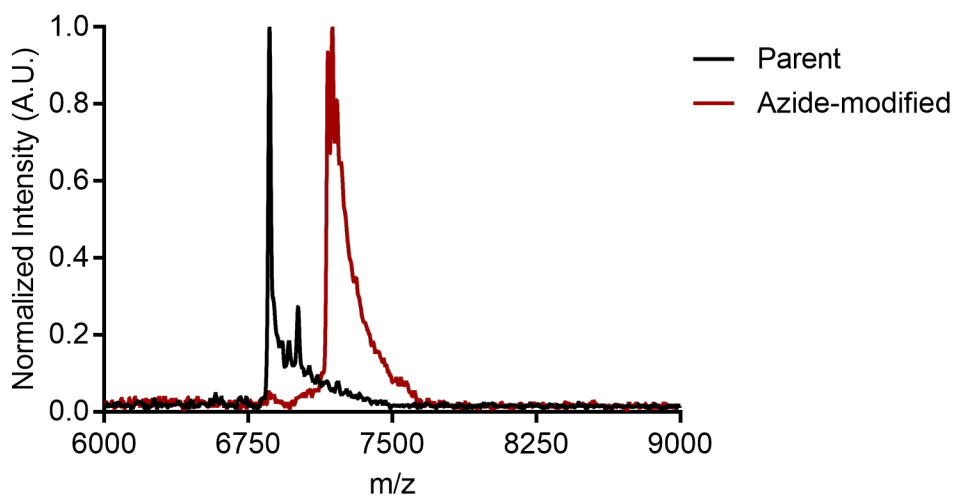
Figure A5. 1. MALDI-MS analysis of azide-modified DNA.
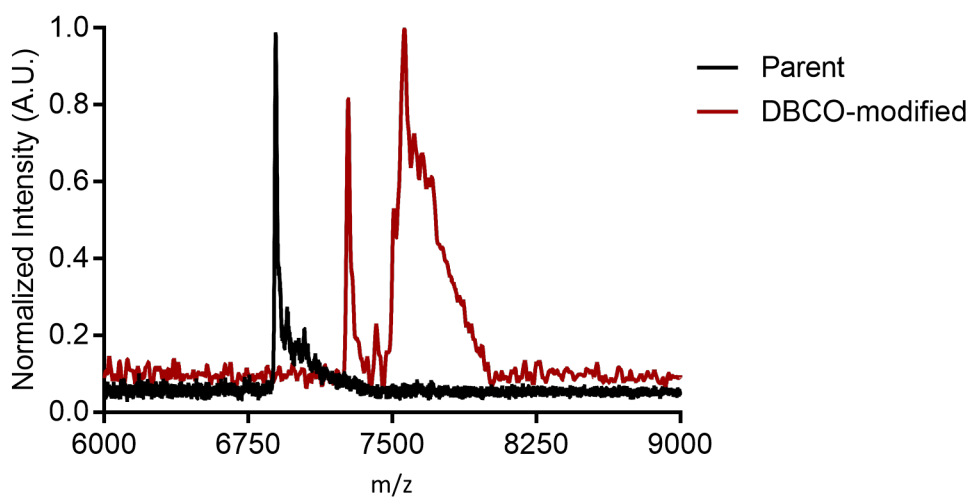
Figure A5. 2. MALDI-MS analysis of DBCO-modified DNA.

Synthesis of Cleavable, Fluorophore-modified DNAs for IEDDA Conjugation
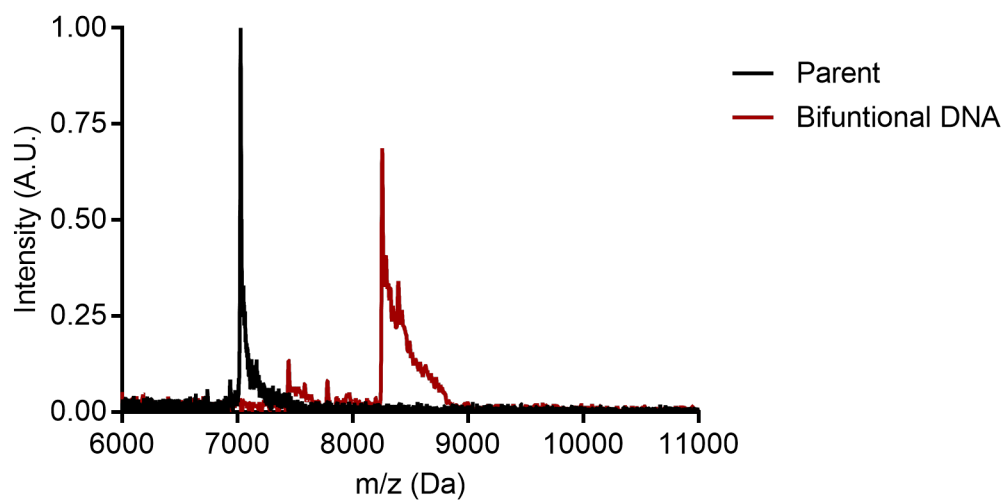
Figure A5. 3. MALDI-MS analysis of cleavable-TCO, Alexa Fluor 647-modified DNA

Synthesis of "A10" Lipid
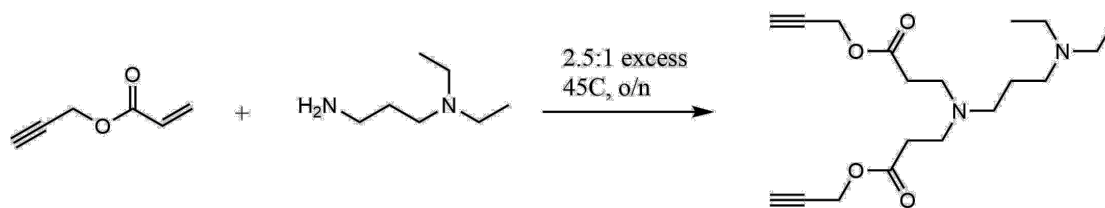
Figure A5. 4. Synthesis scheme for first step of A10 lipid synthesis.
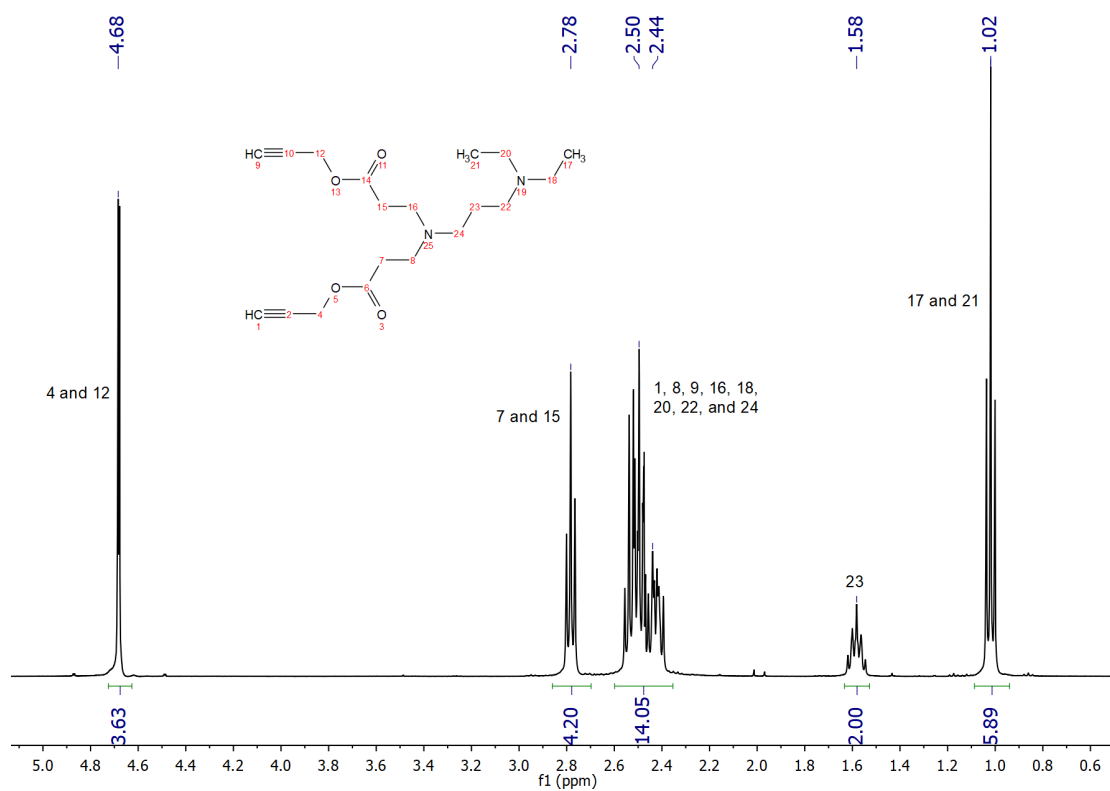
Figure A5. 5. ¹H NMR of A10 lipid intermediate (400 MHz, CDCl₃)
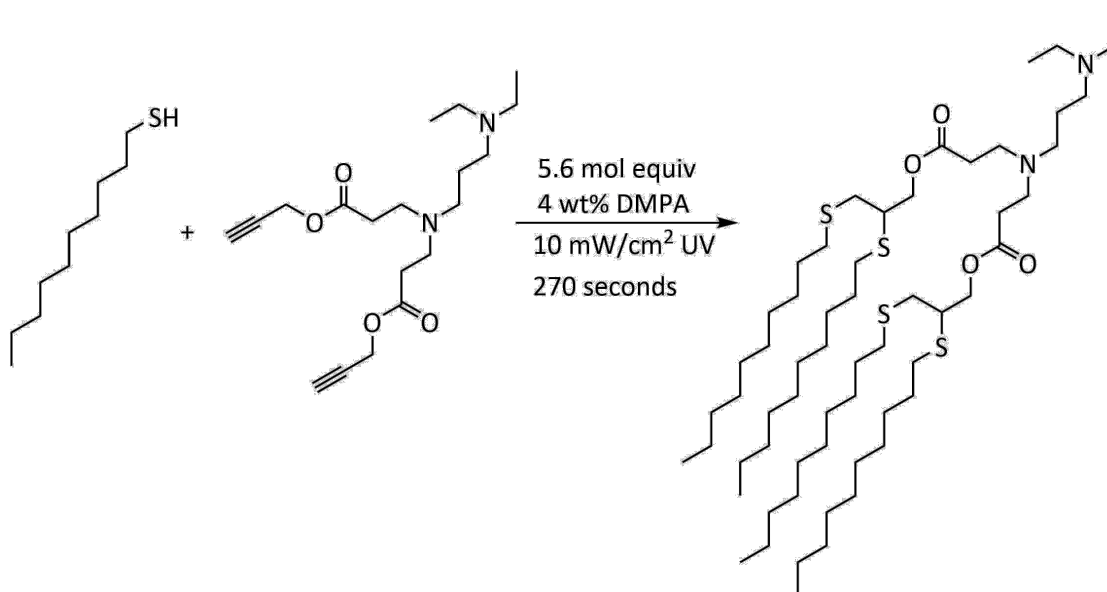
Figure A5. 6. Synthesis scheme for second step of A10 lipid synthesis.
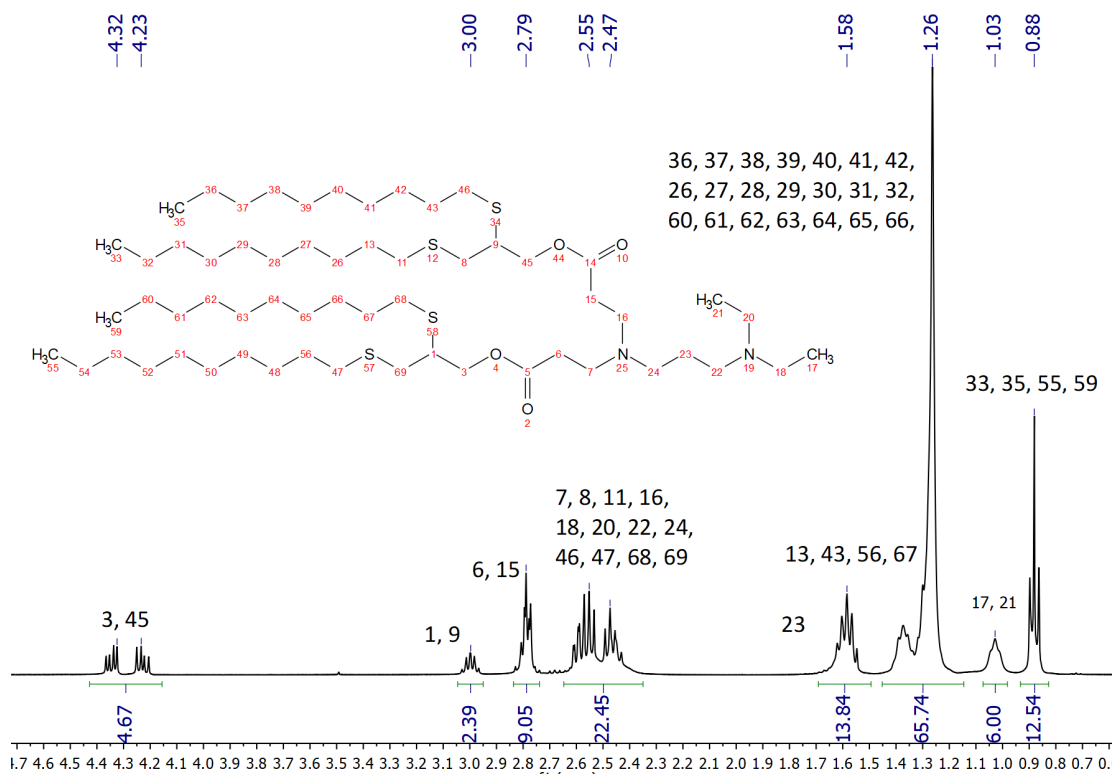
Figure A5. 7. ¹H NMR of A10 lipid (400 MHz, CDCl₃).

Synthesis of Biotinylated LNPs
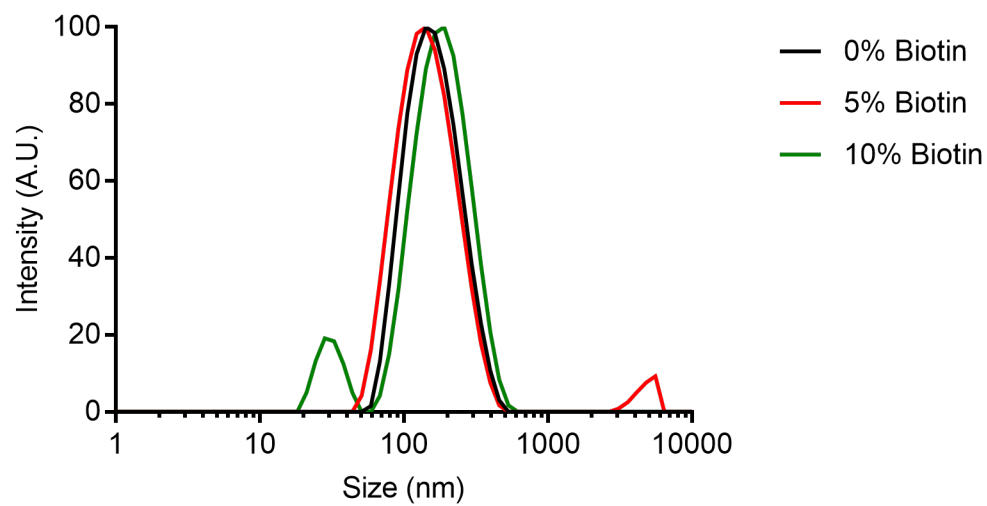
Figure A5. 8. Dynamic light scattering of biotinylated LNPs.

Synthesis of Compounds 1 – 3
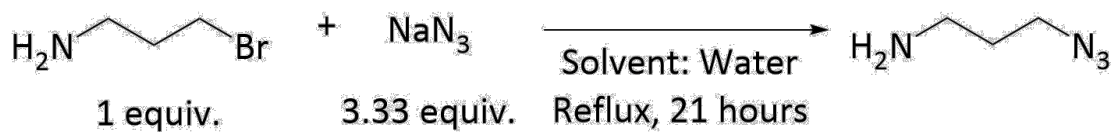
Figure A5. 9. Synthesis scheme for compound **(1)**.
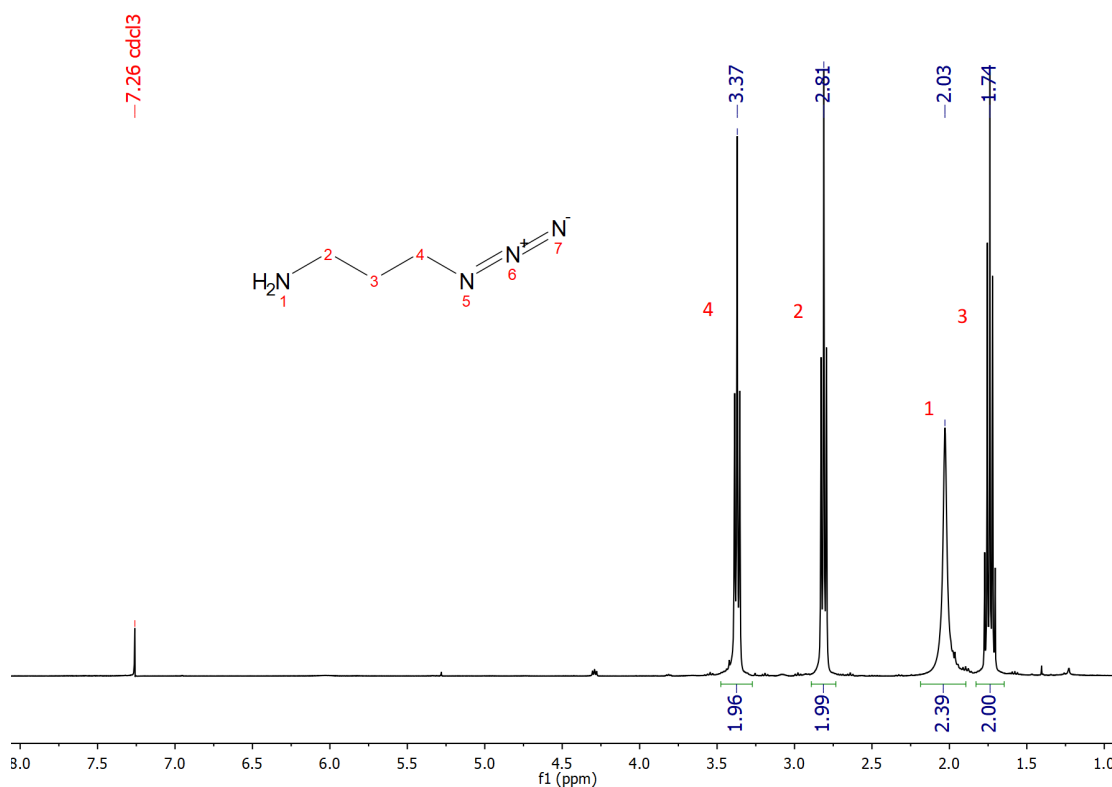
Figure A5. 10. ¹H NMR of compound **(1)** (400 MHz, CDCl₃).
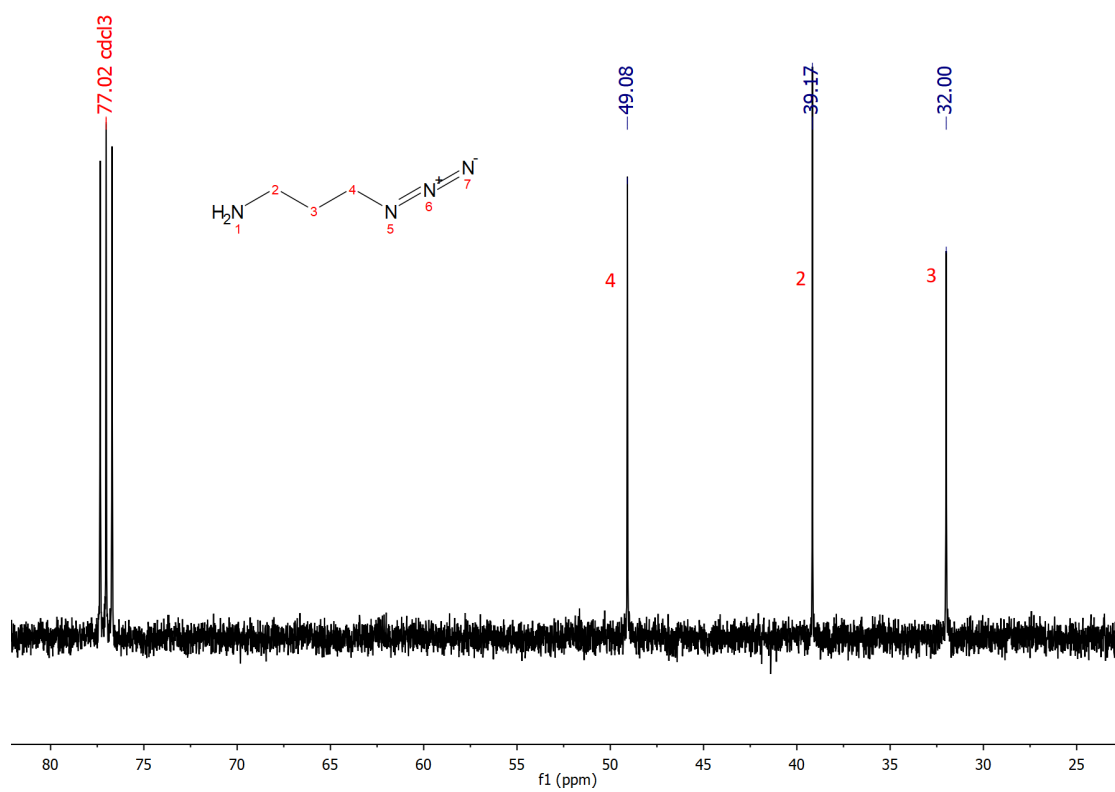
Figure A5. 11. ^{13}C NMR of compound **(1)** (400 MHz, CDCl$_3$).
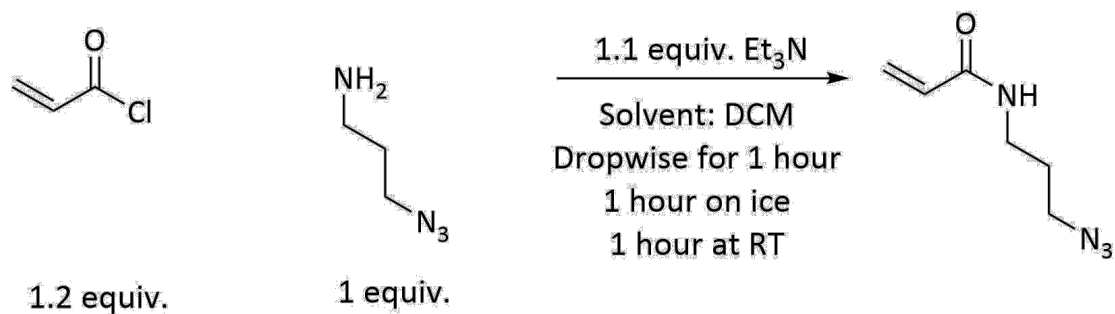
Figure A5. 12. Synthesis scheme for compound **(2)**.
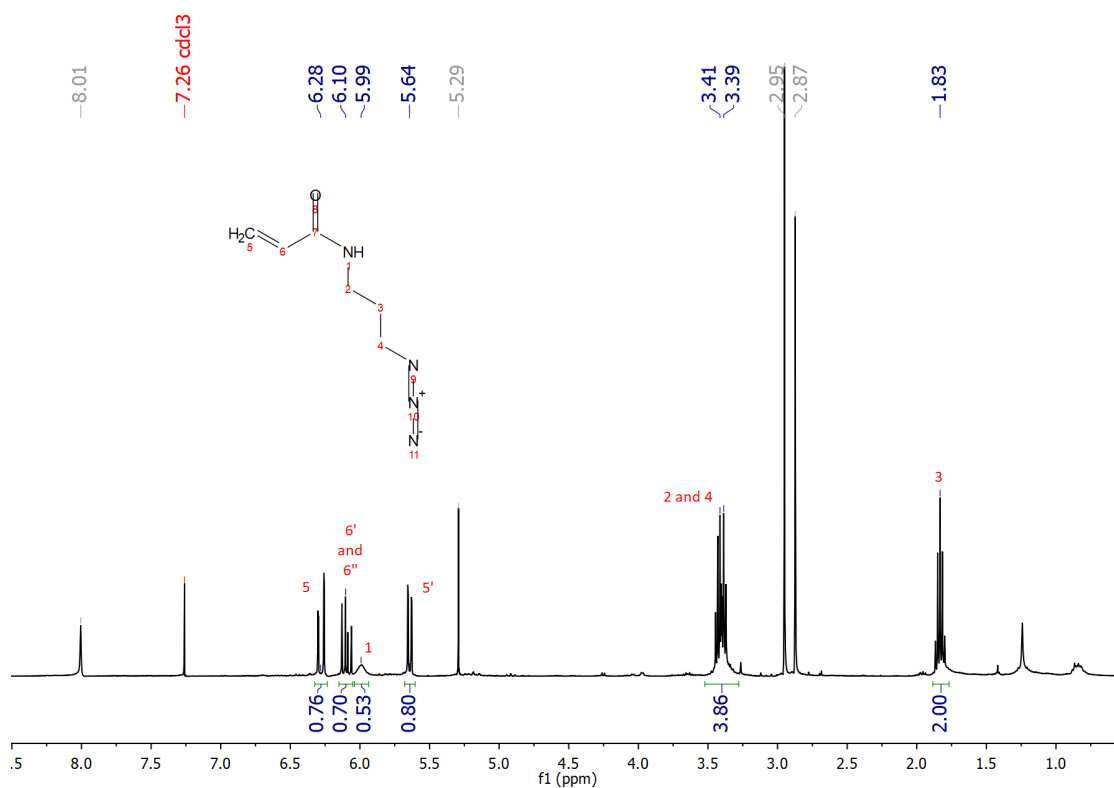
Figure A5. 13. ^{1}H NMR of compound **(2)** (400 MHz, CDCl$_3$).
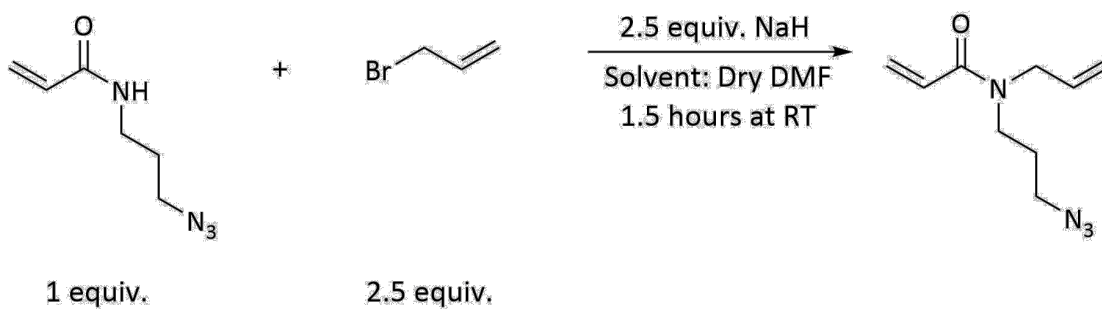
Figure A5. 14. Synthesis scheme for compound **(3)**.
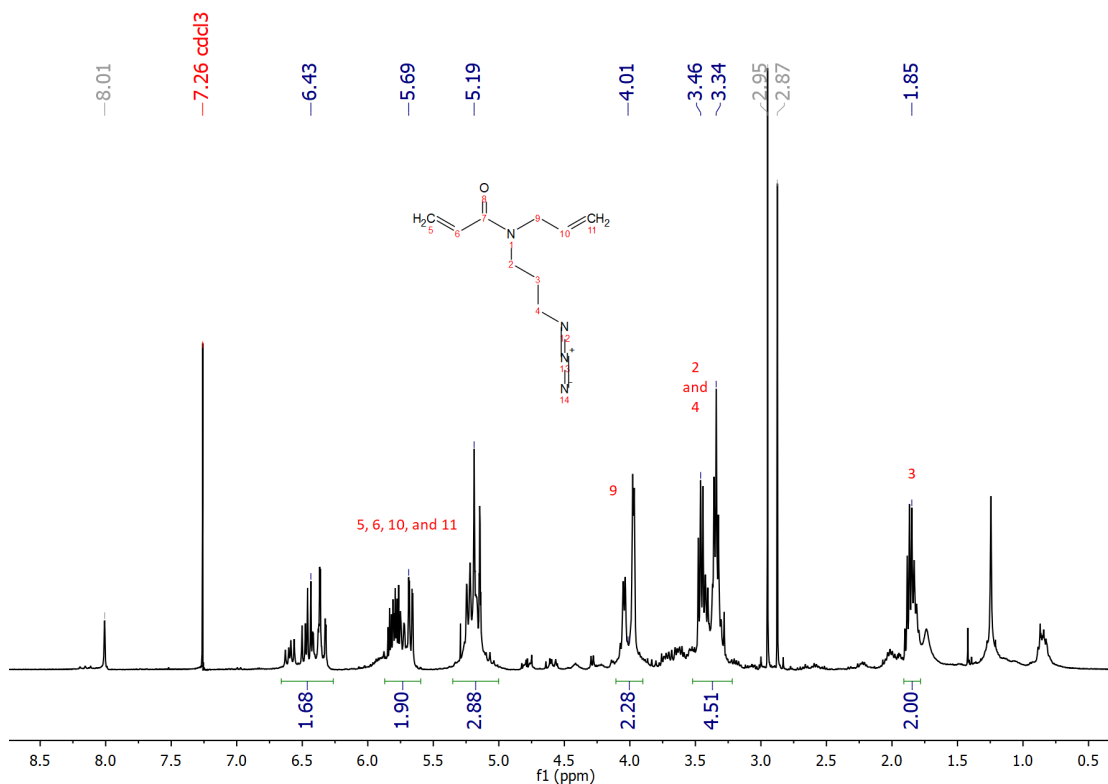
Figure A5. 15. ^{1}H NMR of compound **(3)** (400 MHz, CDCl$_3$).

Synthesis of Compound 4
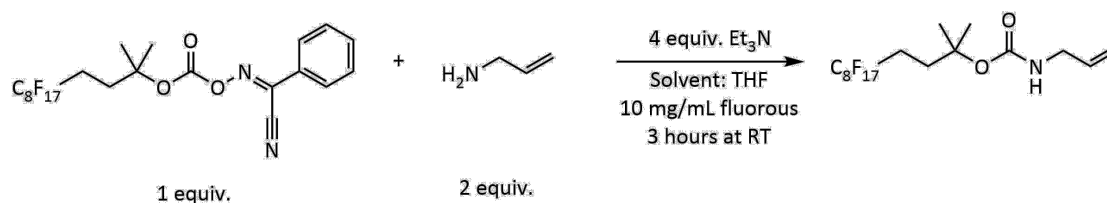
Figure A5. 16. Synthesis scheme for compound **(4)**.
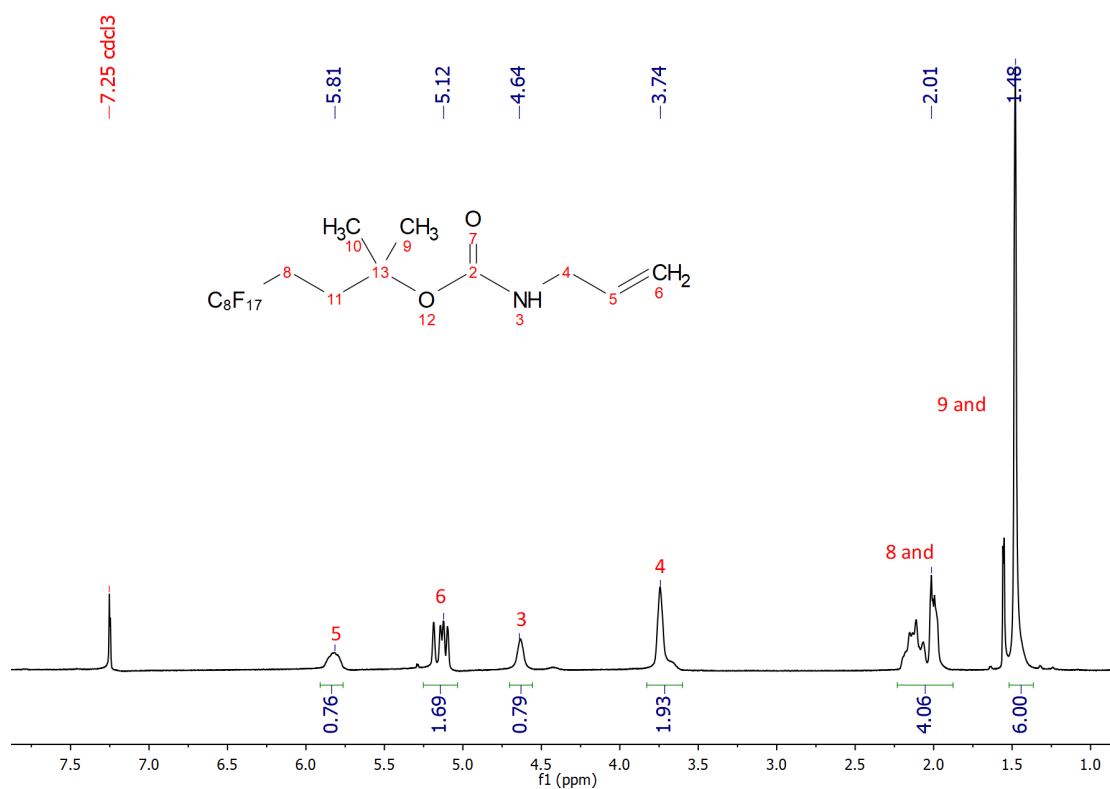
Figure A5. 17. ^{1}H NMR of compound **(4)** (400 MHz, CDCl$_3$).

Synthesis of Compounds 5 – 14
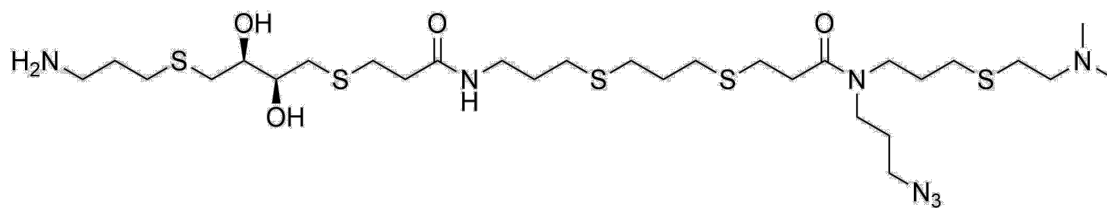
Figure A5. 18. Structure of compound **(5)**.
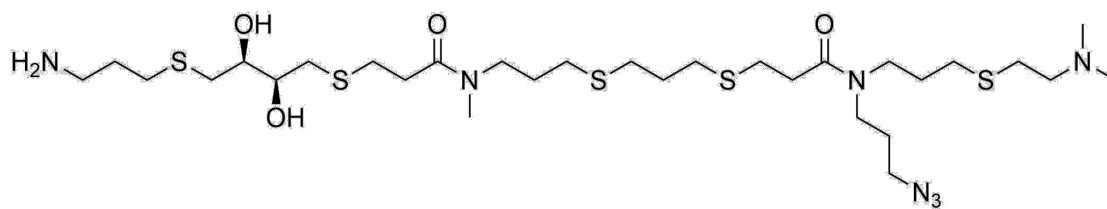
Figure A5. 19. Structure of compound **(6)**.
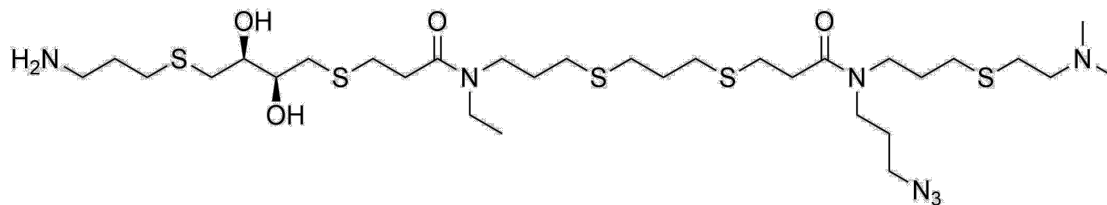
Figure A5. 20. Structure of compound **(7)**.
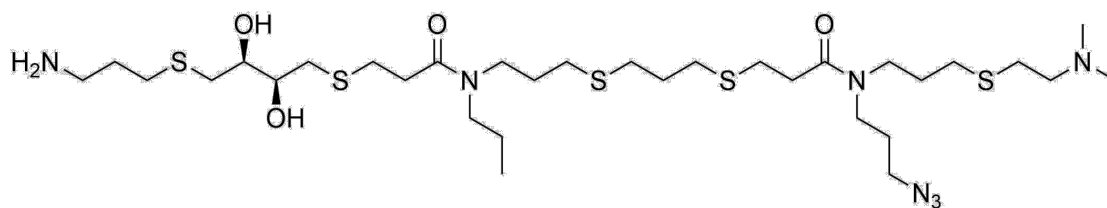
Figure A5. 21. Structure of compound **(8)**.
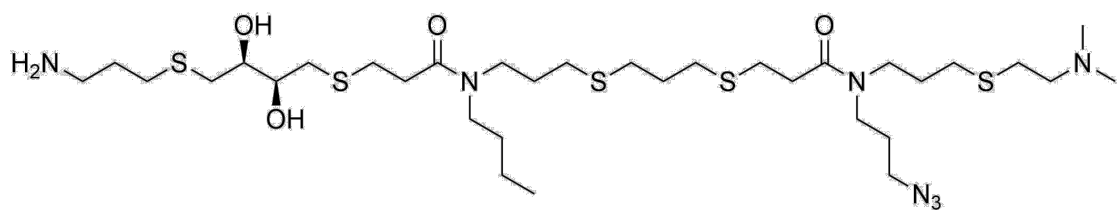
Figure A5. 22. Structure of compound **(9)**.
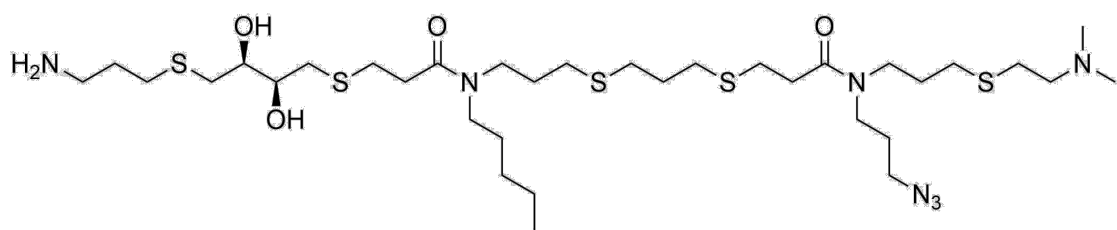
Figure A5. 23. Structure of compound **(10)**.
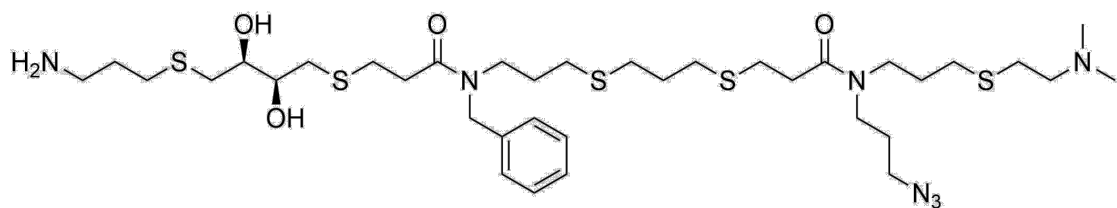
Figure A5. 24. Structure of compound **(11)**.
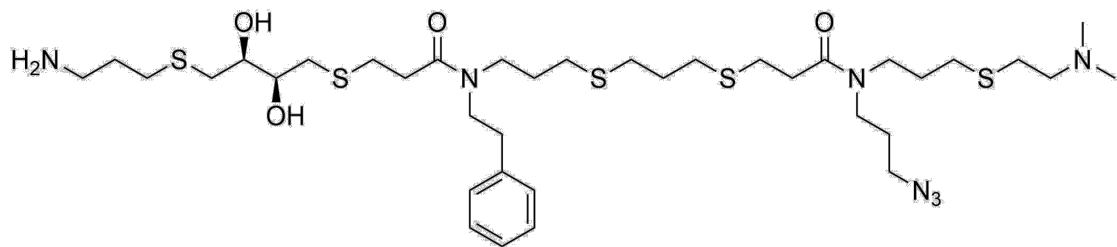
Figure A5. 25. Structure of compound **(12)**.
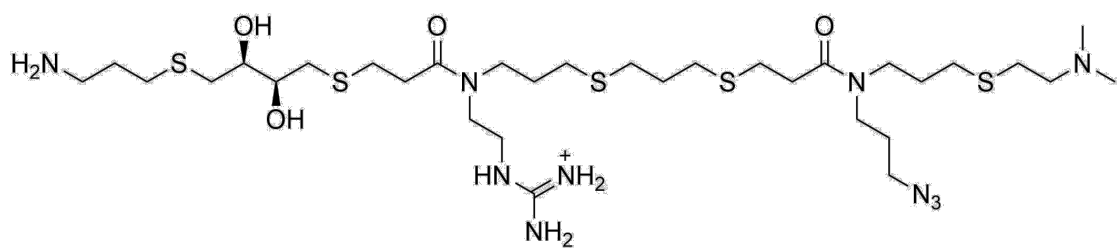
Figure A5. 26. Structure of compound **(13)**.
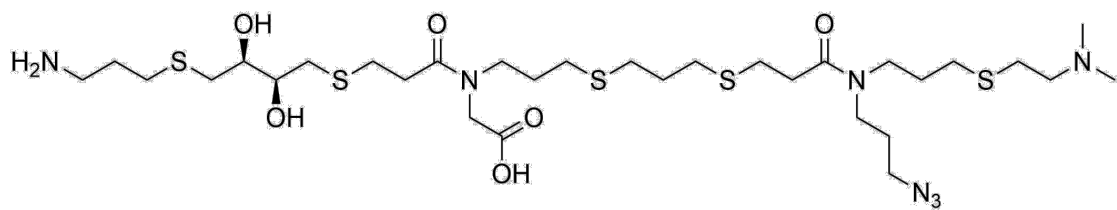
Figure A5. 27. Structure of compound **(14)**.

Synthesis of Compounds 15 – 17

Figure A5. 28. Synthesis scheme for compound **(15)**.

Figure A5. 29. ^{1}H NMR of compound **(15)** (400 MHz, CDCl$_3$).

Figure A5. 30. Synthesis scheme for compound **(16)**.
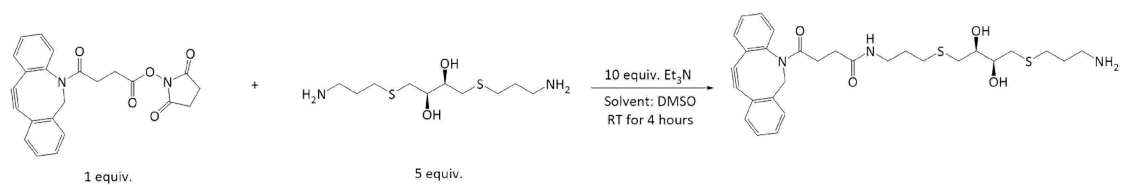
Figure A5. 31. Synthesis scheme for compound **(17)**.

Chapter 5 References

1.Luga, V. *et al.* Exosomes mediate stromal mobilization of autocrine Wnt-PCP signaling in breast cancer cell migration. *Cell* **151,** 1542–1556 (2012).

2.Webber, J. P., Spary, L. K., Sanders, A. J. & Chowdhury, R. Differentiation of tumour-promoting stromal myofibroblasts by cancer exosomes. *Oncogene* **34,** 290 (2014).

3.Peinado, H. *et al.* Melanoma exosomes educate bone marrow progenitor cells toward a pro-metastatic phenotype through MET. *Nature medicine* **18,** 883–891 (2012).

4.Li, J. *et al.* Exosomes mediate the cell-to-cell transmission of IFN-α-induced antiviral activity. *Nat Immunol* **14,** 793 (2013).

5.Al-Nedawi, K., Meehan, B., Kerbel, R. S., Allison, A. C. & Rak, J. Endothelial expression of autocrine VEGF upon the uptake of tumor-derived microvesicles containing oncogenic EGFR. *Proc Natl Acad Sci USA* **106,** 3794–3799 (2009).

6.Putz, U. *et al.* The tumor suppressor PTEN is exported in exosomes and has phosphatase activity in recipient cells. *Science … ***5,** ra70 (2012).

7.Alexander, M. *et al.* Exosome-delivered microRNAs modulate the inflammatory response to endotoxin. *Nat Commun* **6,** 7321 (2015).

8.Valadi, H. *et al.* Exosome-mediated transfer of mRNAs and microRNAs is a novel mechanism of genetic exchange between cells. *Nat Cell Biol* **9,** 654–659 (2007).

9.Umezu, T., Ohyashiki, K., Kuroda, M. & Ohyashiki, J. H. Leukemia cell to endothelial cell communication via exosomal miRNAs. *Oncogene* **32,** 2747–2755 (2012).

10.Mittelbrunn, M. *et al.* Unidirectional transfer of microRNA-loaded exosomes from T cells to antigen-presenting cells. *Nat Commun* **2,** 282 (2011).

11.Hornick, N. I. *et al.* AML suppresses hematopoiesis by releasing exosomes that contain microRNAs targeting c-MYB. *Science … ***9,** ra88 (2016).

12. Kim, D.-K., Nishida, H. & An, S. Y. Chromatographically isolated CD63 + CD81 + extracellular vesicles from mesenchymal stromal cells rescue cognitive impairments after TBI. *Proc Natl Acad Sci USA* **113,** 170 (2015).

13. Zernecke, A. *et al.* Delivery of microRNA-126 by apoptotic bodies induces CXCL12-dependent vascular protection. *Science …* **2,** ra81 (2009).

14. Hu, L. *et al.* Exosomes derived from human adipose mensenchymal stem cells accelerates cutaneous wound healing via optimizing the characteristics of fibroblasts. *Scientific reports* **6,** 32993 (2016).

15. Meckes, D. G. *et al.* Modulation of B-cell exosome proteins by gamma herpesvirus infection. *Proc Natl Acad Sci USA* **110,** E2925–33 (2013).

16. Wolfers, J. *et al.* Tumor-derived exosomes are a source of shared tumor rejection antigens for CTL cross-priming. *Nature medicine* **7,** 297–303 (2001).

17. Wiley, R. D. & Gummuluru, S. Immature dendritic cell-derived exosomes can mediate HIV-1 trans infection. *Proc Natl Acad Sci USA* **103,** 738–743 (2006).

18. Costa-Silva, B. *et al.* Pancreatic cancer exosomes initiate pre-metastatic niche formation in the liver. *Nat Cell Biol* **17,** 816–826 (2015).

19. Melo, S. A., Sugimoto, H., O'Connell, J. T. & Kato, N. Cancer exosomes perform cell-independent microRNA biogenesis and promote tumorigenesis. *Cancer cell* (2014).

20. Al-Nedawi, K. *et al.* Intercellular transfer of the oncogenic receptor EGFRvIII by microvesicles derived from tumour cells. *Nat Cell Biol* **10,** 619–624 (2008).

21. Bukong, T. N., Momen-Heravi, F., Kodys, K., Bala, S. & Szabo, G. Exosomes from hepatitis C infected patients transmit HCV infection and contain replication competent viral RNA in complex with Ago2-miR122-HSP90. *PLoS Pathog* **10,** e1004424 (2014).

22.Mack, M. *et al.* Transfer of the chemokine receptor CCR5 between cells by membrane-derived microparticles: a mechanism for cellular human immunodeficiency virus 1 infection. *Nature medicine* **6,** 769–775 (2000).

23.Meckes, D. G. *et al.* Human tumor virus utilizes exosomes for intercellular communication. *Proc Natl Acad Sci USA* **107,** 20370–20375 (2010).

24.Narayanan, A. *et al.* Exosomes derived from HIV-1-infected cells contain trans-activation response element RNA. *Journal of Biological Chemistry* **288,** 20014–20033 (2013).

25.Rajendran, L. *et al.* Alzheimer's disease beta-amyloid peptides are released in association with exosomes. *Proc Natl Acad Sci USA* **103,** 11172–11177 (2006).

26.Fevrier, B., Vilette, D., Archer, F. & Loew, D. Cells release prions in association with exosomes. *Proc Natl Acad Sci USA* **101,** 9683 (2004).

27.Robbins, P. D. & Morelli, A. E. Regulation of immune responses by extracellular vesicles. *Nature Reviews Immunology* **14,** 195–208 (2014).

28.EL Andaloussi, S., Mäger, I., Breakefield, X. O. & Wood, M. J. A. Extracellular vesicles: biology and emerging therapeutic opportunities. *Nat Rev Drug Discov* **12,** 347–357 (2013).

29.Vlassov, A. V., Magdaleno, S., Setterquist, R. & Conrad, R. Exosomes: current knowledge of their composition, biological functions, and diagnostic and therapeutic potentials. *Biochim Biophys Acta* **1820,** 940–948 (2012).

30.Buzas, E. I., György, B., Nagy, G., Falus, A. & Gay, S. Emerging role of extracellular vesicles in inflammatory diseases. *Nat Rev Rheumatol* **10,** 356–364 (2014).

31.Théry, C., Amigorena, S., Raposo, G. & Clayton, A. Isolation and characterization of exosomes from cell culture supernatants and biological fluids. *Curr Protoc Cell Biol* **Chapter 3,** Unit–3.22 (2008).

32.Lane, R. E., Korbie, D., Anderson, W., Vaidyanathan, R. & Trau, M. Analysis of exosome purification methods using a model liposome system and tunable-resistive pulse sensing. *Scientific reports* **5,** 7639 (2015).

33.Gámez-Valero, A., Monguió-Tortajada, M., Carreras-Planella, L., la Franquesa, M. & Beyer, K. Size-Exclusion Chromatography-based isolation minimally alters Extracellular Vesicles' characteristics compared to precipitating agents. *Scientific reports* **6,** 33641 (2016).

34.Sódar, B. W. *et al.* Low-density lipoprotein mimics blood plasma-derived exosomes and microvesicles during isolation and detection. *Scientific reports* **6,** 24316 (2016).

35.Kanada, M. *et al.* Differential fates of biomolecules delivered to target cells via extracellular vesicles. *Proc Natl Acad Sci USA* **112,** E1433–42 (2015).

36.Chevillet, J. R. *et al.* Quantitative and stoichiometric analysis of the microRNA content of exosomes. *Proc Natl Acad Sci USA* **111,** 14888–14893 (2014).

37.Willms, E. *et al.* Cells release subpopulations of exosomes with distinct molecular and biological properties. *Scientific reports* **6,** 22519 (2016).

38.Ferguson, S. W. & Nguyen, J. Exosomes as therapeutics: The implications of molecular composition and exosomal heterogeneity. *Journal of controlled release : official journal of the Controlled Release Society* **228,** 179–190 (2016).

39.Lewis, W. G. *et al.* Click chemistry in situ: acetylcholinesterase as a reaction vessel for the selective assembly of a femtomolar inhibitor from an array of building blocks. *Angew Chem Int Ed Engl* **41,** 1053–1057 (2002).

40.Manetsch, R. *et al.* In situ click chemistry: enzyme inhibitors made to their own specifications. *J Am Chem Soc* **126,** 12809–12818 (2004).

41.Kolb, H. C., Finn, M. G. & Sharpless, K. B. Inhibitors of HIV-1 Protease by Using In Situ Click Chemistry. *Angew Chem Int Ed Engl* **45,** 1435 (2006).

42.Mocharla, V. P. *et al.* In situ click chemistry: enzyme-generated inhibitors of carbonic anhydrase II. *Angew Chem Int Ed Engl* **44,** 116–120 (2004).

43.Lee, L. V. *et al.* A potent and highly selective inhibitor of human alpha-1,3-fucosyltransferase via click chemistry. *J Am Chem Soc* **125,** 9588–9589 (2003).

44.Nag, A. *et al.* A chemical epitope-targeting strategy for protein capture agents: the serine 474 epitope of the kinase Akt2. *Angew Chem Int Ed Engl* **52,** 13975–13979 (2013).

45.Millward, S. W. *et al.* Iterative in situ click chemistry assembles a branched capture agent and allosteric inhibitor for Akt1. *J Am Chem Soc* **133,** 18280–18288 (2011).

46.Agnew, H. D. *et al.* Iterative in situ click chemistry creates antibody-like protein-capture agents. *Angew Chem Int Ed Engl* **48,** 4944–4948 (2009).

47.Farrow, B. *et al.* Epitope Targeting of Tertiary Protein Structure Enables Target-Guided Synthesis of a Potent In-Cell Inhibitor of Botulinum Neurotoxin. *Angew Chem Int Ed Engl* **54,** 7114–7119 (2015).

48.Porel, M. & Alabi, C. A. Sequence-defined polymers via orthogonal allylacrylamide building blocks. *J Am Chem Soc* **136,** 13162–13165 (2014).

49.Porel, M., Thornlow, D. N., Phan, N. N. & Alabi, C. A. Sequence-defined bioactive macrocycles via an acid-catalysed cascade reaction. *Nat Chem* **8,** 590–596 (2016).

50.Phan, N. N., Li, C. & Alabi, C. A. Intracellular Delivery via Noncharged Sequence-Defined Cell-Penetrating Oligomers. *Bioconjugate Chemistry* **29,** 2628–2635 (2018).

51.Brown, J. S. *et al.* Synthesis and Solution-Phase Characterization of Sulfonated Oligothioetheramides. *Macromolecules* **50,** 8731–8738 (2017).

52.Robinson, P. V., de Almeida-Escobedo, G., de Groot, A. E., McKechnie, J. L. & Bertozzi, C. R. Live-Cell Labeling of Specific Protein Glycoforms by Proximity-Enhanced Bioorthogonal Ligation. *J Am Chem Soc* **137,** 10452–10455 (2015).

53.Alabi, C. A. *et al.* Multiparametric approach for the evaluation of lipid nanoparticles

for siRNA delivery. *Proc Natl Acad Sci USA* **110,** 12881–12886 (2013).

Chapter 6 – Peptide-DNA Conjugates to Quantify Endosomal Escape

6.1 – Background

Nucleic acid-based therapeutics such as short interfering RNA (siRNA) have the potential to fundamentally alter disease treatment by selectively[1] and reversibly[2] degrading otherwise undruggable protein targets[3]. However, due to their large size and highly negative charge, siRNAs cannot passively diffuse across the mammalian cell membrane and must enter the cell via endocytosis. Upon endocytosis, siRNA is sequestered inside of an endosome, a lipid bilayer-bound vesicle. During lysosomal maturation, nucleases are shuttled into the endosome to degrade exogenous nucleic acids. Therefore, the potency of siRNA-based therapeutics is limited by their ability to undergo "endosomal escape" before lysosomal degradation[4].

To solve the problem of endosomal escape, researchers have relied on GalNAc-conjugated siRNAs and nanoparticle encapsulation. GalNAc-conjugated siRNAs[5-8], which are targeted to the liver by the asialoglycoprotein receptor (ASGRP) expressed on hepatocytes[9], are thought to rely on a fortuitous combination of high receptor expression, fast recycling rate, and "leaky" endosomal escape to achieve therapeutic levels of cytosolic siRNA[4]. Nanoparticles, which passively accumulate in the liver[10], typically use ionizable lipids to disrupt the endosomal membrane and deliver siRNA into the cytosol[11-16]. These approaches have led to, patisiran (ONPATTRO®)[17], the first FDA approved siRNA therapeutic, and have opened the door for a plethora of liver-targeted siRNA therapeutics currently in clinical trials.

The next frontier in siRNA therapeutics is tissue-specific, extra-hepatic delivery. To enable extra-hepatic delivery, alternative carriers are needed. Due to their ability to target specific tissues, antibody-based carriers have the potential to achieve extra-hepatic delivery[18-20]. However, antibodies do not possess an active mechanism for

endosomal escape[21]. Nevertheless, a variety of strategies have been pursued to deliver antibody-conjugated siRNA both *in vitro* and *in vivo*. Several such approaches sought to incorporate active release mechanisms[22-24]. However, surprisingly, other approaches as well as the GalNAc-siRNA conjugate[4] possessed no obvious mechanism of endosomal escape[25,26]. These conflicting results highlight one of the major hurdles to developing efficient antibody-siRNA conjugates – understanding their processing inside of cells. A variety of readouts have been developed to quantify gene knockdown, the functional output of siRNA delivery[27-29]. These methods are valuable tools, but they are indirect indicators of endosomal escape. A comprehensive analysis of intracellular antibody-conjugated siRNA processing must directly assay endosomal escape.

A variety of methods have been developed to study the endosomal escape of macromolecular therapeutics. The split GFP-complementation assay[30,31] has been adapted to study the intracellular delivery of protein-based therapeutics[32,33]. These assays are high throughput, but do not provide molar quantification of the delivered macromolecular therapeutic. Live-cell imaging has been used to visualize siRNA release from lipid nanoparticles[34] and study intracellular trafficking[35]. These works provide insight into the molecular basis of endosomal escape, but these techniques are low throughput and are only able to estimate the amount of cytosolically delivered siRNA. Other researchers have developed an assay based on biotin ligase[36,37] to quantify the cytosolic delivery of proteins[38-40]. This approach is quantitative but is not amenable to high through-put or live-cell analysis. Taken together, these methods provide a valuable blueprint for the development of a universal assay for the endosomal escape of siRNA.

An ideal approach would be compatible with a variety of delivery systems and cell lines (i.e. does not require genetic manipulation). This would pave the way for a plug-and-play approach to studying and optimizing conjugate-based siRNA therapeutics. Additionally, it would possess detection modalities compatible with high throughput measurements, live-cell imaging, and precise molar quantification. Measurements that can be performed with high throughput would enable the rapid screening of libraries of conjugate-based carriers. Further, kinetic measurements of endosomal escape would enable the determination of the rate of endosomal escape. Once quantified, this fundamental parameter could be used to predict the kinetics of cytosolic siRNA delivery and inform the design of future siRNA-carriers. Live-cell imaging would facilitate visualization of the intracellular trafficking of cytosolic siRNA. In combination with colocalization studies, this could inform the molecular basis of endosomal escape. Finally, molar quantification of the cytosolically delivered fraction could be correlated to gene knockdown to determine the true dose-response behavior of siRNA therapeutics. In this work, we sought to devise an endosomal escape assay capable of fulfilling the above criteria.

6.2 – Results and Discussion

Any endosomal escape assay must be built around a physical or chemical trigger which distinguishes between the cytosolic and endosomal compartments. To design our trigger, we were inspired by thimet oligopeptidase (THOP1). THOP1 is a ubiquitously expressed peptidase, which is reported to be present only in the cytosol of mammalian cells[41,42]. This would provide a means of detecting endosomal escape in any cell line of interest without the need to express an exogenous protein. Further, THOP1 cleaves a five amino acid model peptide substrate (PLGPdK)[43,44]. This should provide a minimally perturbative "tag" for detecting endosomal escape.
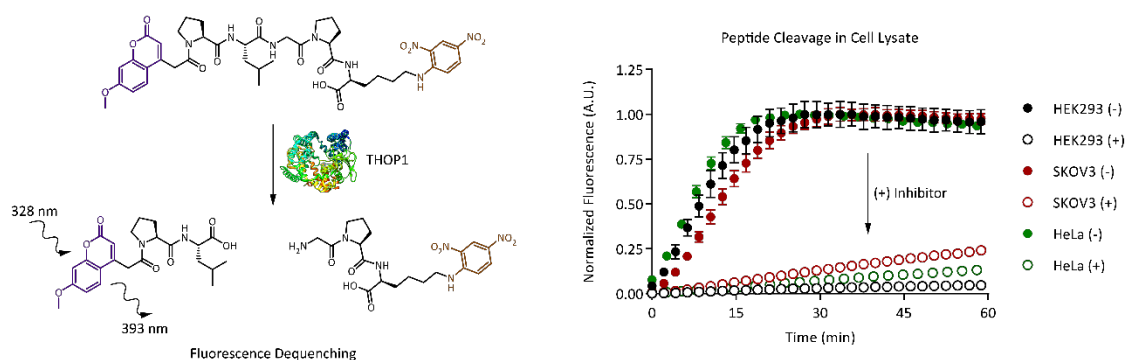
Figure 6.1. THOP1-specific cleavage of MCA-PLGPdK-DNP in cell lysate. Peptide cleavage measured via excitation at 328 nm and methoxy coumarin-specific emission at 393 nm. Cleavage specificity assessed via incubation with THOP-specific inhibitor. Data represents average of two measurements.

In a preliminary study, we tested the specificity of THOP1 cleavage in cell lysate using a commercially available substrate for THOP1 (**Figure 6.1**). The amino acid sequence for this peptide is PLGPdK. Interestingly, the C-terminal lysine residue of this peptide is the D-isomer while all other residues are the natural L-isomers. The N-terminus of the peptide is modified with a methoxy coumarin (MCA)-based fluorescent reporter. This dye is quenched by a 2,4-dintirophenol (DNP)-based static quencher placed on the lysine side chain. Upon cleavage between the leucine and glycine residues, fluorescence is observed by excitation at 328 nm and emission at 393 nm. Cleavage of the peptide was observed upon incubation with lysate from HEK293, SKOV3, and HeLa cell lines. Further, the addition of Cpp-AAF-pAb, a THOP1-specific inhibitor, greatly reduced peptide cleavage. The low level of cleavage observed in the presence of inhibitor could be due to off-target cleavage by another protease or low levels of residual THOP1 activity. This experiment was unable to distinguish between these two interpretations. This data suggests that THOP1 is expressed at significant levels in a variety of cell lines, and that the amino acid sequence PLGPdK is specific for THOP1.
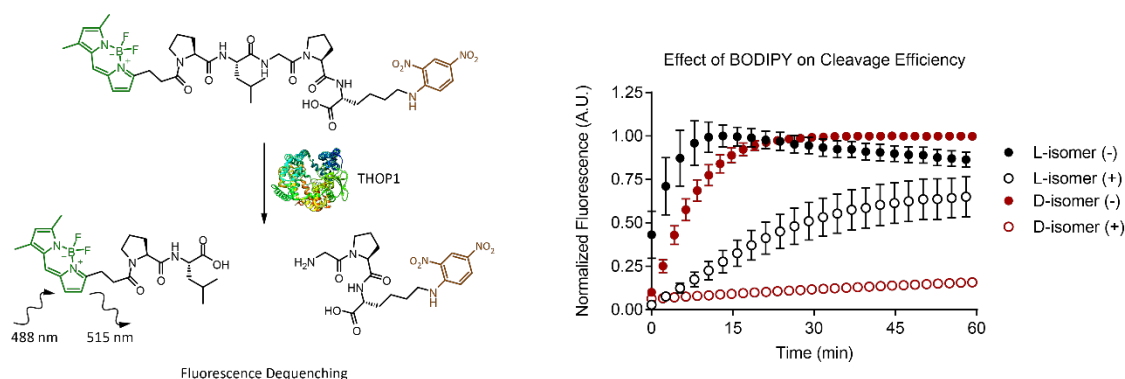
Figure 6.2. Effect of BODIPY modification on peptide cleavage. Peptide cleavage measured in lysate generated from HeLa cells. Cleavage was measured via excitation at 488 nm and BODIPY-specific emission at 515 nm. Cleavage specificity assessed via incubation with THOP-specific inhibitor. Data represents average of two measurements.

Specific cleavage of PLGPdK in cell lysate demonstrated the potential for this peptide to serves as a scaffold for building an intracellular probe for endosomal escape. The N-terminal coumarin dye is dim and not suitable for intracellular fluorescence measurements. Therefore, we synthesized two analogs of the commercially available substrate containing an N-terminal BODIPY modification. Cleavage of these probes can be assayed by fluorescence emission at 515 nm upon excitation at 488 nm. We selected BODIPY because it is bright, photostable, and known to be quenched by DNP[45]. The two BODIPY-modified substrates differed in the isomerization of the C-terminal lysine residue. Hereafter, the substrates will be referred to as BODIPY-Lys and BODIPY-dLys. Cleavage specificity for BODIPY-Lys and BODIPY-dLys was tested in HeLa cell lysate (**Figure 6.2**). Encouragingly, both peptides demonstrated bond cleavage efficiency comparable to that of the commercial substrate (**Figure 6.1**). This indicated that THOP1 can accept different N-terminal modifications on the PLGPdK sequence. Further, BODIPY-dLys showed a greater decrease in bond cleavage upon the addition of inhibitor, which indicated greater THOP1 specificity than BODIPY-Lys. However, BODIPY-dLys was synthetically less accessible and low yield. Therefore,

BODIPY-Lys was used for preliminary studies. This choice may lead to false positive

data but should not lead to false negatives.
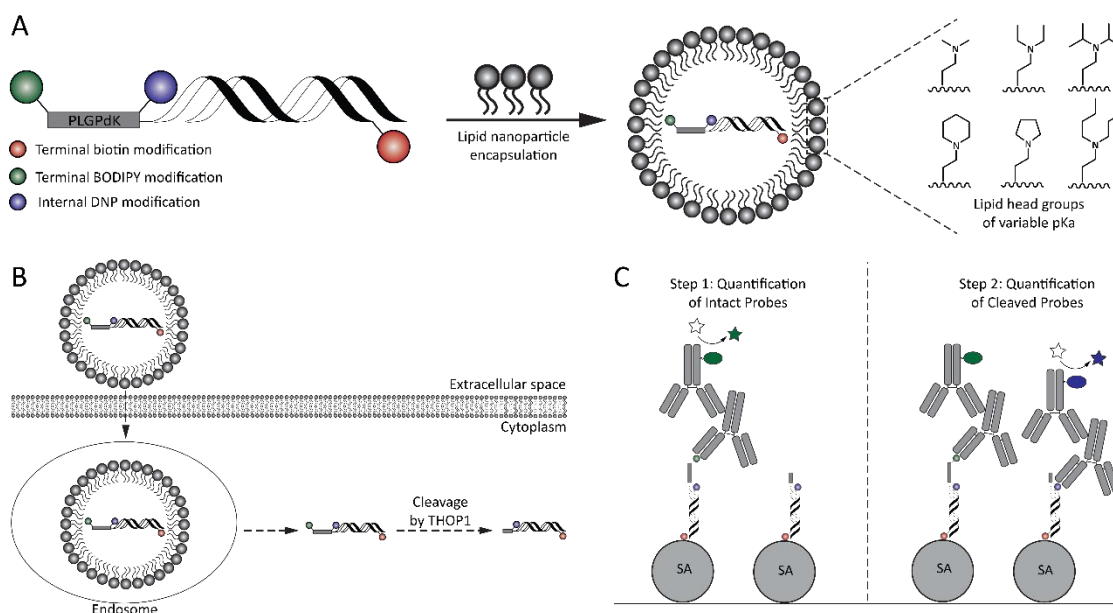
Figure 6.3. Design of THOP1-based endosomal escape assay. A) BODIPY-Lys is covalently attached via the peptide C-terminus to 20mer, biotinylated dsDNA. The resulting peptide-DNA conjugate is encapsulated in lipid nanoparticles. B) Delivered conjugate escapes the endosome where it is cleaved by cytosolically-localized THOP1. C) Intact (endosomal) and cleaved (cytosolic) conjugates are quantified via BODIPY- and 2,4-DNP-specific ELISAs.

Encouraged by this data, we envisioned the following assay for endosomal

escape (**Figure 6.3**). BODIPY-Lys would be chemically conjugated to a biotinylated

ssDNA, forming the so called "probe" strand. The length of this DNA would be 20

nucleotides to mimic the size, shape, and charge of siRNA. The probe strand would be

duplexed and incapsulated in a lipid nanoparticle (LNP). Probe-loaded LNPs would be

used to transfect cells. Upon endosomal escape, BODIPY-Lys is cleaved by

cytosolically-localized THOP1. This cleavage event leads to fluorescence

dequenching, which can be measured in a high throughput manner via flow cytometry

or by live-cell confocal microscopy to ascertain the intracellular trafficking of the probe

strand. Finally, BODIPY and DNP are haptens, which enables detection via enzyme-linked immunosorbent assay (ELISA). The terminal biotin modification is used to immobilize probes on streptavidin-coated plates. Quantification of intact DNP modifications represents the total amount of delivered probe. Quantification of intact BODIPY modifications represents the total amount of endosome-localized probes.
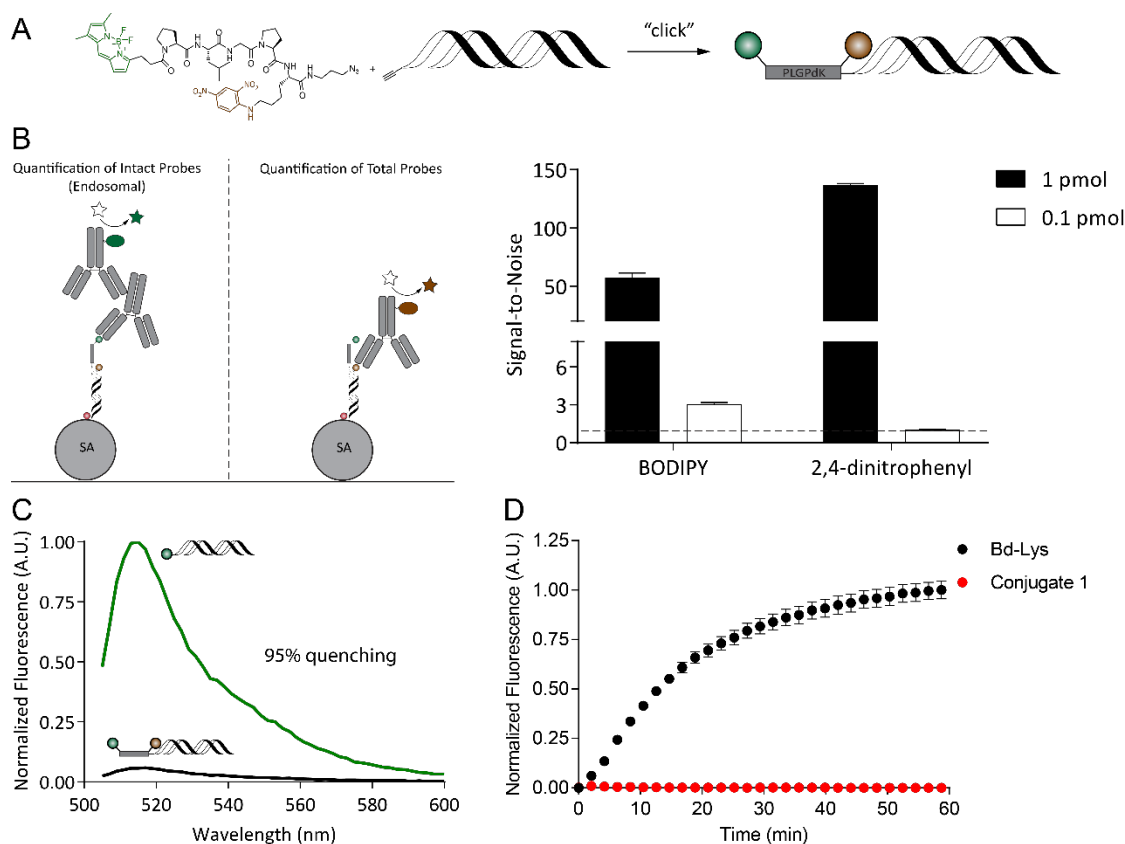
Figure 6.4. Functional testing of peptide-DNA conjugate. A) Scheme for synthesizing peptide-DNA conjugate. B) Determination of ELISA-based detection limit of conjugate. C) Efficiency of BODIPY-DNP quenching within the peptide-DNA conjugate. D) Activity of THOP1 towards BODIPY-Lys conjugated to dsDNA.

To realize this vision, we conjugated BODIPY-Lys to a 20mer biotinylated DNA. Conjugation was performed by first derivatizing the C-terminus of BODIPY-Lys via EDC/NHS coupling with azido propylamine, a small "click" handle. The azide-functionalized peptide was conjugated to a DNA modified with a dibenzocyclooctyne

(DBCO) functional group (**Figure 6.4**). This construct, conjugate 1, was used to determine the detection limit of ELISA-based quantification. In the assay shown above, signal greater than 1 is considered signal above background. For both BODIPY and DNP, the ELISA detection limit was between 1 and 0.1 pmol of sample in a 96-well plate format. Next, the quenching efficiency of conjugate 1 was determined. DNP is a static quencher; therefore, the efficiency of quenching can be strongly dependent on the chemical environment of they dye. Comparison a non-quenched, BODIPY-modified DNA showed a quenching efficiency of approximately 95% at 515 nm up excitation at 488 nm. Finally, the cleavage efficiency of conjugate 1 was assessed using commercially available recombinant THOP1. Conjugate 1 was compared to a control of BODIPY-Lys. No cleavage was observed over the course of 1 hour at 37°C. Cleavage was again assessed after 4 days at 37°C, with no observable bond cleavage (data not shown). This data suggests, that THOP1 does not accept bulky modifications at the C-terminus of PLGPK.
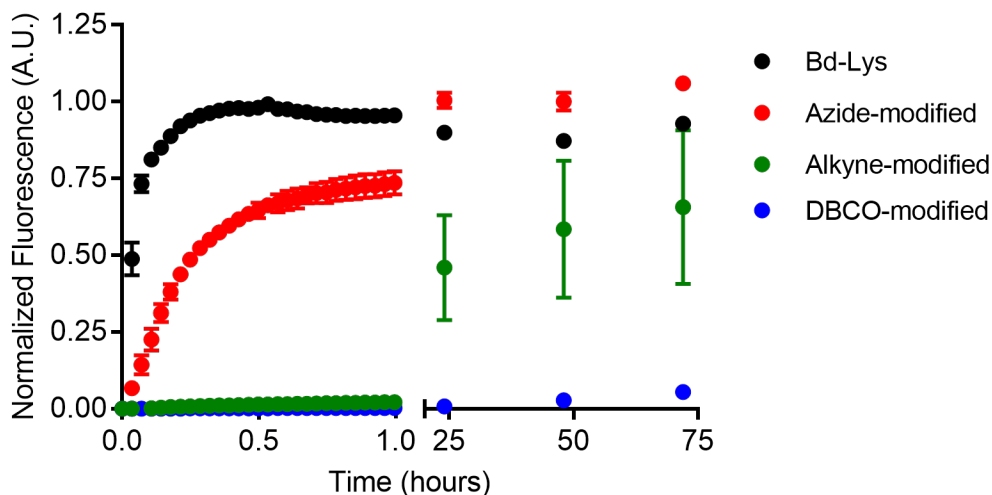
Figure 6.5. Effect of C-terminal modifications on THOP1 cleavage. Peptide cleavage assessed using recombinant THOP1 and BODIPY-specific excitation at 488 nm and emission at 515 nm. Data represents the average of two measurements

To test the effect of C-terminal modifications on THOP1 cleavage, azide-modified BODIPY-Lys was reacted with either a DBCO containing no PEG spacer or a linear alkyne containing a PEG4 spacer. These peptides were purified via RP-HPLC and characterized via LC-MS. Bond cleavage was assayed using recombinant THOP1 (**Figure 6.5**). In agreement with **Figure 6.4**, the DBCO-modified peptide displayed negligible bond cleavage over 72 hours. Interestingly, modification of the C-terminus with azido propylamine caused a noticeable drop in cleavage efficiency. Cleavage efficiency dropped further up on cycloaddition of a linear alkyne-PEG4 cross-linker. Despite the decreased efficiency, the alkyne-modified peptide showed significant bond cleavage after 24 hours. After 72 hours, fluorescence was comparable to that of BODIPY-Lys and its azide-modified derivative. This highlights the importance of reducing steric bulk at the C-terminal lysine of PLGPK and points to the potential importance of the anionic charge of the C-terminal carboxylic acid. The linear alkyne-

modified peptide was taken as our optimal design, recapitulated in a DNA conjugate (conjugate 3), and used for intracellular testing.
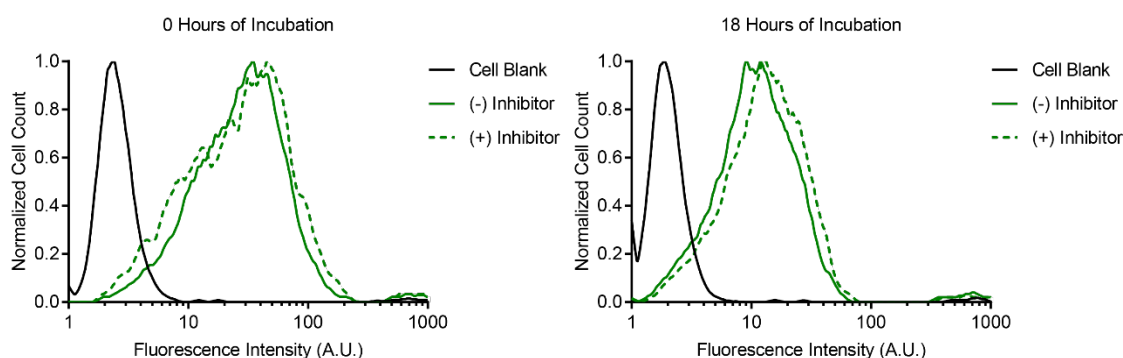
Figure 6.6. Endosomal escape assay with conjugate 3. Conjugate 3 was delivered to HeLa cells via Lipofectamine. THOP1 specificity was assessed via incubation in the presences or absence of THOP1-specific inhibitor. Endosomal escape was assessed after either 0 hours (left) or 18 hours (right) of post transfection incubation. Endosomal escape was analyzed by monitoring BODIPY-specific fluorescence. Each measurement was performed in duplicate.

Conjugate 3 was used to assess the potential of BODIPY-Lys to serve as a probe for endosomal escape (**Figure 6.6**). In short, conjugate 3 was transfected into SKOV3 cells using lipofectamine as a model transfection reagent. To assess the specificity of intracellular BODIPY-Lys cleavage, transfected cells were incubated with and without THOP1-specific inhibitor. Transfections were carried out for 6 hours followed by incubation for the indicated amounts of time. After both 0 hours and 18 hours of incubation, the histograms for cells incubated with and without inhibitor were indistinguishable. There are a variety of interpretations of this data. It is possible that the THOP1 inhibitor is not cell permeable at the concentration tested (25 µM). In this case, it would be impossible to distinguish between specific and non-specific degradation intracellularly, which would obscure our results. Another possibility is that conjugate 3 was delivered into the cytosol but was not cleaved by THOP1. Figure 6.5 indicates that THOP1 cleavage should be less efficient on the conjugate compared to

the free peptide, but it is difficult to directly compare these experiments. Another possibility is that conjugate 3 was delivered to the cytosol and cleaved by THOP1, but the liberated BODIPY fluorophore was not retained inside the cell or was removed from the cell by exocytosis[46]. Indeed, some level of exocytosis of either conjugate or cleaved BODIPY has occurred as evidenced by the shift towards lower fluorescence after 18 hours of incubation. A final interpretation is that conjugate 3 was delivered to the cytosol and cleaved, but the detection limit for dequenching inside of cells in incompatible with the small amount of conjugate that is expected to escape the endosome[34,35]. The true answer is likely some combination of these interpretations.
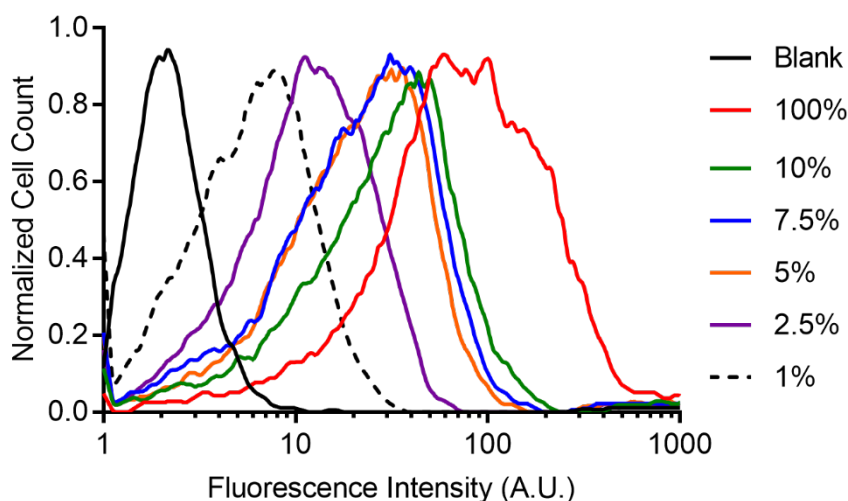
Figure 6.7. Flow cytometry detection limit of lipofectamine transfection. Mixtures of BODIPY-labeled and unlabeled dsDNA were delivered to HeLa cells via Lipofectamine. A standard curve of fluorescence was generated by measuring BODIPY-specific fluorescence. Each measurement was performed in duplicate.

To assess the fundamental detection limit of a flow cytometry-based endosomal escape assay, cells were transfected with non-quenched, DNA-conjugated BODIPY (**Figure 6.7**). To mimic transfection with a quenched conjugated and THOP1-mediated dequenching, cells were transfected with standard mixtures of labeled and non-labeled

dsDNA. The quenching efficiency of BODIPY-Lys conjugated to DNA is approximately 95% (**Figure 6.4**). This is equivalent to the "5%" transfection case in Figure 6.7. The 7.5% and 10% transfection conditions cannot be reliably distinguished from the 5% transfection. This can be interpreted to mean that endosomal escape below a threshold of approximately 5% cannot be detected with conjugate 3. Current best estimates are that only 1 – 2% of siRNA escapes the endosome. Therefore, the quenching efficiency of conjugate 3 is not sufficient. However, comparison of the 1%, 2.5%, and 5% transfection conditions reveals that as little as 1.5% escape should be detectable provided that the quenching efficiency of the probe is at least 99%.
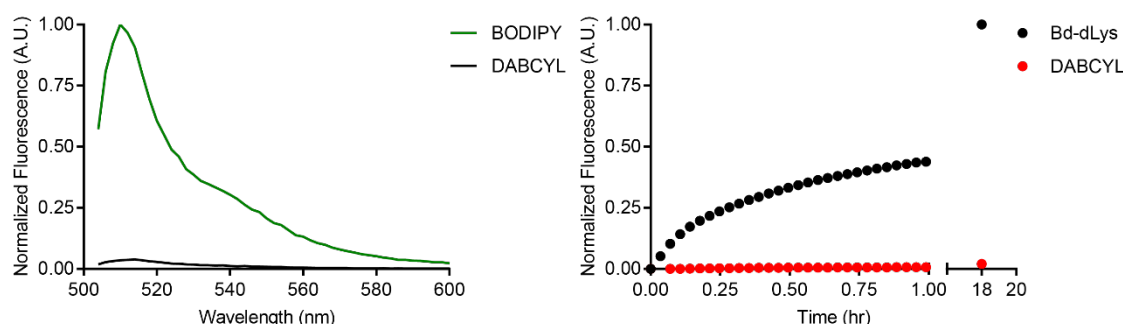
Figure 6.8. Characterization of DABCYL-modified peptide by THOP1. Efficiency of DBACYL-based BODIPY quenching (left). Cleavage of DABCYL-modified peptide (right). Peptide cleavage assessed using recombinant THOP1 and BODIPY-specific excitation at 488 nm and emission at 515 nm. Data represents the average of two measurement.

To improve the quenching efficiency of the PLGPdK probe, a version of the probe was synthesized containing a DABCYL-based quencher on the lysine side chain. DABCYL was shown to be a more efficient quencher of BODIPY (**Figure 6.8**). The quenching efficiency was found to be approximately 99%. Highly efficient quenching should enable sensitive detection of endosomal escape as demonstrated in Figure 6.7. The cleavage efficiency of this peptide was measured using recombinant THOP1 (**Figure 6.8**). That DABCYL-modified peptide was synthesized with the C-terminal D-

lysine isomer. Therefore, cleavage efficiency was compared to BODIPY-dLys. This data indicates that a DABCYL modification on the lysine residue is not tolerated by THOP1. This further highlights the C-terminal sensitivity that we have observed with other modifications of the PLGPdK and PLGPK peptides.

6.3 – Conclusions

In conclusion, with an eye towards studying siRNA therapeutics, we sought to co-opt THOP1, a ubiquitously expressed cytosolic peptidase, to develop a high throughput, quantitative assay for endosomal escape. A commercial substrate for THOP1, MCA-PLGPdK-DNP, was used as a starting point for probe development. The N-terminal coumarin dye was replaced with BODIPY to improve brightness and suitability for live-cell imaging. An N-terminal BODIPY modification was well tolerated and maintained THOP1 specificity in cell lysate. The C-terminus of the peptide was modified with an azide "click" handle for conjugation to DNA. A large decrease in THOP1 cleavage activity was observed for progressively larger C-terminal modifications. It was determined that the quenching efficiency DNP is insufficient for live-cell studies of endosomal escape via flow cytometry. A DABCYL-based quencher was used to improve quenching efficiency. However, the addition of a bulky modification on the C-terminal lysine was shown to abolish THOP1 cleavage activity. Taken together, these data highlight the potential perils of developing an endosomal escape assay within the constraints of an existing biological system. The ubiquitous expression of THOP1 would have proven to be a convenient, universal trigger to detect endosomal escape. However, our substrate-design based approach was unable to uncover a suitable peptide-DNA conjugate substrate for THOP1. In future work, it may be advantageous to turn towards bioorthogonal chemistry or orthogonal biological

processes with predictable performance as a starting point to develop an endosomal

escape assay.

6.4 – Materials and Methods

Reagents for Chemical Synthesis

All chemicals were purchased from MilliporeSigma unless stated otherwise.

Reagents for Molecular Biology and Cell Culture

All cell culture reagents were purchased from ThermoFisher Scientific unless stated otherwise. SKOV3, HeLa, and HEK293 cells were cultured in Dulbecco's Modified Eagle Medium (DMEM).

Liquid Chromatography Mass Spectrometry (LC-MS)

LC-MS analysis was carried out on an Agilent 1100 Series LC with a Poroshell 120 EC-C18 column (100 × 3 mm, 2.7 µm, Agilent Technologies) and an Agilent G1956B Series Single Quadripole MS in positive ion mode for mass detection. The mobile phase for LC-MS (solvent A) was water with 0.1% (v/v) acetic acid, and the stationary phase (solvent B) was acetonitrile with 0.1% (v/v) acetic acid. Compounds were eluted at a flow rate of 0.6 mL/min using a gradient of 5-100% solvent B (0-10 minutes) followed by 100% solvent B (10-12 minutes) and equilibrated back to 5% solvent B (12-15 minutes).

Reverse Phase High Performance Liquid Chromatography (RP-HPLC)

HPLC purification was performed on an Agilent 1100 Series HPLC system equipped with a UV diode array detector and an 1100 Infinity fraction collector. Semi-preparative RP-HPLC was performed with a C18 column (Agilent Eclipse XDB-C18, 9.4 x 250 mm, 5 µm). Analytical RP-HPLC was performed with a C18 column (Agilent Eclipse Plus C18, 4.6 x 150 mm, 5 µm). The mobile phase for HPLC was water with 0.1% (v/v) trifluoroacetic acid (solvent A) and acetonitrile with 0.1% (v/v) trifluoroacetic acid (solvent B) unless specified otherwise. Compounds were eluted at a flow rate of either

4 mL/min (semi-preparative) or 1 mL/min (analytical) using a linear solvent gradient as specified below.

Purification of Modified DNAs

HPLC purification was performed on an Agilent 1100 Series HPLC system equipped with a UV diode array detector and an 1100 Infinity fraction collector. Purification of modified DNAs was performed using an analytical RP-HPLC with a C18 column (Agilent Eclipse Plus C18, 4.6 x 150 mm, 5 µm). The mobile phase for HPLC was TEAA buffer (100 mM triethylamine, 100 mM acetic acid, pH 7.2, solvent A) and acetonitrile (solvent B). Compounds were eluted at a flow rate of either 1 mL/min using a linear solvent gradient as specified below.

Analysis of THOP1 Activity using Recombinant THOP1

Recombinant THOP1 was mixed with peptide substrate in assay buffer (25 mM Tris, 150 mM NaCl, pH 7.5). Activity was tested at 37°C with THOP1 at a concentration of 5 nM and the peptide substrate at a concentration of 10 µM. For methoxy coumarin-peptides, fluorescence was measured by excitation at 328 nm and emission at 393 nm. For BODIPY-modified peptides, fluorescence was measured by excitation at 490 nm and emission at 515 nm.

Generation of Cell Lysate

Cells were expanded in three T75 flasks until the cells reached 70% confluent. The cells were washed with phosphate buffer saline (PBS), pH 7.4. Trypsin (3 mL) was added to each T75 flask to dislodge the cells. The cells were removed from each flask and pooled together. Cells were pelleted by centrifugation at 500xg for 5 minutes. Trypsin was aspirated and the cells were suspended in 15ml of PBS. Again, cells were pelleted by centrifugation at 500xg for 5 minutes. This process was repeated once more. The washed cells were suspended in 350 µL of assay buffer (25 mM Tris, 150

mM NaCl, pH 7.5). To disrupt the cell membrane, the cell suspension was frozen in a dry ice-isopropyl alcohol bath for 1 minute then placed in a water bath at 37°C for 2 minutes. The thawed suspension was vortexed briefly. This cycle was repeated a total of 5 times. Cell debris was removed by centrifugation at 10,000xg for 10 minutes. To remove residual cell debris, the supernatant was transferred to a new Eppendorf tube and centrifuged at 10,000xg for 10 minutes. This supernatant was taken as the final cell lysate preparation. A Bradford Assay was performed to determine the protein concentration in the generated cell lysate. The cell lysate sample was diluted at ratios from 1:50 to 1:400 for Bradford analysis. Cell lysate was stored at a concentration of 2.5 mg/mL as 150 µL aliquots for single use. Aliquots were stored frozen at -20°C until use.

Analysis of THOP1 Activity in Cell Lysate

Cell lysate was added to peptide substrate at final concentration of 10 µM peptide and 0.75 mg/mL protein in assay buffer (25 mM Tris, 150 mM NaCl, pH 7.5). Cleavage reactions were carried out at 37°C for the indicated amounts of time. Peptide cleavage was reported by dequenching of the N-terminal fluorophore. For methoxy coumarin-peptides, fluorescence was measured by excitation at 328 nm and emission at 393 nm. For BODIPY-modified peptides, fluorescence was measured by excitation at 490 nm and emission at 515 nm. To test the specificity of peptide cleavage, N-[(RS)-1-Carboxy-3-phenyl-propyl]-Ala-Ala-Phe-4-Abz-OH (Cpp-AAF-pAb), a THOP1-specific inhibitor[47], was added at a concentration of 200 µM.

Lipofectamine Transfection of Conjugate 3

On day 1, SKOV3 cells were plated at a density 25,000 cells per well in a 24-well plate. On day 3, a duplex of DNA conjugate 3 was prepared and allowed to anneal at room temperature for 5 minutes. The cells were washed with PBS, pH 7.4 and placed in

Optimem (225 µL). To test the effect of THOP1 inhibition, Cpp-AAF-pAb (1.5 µL) was added to cells at 25 µM. Dimethyl sulfoxide (1.5 µL) was added as a vehicle control in the case of cell not treated with inhibitor. The DNA duplex was complexed with Lipofectamine as follows. DNA duplex (49.5 pmol) was prepared at 2.7 µM in Optimem. Separately, lipofectamine (3.7 µL) was added to Optimem (33 µL). The DNA duplex and lipofectamine solutions were incubated at room temperature for 5 minutes. Then the DNA duplex and lipofectamine solutions were combined and incubated at room temperature for 20 minutes. The lipofectamine complex (25 µL) was then added to cells. The final concentration of DNA duplex used for transfection at 100 nM. Transfection was carried out at 37°C for 6 hours. Cells were washed with PBS and incubated in Dulbecco's Modified Eagle Medium (DMEM) for the indicated amount of time (0 hours or 18 hours). Cells were washed with PBS, removed by trypsinization, pelleted by centrifugation at 500xg for 5 minutes, and suspended in PBS for analysis by flow cytometry.

Lipofectamine Transfection of Conjugate 4

On day 1, SKOV3 cells were plated at a density 50,000 cells per well in a 24-well plate. On day 2, a duplex of DNA conjugate 4 was prepared and allowed to anneal at room temperature for 5 minutes. The BODIPY-labeled duplex was mixed with an unlabeled DNA duplex to generate duplex solutions that contained 1%, 2.5%, 5%, 7.5%, 10%, or 100% labeled DNA. The cells were washed with PBS, pH 7.4 and placed in Optimem (225 µL). The mixtures of DNA duplex were complexed with Lipofectamine as follows. DNA duplex (49.5 pmol) was prepared at 2.7 µM in Optimem. Separately, lipofectamine (3.7 µL) was added to Optimem (33 µL). The DNA duplex and lipofectamine solutions were incubated at room temperature for 5 minutes. Then the DNA duplex and lipofectamine solutions were combined and incubated at room temperature for 20

291

minutes. The lipofectamine complex (25 µL) was then added to cells. The final concentration of DNA duplex used for transfection at 100 nM. Transfection was carried out at 37°C for 6 hours. Cells were washed with PBS, removed by trypsinization, pelleted by centrifugation at 500xg for 5 minutes, and suspended in PBS for analysis by flow cytometry.

Synthesis of Bd-PLGPdK-DNP (compound 1)

Step 1

1 equivalency of Fmoc-PLGPdK was dissolved at 22 mM in dimethyl sulfoxide. 7 equivalencies of triethylamine and 1.5 equivalencies of 1-chloro-2,4-dinitrobenzene were added. The mixture was reacted overnight at 40°C. The product was purified via analytical RP-HPLC. The reaction mixture was separated using a linear solvent gradient of 5 – 95% solvent B over 45 minutes Elution: 31 minutes.

Step 2

1 equivalency of step 1 product was dissolved at 5.7 mM in dimethyl sulfoxide. 5 equivalencies of piperidine were added. The mixture was reacted overnight at room temperature. The product was purified via analytical RP-HPLC. The reaction mixture was separated using a linear solvent gradient of 5 – 95% solvent B over 45 minutes Elution: 19 minutes.

Step 3

1 equivalency of step 2 product was dissolved at 7 mM in dimethyl sulfoxide. 5 equivalencies of triethylamine and 2 equivalencies of BODIPY-NHS were added. The mixture was reacted at room temperature overnight. The product was purified via analytical RP-HPLC. The reaction mixture was separated using a linear solvent gradient of 5 – 95% solvent B over 45 minutes Elution: 28 minutes. The product **(1)**

was characterized via LC-MS (**Figure A6. 1**, calculated: 931.43, observed: 931.20 [M-F]$^+$).

Synthesis of Bd-PLGPdK-DABCYL (compound 2)

Step 1

1 equivalency of Fmoc-PLGPdK was dissolved at 6.8 mM in dimethyl sulfoxide. 7 equivalencies of triethylamine and 3 equivalencies of 2,5-dioxopyrrolidin-1-yl (E)-4-((4-(dimethylamino)phenyl)diazenyl)benzoate (DABCYL-NHS ester) were added. The mixture was reacted overnight at room temperature. Removal of the Fmoc protecting group was achieved by treatment with 10% (v/v) piperidine for 5 hours. The product was purified via semi-preparative RP-HPLC.

Step 2

1 equivalency of step 1 product was dissolved at 3 mM in dimethyl sulfoxide. 5 equivalencies of triethylamine and 5 equivalencies of BODIPY-NHS were added. The mixture was reacted at room temperature overnight. The product **(2)** was purified via analytical RP-HPLC. (**Figure A6. 2**, calculated: 1036.53, observed: 1036.40 [M+H]$^+$).

Synthesis of Bd-PLGPK-DNP (compound 3)

1 equivalency of PLGPK-DNP was dissolved at 6 mM in dimethyl sulfoxide. 4 equivalencies of triethylamine and 2 equivalencies of BODIPY-NHS were added. The mixture was reacted at room temperature overnight. The product was purified via analytical RP-HPLC. The reaction mixture was separated using a linear solvent gradient of 5 – 95% solvent B over 30 minutes Elution: 21 minutes. The product **(3)** was characterized via LC-MS (**Figure A6. 3**, calculated: 931.43, observed: 931.10 [M-F]$^+$).

Synthesis of Azide-modified THOP1 Peptide (compound 4)

1 equivalency of compound (3) was dissolved at 4 mM in dimethyl sulfoxide. 5 equivalencies of triethylamine, 5 equivalencies of EDC, 2 equivalencies of NHS, and 3 equivalencies of 3-azidopropan-1-amine were added. The mixture was reacted at room temperature overnight. The product was purified via analytical RP-HPLC. The reaction mixture was separated using a linear solvent gradient of 5 – 95% solvent B over 30 minutes Elution: 25 minutes. The product (4) was characterized via LC-MS (**Figure A6. 4**, calculated: 1013.49, observed: 1013.25 $[M-F]^+$).

Synthesis of DBCO-modified THOP1 Peptide (compounds 5)

1 equivalency of compound (4) was dissolved at 1 mM in 10% (v/v) water in dimethyl sulfoxide. 2 equivalencies of DBCO-NHS ester were added. The mixture was reacted overnight at room temperature. The product was purified via analytical RP-HPLC. The reaction mixture was separated using a linear solvent gradient of 5 – 95% solvent B over 90 minutes Elution: 59 minutes. The product (5) was characterized via LC-MS (**Figure A6. 5**, calculated: 1415.61, observed: 1415.20 $[M-F]^+$).

Synthesis of DBCO-PEG13-modified THOP1 Peptide (compound 6)

1 equivalency of compound (4) was dissolved at 1 mM in 10% (v/v) water in dimethyl sulfoxide. 2 equivalencies of DBCO-PEG13-NHS ester were added. The mixture was reacted overnight at room temperature. The product was purified via analytical RP-HPLC. The reaction mixture was separated using a linear solvent gradient of 5 – 95% solvent B over 90 minutes Elution: 54 minutes. The product (6) was characterized via LC-MS (**Figure A6. 6**, calculated: 1030.00, observed: 1030.1 $[M-F+H]^{2+}$).

Synthesis of Alkyne-modified THOP1 Peptide (compound 7)

1 equivalency of compound (4) was dissolved at 2 mM in 25% (v/v) water in dimethyl sulfoxide. 2 equivalencies of alkyne-PEG4-NHS, 0.5 equivalencies of copper sulfate, 1

equivalency of TBTA, and 5 equivalencies of sodium ascorbate were added. The mixture was reacted overnight at room temperature. The product **(7)** was purified via analytical RP-HPLC. The reaction mixture was separated using a linear solvent gradient of 5 – 65% solvent B over 60 minutes Elution: 50 minutes.

Reaction of Compound 2 with DBCO-modified DNA (Conjugate 1)

Step 1: Acylation of 3' Amine Modification

1 equivalency (100 µg, 14 nmol) of bifunctional DNA (3' C6 spacer, Amine; 5' Biotin) was reacted with 40 equivalencies of DBCO-NHS at a DNA concentration of 100 µM. The solvent for the reaction was 40% (v/v) dimethyl sulfoxide in borate buffered saline (BBS), pH 8.2 (100 mM borate, 150 mM NaCl). The reaction was carried out at room temperature overnight. The product was dialyzed against water to remove excess DBCO and concentrated under vacuum. The product was used without further characterization or purification.

Step 2: SPAAC Reaction

Modification of the 3' DBCO modification was achieved by reacting 1 equivalency of crude step 1 product with 1.5 equivalencies of compound **(4)** at a DNA concentration of 350 µM. The reaction solvent was 50% (v/v) dimethyl sulfoxide in PBS, pH 7.4. The reaction was carried out at room temperature overnight. The product was dialyzed against water to remove excess compound **(4)** and concentrated under vacuum. The crude product (conjugate 1) was purified via analytical RP-HPLC and dried under vacuum to yield the final product. The reaction mixture was separated using a linear solvent gradient of 5 – 95% solvent B over 45 minutes Elution: 21 minutes.

Reaction of Compound 2 with DBCO-PEG4-modified DNA (Conjugate 2)

Step 1: Acylation of 3' Amine Modification

1 equivalency (400 µg, 55 nmol) of bifunctional DNA (3' C6 spacer, Amine; 5' Biotin) was reacted with 40 equivalencies of DBCO-PEG4-NHS at a DNA concentration of 100 µM. The solvent for the reaction was 5% (v/v) dimethyl sulfoxide in borate buffered saline (BBS), pH 8.2 (100 mM borate, 150 mM NaCl). The reaction was carried out at room temperature overnight. The product was dialyzed against water to remove excess DBCO and concentrated under vacuum. The product was used without further characterization or purification.

Step 2: SPAAC Reaction

Modification of the 3' DBCO-PEG4 modification was achieved by reacting 1 equivalency of crude step 1 product with 1.5 equivalencies of compound **(4)** at a DNA concentration of 350 µM. The reaction solvent was 50% (v/v) dimethyl sulfoxide in PBS, pH 7.4. The reaction was carried out at room temperature overnight. The product was dialyzed against water to remove excess compound **(4)** and concentrated under vacuum. The crude product (conjugate 2) was purified via analytical RP-HPLC and dried under vacuum to yield the final product. The reaction mixture was separated using a linear solvent gradient of 5 – 95% solvent B over 45 minutes Elution: 21 minutes.

Reaction of Compound 2 with Alkyne-PEG4-modified DNA (Conjugate 3)

Step 1: Acylation of 3' Amine Modification

1 equivalency (100 µg, 14.5 nmol) of monofunctional DNA (3' C9 spacer) was reacted with 40 equivalencies of Alkyne-PEG4-NHS at a DNA concentration of 170 µM. The solvent for the reaction was 35% (v/v) dimethyl sulfoxide in borate buffered saline (BBS), pH 8.2 (100 mM borate, 150 mM NaCl). The reaction was carried out at room temperature overnight. The crude product was purified via analytical RP-HPLC and dried under vacuum to yield the final product. The reaction mixture was separated using a linear solvent gradient of 5 – 35% solvent B over 15 minutes Elution: 10 minutes.

Step 2: Azide-Alkyne Copper Click Reaction

Modification of the 3' Alkyne-PEG4 modification was achieved by reacting 1 equivalency of crude step 1 product with 5 equivalencies of compound **(4)** at a DNA concentration of 180 μM. 5 equivalencies of copper sulfate, 10 equivalencies of TBTA, and 50 equivalencies of sodium ascorbate were added. The reaction solvent was 50% (v/v) dimethyl sulfoxide in water. The reaction was carried out at room temperature overnight. The crude product was purified via analytical RP-HPLC and dried under vacuum to yield the final product. The reaction mixture was separated using a linear solvent gradient of 5 – 55% solvent B over 25 minutes Elution: 20 minutes.

Reaction of BODIPY-NHS with DNA-Amine (Conjugate 4)

1 equivalency (100 μg, 14.5 nmol) of monofunctional DNA (3' C9 spacer) was reacted with 10 equivalencies of BODIPY-NHS at a DNA concentration of 150 μM. The solvent for the reaction was 20% (v/v) dimethyl sulfoxide in borate buffered saline (BBS), pH 8.2 (100 mM borate, 150 mM NaCl). The reaction was carried out at room temperature overnight. The crude product was purified via analytical RP-HPLC and dried under vacuum to yield the final product.

Chapter 6 Appendix

Peptide-DNA Conjugates to Quantify Endosomal Escape

Synthesis of Bd-PLGPdK-DNP (compound 1)
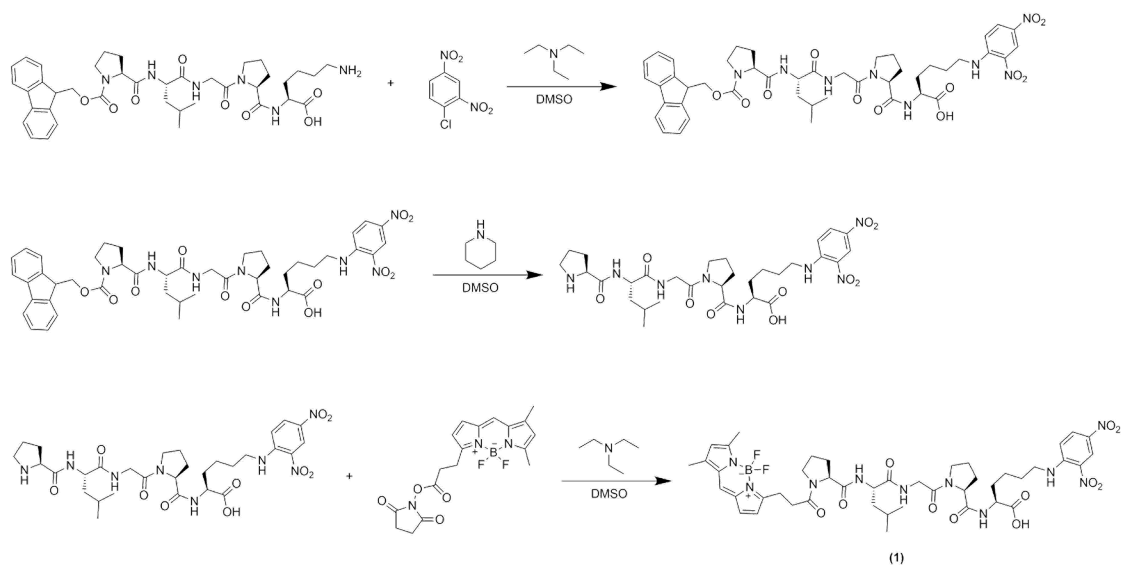
Figure A6. 1. Synthesis scheme for compound 1.

Synthesis of Bd-PLGPdK-DABCYL (compound 2)
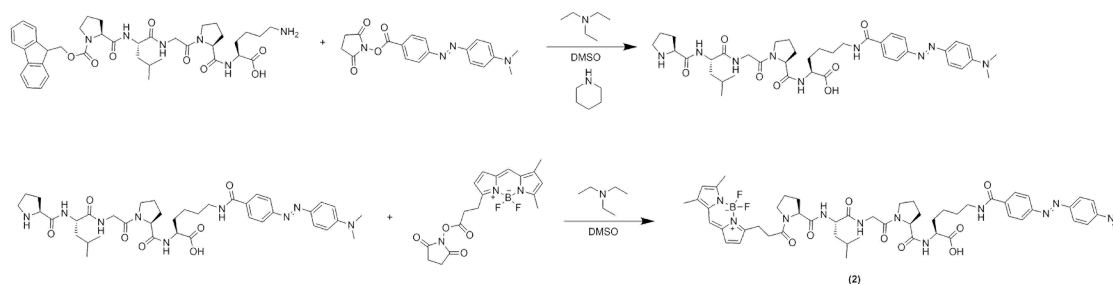
Figure A6. 2. Synthesis scheme for compound 2.

Synthesis of Bd-PLGPK-DNP (compound 3)
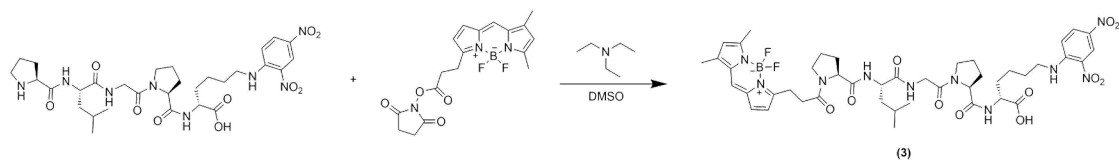
Figure A6. 3. Synthesis scheme for compound 3.

Synthesis of Azide-modified THOP1 Peptide (compound 4)
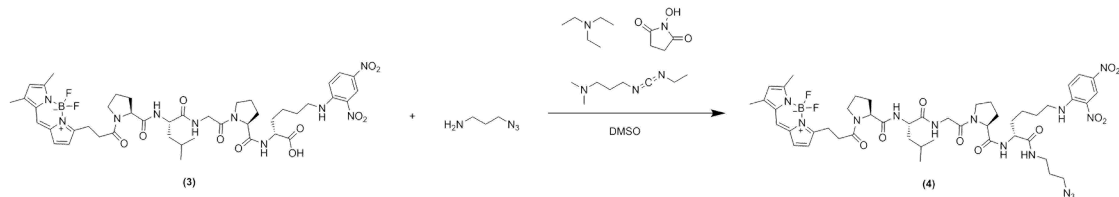
Figure A6. 4. Synthesis scheme for compound 4.

Synthesis of DBCO-modified THOP1 Peptide (compounds 5)

Figure A6. 5. Synthesis scheme for compound 5.

Synthesis of DBCO-PEG13-modified THOP1 Peptide (compound 6)
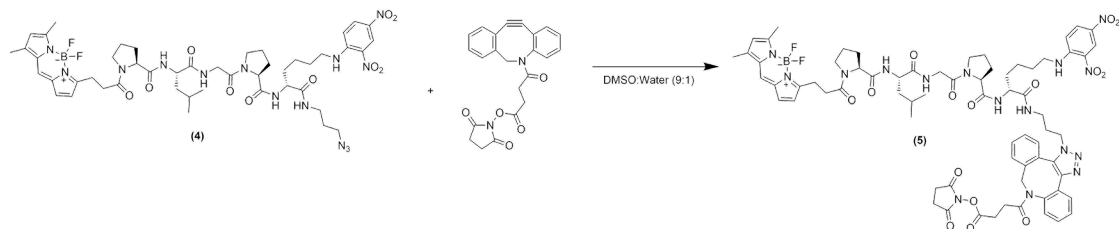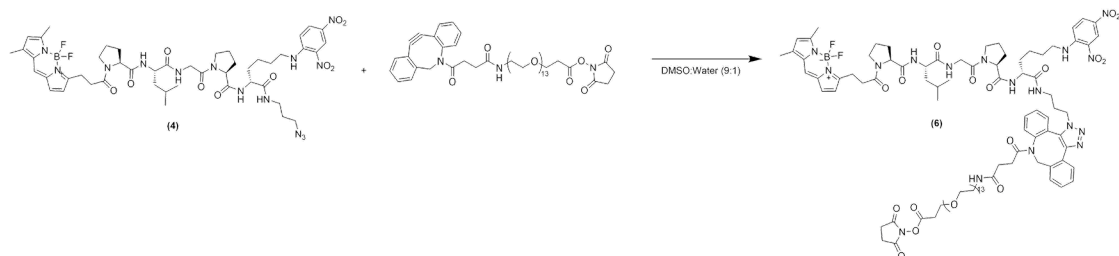

Figure A6. 6. Synthesis scheme for compound 6.

Synthesis of Alkyne-modified THOP1 Peptide (compound 7)
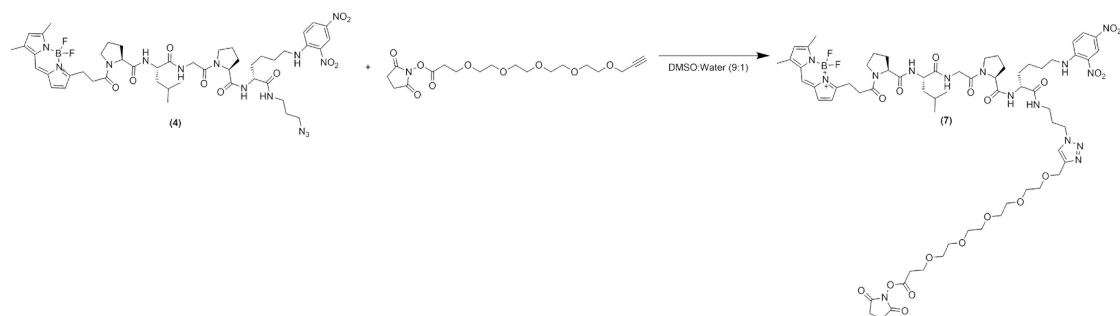
Figure A6. 7. Synthesis scheme for compound 7.

Chapter 6 References

1.Janas, M. M. *et al.* Selection of GalNAc-conjugated siRNAs with limited off-target-driven rat hepatotoxicity. *Nat Commun* **9,** 723 (2018).

2.Zlatev, I. *et al.* Reversal of siRNA-mediated gene silencing in vivo. *Nat Biotechnol* **36,** 509–511 (2018).

3.Scherman, D., Rousseau, A., Bigey, P. & Escriou, V. Genetic pharmacology: progresses in siRNA delivery and therapeutic applications. *Gene Ther* **24,** 151–156 (2017).

4.Dowdy, S. F. Overcoming cellular barriers for RNA therapeutics. *Nat Biotechnol* **35,** 222–229 (2017).

5.Nair, J. K. *et al.* Multivalent N-acetylgalactosamine-conjugated siRNA localizes in hepatocytes and elicits robust RNAi-mediated gene silencing. *J Am Chem Soc* **136,** 16958–16961 (2014).

6.Matsuda, S. *et al.* siRNA conjugates carrying sequentially assembled trivalent N-acetylgalactosamine linked through nucleosides elicit robust gene silencing in vivo in hepatocytes. *ACS Chemical Biology* **10,** 1181–1187 (2015).

7.Foster, D. J. *et al.* Advanced siRNA Designs Further Improve In Vivo Performance of GalNAc-siRNA Conjugates. *Mol Ther* **26,** 708–717 (2018).

8.Meade, B. R. *et al.* Efficient delivery of RNAi prodrugs containing reversible charge-neutralizing phosphotriester backbone modifications. *Nat Biotechnol* **32,** 1256–1261 (2014).

9.Bon, C., Hofer, T., Bousquet-Mélou, A., Davies, M. R. & Krippendorff, B.-F. Capacity limits of asialoglycoprotein receptor-mediated liver targeting. *MAbs* **9,** 1360–1369 (2017).

10. Zhang, Y.-N., Poon, W., Tavares, A. J., McGilvray, I. D. & Chan, W. C. W. Nanoparticle-liver interactions: Cellular uptake and hepatobiliary elimination. *Journal of controlled release : official journal of the Controlled Release Society* **240,** 332–348 (2016).

11. Jayaraman, M. *et al.* Maximizing the potency of siRNA lipid nanoparticles for hepatic gene silencing in vivo. *Angew Chem Int Ed Engl* **51,** 8529–8533 (2012).

12. Semple, S. C. *et al.* Rational design of cationic lipids for siRNA delivery. *Nat Biotechnol* **28,** 172–176 (2010).

13. Whitehead, K. A., Langer, R. & Anderson, D. G. Knocking down barriers: advances in siRNA delivery. *Nat Rev Drug Discov* **8,** 129–138 (2009).

14. Alabi, C. A. *et al.* Multiparametric approach for the evaluation of lipid nanoparticles for siRNA delivery. *Proc Natl Acad Sci USA* **110,** 12881–12886 (2013).

15. Kumar, V. *et al.* Shielding of Lipid Nanoparticles for siRNA Delivery: Impact on Physicochemical Properties, Cytokine Induction, and Efficacy. *Molecular Therapy— …* **3,** e210 (2014).

16. Ball, R. L., Hajj, K. A., Vizelman, J., Bajaj, P. & Whitehead, K. A. Lipid Nanoparticle Formulations for Enhanced Co-delivery of siRNA and mRNA. *Nano Lett* **18,** 3814–3822 (2018).

17. Adams, D. *et al.* Patisiran, an RNAi Therapeutic, for Hereditary Transthyretin Amyloidosis. *N Engl J Med* **379,** 11–21 (2018).

18. Sievers, E. L. & Senter, P. D. Antibody-drug conjugates in cancer therapy. *Annu Rev Med* **64,** 15–29 (2012).

19. van Buggenum, J. A. G. L. *et al.* A covalent and cleavable antibody-DNA conjugation strategy for sensitive protein detection via immuno-PCR. *Scientific reports* **6,** 22675 (2016).

20. Hughes, B. Antibody-drug conjugates for cancer: poised to deliver? *Nat Rev Drug Discov* **9,** 665–667 (2010).

21. Varkouhi, A. K., Scholte, M., Storm, G. & Haisma, H. J. Endosomal escape pathways for delivery of biologicals. *Journal of controlled release : official journal of the Controlled Release Society* **151,** 220–228 (2010).

22. Ma, Y. *et al.* Humanized Lewis-Y specific antibody based delivery of STAT3 siRNA. *ACS Chemical Biology* **6,** 962–970 (2011).

23. Bäumer, N. *et al.* Antibody-coupled siRNA as an efficient method for in vivo mRNA knockdown. *Nature protocols* **11,** 22–36 (2015).

24. Song, E. *et al.* Antibody mediated in vivo delivery of small interfering RNAs via cell-surface receptors. *Nat Biotechnol* **23,** 709–717 (2005).

25. Sugo, T. *et al.* Development of antibody-siRNA conjugate targeted to cardiac and skeletal muscles. *Journal of controlled release : official journal of the Controlled Release Society* **237,** 1–13 (2016).

26. Cuellar, T. L. *et al.* Systematic evaluation of antibody-mediated siRNA delivery using an industrial platform of THIOMAB-siRNA conjugates. *Nucleic Acids Res* **43,** 1189–1203 (2014).

27. Paddison, P. J., Caudy, A. A. & Hannon, G. J. Stable suppression of gene expression by RNAi in mammalian cells. *Proc Natl Acad Sci USA* **99,** 1443–1448 (2002).

28. Reynolds, A. *et al.* Rational siRNA design for RNA interference. *Nat Biotechnol* **22,** 326–330 (2004).

29. Robb, G. B., Brown, K. M., Khurana, J. & Rana, T. M. Specific and potent RNAi in the nucleus of human cells. *Nat Struct Mol Biol* **12,** 133–137 (2005).

30.Cabantous, S. & Waldo, G. S. In vivo and in vitro protein solubility assays using split GFP. *Nat Methods* **3,** 845–854 (2006).

31.Cabantous, S., Terwilliger, T. C. & Waldo, G. S. Protein tagging and detection with engineered self-assembling fragments of green fluorescent protein. *Nat Biotechnol* **23,** 102–107 (2004).

32.Lönn, P. *et al.* Enhancing Endosomal Escape for Intracellular Delivery of Macromolecular Biologic Therapeutics. *Scientific reports* **6,** 32301 (2016).

33.Milech, N. *et al.* GFP-complementation assay to detect functional CPP and protein delivery into living cells. *Scientific reports* **5,** 18329 (2015).

34.Wittrup, A. *et al.* Visualizing lipid-formulated siRNA release from endosomes and target gene knockdown. *Nat Biotechnol* **33,** 870 (2015).

35.Gilleron, J. *et al.* Image-based analysis of lipid nanoparticle-mediated siRNA delivery, intracellular trafficking and endosomal escape. *Nat Biotechnol* **31,** 638–646 (2013).

36.Beckett, D., Kovaleva, E. & Schatz, P. J. A minimal peptide substrate in biotin holoenzyme synthetase-catalyzed biotinylation. *Protein Sci* **8,** 921–929 (1999).

37.Schatz, P. J. Use of peptide libraries to map the substrate specificity of a peptide-modifying enzyme: a 13 residue consensus peptide specifies biotinylation in Escherichia coli. *Biotechnology (NY)* **11,** 1138–1143 (1993).

38.Verdurmen, W. P. R., Mazlami, M. & Plückthun, A. A Biotin Ligase-Based Assay for the Quantification of the Cytosolic Delivery of Therapeutic Proteins. *Methods Mol Biol* **1575,** 223–236 (2017).

39.Verdurmen, W. P. R., Mazlami, M. & Plückthun, A. A quantitative comparison of cytosolic delivery via different protein uptake systems. *Scientific reports* **7,** 13194 (2017).

40. Verdurmen, W. P. R., Luginbühl, M., Honegger, A. & Plückthun, A. Efficient cell-specific uptake of binding proteins into the cytoplasm through engineered modular transport systems. *Journal of controlled release : official journal of the Controlled Release Society* **200,** 13–22 (2014).

41. Fontenele-Neto, J. D., Massarelli, E. E., Garrido, P. A. G., Beaudet, A. & Ferro, E. S. Comparative fine structural distribution of endopeptidase 24.15 (EC3.4.24.15) and 24.16 (EC3.4.24.16) in rat brain. *J Comp Neurol* **438,** 399–410 (2001).

42. Rioli, V. *et al.* Novel natural peptide substrates for endopeptidase 24.15, neurolysin, and angiotensin-converting enzyme. *J Biol Chem* **278,** 8547–8555 (2002).

43. Tisljar, U., Knight, C. G. & Barrett, A. J. An alternative quenched fluorescence substrate for Pz-peptidase. *Anal Biochem* **186,** 112–115 (1990).

44. Shrimpton, C. N. *et al.* Thiol activation of endopeptidase EC 3.4.24.15. A novel mechanism for the regulation of catalytic activity. *J Biol Chem* **272,** 17395–17399 (1997).

45. Hendrickson, H. S., Hendrickson, E. K., Johnson, I. D. & Farber, S. A. Intramolecularly quenched BODIPY-labeled phospholipid analogs in phospholipase A(2) and platelet-activating factor acetylhydrolase assays and in vivo fluorescence imaging. *Anal Biochem* **276,** 27–35 (1999).

46. Cilliers, C., Liao, J., Atangcho, L. & Thurber, G. M. Residualization Rates of Near-Infrared Dyes for the Rational Design of Molecular Imaging Agents. *Mol Imaging Biol* **17,** 757–762 (2015).

47. Knight, C. G. & Barrett, A. J. Structure/function relationships in the inhibition of thimet oligopeptidase by carboxyphenylpropyl-peptides. *FEBS Lett* (1991).

Chapter 7 – Conclusions and Future Directions

Multifunctional Substrates for Microbial Transglutaminase

Through systematic substrate design, we have shown that microbial transglutaminase (MTG) accepts heterobifunctional substrates containing two bioorthogonal chemical handles; an aliphatic azide and a methyltetrazine. We characterized the conjugation efficiency of five substrate designs and identified spacer flexibility alpha to the primary amine as a key structural feature. This conjugation strategy was used to synthesize a multifunctional antibody-drug conjugate (ADC) containing DM1, a cytotoxic drug, and a hydrophobicity masking a polyethylene glycol (PEG) chain. This work is an important addition to the literature regarding MTG-based antibody modification and could be built upon in a few ways.

In this work, we utilized the dual "click" functionality to attach a drug and PEG chain. This was a convenient demonstration of the capability of this conjugation strategy. However, the true power of our conjugation strategy lies not in the ability to attach two cargoes in a one-pot fashion. The power of our approach is that it utilizes two bioorthogonal chemistries, which enables conjugation to complex biomolecules or within biological environments. One potential application is the *in vivo* delivery of "click"- modified antibodies. This has been used to pre-label cancer cells with chemical handles that can be used to direct therapeutics to the target site. Our conjugate could enable the delivery of two therapeutic cargos in a mix-and-match fashion. This conjugation strategy could also be a powerful tool for the combinatorial assembly of antibody-siRNA conjugates (ARCs). ARCs required a two-component strategy in which an endosomalytic agent facilitates the delivery of a conjugated siRNA into the cytosol. However, it is unclear what properties constitute an effective endosomalytic agent. This necessitates the need to screen a large library of antibody conjugates with chemical

diverse cargoes. Using bioorthogonal chemistry would streamline the workflow of conjugate synthesis – accelerating the discovery of endosomalytic agents.

Support-free Synthesis of OligoTEAs

We developed two methods for the support-free synthesis of oligoTEAs. These methods eliminated the use of a fluorous tag to perform iterative purification. This is particularly useful for synthesizing hydrophilic structures which can cause inefficient partitioning onto the fluorinated solid phase. The first method was based on a bifunctional monomer containing both an acrylamide and an acetylated thiol. The second method utilized a traditional *N*-allylacrylamide monomer and an acetylated dithiol monomer, which were assembled via sequential thiol-Michael and thiol-ene reactions. Both methods were applied to the synthesis of multifunctional chemical cross-linkers containing three pendant group functionalities. The first method requires multistep monomer synthesis but eliminates the need for excess reagents when assembling the final cross-linker. The second method is compatible with one or two step monomer synthesis but requires the use of excess reagents to assemble the final cross-linker. Because of this, method one is better suited for the synthesis of short cross-linkers at scales approaching 100 mg. Meanwhile method two is best applied to cross-linker synthesis on the scale of approximately 10 mg. This work has provided insight into the challenges of synthesizing sequence-defined polymers without the use of a support.

Both strategies pursued here utilized iterative purification via RP-HPLC. However, method one was envisioned to synthesize oligoTEAs in a one-pot fashion without the need for stepwise purification – the holy grail of polymer synthesis. This vision was not realized due to the ability of the thiolate ion to perform both a thiol-Michael addition and deprotect the acetylated thiol which can cause uncontrolled

307

polymerization. Sterically hindered acetate protecting groups can be used to suppress unwanted deprotection. However, these protecting groups also become increasingly difficult to remove. An ideal approach would employ a protecting group that is stable to nucleophiles such as the thiolate ion. The protecting group must be traceless or generate no byproducts that interfere with oligomer synthesis. These challenges are not limited to oligoTEA synthesis. Identifying a methodology capable of synthesizing sequence-defined polymers in a one-pot, support-free manner remains a grand challenge in polymer chemistry. Solving this problem will accelerate the discovery of bioactive synthetic polymers by enabling large scale combinatorial screening.

Effect of Cross-linker Sequence on the Biophysical Properties of ADCs

We utilized multifunctional, PEGylated cross-linkers to explore the effect of sequence on the biophysical properties of antibody-drug conjugates. These cross-linkers were shown to shield dansyl, a model cargo, from the surrounding aqueous environment. Within the context of an antibody-drug conjugate (ADC), these cross-linkers were shown to screen the hydrophobicity of monomethyl auristatin E (MMAE). Placement of PEG chains distally from the cargo yielded the most hydrophilic ADC. Cross-linker sequence was shown to influence the ability of these ADCs to bind their receptor, but it had no effect on *in vitro* potency.

To the best of our knowledge, this work was the fist study of the effect of cross-linker sequence on ADC properties. The data presented here would benefit from additional *in vivo* work to address the full scope of the effect of sequence on efficacy. The cargo we investigated has been successfully employed in two FDA approved ADCs. While this made for a good test system, this indicates that MMAE does not require hydrophobicity masking PEG chains to achieve therapeutically relevant drug loading. The system developed here would be best applied to drug candidates that

have low potency or a highly hydrophobic character. In ADC design, a drug that has low potency requires a higher degree of drug loading. This would naturally lead to greater ADC aggregation, which our system may help prevent. Similarly, highly potent compounds that are too hydrophobic to yield a stable conjugate are good candidates for this system. Ultimately, work in this area will expand the range of therapeutic compounds assessible to ADC design.

DNA- and Polymer-Protein Conjugates to Characterize Extracellular Vesicles

We sought to develop target-guided synthesis as a method to probe protein-protein proximity on the surface of extracellular vesicles. In this effort we initially pursued a strategy based on protein-DNA conjugates. However, the highly charged nature of DNA-based cross-linkers prevented binding of our conjugates in proximity on the nanoparticle surface. An alternative approach utilizing oligoTEA-based molecular barcodes detectable by LC-MS was explored. Ultimately, the detection limit of this assay was too low to achieve detectable signal within the constraints of our experiment. Despite these setbacks, concurrent work by Carolyn Bertozzi's lab supports that the concept of employing target-guided synthesis to probe interactions on the nanoscale is sound. Further, Bertozzi's work informs us as to the shortcomings our approach and points to a viable direction for future work.

The work from Carolyn Bertozzi's lab utilized a biotin functionalized aptamer to isolate the product from their target-guided synthesis reaction. This could then be fed into a detection scheme based on Western Blot analysis, which provided enzymatic signal amplification. A similar detection scheme may have aided our proof-of-concept studies. In future work, biotinylation would have also proved to be a convenient handle for isolating extracellular vesicles subpopulations for further analysis. However, closer

collaboration with biologist is needed to identify the important biological questions that need to be answered.

Peptide-DNA Conjugates to Quantify Endosomal Escape

We developed a peptide-DNA conjugate to study the endosomal escape of siRNA therapeutics. This conjugate was based on the activity of thimet oligopeptidase (THOP1), a cytosolically localized peptidase. THOP1 was found to tolerate functionalization of its substrate at the N-terminus with either a methoxy coumarin or BODIPY FL dye. However, functionalization of the C-terminal carboxylic acid with both PEG spacers and DNA caused a sharp decrease in THOP1 activity. Ultimately, it was determined that THOP1 does not accept DNA-conjugated substrates. This was one of the major contributing factors in determining that this assay for endosomal escape would not be feasible.

Our attempt to devise an assay for endosomal escape was ultimately undone by our decision to rely on an existing biological mechanism to distinguish between endosome and cytosol. This type of approach simplifies the implementation of an assay by not requiring engineering of each cell line to be tested. A downside of this approach is that we were left with systematic substrate design as the only means to optimize assay performance. In this instance, harsh constraints on THOP1 substrate recognition could not be overcome by systematic substrate design. An alternative approach could be to engineer a cell line to express an exogenous protein that differentiates subcellular localization of a peptide tag. Mechanistically, this would be very similar to our approach using THOP1. However, the performance of this assay could be optimized via conjugate design, protein overexpression, and protein engineering. These additional optimization handles may facilitate assay development. However, the field of antibody-siRNA conjugates (ARCs) is limited by more than mechanistic studies of endosomal

escape. Traditionally, siRNA has been delivered via nanoparticle encapsulation. Potent nanoparticle carriers were identified via combinatorial screening of ionizable lipids and particle formulations. Similarly, combinatorial screening holds the promise to identify bioactive ARCs. However, in comparison to nanoparticles, ARCs require labor intensive synthesis and characterization. Therefore, new methods are needed to rapidly synthesize libraries of endosomalytic agents and deploy them in ARCs. Together with improving our mechanistic understanding of endosomal escape, this holds the promise to identify potent ARCs capable of targeting tissues beyond the liver.

Conclusion

In this work, we have developed a variety of synthetic tools to construct multifunctional bioconjugates. These bioconjugates were applied to study site-specific antibody modification and the biophysical properties of ADCs as well as develop molecular probes for protein-protein clustering and the intracellular processing of siRNA. The breadth of topics discussed underscores the central role that chemical cross-linker synthesis plays in the design of bioconjugates. However, effectively working with bioconjugates requires equivalent expertise in both protein engineering, and molecular biology. In recent years, we and others have developed a host of tools that enable the synthesis of homogeneous, multifunctional bioconjugates. Looking towards the future, tools are needed to streamline the synthesis of bioconjugates and quantitatively study their interactions inside of cells. This will accelerate the development of bioconjugate-based therapeutics by enabling combinatorial screening of bioconjugates and demystifying their intracellular processing.